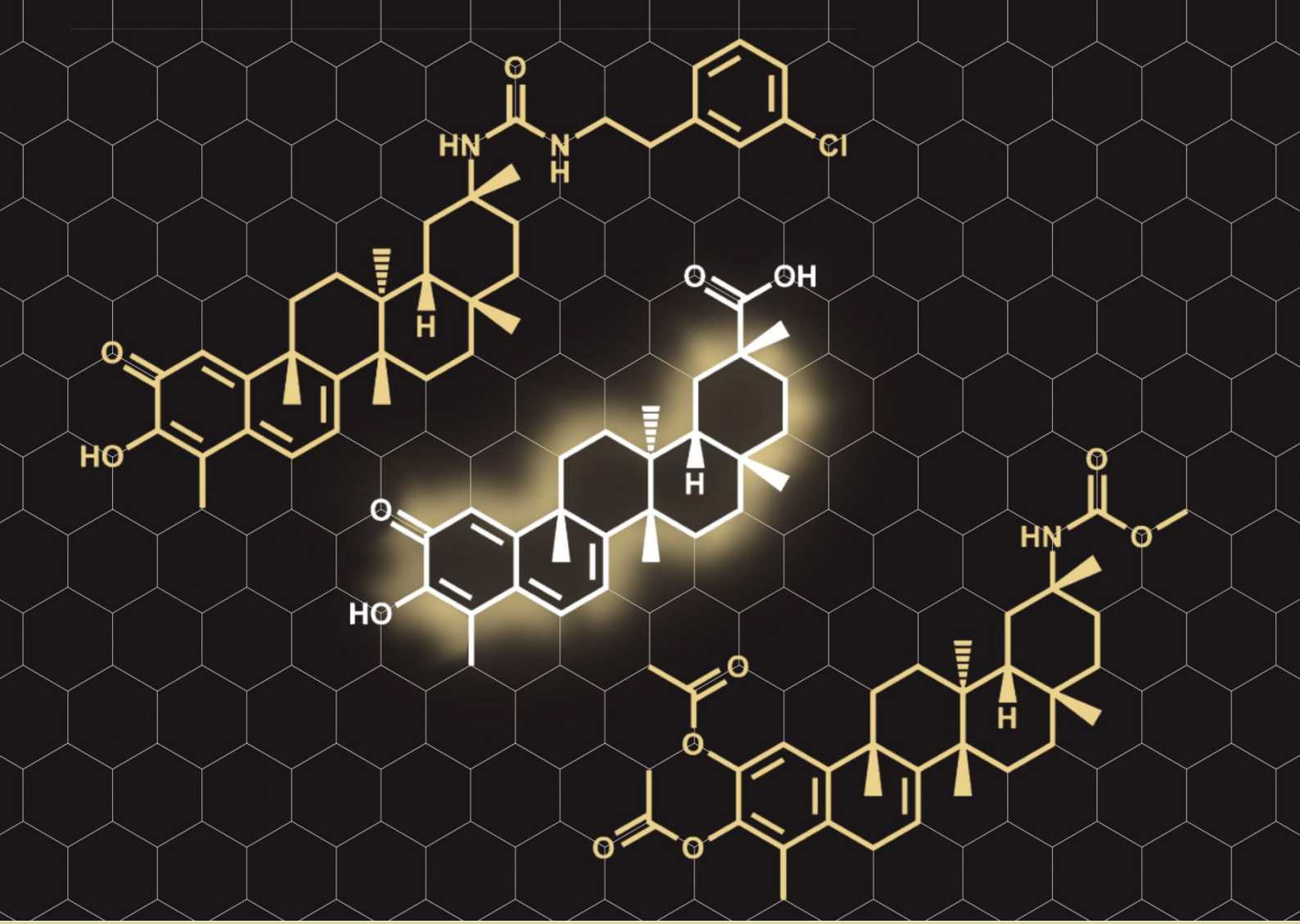

Sandra Antónia Cordeiro Figueiredo

Pentacyclic Triterpenoids: Discovery of New Drugs with Antitumour Activity

Doctoral Thesis in Pharmaceutical Sciences in the specialty of Pharmaceutical Chemistry, supervised by Professor Jorge António Ribeiro Salvador and presented to the Faculty of Pharmacy of the University of Coimbra

August/2017

· U C ·

Pentacyclic Triterpenoids: Discovery of New Drugs with Antitumour Activity

Thesis submitted to the Faculty of Pharmacy of the University of Coimbra in partial fulfilment of the requirements for the degree of Doctor of Philosophy in Pharmaceutical Sciences in the specialty of Pharmaceutical Chemistry

By

Sandra Antónia Cordeiro Figueiredo

Coimbra, Portugal, 2017

Pentacyclic Triterpenoids: Discovery of New Drugs with Antitumour Activity

The present PhD thesis was developed under the supervision of:

Professor Jorge António Ribeiro Salvador, PhD

Laboratory of Pharmaceutical Chemistry, Faculty of Pharmacy, University of Coimbra, and Centre for Neuroscience and Cell Biology,

University of Coimbra, Portugal

With the collaboration of:

Professor Marta Cascante Serratosa, PhD

Department of Biochemistry and Molecular Biology, Faculty of Biology, University of Barcelona, Spain

Pentacyclic Triterpenoids: Discovery of New Drugs with Antitumour Activity

This work was financially supported by Fundação para a Ciência e a Tecnologia under the Programa Operacional Potencial Humano (POPH) of Quadro de Referência Estratégica Nacional (QREN) Portugal 2007-2013:

SFRH/BD/86163/2012

Front Cover:

Representation of the chemical structures of celastrol and the most cytotoxic derivatives prepared in this work.

“A espantosa realidade das coisas

é a minha descoberta de todos os dias”

Alberto Caeiro (Fernando Pessoa)

Aos meus pais,

À minha irmã,

Aos meus avós,

Ao Jorge

AGRADECIMENTOS | *ACKNOWLEDGEMENTS*

Esta dissertação é o resultado de inúmeros contributos, partilhas e apoios, todos eles fundamentais para a sua realização.

Ao Professor Doutor Jorge Salvador, pela orientação científica desta tese de doutoramento. Pela oportunidade e confiança que depositou em mim desde o início. Pelo seu exemplo de motivação, determinação e otimismo. O seu dinamismo e entusiasmo incomparáveis permitiram a concretização deste projeto. Agradeço ainda as sugestões e a revisão crítica do presente texto.

To Professor Marta Cascante Serratosa, for welcoming me in her laboratory, for the scientific support and for the opportunity to work with such wonderful people. It was an honour to work under her supervision and witness her enthusiasm for science.

To Roldán Cortés, PhD for all the countless help throughout this project. For his important feedback regarding the interpretation of the results, the revision process and sharing scientific knowledge. For the patience, competence, constant availability, help, dedication and friendship. It was a pleasure to work with him.

À Fundação para a Ciência e a Tecnologia, pelo apoio financeiro a este projeto (SFRH/BD/86163/2012).

Aos docentes e funcionários do Laboratório de Química Farmacêutica da Faculdade de Farmácia da Universidade de Coimbra. Um agradecimento especial à D. Graça Santiago por ter sido minha confidente em tantos momentos, pela sua dedicação e amizade. À D. Anabela Pinto pela partilha e boa-disposição.

Aos meus colegas do Laboratório de Química Farmacêutica da Faculdade de Farmácia, pela partilha, pela boa-disposição, ajuda e encorajamento. Ao Bruno Gonçalves que desde o primeiro momento me acolheu no laboratório, pela ajuda e disponibilidade constante até ao último momento. À Vanessa Mendes pelas opiniões e sugestões que contribuíram para um melhor trabalho, pela dedicação e partilha. À Ana Sofia Valdeira, Daniela Alho e Judite Coimbra pelos bons momentos que partilhámos. Acima de tudo, à Maria de Salete Baptista pela amizade infinita. Por me ter demonstrado que um doutoramento é muito mais do que experiências laboratoriais, mas essencialmente a partilha de experiências de vida. Por tudo o que partilhámos, pela sua força e incentivo. Por ter percorrido comigo todo este percurso e ter sido o melhor que nele encontrei.

Ao Doutor Pedro Cruz pela partilha de conhecimento e ajuda técnica na elucidação estrutural das amostras.

To Anusha Jayaraman, Alfonso Martín, Carles Foguet, Cristina Balcells, Effi Karakitsou, Erika Zodda, Ibrahim Halil Polat, Inês Baptista, Jordi Perarnau, Josep Centelles, Josep Tarragó, Miriam Contreras, Míriam Tarrado, Pedro de Atauri, Silvia Marín, Vitaly Selivanov: the awesome multicultural team at Marta Cascante's lab for welcoming me and for the scientific support. Above all, for their friendship, for the fantastic moments we shared, and essentially for making me feel that I was at home. Each one of them was unique, and their support meant more than they will ever know.

Aos meus pais, à minha irmã e aos meus avós pela dedicação, compreensão, incentivo e apoio incondicional. Pela confiança e por nunca terem deixado de acreditar em mim. Por tornarem este trabalho possível. A eles lhes devo tudo.

Aos restantes familiares, aos amigos que fiz durante este percurso e aos amigos de sempre. Por todo o apoio e motivação. Por sempre me apoiarem independentemente do tempo que tive de abdicar em prol deste projeto. Às minhas companheiras: Nala, Riscas e Pintas. Pela alegria infinita e por tornarem tudo mais fácil. À Norte, por apenas com aquele olhar doce me conseguir desacelerar a pressa dos pensamentos.

Acima de tudo, ao Jorge, por todo o apoio e amor incondicional. Por ser a minha base e o meu suporte ao longo de todos estes anos. Por nunca ter deixado de acreditar em mim.

A todos,

Obrigada

Thank you

Gràcies

Gracias

Grazie

धन्यवाद

Teşekkürler

Σας ευχαριστώ

Благодарю вас

TABLES OF CONTENTS

ABSTRACT

Cancer is a major public health problem and, one of the leading causes of morbidity and mortality worldwide. Cancer treatments, including chemotherapy, are crucial to the clinical management of the disease. However, conventional cancer therapies often cause serious side effects and in the majority of advanced cases, offer only modest improvement in survival rates. Therefore, there is an urgent therapeutic need for the development of new active agents against cancer.

Plants are a key source of pharmaceuticals and serve as the basis for numerous medicines, including anticancer agents. Pentacyclic triterpenoids are a group of promising secondary plant metabolites that, present a broad range of biological activity, including antitumour activity. They are often used in traditional medicine and are an important source of hits in drug discovery. Celastrol is one of the most active antitumour compounds among the natural triterpenoids. It has been reported to be highly active against a wide variety of tumours and to affect multiple cellular pathways. Considering its biological potential, some semisynthetic derivatives of celastrol have been previously prepared. These studies suggest that structural modification of celastrol may be important to improve its anticancer activity.

In the present work, the design and synthesise of new semisynthetic derivatives of celastrol with improved selectivity and enhanced anticancer activity was intended. For that purpose, different synthetic strategies were exploited and new series of celastrol derivatives, including compounds bearing a urea and a carbamate group at C(29), were prepared and their anticancer activity was evaluated.

The chemical structures and high purity of the new celastrol derivatives were corroborated by melting point determination, infrared spectroscopy, nuclear magnetic resonance spectroscopy (^{1}H NMR, ^{13}C NMR and DEPT-135), mass spectrometry and elemental analyses. To determine their anticancer potential, the activity of all synthesised analogues over the viability of cancer cells was evaluated against several human tumour cell lines, including lung carcinoma

(A549) and pancreatic carcinoma (MIA PaCa-2) cell lines, using the MTT assay. Furthermore, preliminary studies of the mechanism of action of the most promising derivatives were performed in ovarian carcinoma cells (SKOV-3) using techniques, such as flow cytometry, fluorescence microscopy and western blotting.

Several of these new celastrol derivatives exhibited an improved growth-inhibition effect on human cancer cells compared with the parent compound, with IC_{50} values around or below 1 μM. Additionally, to assess selectivity, the best compounds of each series were further tested against a human non-tumour fibroblast cell line (BJ) and showed lower toxicity, which indicated a selective cytotoxic activity for malignant cells.

Compound **3.21** — a quinonemethide urea derivative — and compound **4.11** — a dihydrocelastrol diacetate carbamate derivative — were the most promising synthesised compounds. Preliminary studies of the mechanism underlying their anticancer effect showed that both might induce apoptosis through the activation of the extrinsic death receptor pathway. Additionally, a synergistic anticancer effect was evidenced when SKOV-3 cells were simultaneously treated with compound **3.21** and cisplatin and a similar effect was observed when SKOV-3 cells were treated concomitantly with compound **4.11** and carboplatin.

Taken together, these results provided a deeper understanding of the structure-activity relationship, chemical reactivity and stability of celastrol derivatives. Moreover, these results demonstrated the remarkable potential of celastrol derivatives, such as compounds **3.21** and **4.11**, as promising leads for the development of new cancer therapies.

Keywords: Celastrol, triterpenoids, semisynthetic derivatives, ureas, carbamates, anticancer, apoptosis, drug synergy.

RESUMO

O cancro representa um importante problema de saúde pública, sendo uma das principais causas de morbilidade e mortalidade a nível mundial. Os tratamentos utilizados atualmente em clínica, incluindo a quimioterapia, são essenciais para o controlo clínico da doença. No entanto, os tratamentos antineoplásicos convencionais causam frequentemente efeitos secundários graves e, nas fases mais avançados do cancro, apenas aumentam ligeiramente a taxa de sobrevivência. Isto indica que há uma necessidade emergente de desenvolvimento terapêutico de novas substâncias ativas anticancerígenas mais eficazes e menos tóxicas.

As plantas são uma fonte fundamental de produtos farmacêuticos, sendo a base de inúmeros fármacos, entre eles medicamentos de quimioterapia. Os triterpenóides pentacíclicos são um grupo promissor de metabolitos secundários das plantas e apresentam uma atividade biológica muito diversificada, entre elas a atividade antitumoral. Estes compostos são frequentemente utilizados na medicina tradicional e são uma fonte importante de novas moléculas para a indústria farmacêutica. O celastrol é dos compostos antitumorais mais activos entre os triterpenóides, demonstrando elevada atividade em diferentes tipo de tumores e afetando diversos mecanismos celulares. Considerando o seu elevado potencial biológico, foram realizados alguns estudos com derivados semissintéticos do mesmo, os quais sugeriram que modificações estruturais da molécula do celastrol poderiam ser vantajosas para otimizarem a sua atividade antitumoral.

Assim, neste presente trabalho pretendeu-se preparar novos derivados semissintéticos do celastrol com melhor atividade antitumoral e melhor seletividade. Para tal, explorou-se diferentes estratégias sintéticas de forma a preparem-se novos painéis de derivados do celastrol, entre eles ureias e carbamatos na posição C(29).

As estruturas químicas e elevada pureza dos novos derivados do celastrol foram confirmadas por determinação do ponto de fusão, espectroscopia de

infravermelho, ressonância magnética nuclear (^{1}H RMN and ^{13}C RMN), espectrometria de massa e análise elemental. De forma a determinar-se o potencial anticancerígeno dos novos compostos, avaliou-se a sua atividade na viabilidade celular de várias linhas celulares tumorais humanas, tais como células do carcinoma de pulmão (A549) e do carcinoma de pâncreas (MIA PaCa-2), através de ensaios de MTT. Foram ainda feitos estudos preliminares do mecanismo de ação dos derivados mais promissores em células do carcinoma do ovário (SKOV-3), utilizando técnicas diversas, tais como, citometria de fluxo, microscopia de fluorescência e *western blotting*.

Muitos dos novos derivados do celastrol apresentaram melhores efeitos de inibição do crescimento celular das células tumorais, comparativamente ao celastrol, apresentando valores de IC_{50} próximos ou inferiores a 1 μM. Os melhores compostos de cada painel foram também avaliados em relação à sua seletividade, utilizando células humanas não tumorais (fibroblastros BJ). Estes compostos revelaram ser menos tóxicos para este tipo de células, o que indica uma seletividade citotóxica para células malignas.

O composto **3.21** — um derivado ureia quinonametídeo — e o composto **4.11** — um derivado carbamato diacetato dihidrocelastrol — demonstraram ser os mais promissores entre todos os compostos sintetizados. Os estudos preliminares do mecanismo de ação indicaram que ambos os compostos induzem a morte celular através da ativação da via extrínseca da apoptose. Demonstrou-se ainda uma sinergia antitumoral nas células SKOV-3 quando estas foram tratadas concomitantemente com o composto **3.21** e cisplatina, assim como quando tratadas com o composto **4.11** e carboplatina.

Em conclusão, estes resultados permitiram obter uma compreensão mais detalhada da relação estrutura-atividade, reatividade química e estabilidade dos derivados do celastrol. Além disso, demonstrou-se o potencial notável dos derivados do celastrol, tais como os compostos **3.21** e **4.11**, como moléculas promissoras para o desenvolvimento de terapias antineoplásicas.

Palavras-chave: Celastrol, triterpenóides, derivados semissintéticos, ureias, carbamatos, antitumorais, apoptose, sinergia.

LIST OF ABBREVIATIONS

17-AAG	17-N-allylamino-17-demethoxygeldanamycin
ADP	Adenosine diphosphate
Aha1	Activator of heat shock protein ATPase 1
Akt	Protein kinase B
AML	Acute myeloid leukaemia
AMP	Adenosine monophosphate
AMPK	AMP-activated protein kinase
Apaf-1	Apoptotic protease-activating factor 1
ATCC	American type culture collection
ATF2	Activating transcription factor-2
ATP	Adenosine triphosphate
Bad	Bcl-2-associated death promoter
Bak	Bcl-2 homologous antagonist/killer
Bax	Bcl-2-associated X
Bcl-2	B-cell lymphoma 2
Bcr-Abl	Breakpoint cluster region-Abelson
BH	Bcl-2 homology domain
Bik	Bcl-2 interacting killer
Bim	Bcl-2-like protein 11
cAMP	Cyclic adenosine monophosphate
CCK-8	Cell counting Kit-8
Cdc37	Cell division cycle 37
CDK	Cyclin-dependent kinase
CI	Combination index
cIAP	Cellular inhibitor of apoptosis protein
CIP2A	Cancerous inhibitor of PP2A
CLL	Chronic lymphocytic leukaemia
CML	Chronic myelogenous leukaemia
COPD	Chronic obstructive pulmonary disease
CREB	cAMP response element binding protein
CXCR4	C-X-C chemokine receptor type 4
d	Doublet (NMR)
dd	Doublet of doublets (NMR)

DEPT	Distortionless enhancement by polarization transfer
DIABLO	Direct inhibitor of apoptosis-binding protein with low isoeletric point
DI-ESI	Direct infusion electrospray ionization
DISC	Death inducing signalling complex
DMAP	4-(Dimethylamino)pyridine
DMEM	Dulbecco's modified eagle's medium
DMF	Dimethylformamide
DMSO	Dimethyl sulfoxide
DNA	Deoxyribonucleic acid
DNase	Deoxyribonuclease
DR	Death receptor
EDTA	Ethylenediaminetetraacetic acid
EGFR	Epidermal growth factor receptor
eIF2α	Eukaryotic translation initiation factor 2α
eIF4e	Eukaryotic translation initiation factor 4E
eNOS	Endothelial nitric oxide synthase
ER	Endoplasmic reticulum
ERK	Extracellular signal-regulated kinase
FACS	Fluorescence-activated cell sorting
FADD	Fas-associated death domain
Fas	First apoptosis signal
FasL	Fas ligand
FasR	Fas receptor
FBS	Fetal bovine serum
FCM	Cell counting by flow cytometry
FDA	Food and drug administration
FLICE	FADD-like interleukin-1β-converting enzyme inhibitory protein
FLIP	FLICE-inhibitory protein
FT-NMR	Fourier-transform-NMR
GSK3	Glycogen synthase kinase 3
hERG	Human *ether-a-go-go*-related gene
HER1	Human epidermal growth factor receptor 1
HIF-1α	Hypoxia-inducible factor 1α
Hop	Hsp70-Hsp90 organizing protein
HSF-1	Heat shock factor 1

Hsp	Heat-shock protein
hTERT	Human telomerase reverse transcriptase
Hz	Hertz
IAPs	Inhibitors of apoptosis proteins
IC_{50}	Concentration of compound required to reduce 50% of cell viability
ICAM	Intercellular adhesion molecule
IκB	Inhibitor of kappa B
IKK	IκB kinase
IL	Interleukin
IR	Infrared spectroscopy
J	Coupling constant
JAK	Janus kinase
JNK	c-Jun N-terminal kinase
KRAS	V-KI-RAS2 Kirsten rat sarcoma viral oncogene homolog
LPS	Lipopolysaccharide
LTBA	Lithium tri-*tert*-butoxyaluminum hydride
m	Multiplet (NMR)
M^+	Molecular ion (MS)
Mcl-1	Induced myeloid leukaemia cell differentiation protein
miR	MicroRNA
MAPK	Mitogen-activated protein kinase
MEF2D	Myocyte enhancer factor 2D
MEM	Minimum essential medium
MMP	Matrix metalloproteinase
Mp	Melting point
MRC	Mammalian respiratory complex
MS	Mass spectrometry
mTOR	Mammalian target of rapamycin
MTS	3-(4,5-Dimethylthiazol-2-yl)-5-(3-carboxymethoxyphenyl)-2-(4-sulfophenyl)-2H-tetrazolium
MTT	3-(4,5-Dimethylthiazol-2-yl)-2,5-diphenyltetrazolium bromide
m/z	Ion mass/charge ratio (MS)
ND	Not determined
NF-κB	Nuclear factor kappa-light-chain-enhancer of activated B cells
NMR	Nuclear magnetic resonance

NOS	Nitric oxide synthase
p70S6K	Ribosomal protein S6 kinase beta-1
***p*-QM**	*para*-Quinonemethide
pAkt	Phospho-Akt
PARP	Poly (ADP-ribose) polymerase
PBS	Phosphate buffered saline
PBST	PBS containing Tween-20®
PDGFR	Platelet derived growth factor receptor
PDK1	Phosphoinositide-dependent protein kinase 1
PERK	Protein kinase RNA-like endoplasmic reticulum kinase
PI	Propidium iodide
PI3K	Phosphatidylinositol 3-kinase
ppm	Parts per million
P/S	Penicillin/Streptomycin
PS	Phosphatidylserine
PT	Pentacyclic triterpenoid
PUMA	p53 upregulated modulator of apoptosis
PVDF	Hydrophobic polyvinylidene fluoride
QM	Quinonemethide
QT	Quinonemethide triterpenoid
ROS	Reactive oxygen species
RNA	Ribonucleic acid
R.T.	Room temperature
s	Singlet (NMR)
S6	Ribosomal protein S6
S6K	S6 kinase
SAHA	Suberanilohydroxamic acid
SAR	Structure-activity relationship
SD	Standard deviation
SDS	Sodium dodecyl sulfate
SEM	Standard error of mean
SHH	Sonic hedgehog
Smac	Second mitochondria derived activator of caspase
STAT	Signal transducer and activator of transcription proteins
t	Triplet (NMR)

tBid	Truncated Bid
TBS	Tris-Buffered Saline
THF	Tetrahydrofuran
TLC	Thin layer chromatography
TMS	Tetramethylsilane
TNF	Tumour necrosis factor
TNF-R	TNF receptor
TRADD	TNF-R-associated death domain
TRAIL	TNF-related apoptosis-inducing ligand
TRAIL-R	TRAIL receptor
UPR	Unfolded protein response
UV	Ultraviolet
VCAM1	Vascular cell adhesion molecule 1
VEGF	Vascular endothelial growth factor
VEGFR	Vascular endothelial growth factor receptor
WHO	World Health Organization
WST-8	2-(2-Methoxy-4-nitrophenyl)-3-(4-nitrophenyl)-5-(2,4-disulfophenyl)-2H-tetrazolium, monosodium salt
XIAP	X-linked inhibitor of apoptosis protein
δ	Chemical shifts values (NMR)

LIST OF FIGURES

LIST OF TABLES

LIST OF SCHEMES

THESIS ORGANIZATION

This thesis is structured as follows:

Chapter 1 gives a general introduction to cancer by taking a brief look at its pathophysiology, statistics and anticancer treatments. Additionally, the importance of natural products and their semisynthetic derivatives in drug discovery is discussed, focusing mainly on the anticancer activity of pentacyclic triterpenoids. In the last part of this chapter the antitumour activity of celastrol in particular is highlighted, and a description of the current status of research on the anticancer activity of its semisynthetic analogues is also provided.

Chapter 2 presents the aim of the work described in this thesis.

In the subsequent chapters, **Chapters 3** and **4**, the design, synthesis and biological evaluation on human cancer cell lines of new celastrol derivatives, including urea (**Chapter 3**) and carbamate (**Chapter 4**) derivatives, are described. In both chapters, further studies of the best compounds were performed, such as preliminary mechanistic studies of the antitumour activity, studies of selectivity and synergistic determinations.

Chapter 5 includes an additional structural diversification of celastrol derivatives and new insights into celastrol analogues previously prepared, including their effects on cell viability and analysis of structure-activity relationship (SAR).

Chapters 3–5 are similarly structured: a brief introduction is followed by the main results and discussion outlining the synthetic strategies that were used for the preparation of the new derivatives and the biological studies that were performed using them. Each chapter closes with a conclusion and an experimental section describing the biological and chemical procedures used in this work, as well as the structural elucidation of the new derivatives.

Finally, **Chapter 6** includes a summary of the main outcomes of this study and suggestions for future work.

The closing chapter, **Chapter 7** presents the bibliographical references used in this thesis, which were cited accordingly to the *American Chemical Society style guide.*

CHAPTER I

INTRODUCTION

1. CHAPTER I

Introduction

1.1. CANCER

1.1.1. Understanding cancer

Cancer is a complex and heterogeneous disease that presents many subtypes and affects, various tissues in different ways. The uncontrolled, abnormal growth of cells is the defining characteristic of cancer, among several common biological properties that identify this condition [*1*].

With the development of cancer, the atypical cells may proliferate without stopping and create tumours, which can spread into nearby tissues or invade other parts of the body, via the bloodstream and lymphatic system. Tumour growth can disrupt the normal function of tissues and vital organs, which can lead to death [*2*].

1.1.2. Cancer statistics

Cancer is a major public health problem, and is one of the leading causes of morbidity and mortality worldwide [*3*]. In fact, cancer was the second cause of death in 2015, which indicates that nearly one in six deaths were related to cancer [*4*]. Moreover, cancer is the leading cause of death among specific age groups, namely women aged 40 to 79 and men aged 45 to 79 years [*5*]. Around 30% of cancer deaths are linked to one of these five behavioural and dietary risks: low fruit and vegetable consumption, insufficient physical activity, high body mass index and, alcohol and tobacco use. Unfortunately, the number of new cancer cases is expected to increase by about 70% in the next 20 years [*4*]. Therefore, it is not surprising that the economic impact of cancer is massive and keeps increasing: in 2010 the total annual economic cost associated with this condition was estimated at around US$ 1.16 trillion [*6*].

1.1.3. Anticancer drugs

Cancer treatments include different therapeutic modalities, such as surgery, radiotherapy and systemic therapy. Although chemotherapy is central to the clinical management of cancer, it remains among the life-threatening diseases that are the most difficult to treat. In the majority of advanced cases of cancer, chemotherapy only offers a modest increase in the survival rate. This is in part due to tumour diversity, drug resistance, dose-limiting toxicities and limitations of the animal models available [*7*]. Even after over half a century of chemotherapy research, it remains one of the most crucial fields of medicinal chemistry.

1.1.3.1. Strategies of anticancer drug development: targeted drugs

Targeted therapy is a specific type of chemotherapy that targets different characteristics between cancer cells and non-tumour cells. This type of therapy is expected to be more effective and safer as it interferes with specific target molecules that are involved in carcinogenesis, rather than interfering with all — healthy or abnormal — rapidly proliferating cells [*8*][*9*].

Advances in this field of genetics and molecular biology provide an essential understanding of the regulatory and signalling networks that act in cells that control critical cellular processes, such as growth, differentiation, proliferation and vascularisation. As pointed out by Douglas Hanahan and Robert Weinberg, tumour cells present further enhancements of some of these biological capabilities, the so-called hallmarks categories of cancer [*1*, *10*]. These hallmarks comprise resisting cell death, sustaining proliferative signalling, evading growth suppressors, enabling replicative immortality, inducing angiogenesis, and activating invasion and metastasis [*10*]. Additionally, two emerging hallmarks were added to this list: reprogramming of the energy metabolism and evading immune destruction [*1*]. Each of these hallmarks of cancer represents an opportunity for seeking molecular targets that are critical to the malignant tumour phenotype but not essential for normal tissues and organs [*11*].

Researchers and the pharmaceutical industry have been exploring this approach and, since the mid-1990s, several new targeted drugs have been approved (Table 1.1).

Table 1.1 Examples of approved targeted cancer drugs

Drug	Classification	Clinical uses	Molecular targets	Ref.
Bevacizumab	Monoclonal antibody	Cervical cancer, colorectal cancer, fallopian tube cancer, glioblastoma, non-small cell lung cancer, ovarian cancer, peritoneal cancer, renal cell carcinoma.	VEGF ligand	[12]
Bortezomib	Small molecule	Multiple myeloma, mantle cell lymphoma.	Proteasome	[*13*]
Cetuximab	Monoclonal antibody	Colorectal cancer (KRAS wild type), squamous cell cancer of the head and neck.	EGFR (HER1/ERBB1)	[14]
Imatinib	Small molecule	CML, gastrointestinal stromal tumour, dermatofibrosarcoma protuberans, multiple hematologic malignancies.	KIT, PDGFR, Bcr-Abl	[*15*]
Rituximab	Monoclonal antibody	Non-Hodgkin's lymphoma, CLL, rheumatoid arthritis, granulomatosis with polyangiitis.	CD20	[16]

The more rational approach that leads to these treatment advances is based on not only the increasing knowledge on the biology of the targets, but also on developments in this field of screening technology and chemical synthesis. In fact, medicinal chemistry plays a key role in anticancer drug development, with an emphasis on finding and optimizing chemical leads with activity against specific targets [*17*].

The discovery of the Bcr-Abl tyrosine kinase inhibitor, imatinib **1.3**, which is a drug that has been approved for the treatment of chronic myelogenous leukaemia (CML), is a good illustration of the optimization of a lead compound (Table 1.1, Figure 1.1). First, the molecular target was chosen, i.e., the oncogene tyrosine kinase *Bcr-Abl*, which is found only in CML cells [*18*]. Then, a chemical lead (compound **1.1**) was identified in a screen and chosen as the starting point. Introduction of an amide group in the phenyl ring added potency, while substitution of a methyl group added selectivity (compound **1.2**). Finally, addition of a polar piperazinylmethyl group improved water solubility and oral bioavailability, resulting

in the compound imatinib **1.3** [*19*]. Furthermore, an X-ray structural analysis of imatinib **1.3** bound to Bcr-Abl revealed that the piperazine ring not only improved the physical properties of the molecule, but also promoted significant contacts with the enzyme [*20*]. This knowledge unlocked the potential for designing new drugs to overcome the drug-resistance developed by mutations in the *Bcr-Abl* gene [*21*].

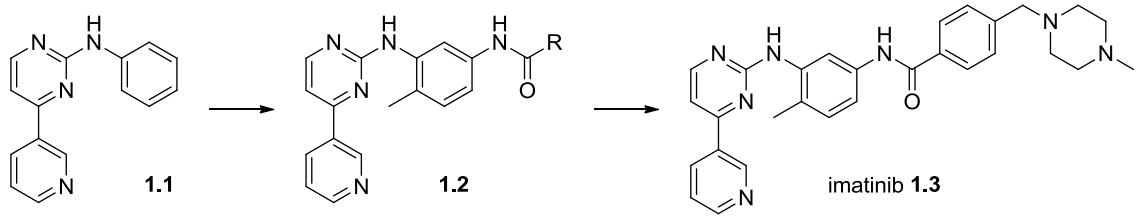

Figure 1.1 Discovery of imatinib **1.3.**

Targeted cancer therapy can be categorised by the underlying mechanism of action: for instance, signal transduction inhibitors, gene expression modulators, hormone therapies, angiogenesis inhibitors, immunotherapies, toxin delivery molecules and apoptosis inducers [*22*]. In the next subsection, we will focus on the latter mechanism.

1.1.3.2. Targeting apoptosis

Apoptosis is a process of programmed cell death that involves several biochemical and genetic pathways via which the proper survival/death balance is maintained in normal tissues [*23*]. Apoptosis is essential in normal organisms: it regulates embryonic development; controls cell number and proliferation; controls the immune function and infection resistance; and eliminates useless, degenerative, damaged and stressed cells, among several other functions [*24*, *25*].

Apoptosis causes minor damage and inflammation in the surrounding tissues [*26*]. This is reflected in the typical morphological features of apoptosis, such as cell shrinkage, dilatation of the endoplasmic reticulum, fragmentation into membrane-bound apoptotic bodies (membrane blebbing) and rapid phagocytosis by nearby cells [*27*].

The malfunction of apoptosis is central to cancer development. In fact, resistance against cell death is one of the prominent hallmarks of cancer, as it allows cells an accumulation of mutations in the cell that is sufficient for them to become malignant and continue their uncontrolled proliferation [*10*]. Additionally, evasion of apoptosis is a major contributor to treatment resistance, as most of the current approved cytotoxic drugs induce apoptosis in cancer cells [*28*].

Thus, targeting apoptosis is an obvious strategy for cancer therapy, and several molecules involved in this process have been listed as potential targets to stimulate apoptosis in different types of cancer [*29*]. Although apoptotic mechanisms are often described as separated mechanisms, they are interwoven with many other cellular pathways: e.g., cell-cycle, metabolism and receptor transduction pathways [*30*]. Conventionally, the complex mechanisms of apoptosis involve an energy-dependent cascade of molecular events and are divided in two main pathways: the intrinsic, stress or mitochondrial pathway and the extrinsic or death receptor-mediated pathway. However, the two pathways are linked and their molecules converge on downstream effector caspases that lead to the execution of the death signal [*31*]. Caspases are synthesised as inactive enzymes — procaspases — that require cleavage at aspartate residues for their activation. As procaspases are cleaved, the released caspases participate in a cascade of activation whereby one caspase can activate another one in a chain reaction that leads to the amplification of the apoptotic signal [*9*].

Intrinsic pathway

The intrinsic pathway (Figure 1.2) is induced by stimuli stemming from inside the cell and is chiefly controlled by the Bcl-2 protein family. These proteins share at least one Bcl-2 homology (BH) domain which mediates protein-protein interactions. Regarding their function, Bcl-2 family proteins are classified into two groups: antiapoptotic proteins that promote cell survival, and proapoptotic proteins that mediate receptor-, mitochondria- or endoplasmic reticulum (ER) stress-dependent apoptosis (Table 1.2) [*29*].

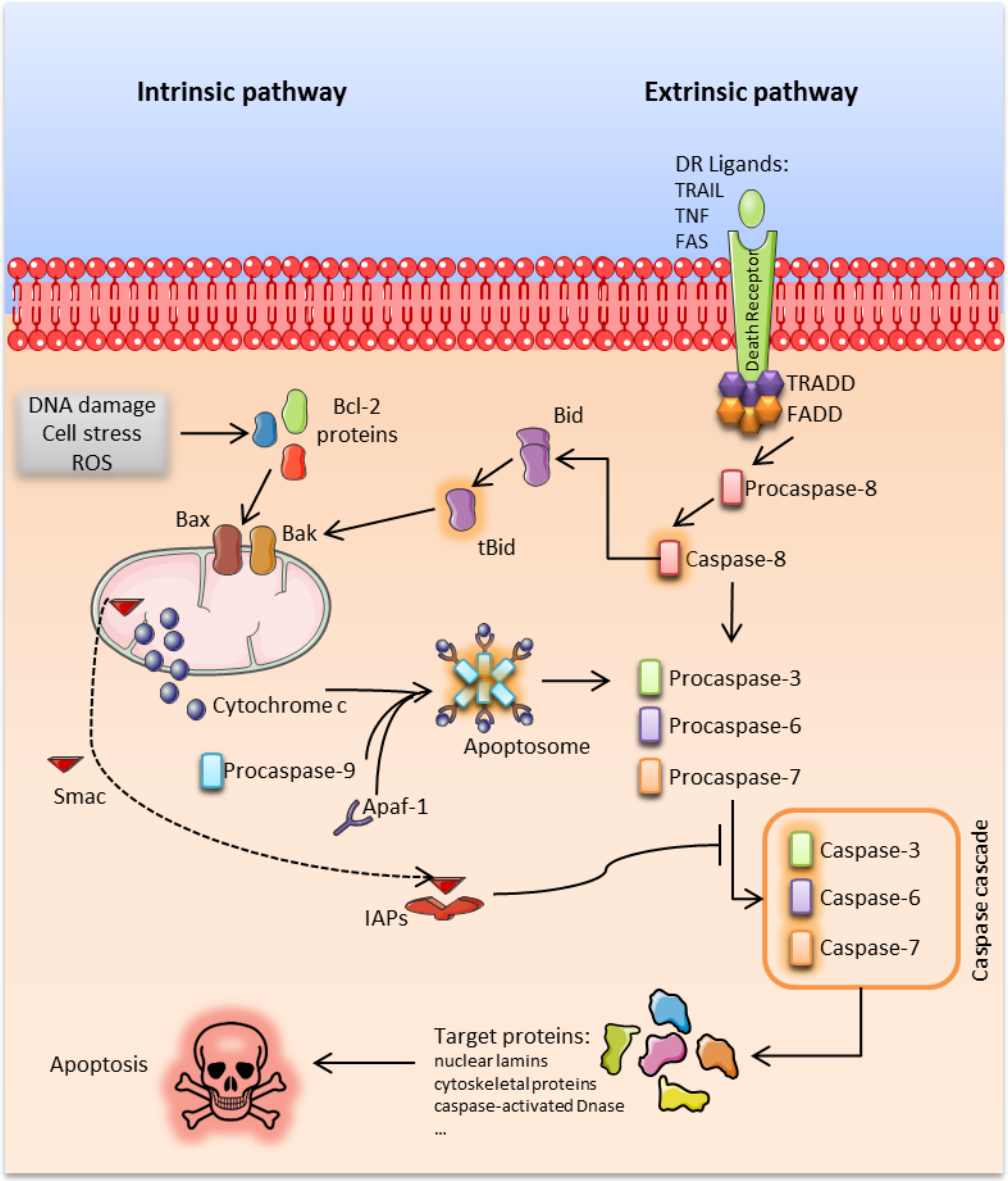

Figure 1.2 Apoptotic pathways.

The apoptosis process progresses essentially through three stages. First, during the initiation phase, cytotoxic stimuli inside the cell (e.g., oxidative stress and DNA damage, activation of oncogenes, overload of Ca^{2+} and deprivation of growth factors) lead to an increase in mitochondrial permeability and the release of molecular apoptotic mediators from mitochondria [*29*]. The intermembrane space (between the inner and outer mitochondrial membranes) works as a supply of apoptotic mediators [*32*]. Second, during the regulatory phase, BH3-only family proteins (e.g., the Bcl-2-associated death promoter protein (Bad) and the Bcl-2 interacting killer (Bik)) act as sensitizers by activating proapoptotic effectors (Bcl-2-

associated X (Bax) and Bcl-2 homologous antagonist/killer (Bak)) (Table 1.2). Thus, the mitochondrial membrane is disrupted and leaks cytochrome c (an apoptosis-inducing factor) into the cytosol. The released cytochrome c forms a multi-protein caspase-activating structure called “apoptosome”. This complex consists of caspase-9, the apoptotic protease activating factor 1 (Apaf-1) and cytochrome c, and is responsible for activating effector caspases (downstream caspase-3, caspase-6, and caspase-7) [*33*]. This is the third and final phase, the execution phase, during which caspases are cleaved and cells are further engulfed by neighbouring phagocytic cells [*34*].

Table 1.2 Members of the Bcl-2 family and respective function.

Bcl-2 family protein	Apoptotic function	BH domain
Bcl-2	Antiapoptotic	BH 1-4
Bcl-xL	Antiapoptotic	BH 1-4
Bcl-w	Antiapoptotic	BH 1-4
Bfl-1	Antiapoptotic	BH 1-4
Mcl-1	Antiapoptotic	BH 1-4
Bax	Proapoptotic — effector	BH 1-3
Bak	Proapoptotic — effector	BH 1-3
Bim	Proapoptotic — sensitizer	BH3-only
Bid	Proapoptotic — sensitizer	BH3-only
Bad	Proapoptotic — sensitizer	BH3-only
Bik	Proapoptotic — sensitizer	BH3-only
Noxa	Proapoptotic — sensitizer	BH3-only
Puma	Proapoptotic — sensitizer	BH3-only

This complex process is modulated by multiple additional proteins, such as inhibitors of apoptosis proteins (IAPs) and second mitochondria derived activator of caspase/direct inhibitor of apoptosis-binding protein with low isoeletric point (Smac/DIABLO). Smac has a proapoptotic function by blocking the X-linked inhibitor of apoptosis protein (XIAP), which is a pro-survival protein that binds to and inhibits caspase-3, caspase-7 and caspase-9 [*35*].

Because of their ability to control cell death, as well as the elevated expression of its member proteins in a variety of cancer cell types, the intrinsic apoptotic pathway holds promising potential for cancer therapeutic strategies.

Moreover, several tumours develop resistance to chemotherapy and radiotherapy because of aberrant expression of Bcl-2 family proteins, which allows them to evade apoptosis. Therefore, treating cells with drugs that modulate the Bcl-2 pathway might be useful for achieving an efficient cancer therapy. Some advances have been made toward this achievement, such as the development of antisense-mediated inhibitors, peptide inhibitors and small molecule inhibitors [*36*]. The first Bcl-2 inhibitor, venetoclax, was recently approved by the FDA (2016). Venetoclax is indicated for the treatment of an aggressive form of chronic lymphocytic leukaemia (CLL). The approval of venetoclax constitutes a milestone in cancer treatment, as it represents the first apoptosis-targeting drug available in a clinical setting, and the first drug that addresses the "resisting cell death" hallmark of cancer [*37*].

Extrinsic pathway

Conversely, the extrinsic pathway (Figure 1.2) is triggered by extracellular signals — death ligands or death factor — that couple to a death receptor (DR) at the cellular surface. The first apoptosis signal (Fas) ligand (FasL) is an example of a death factor that is bound to the plasma membrane of neighbouring cells and binds to a Fas receptor (FasR), a transmembrane death receptor, to induce apoptosis. Another example of a death factor is the tumour necrosis factor (TNF), which is a soluble factor that binds to another transmembrane death receptor, the TNF receptor (TNF-R) [*29*]. After the ligands bind to the DRs, the receptors undergo a conformational change and oligomerize, which enable the exposure of the death domains — located on the cytoplasmic tail of the receptors. Therefore, the death signal can be transduced into the cell by intracellular adaptor proteins, such as the Fas-associated death domain (FADD) and the TNF-R-associated death domain (TRADD). The adaptor proteins recruit several molecules of procaspase-8, which is an initiator caspase that links the receptor to the apoptotic

proteases. Thus, the death inducing signalling complex (DISC) is formed, which is composed of death ligands, receptors, adaptors and caspase-8. DISC transduces a downstream signal cascade: cascape-8 initiates a caspase cascade by activating the executioner caspases (caspase-3, caspase-6, and caspase-7). The caspase cascade induces the cleavage of specific protein targets, such as nuclear lamins, cytoskeletal proteins (e.g., actin and intermediate filaments), specific kinases and other enzymes (e.g., caspase-activated deoxyribonuclease (DNase). The proteolysis of these target proteins leads to nuclear shrinkage, rearrangement of cell structure, cell signalling and cleavage of chromatin, ultimately resulting in apoptosis [*38*, *39*].

The extrinsic pathway encloses promising targets for cancer therapy, as cytotoxic drugs and X-irradiation rely on the mitochondrial pathway for cell death, leading to the frequent development of chemorefractory cells [*40*].

Common mutations that affect the extrinsic pathway of apoptosis and result in cancer are those that occur in the genes that encode the *FasR* and the TNF-related apoptosis-inducing ligand (TRAIL) receptor (*TRAIL-R*) [*9*]. TRAIL is a member of the TNF family that induces a differential sensitivity to apoptosis between non-tumour and tumour cells. TRAIL-R1 and TRAIL-R2, — also called DR4 and DR5 — are expressed at higher levels in solid tumours [*41*]. The differential activity of TRAIL and its receptors in non-tumour cells vs cancer cells creates an opportunity for designing safer drugs that target this pathway. In fact, a recombinant human TRAIL ligand has been developed, and to date, two therapeutic strategies have been enrolled in clinical trials: recombinant human TRAIL and antibodies directed against TRAIL-R1 or TRAIL-R2. Despite promising initial results, these agonists have not been successful because of resistance to apoptosis induction. However, novel agents targeting TRAIL-R are currently being developed, to overcome this limitation [*42*].

Cross-talk between the intrinsic and extrinsic pathways

The intrinsic and extrinsic pathways converge on downstream effector caspases (Figure 1.2). The following is an illustration of the cross-talk between the

two pathways: caspase-8 — a key regulator of the extrinsic pathway — can cleave Bid into the active form, truncated Bid (tBid). Bid is a proapoptotic member of the Bcl-2 family of proteins that regulates mitochondria-mediated apoptosis by directly activating Bax and Bak, thus inducing mitochondrial outer-membrane permeabilization, facilitating the release of cytochrome c from the mitochondria, and inducing the subsequent activation of downstream caspases [*43*].

Both the extrinsic and intrinsic apoptotic pathways are regulated by several other agents, including the p53 protein, the phosphatidylinositol 3-kinase (PI3K) pathway and heat-shock proteins (Hsps) [*29*].

p53

The p53 protein is a tumour suppressor protein that is often called the guardian of the genome because of its important role in several cellular mechanisms, such as cell-cycle arrest, DNA repair and apoptosis [*44*]. In the face of stress signals, such as DNA damage, p53 becomes functionally active and can either trigger a transient or permanent cell-cycle arrest; alternatively it can trigger apoptosis-mediated cell death to prevent the development of the damaged cell into a tumour [*45*]. It does this by using both transcription-dependent and transcription-independent pathways [*9*].

Through the transcription-dependent pathway, p53 acts as a transcription factor that regulates the expression of apoptosis-related genes that affect the intrinsic or extrinsic pathways. Essentially, p53 induces the expression of proapoptotic factors (e.g., NOXA, Bax, Bak, FasR and PUMA) and represses the expression of antiapoptotic factors (e.g., Bcl-2, Bcl-x and IAPs) [*46*]. Conversely, the transcription-independent mechanism involves the p53-mediated activation of Bax in the cytoplasm, followed by the release of cytochrome c and the activation of the caspase cascade [*47*].

The critical role of p53 is evidenced by the fact that more than 50% of tumours bear a mutation in this gene. *p53* mutations offer cancer cells a survival advantage by disrupting apoptosis and, therefore, contributing to drug resistance

[*48*]. It has recently been demonstrated that mutant p53 proteins do not only lead to the loss of wild-type p53 tumour-suppressor functions, but may also be responsible for an oncogenic gain-of-function. These newly described oncogenic properties of mutant p53 proteins can favour the maintenance, expansion, spreading and resistance of tumour cells, thus promoting the proliferation of cells bearing mutant p53 [*49*, *50*].

Consequently, the tumour suppressor gene *p53* is an attractive therapeutic target. Although several clinical trials using gene-therapy-based approaches for restoring the wild-type p53 function in tumours have been conducted, this therapy is not widely used at the moment [*51*].

PI3K/Akt/mTOR pathway

The PI3K/Akt/mTOR is a complex pathway that plays a central role in several cellular mechanisms, such as cell survival, proliferation, motility and tissue neovascularization [*52*]. This pathway is initiated by several mechanisms, and its upregulation is associated with several types of cancer [*53*]. Initial signalling activation of the PI3K/Akt/mTOR pathway occurs at the cell membrane; subsequently, the signal is propagated via the activation of PI3K class Ia. In turn, activation of PI3K leads to the phosphorylation of inositol lipids in the plasma membrane that attract protein kinase B (PKB/Akt). Subsequently, Akt — the primary mediator of PI3K-initiated signalling — is phosphorylated and activated. Fully activated Akt translocates to the cytosol and the nucleus, where it can phosphorylate its substrates. Akt can regulate various target proteins related to the control of apoptosis and cell proliferation, such as Bad, caspase-9, IκB kinase (IKK) and the cAMP response element binding protein (CREB). The mammalian target of rapamycin (mTOR), which is a key regulator of protein translation and cell growth, is an additional substrate of Akt [*54*, *55*].

The PI3K/Akt/mTOR pathway regulates numerous non-tumour cellular mechanisms that are also critical for carcinogenesis. In addition, in some cancers, this pathway can be aberrantly activated. Therefore, its components constitute attractive therapeutic targets in cancer [*54*]. Currently, some compounds targeting

the PI3K/Akt/mTOR pathway are being tested in clinical trials for the treatment of solid tumours. Compared with the mTOR inhibitors, PI3K and Akt inhibitors are still at an early phase of development [*55*].

Hsp90

Hsps are a family of proteins that are produced in response to different types of stressful conditions, such as heat shock, pH shift or hypoxia. They function as molecular chaperones that enable the synthesis and folding of other proteins, termed clients [*56*]. Under normal conditions, Hsps play several roles in cells, including protein assembly, protein degradation within the proteasome pathway and modulation of protein activity by changing their conformation. Under stressful conditions, cells increase the production of Hsps to stabilize unfolded proteins, thus giving the cells more time to repair or re-synthesize the damaged proteins. In addition to affording resistance to stress-induced cell damage, Hsps have been reported to regulate apoptosis and cell death [*57*].

Hsp90s are the most common and widely studied Hsps. Hsp90s are commonly associated with cancer development and malignant phenotypes, such as drug resistance, invasion, angiogenesis, and metastasis [*58*]. In fact, Hsp90 is upregulated to 10-fold in tumour cells, and its client proteins include several oncogenic proteins, such as Bcr-Abl, Raf-1, p53, ErbB2, NF-κB and HIF-1α (hypoxia-inducible factor 1α) [*29*, *59*]. Hsp90s also play a role in modulating the Akt pathway: the interruption of the interaction between Hsp90 and Akt leads to the dephosphorylation of Akt and increases the likelihood of apoptosis [*60*]. Hsp90 requires molecular co-chaperone proteins (e.g., Cdc37, Hop, p23, Hsp110 and Aha1) for the assembly and activity of client proteins. The complex between Hsp90 and its co-chaperone proteins allows the interaction between client proteins in an ATP-dependent way [*59*].

Several molecular studies have suggested that small molecule inhibitors that act on Hsp90 directly or that interfere with its molecular co-chaperones may be a promising strategy to enhance apoptosis and treat a vast range of tumours

[*57*]. Tanespimycin, a geldanamycin derivative, is one of those compounds, and has yielded some promising results in clinical trials [*61*].

1.1.3.3. Combination chemotherapy

Despite numerous reports of development in cancer therapies of targeted drugs, some important limitations remain, such as incomplete remission, high toxicity and development of drug resistance [*62*]. This is mainly caused by the complexity and high heterogeneity of tumour cells and the genomic instability of cancer [*63*].

As targeting a single protein does not necessarily eliminate the tumour, the use of multi-targeting therapies might offer advantageous in this context. The combination of cytotoxic agents that co-inhibit more than one target in a single pathway or in compensatory pathways may be more effective and safer by decreasing drug doses and non-overlapping toxicities, preventing drug resistance and promoting a synergistic effect between two or more drugs [*64*].

1.2. NATURAL PRODUCTS

1.2.1. Natural products in drug discovery

Currently, it is estimated that 391,000 vascular plant species are known to science [*65*]. Plants have always been essential for the survival and well-being of mankind and other animals. Plants not only provide oxygen and food, they also have been the main source of therapeutic products for the prevention and treatment of several diseases [*66*]. In fact, one of the first references of medicinal plants, written on Sumerian clay slabs, dates back to around 5,000 years ago and presents recipes for drug preparations for over 200 different plants [*67*].

Often, one single plant species contains approximately 1000 different chemical compounds. This results in a huge number of different chemical structures that could hardly be synthesised in the laboratory [*68*]. About 50,000 metabolites have already been identified in plants, and this number is predicted to

increase to over 200,000. A large portion of these natural compounds are still available to be studied and exploited for their potential therapeutic activities [*69*]. Although plants provide a very rich, variable and complex set of chemical structures, many of them are currently threatened with extinction because of environmental changes and unsustainable agricultural practices [*70*]. This renders the advancement of research in the area of botany even more imperative.

Despite recent enormous technological advances in the pharmaceutical industry, plants continue to be a key source of pharmaceuticals and serve as the basis for the majority of medicines and cosmetics [*71*]. According to data from the World Health Organization (WHO), primary health care for 80% of the population is still based on natural sources, the so-called traditional medicine [*72*, *73*]. As for conventional medicine, 4% of the drugs that were approved worldwide between 1981 and 2014 were unaltered natural products. Moreover, 21% were natural product derivatives, as natural products have been a precious source for organic chemists to synthesise novel drug candidates. In total, only 27% of the new chemical entities approved can be classified as being truly synthetic [*74*].

The reason why so many compounds in nature have biological effects in humans and other species is not fully understood. One hypothesis is that these compounds are produced by living organisms and aim to interact with receptors and enzymes in those organisms, thus mimicking endogenous metabolites that are involved in signalling pathways. In general, drugs also aim to interact with this type of biomolecules in the human body, which is a huge structural advantage. The fact that plants and humans share a common evolutionary origin is also related with this explanation. Thus, the common ancestor had molecules, receptors and enzymes that interacted with each other, and although the organisms evolved differently, these molecules retained common features that keep them somehow compatible [*75*]. A third theory is related to the long-term co-evolution within biological communities: organisms that live in the same environment evolved to interact actively with each other, so they can influence them (e.g., defence and chemical communication functions) [*76*].

1.2.2. Semisynthetic derivatives

Despite the enormous potential of natural products as therapeutic agents, their use in clinical settings is not always straightforward. This is because natural compounds often show pharmacokinetics limitations, such as low solubility in water, which can lead to poor systemic absorption. In addition, natural compounds can cause undesirable side effects in humans and/or present insufficient biological activity [*77*]. The optimization of natural products through semisynthesis is a convenient way of overcoming these limitations [*78*]. Analytical and structural chemistry approaches provide the perfect tools to modify natural compounds in order to enhance their activity and other characteristics, such as solubility and stability [*76*].

The natural cyclolignan podophyllotoxin **1.4** (Figure 1.3) is an excellent example of a natural product that was used as a lead in medicinal chemistry, the structural modification of which has afforded compounds with extraordinary pharmacological activity [*79*]. Podophyllotoxin **1.4**, isolated from species of the genus *Podophyllum* (Berberidaceae), has been used for medicinal purposes since ancient times, and its current most relevant biological activities are cytotoxicity and antiviral activity [*80*]. Podophyllotoxin **1.4** itself is effective in the treatment of Wilms' tumours, different types of genital tumours, lung cancer and, non-Hodgkin and other lymphomas [*81*]. However, its clinical results were disappointing because of the severe gastrointestinal side effects associated with this drug. To optimize its activity and develop new compounds with better antitumour activity, many structural modifications have been performed on the cyclolignan skeleton [*82*]. Three semisynthetic podophyllotoxin derivatives — etoposide **1.5**, teniposide **1.6** and etopophos **1.7** (Figure 1.3) — are widely used anticancer drugs that display good clinical activity against several types of tumour, including lung cancer, acute leukaemia, lymphoma, testicular carcinoma and Kaposi's sarcoma [*83*]. Other new cyclolignans have been prepared by modification of nearly all the rings of the basic skeleton of the molecule in the search for more potent, less toxic and more selective analogues. GL-331 **1.8** and TOP-53 **1.9** (Figure 1.3) are among the derived compounds that have reached clinical trials [*79*].

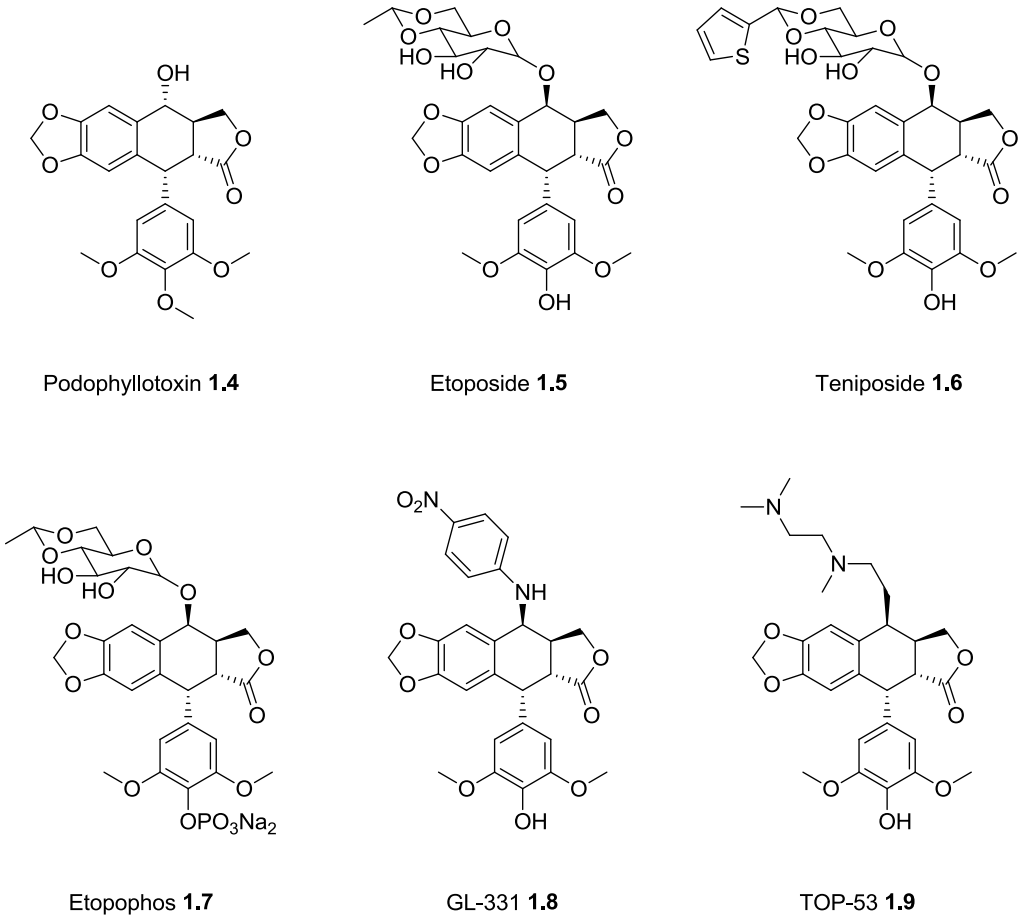

Figure 1.3 Chemical structures of podophyllotoxin **1.4** and its derivatives.

Other examples of natural lead anticancer compounds are vinblastine **1.10** and vincristine **1.11** (Figure 1.4), which are vinca alkaloids isolated from the pink periwinkle plant *Catharantus rosea.* By simple structural modification of these natural leads, other indole compounds were obtained, such as vinorelbine **1.12** and vindesine **1.13** (Figure 1.4) [*84*]. These natural products and their derivatives show extraordinary antineoplastic properties, and, despite their similar chemical structures, they show differences both in their activity spectrum and toxicity. For example, vinblastine **1.10** is used in the treatment of testicular cancer, non-Hodgkin lymphoma, breast cancer, head and neck cancer, cervico-uterine cancer and bladder cancer, while vincristine **1.11** is more effective against non-Hodgkin lymphoma, Hodgkin's disease and paediatric solid tumours than it is against adult solid tumours. Vinorelbine **1.12**, in turn, is more effective against breast and lung cancer, whereas vindesine **1.13** is used in the treatment of acute leukaemia,

malignant lymphoma, Hodgkin's disease, acute erythraemia and acute panmyelosis [*85–87*].

Podophyllotoxin **1.4**, vinblastine **1.10** and vincristine **1.11** are only some examples of lead natural anticancer drugs within the wide arsenal of natural products for which structural modification has led to more potent and less toxic analogues compared with the parent compound.

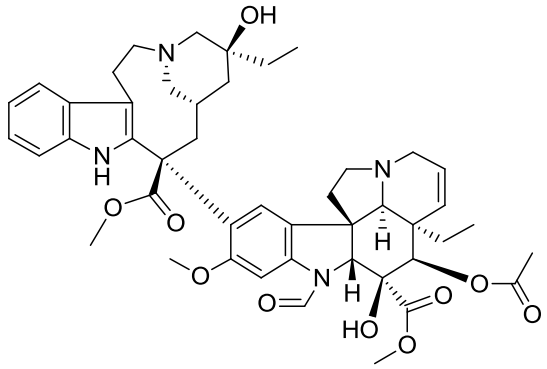

Vinblastine **1.10**

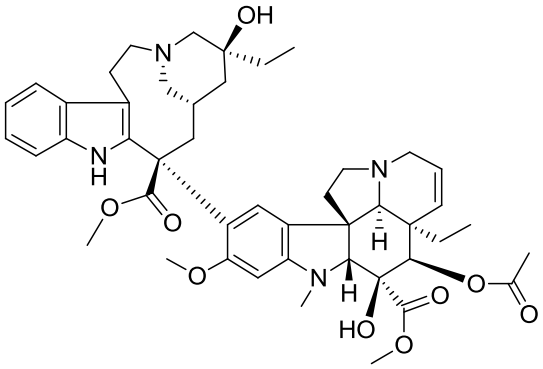

Vincristine **1.11**

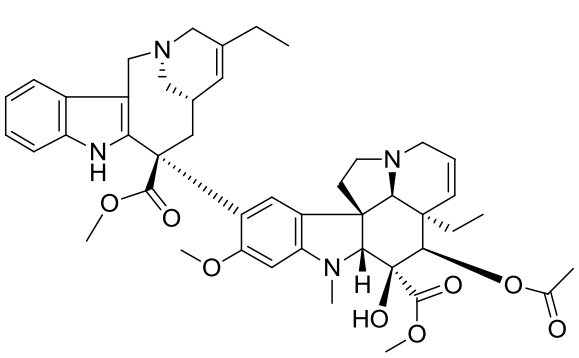

Vinorelbine **1.12**

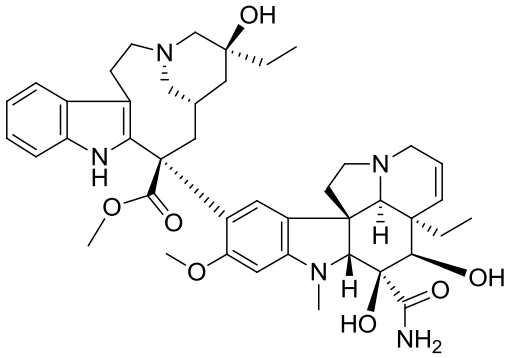

Vindesine **1.13**

Figure 1.4 Chemical structures of vinblastine **1.10**, vincristine **1.11** and its derivatives.

1.2.3. Terpenes

Terpenes and terpenoids are the largest class of natural products [*88*]. The difference between them is that terpenes are hydrocarbons, while terpenoids contain additional functional groups. These compounds come mainly from plants,

in which they play important biological functions. Structurally, these molecules consist of isoprene units (C_5H_8), which can be conjugated in different ways, resulting in a huge diversity of different structures. These compounds constitute the most functionalised and structurally diversified group of secondary plant metabolites, and are also essential components of the human diet [*88*]. Triterpenoids are widely used in traditional medicine and are an important source of hits in drug discovery [*89*]. As detailed in Table 1.3, the main classification of these structures is based on the number of isoprene units [*90*].

Table 1.3 Classification of terpenoids based on the number of isoprene units.

Number of isoprene units	Number of carbons	Classification
1	C5	Hemiterpenoids
2	C10	Monoterpenoids
3	C15	Sesquiterpenoids
4	C20	Diterpenoids
6	C30	Triterpenoids
8	C40	Tetraterpenoids
Other structures		Polyterpenoids

1.2.3.1. Pentacyclic triterpenoids

According to the aforementioned classification (Table 1.3), triterpenoids contain six isoprene units and their basic molecular formula is $C_{30}H_{48}$. These compounds are ubiquitously distributed in nature and include different groups, such as squalene, lanostane, dammarane, friedelane, lupane, oleanane and ursane, among others [*91*]. Triterpenoids show a great biological activity, and their application as bioactive components has grown exponentially. This is reflected in the increasing number of recent publications that associate triterpenoids with treatments for a wide variety of pathologies [*92–94*].

The pentacyclic triterpenoids (PTs) are triterpenoids in which the carbon structure is organised in five rings. PTs are widely distributed in many medicinal plants and are often found in their bark, stem and leaves. They are generally described as ideal drug candidates with a great versatility [*95–97*]. The biological activities attributed to PTs are very broad and include antitumour, antiviral,

antidiabetic, anti-inflammatory, antimicrobial, antiparasitic, analgesic, and cardio-, hepato-, gastro-, and neuro-protective activities [*93*, *95*, *98*]. Additionally, PTs are important components of the natural extracts used in traditional Chinese medicine, in which they have demonstrated their efficacy in tandem with low toxicity and few side effects [*99*].

1.2.3.2. Biosynthesis of pentacyclic triterpenoids

Although the structures of the PTs varies, they all share common patterns of biosynthesis in several species of higher plants (Figure 1.5). PTs are derived from squalene **1.14**, which is oxidised biosynthetically into 2,3-oxidosqualene **1.15** by the squalene epoxidase enzyme [*100*]. Oxidosqualene cyclase catalyses 2,3-oxidosqualene **1.15** to produce the intermediate dammarenyl cation **1.16** [*101*]. Subsequently, the increasing diversification of the dammarenyl cation **1.16** produces the lupenyl cation **1.17,** and the 1,2-methyl rearrangement of the lupenyl cation **1.17** leads to the oleanyl cation **1.18** [*90*]. The other enzymes involved in this process are lupeol synthase and the α/β-amyrin synthases, which convert lupenyl **1.17** and oleanyl **1.18** cations to lupeol **1.19** and α/β-amyrin **1.20/1.21**, respectively [*102*]. These triterpenoid alcohols are further modified by other enzymes (e.g., cytochrome P450s, dehydrogenases and reductases) to produce PTs with great therapeutic interest, such as betulinic **1.22**, ursolic **1.23** and oleanolic **1.24** acids [*100*]. Another PT group with significant biological importance is the quinonemethide (QM) triterpenoids (QT), also known as celastroloids. QTs are derived from the precursor oleanyl cation **1.18**, which is converted to friedelin **1.25** [*103*]. Then via sequential oxidation reactions, most likely by cytochrome P450 enzymes, friedelin **1.25** is converted to different intermediates, for example celastrol **1.26** (Figure 1.5) [*104*].

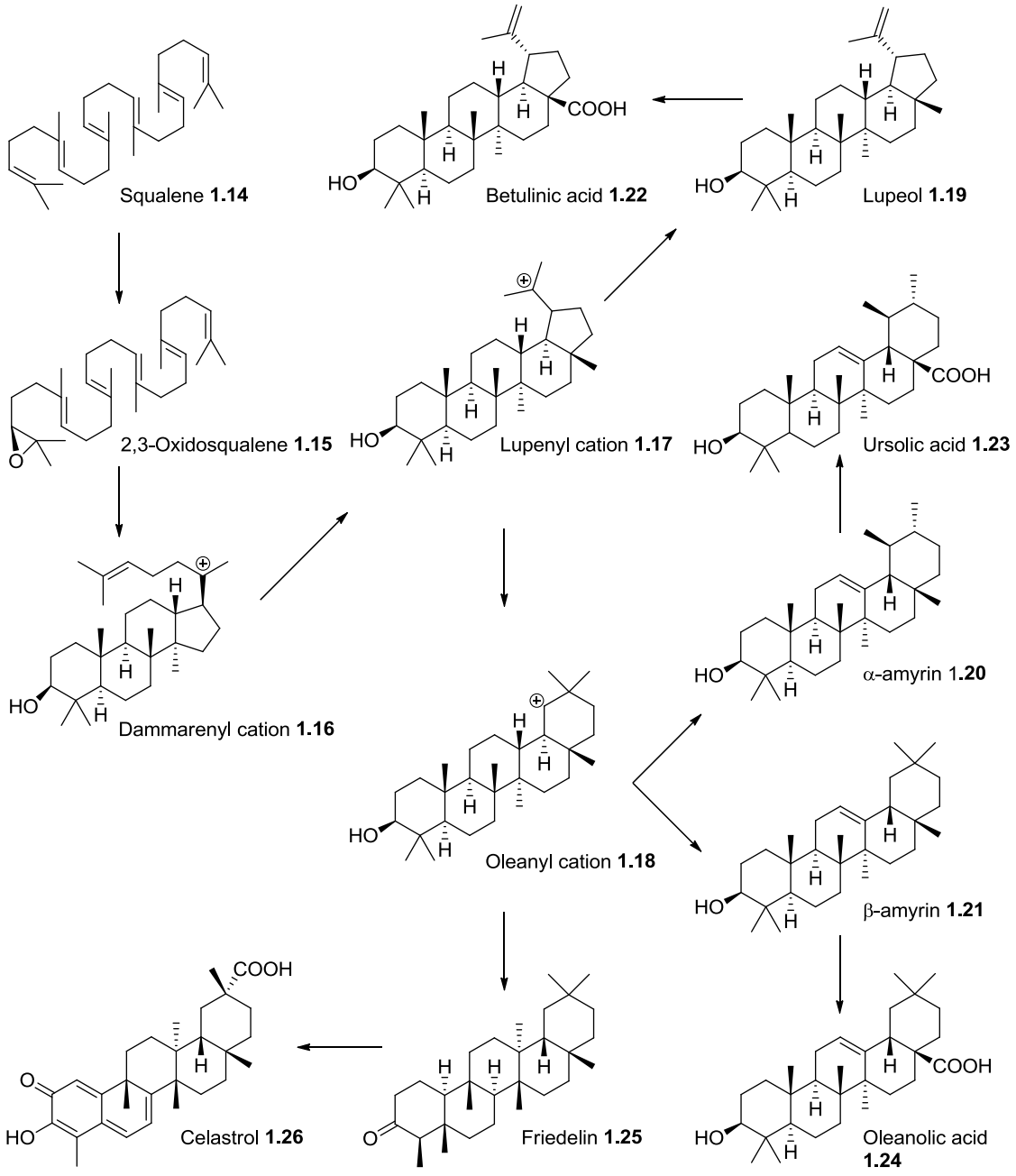

Figure 1.5 Schematic overview of triterpenoid biosynthesis.

1.2.3.3. Natural quinonemethide triterpenoids

QTs belong to a specific PT group called friedelanes, which are characterised by the presence of eight methyl groups at C(4), C(5), C(9), C(13), C(14), C(17) and C(20) (geminal-dimethyl) (Figure 1.6). Friedelane-type triterpenoids are considered as oleanane-type triterpenoids with migrated methyl groups, and for this reason they are also termed D:A-friedo-oleananes [*105*].

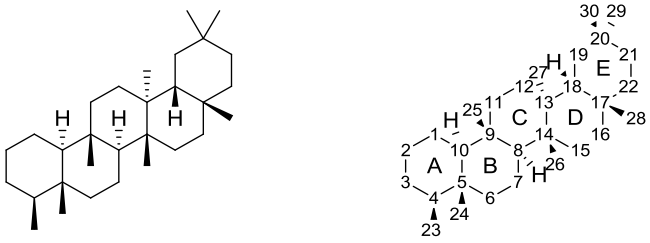

Figure 1.6 Basic skeleton and numbering of the friedelane-type triterpenoids.

Accordingly, QTs, as a subgroup of friedelanes, are also referred as 24-*nor*-friedelanes or D:A-friedo-*nor*-oleananes [*106*]. Structurally, the common feature of QTs is the presence of a *para*-quinonemethide (*p*-QM) group in their skeleton with a specific oxygenation pattern and variable type of unsaturation. The QM group of QTs renders the molecules polarised, and, thus extremely reactive. A Michael acceptor is incorporated when the C(6) position is free, making it highly prone to nucleophilic addition [*107*, *108*]. Therefore, these compounds have the ability to form covalent Michael adducts by reacting with the nucleophilic thiol groups of the cysteine residues of biomolecules, such as DNA and proteins [*109–111*]. This seems to be consistent with the wide range of observed biological activities of QTs [*112–116*].

Celastrol **1.26** is reportedly the first QT to be isolated from the root of *Tripterygium wilfordii* (in 1936) [*117*]. Since then, celastrol **1.26** and several other QTs — around 90 different structures — have been isolated from plants of the *Celastraceae* and *Hippocrateaceae* families, and are considered as chemotaxonomic indicators for those specific families [*106*].

Typically, these QTs have a highly conserved core structure that includes a hydroxyl group at C(3) *ortho* to a ketone group, and an extended conjugated system that involves A/B-rings. The chromophore that extends over the A/B-rings is responsible for the red-orange colour characteristic of many of these compounds [*118*, *119*]. Moreover, this conjugated system can hold an extra carbonyl group in the B-ring, and the extension of the conjugations can also involve C/D-rings [*105*]. As a result, QTs can be classified into three different subgroups (Figure 1.7, Table 1.4): QTs with an extended conjugation with a C=C

bond in the B-ring (**1.26–1.36**); QTs with an extended conjugation with a C=O group in the B-ring (**1.37–1.40**); and QTs with non-extended conjugation (**1.41–1.44**) [*106*].

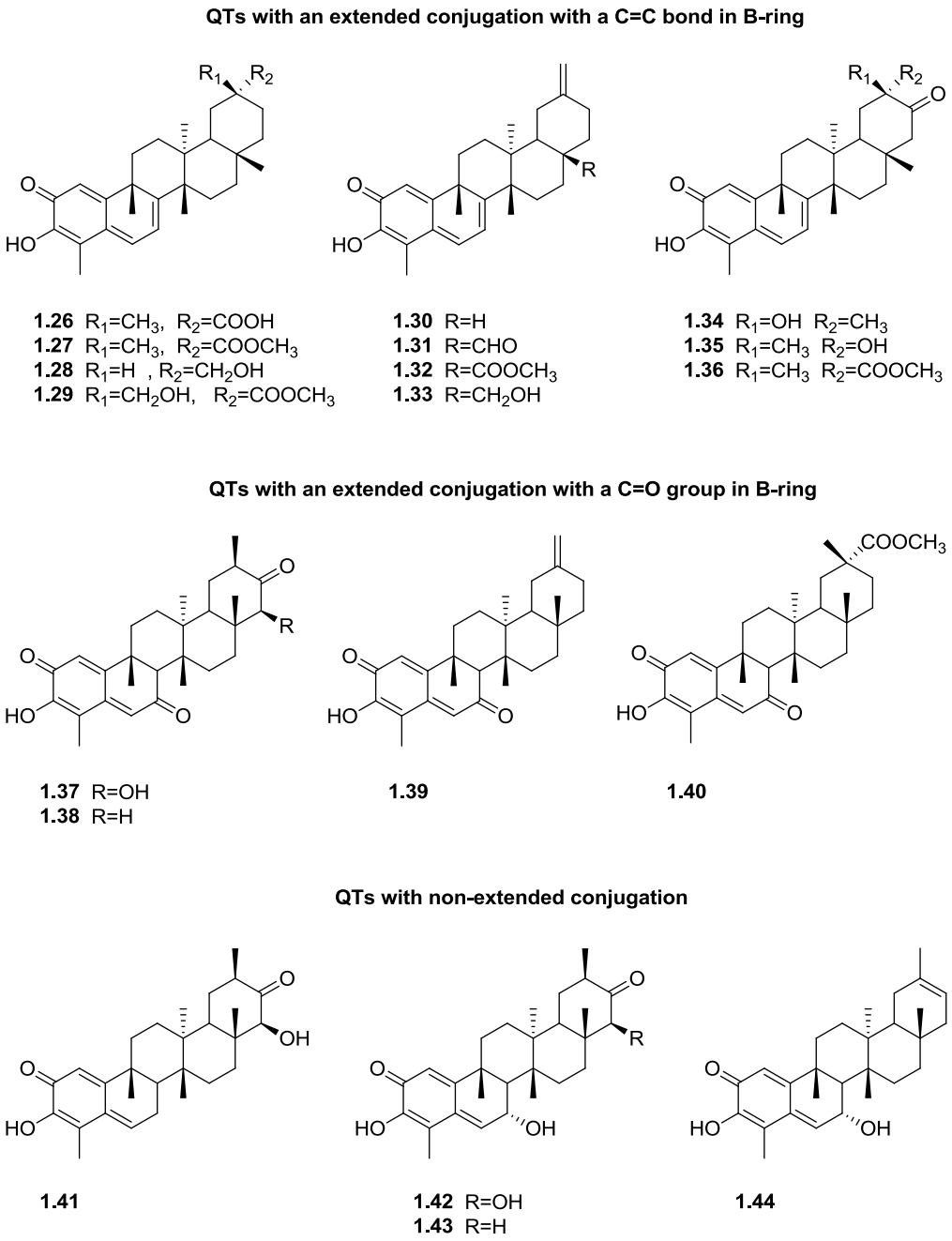

Figure 1.7 QTs found in nature and their classification.

Table 1.4 QTs found in nature and their classification.

Classification (B-ring)	Comp.	Common name	Natural source	Ref.
Extended conjugation with a C=C bond	**1.26**	Celastrol	*Tripterygium wilfordii*	[*117*]
	1.27	Pristimerin	*Pristimera indica*	[*118*]
	1.28	Isoiguesterinol	*Salacia reticulata var. b-diandra*	[*120*]
	1.29	30-Hydroxy pristimerin	*Salacia reticulata var. b-diandra*	[*120*]
	1.30	Isoiguesterin	*Salacia madagascariensis*	[*121*]
	1.31–1.33	—	*Salacia kraussii*	[*114*]
	1.34	20β-Hydroxy-20-epitingenone	*Euonymus tingens*	[*122*]
	1.35	—	*Glyptopetalum sclerocarpum*	[*123*]
	1.36	21-Oxopristimerine	*Maytenus retusa*	[*124*]
Extended conjugation with a C=O group	**1.37**	7,8-Dihydro-22β-hydroxy-7-oxotingenone	*Maytenus amazonica*	[*125*]
	1.38	Amazoquinone	*Maytenus amazonica*	[*125*]
	1.39	Salaciquinone	*Salacia reticulata*	[*126*]
	1.40	Dispermoquinone	*Maytenus dispermus*	[*127*]
Non-extended conjugation	**1.41**	7-Hydroxy-7,8-dihydro-tingenone	*Maytenus amazonica*	[*125*]
	1.42	Macrocarpin D	*Maytenus macrocarpa*	[*128*]
	1.43	7,8-Dihydro-7-hydroxytingenone	*Maytenus amazonica*	[*125*]
	1.44	—	*Maytenus blepharodes*	[*129*]

In addition to these natural compounds, other natural derivatives of QTs bearing a diphenol system in the A-ring have been described (Figure 1.8, Table 1.5). Wilforol A **1.45** is one of those phenolic triterpenoids. It was isolated from *Tripterygium regelii*, and is classified as a 6-oxo-diphenol derivative of celastrol [*115*, *130*].

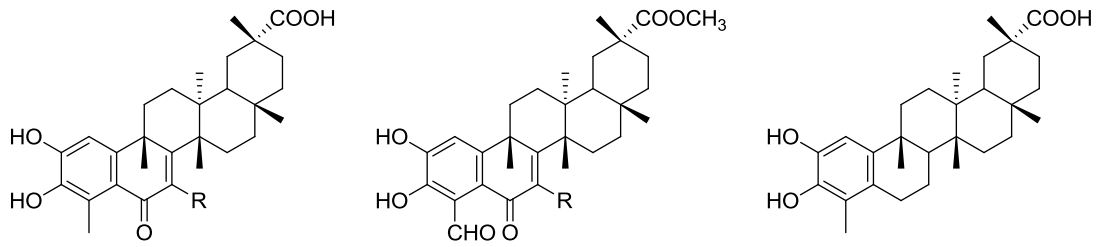

1.45 R=H
1.46 R=OH

1.47

1.48

Figure 1.8 Natural phenolic triterpenoids.

Table 1.5 Natural phenolic triterpenoids.

Classification	Comp.	Common name	Natural source	Ref.
Phenolic triterpenoids	**1.45**	Wilforol A	*Tripterygium regelii*	[*130*]
	1.46	Regeol C	*Tripterygium regelii*	[*131*]
	1.47	Demethylzeylasteral	*Tripterygium regelii*	[*130*]
	1.48	Wilforic acid A	*Salacia chinensis*	[*132*]

1.2.4. Anticancer activity of pentacyclic triterpenoids

As mentioned previously, PTs have been associated with a wide range of pharmacological activities coupled with a low toxicity profile [*133*]. Among these activities, their anticancer effects have attracted great attention. In fact, an increasing number of PTs have been shown to exhibit cytotoxic activity against a variety of tumour cells, without manifesting important toxicity in non-tumour cells [*97*, *134–137*]. Evidence from *in vivo* experiments also supports this antitumour effect [*133*, *138*]. Such properties, in particular their selectivity, indicate them as useful alternatives in cancer prevention and treatment. Hence, it is essential to evaluate the cytotoxic properties and understand the underlying molecular mechanisms of these compounds. Table 1.6 lists several signal transduction pathways that are associated with the anticancer activity of various naturally occurring PTs, including betulinic **1.22**, ursolic **1.23** and oleanolic **1.24** acids, as well as celastrol **1.26.** The main mechanisms via which those PTs act in cancer cells are: cell-cycle arrest, induction of apoptosis and inhibition of angiogenesis and metastasis [*138–140*].

Despite the enormous potential of PTs, many of these molecules are relatively less potent if administrated orally or present other pharmacokinetics limitations [*134*, *141*, *142*]. To overcome these problems and to increase their efficacy, many semisynthetic analogues have been prepared. These often exhibit a significant improvement in bioavailability and therapeutic efficacy over their natural precursors [*135*, *138*, *143*].

Table 1.6 Anticancer activity of some PTs: examples of mechanisms of action and molecular pathways.

Anticancer mechanism	PTs	Signal transduction pathways	Ref.
Cell-cycle arrest	Betulinic acid **1.22**	p53/p21 pathway	[*144*]
	Oleanolic acid **1.24**	miR-122/Cyclin G1/MEF2D pathway	[*145*]
	Celastrol **1.26**	miR-21-mTOR pathway	[*146*]
Induction of apoptosis	Betulinic acid **1.22**	Bax/Bcl-2 pathway	[*144*]
	Ursolic acid **1.23**	pERK1/2 pathway and mitochondrial membrane depolarization	[*147*]
	Celastrol **1.26**	microRNA‑21 and PI3K/Akt/NF-κB pathway	[*148*]
Inhibition of angiogenesis	Ursolic acid **1.23**	VEGF pathway	[*149*]
	Oleanolic acid **1.24**	STAT3 and SHH pathways	[*150*]
	Celastrol **1.26**	IKK/NF-κB pathway	[*151*]
Inhibition of metastasis	Ursolic acid **1.23**	Focal adhesion pathway (e.g., ICAM1, VCAM1, E-selectin, P-selectin)	[*152*]
	Oleanolic acid **1.24**	MAPK/ERK pathway	
	Celastrol **1.26**	PI3K/Akt/NF-κB pathway	[*153*]

1.3. CELASTROL

1.3.1. Physico-chemical properties of celastrol

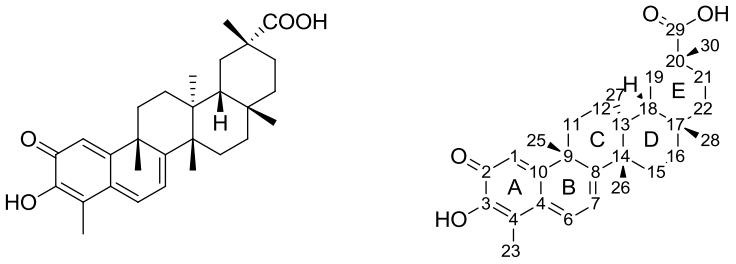

Figure 1.9 Chemical structure and numbering of celastrol **1.26**.

The IUPAC name of celastrol **1.26** is (2R,4aS,6aR,6aS,14aS,14bR)-10-hydroxy-2,4a,6a,6a,9,14a-hexamethyl-11-oxo-1,3,4,5,6,13,14,14b-octahydropicene-2-carboxylic acid, and it is also commonly known as tripterin. Its molecular formula is $C_{29}H_{38}O_4$ and its molecular weight is 450.62 g/mol. At room temperature, celastrol **1.26** is a bright orange solid and its melting point is around 204 °C [*154*]. Celastrol **1.26** shows a maximum ultraviolet (UV)/visible absorption at 253 and 424 nm [*155*]. Celastrol **1.26** is soluble in organic solvents, e.g., ethanol, dimethyl sulfoxide (DMSO) and dimethylformamide (DMF) (solubility of

approximately 10 mg/mL in ethanol and DMSO and 20 mg/mL in DMF), and is sparingly soluble in water.

As mentioned above, celastrol **1.26** has the core structure of the QTs: a hydroxyl group at C(3) *ortho* to a ketone group and extended conjugated system that involves A/B-rings. Additionally, it possesses an acidic group at C(29) (Figure 1.9). These structural characteristics, together with steric effects and its conformation, should influence its reactivity and stability. Celastrol **1.26** is an electrophilic compound and incorporates three potentially electrophilic positions at its QM substructure: C(2), C(4) and C(6). However, the C(4) position seems to be too hindered to be susceptible to nucleophilic addition, and attack at the C(6) position is expected to be favoured over the C(2) position because of the increased thermodynamic stability achieved by aromatization of the A-ring [*119*]. Therefore, the pharmacological effects of celastrol **1.26** seem to rely on its QM moiety, which binds to several functional proteins and disrupts their functions. Apparently, this is one of the mechanisms via which celastrol **1.26** affects the biological functions of proteins.

1.3.2. General pharmacological properties of celastrol

In recent years, the pharmacological activities of celastrol **1.26** have been extensively investigated in diverse clinical areas. Considering its prominent anti-inflammatory activities, celastrol **1.26** has been regarded as a potential therapeutic candidate for rheumatoid arthritis [*156*, *157*], asthma [*158*, *159*], systemic lupus erythematosus [*160*], ulcerative colitis [*161*], multiple sclerosis [*162*], psoriasis [*163*], osteoarthritis [*164*] and hypertension [*165*].

The potent antioxidant and anti-inflammatory effects of celastrol **1.26** in neurodegenerative diseases (e.g., Alzheimer's [*166*, *167*], Huntington's [*168*, *169*] and Parkinson's [*170*] diseases) have also attracted great attention. Accumulating evidence has identified several major cell signalling pathways and molecular targets of celastrol **1.26** that are strategic checkpoints for its anti-inflammatory and neuroprotective properties, such as the NF-κB, PI3K/Akt/mTOR, mitogen-activated

protein kinase (MAPK), JAK/STAT pathways, Hsp response, as well as pathways that regulate ROS homeostasis [*157*, *171*] (Figure 1.10).

Moreover, celastrol **1.26** may be useful in the treatment of other diseases, namely diabetes [*172*], obesity [*173*, *174*], cardiovascular disease [*175*] and malaria [*176*] and dengue [*177*] infections.

Furthermore, a recent report of a clinical trial that combined the use of celastrol **1.26** with nifedipine assessed the outcome of this treatment against preeclampsia. The results showed the potential of celastrol **1.26** as an effective and safe adjuvant to oral nifedipine to treat hypertension in patients with preeclampsia [*178*].

1.3.3. Anticancer activities of celastrol

Among all the pharmacological activities of celastrol **1.26**, its remarkable anticancer activities are the most reported, especially in recent years. Celastrol **1.26**, presents a high cytotoxicity against a wide variety of human cancer cell lines, including bladder [*179*], breast [*180–186*], cervical [*180*, *187*], colorectal [*188–190*], gastric [*146*, *186*, *191*], head and neck [*186*], liver [*186*, *192–195*], lung [*186*, *194*, *196–199*], ovarian [*148*, *154*, *189*], pancreatic [*188*, *200*], prostate [*186*, *197*, *201*, *202*], renal [*186*, *188*, *203*] and thyroid [*204*] cancers, as well as gliomas [*186*], leukaemia [*205–207*], melanoma [*186*, *208*], multiple myeloma [*186*, *209–211*] and sarcoma [*212*, *213*]. The effectiveness of celastrol **1.26** in inhibiting the growth of cancer cells was assessed in the majority of these studies based on IC_{50} value, which is the concentration of a compound that is required for 50% inhibition *in vitro*. The IC_{50} values determined — around or below 1 μM — denote the potential of this compound as an anticancer agent (Table 1.7). Additionally, several *in vivo* studies of celastrol **1.26** have demonstrated its therapeutic efficacy in several animal models [*183*, *189*, *206*, *208*, *213–219*].

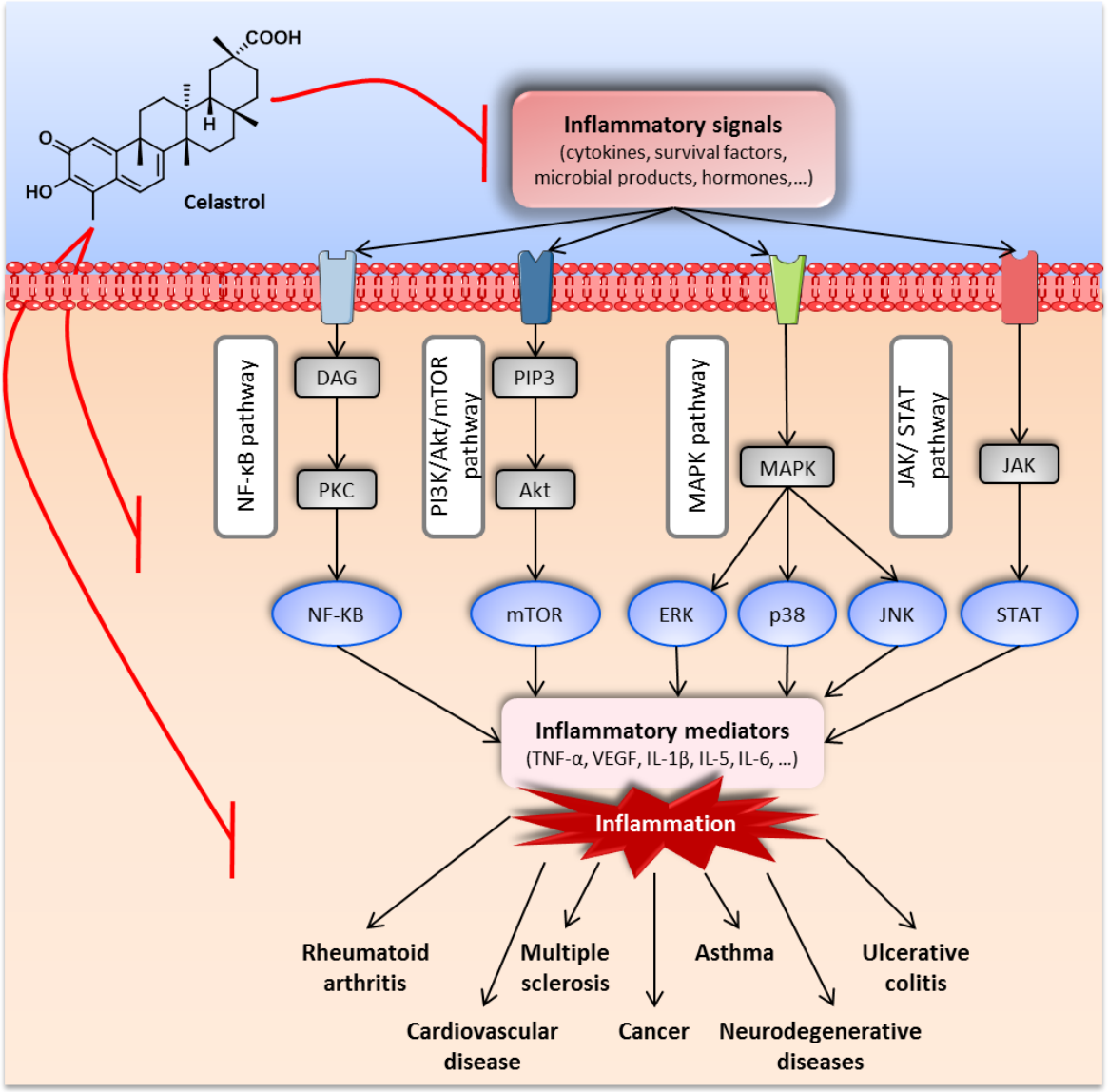

Figure 1.10 Anti-inflammatory activities and cell signalling pathways modulated by celastrol **1.26** for the control of various diseases (adapted from [*220*]).

1.3.3.1. Molecular targets and cell signalling pathways of celastrol

These marked anticancer properties of celastrol **1.26** have been attributed to the modulation of multiple molecular targets and cell signalling pathways involved in tumorigenesis (Figure 1.11), which is briefly discussed below.

Table 1.7 Inhibitory effects of celastrol **1.26** on the proliferation of several human cancer cell lines.

Histological cancer classification	Organ/Tissue	Cell line	IC_{50} values (μM)	Time (h)	Assay	Ref.
Carcinoma	Breast	MCF-7	1.58	72	MTT	[*186*]
	Breast	MDA-MB-231	0.67	72	MTT	[*186*]
	Head and neck	UM-SCC1	0.76	72	MTT	[*186*]
	Liver	Bel-7402	1.12	48	MTT	[*192*]
	Lung	H1650	0.79	72	MTT	[*196*]
	Lung	H1975	0.60	72	MTT	[*196*]
	Prostate	PC3	2.00	24	FCM	[*202*]
	Prostate	DU145	2.35	24	MTT	[*201*]
	Thyroid	8505C	0.94	48	CCK-8	[*204*]
	Thyroid	SW1736	1.08	48	CCK-8	[*204*]
	Stomach	KATOIII	0.54	72	MTT	[*186*]
Sarcoma	Breast	W256	0.43	48	Alamar Blue	[*212*]
	Bone	U-2OS	2.50	48	MTT	[*213*]
Myeloma	Peripheral blood	RPMI 8226	0.52	72	MTT	[*186*]
	Peripheral blood	LP-1	0.88	72	WST-8	[*209*]
	Peripheral blood	U266	0.47	24	MTS	[*210*]
Leukaemia	Peripheral blood	HL-60	0.48	24	CCK-8	[*205*]
	Bone-marrow	K562	0.41	72	MTS	[*206*]

Induction of cell-cycle arrest and cell death

The antitumour effects of celastrol **1.26** can be achieved by the inhibition of cell proliferation and induction of cell death via several mechanisms (Figure 1.12). For example, an increase in the levels of the p27 protein via the inhibition of the miR-21-mTOR signalling pathway was observed, which caused a G2/M cell-cycle arrest in gastric cancer cells treated with celastrol **1.26** [*146*]. A previous study had shown the role of the miR-21 and PI3K/Akt/NF-κB pathways in the induction of apoptosis and inhibition of the growth of gastric cancer cells treated with celastrol **1.26** [*191*]. Jian *et al.* also demonstrated that celastrol **1.26** induced a G1 cell-cycle arrest and apoptosis via p27 upregulation and NF-κB modulation in LP-1 myeloma cells [*209*]. In addition, the effects of celastrol **1.26** of growth inhibition with G0/G1

cell-cycle arrest and apoptosis induction in DU145 prostate cancer cells was attributed to the regulation of the expression of the hERG potassium channel protein [*201*]. Conversely, the effect of celastrol **1.26** of inhibiting cell proliferation through G1 cell-cycle arrest and apoptosis induction in human bladder cancer 5637 cells was attributed to the blockage of the JAK2/STAT3 signalling pathway [*179*].

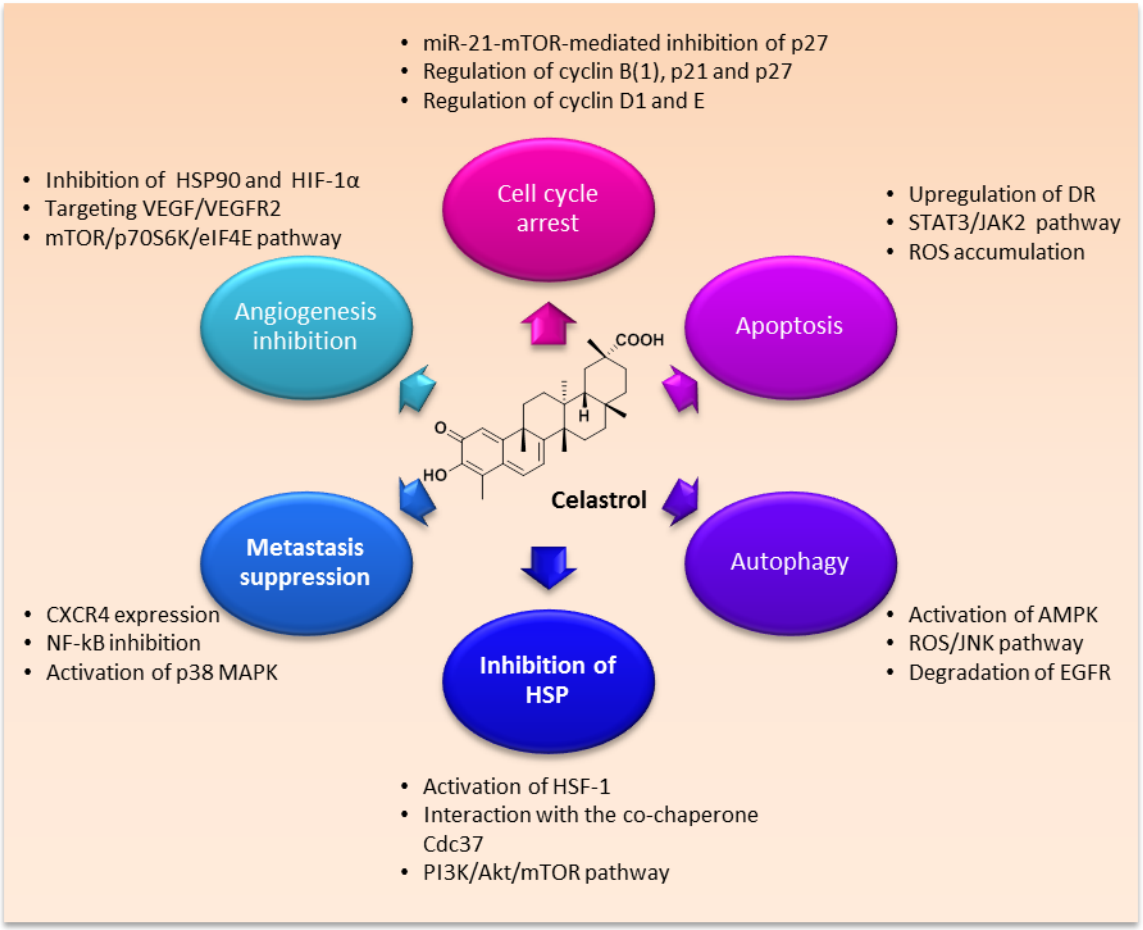

Figure 1.11 Overview of the anticancer mechanism of action of celastrol **1.26**.

Moreover, in numerous studies these effects were accompanied by changes in the expression of several proteins, which is consistent with the multitarget anticancer response induced by celastrol **1.26**, for instance: (1) activation of caspase expression [*209*, *221*, *222*]; (2) downregulation of antiapoptotic proteins (e.g., cIAP1 and cIAP2, FLIP, Bcl-2 and survivin) [*179*, *209*, *223*]; (3) upregulation of proapototic proteins (e.g., Bax and Bak) [*179*, *209*, *224*]; and (4) regulation of the expression of cyclins and cyclin-dependent kinases

(CDKs) [*185*, *186*, *225*]. Table 1.8 lists other mechanisms via which celastrol **1.26** kills cancer cells by apoptosis in different types of cancer.

Table 1.8 Apoptotic pathways via which celastrol **1.26** kills cancer cells.

Cancer type	Molecular pathways	Ref.
Chondrosarcoma	Suppression of CIP2A/c-Myc signalling pathway	[*226*]
Liver cancer and osteosarcoma	Inhibition of MRC complex I, with subsequent ROS accumulation inside cancer cells	[*194*, *227*, *228*]
Breast and colon cancer	Upregulation of DR, enhancing TRAIL-induced apoptosis	[*189*, *229*]
Non-small cell lung cancer	Activation of Fas/FasL pathway	[*230*]
Breast cancer	Destabilization of the ErbB2 and estrogen receptors	[*185*, *224*]
Leukaemia	Inhibition of topoisomerase II	[*231*]
Acute myeloid leukaemia	Downregulation of AML1-ETO fusion protein, with subsequent downregulation of C-KIT kinases and inhibition of Akt, STAT3 and Erk1/2	[*232*]
Hepatocellular carcinoma	Inhibition of STAT3/JAK2 signalling cascade	[*233*]
Acute myeloid leukaemia	Inhibition of the Myb/p300 interaction	[*234*]
Oral squamous cell carcinoma	Induction of the UPR-dependent cell death, ER stress, and PERK/eIF2α/ATF4/CHOP signalling	[*235*]
Prostate cancer	Modulation of AR, ERG, and NF-κB signalling pathways	[*201*, *236*]

In addition to cell-cycle arrest and apoptosis, celastrol **1.26** also induces autophagy, which is a caspase-independent cell-death pathway, in several types of cancer cells (Figure 1.12). Celastrol **1.26** induced cell-cycle arrest, apoptosis and autophagy in gastric cancer cells, and the activation of the AMP-activated protein kinase (AMPK) seemed to play an important role in this process [*237*]; in human osteosarcoma cells, these effects were attributed to the modulation of the ROS/JNK signalling pathway [*213*]. Gefitinib-resistant lung cancer cells treated with celastrol **1.26** exhibited induction of EGFR degradation via induction of autophagy in an intracellular calcium-dependent manner [*238*]. This induction of autophagy in response to celastrol **1.26** treatment was also described in prostate cancer cells, via the downregulation of the miR-17-92a cluster [*239*].

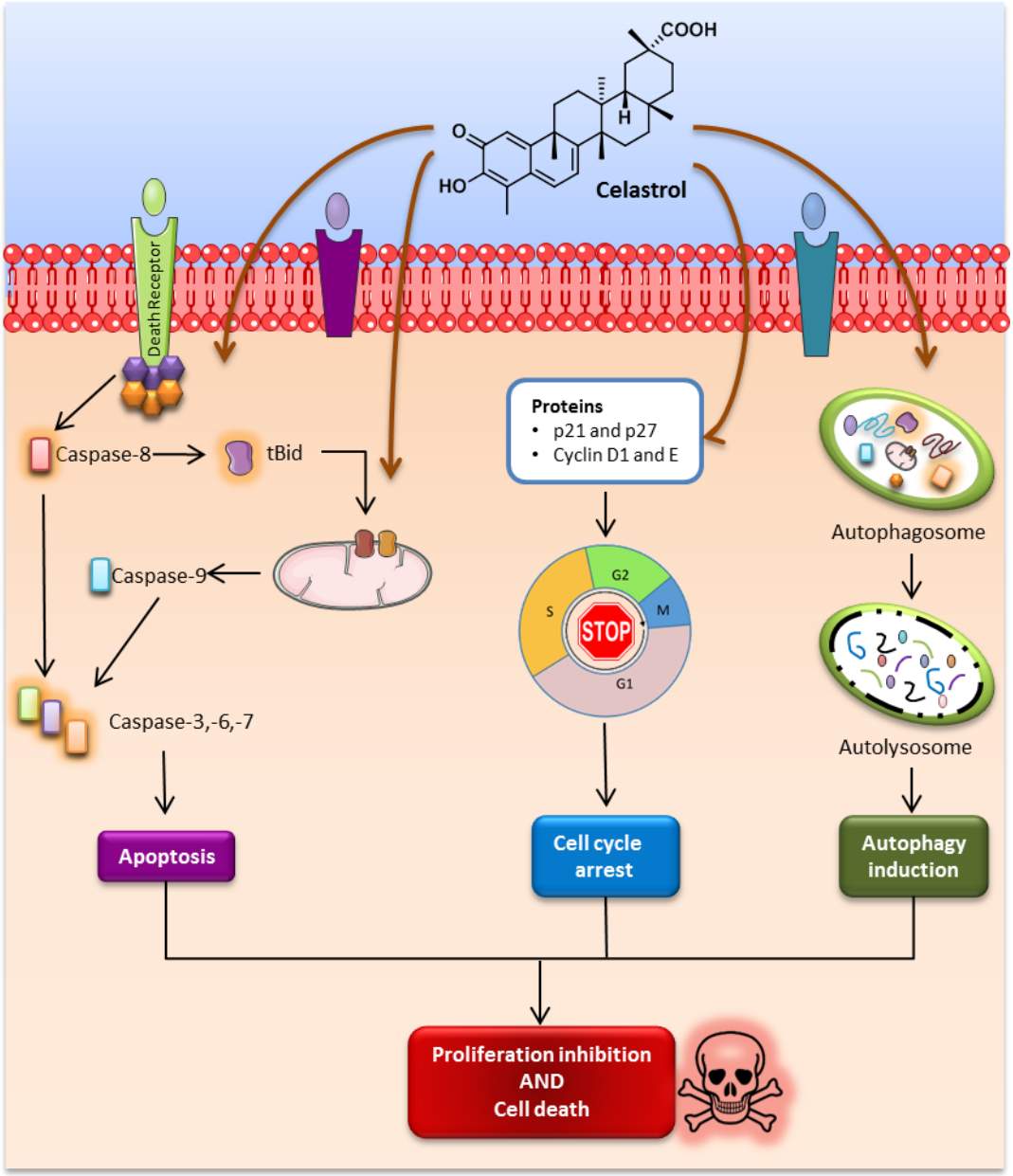

Figure 1.12 Antitumour effects of celastrol **1.26** via the inhibition of cell proliferation and induction of cell death.

Inhibition of molecular chaperones

As mentioned previously, Hsps are molecular chaperones that are essential for cell viability in eukaryotes. They assist the correct folding and assembly of other proteins, stabilize defective proteins, and protect them against denaturation. Hsp90, which is a ubiquitously expressed protein that is highly active in the cytoplasm, is involved in signal transduction and apoptosis, making it a notably

interesting therapeutic target for cancer. Hsp90 and its client proteins interact in a multiprotein complex in association with co-chaperone proteins that are dependent on ATP binding to its intrinsic ATPase domain. The Inhibition of the intrinsic ATPase activity of Hsp90 locks the complex in an open, non-functional state that generally results in the degradation of client proteins via the ubiquitin-proteasome pathway (Figure 1.13) [*59*].

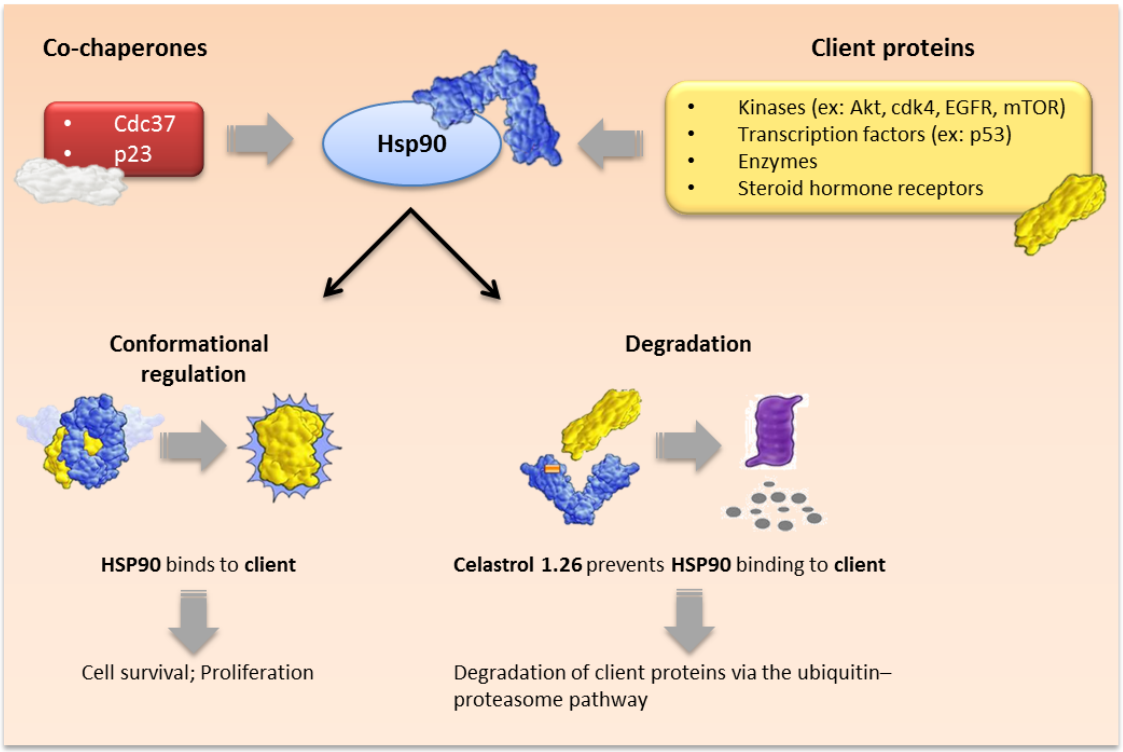

Figure 1.13 Antitumour effect of celastrol **1.26** via the inhibition of Hsp90.

Celastrol **1.26** has been identified as a novel class of Hsp90 inhibitor with unique antitumour properties. It was initially suggested that celastrol **1.26** was an Hsp90 inhibitor, because it was able to induce the heat shock response by activating HSF-1 [*240*]. Subsequently, a gene expression-based strategy was used to demonstrate that celastrol **1.26** inhibited Hsp90 activity by binding to a pocket other than the known ATP-binding site. Hieronymus *et al*. also demonstrated that celastrol **1.26** inhibited Hsp90 client proteins and attenuated the interaction of Hsp90 with the co-chaperone p23 [*241*]. Later, it was demonstrated by molecular docking studies that celastrol **1.26** disrupted the interaction of Hsp90 with another co-chaperone, Cdc37 [*200*]. NMR studies attributed the ability of

celastrol **1.26** to disrupt the Hsp90-Ccd37 interaction to its ability to modify cysteine free thiols and form Michael adducts with Cdc37 [*119*, *242*]. Although other studies confirmed that celastrol **1.26** targets the Hsp90/Cdc37 complex [*243–245*], the exact chemical basis for the interaction of celastrol with Hsp90 is not completely understood.

Effect on the PI3K/Akt/mTOR signalling cascade

The Akt protein is one of the most important proteins that are regulated by Hsp90 [*246*], and Hsp90 has been proven to be responsible for the stabilization of its active form, phospho-Akt (pAkt) [*60*]. As discussed above, the disruption of the PI3K/Akt/mTOR pathway plays an important role in the oncogenic process, as it is one of the most important intracellular signalling pathways in cancer cells [*247*]. Activated PI3K recruits phosphoinositide-dependent protein kinase 1 (PDK1) and Akt at the plasma membrane, leading to Akt activation. This triggers the activation of the downstream effector mTOR, which is another conserved serine/threonine kinase [*246*, *248*]. The potent growth-inhibitory and apoptosis-inducing effects of celastrol **1.26** in cancer cells have been attributed to the following processes: inhibition of Akt/mTOR/p70S6 kinase signalling [*186*, *217*]; downregulation of Akt leading to suppression of the phosphorylation of glycogen synthase kinase 3 (GSK3), which is a substrate of Akt [*186*]; reduction of phosphorylated Akt, mTOR and S6 kinase (S6K) and increase in AMPK phosphorylation in gastric cancer cell lines and xenografts [*249*]; and mitochondrial dysfunction and PI3K/Akt/mTOR pathway inhibition in triple-negative breast cancer [*180*] and melanoma cells [*250*], as well as several other types of cancer [*186*].

Suppression of invasion and metastasis

Metastases are normally related to a poor prognosis and rapid progression of cancers. Celastrol **1.26** has the potential to inhibit metastases through the modulation of multiple pro-inflammatory cytokines, chemokines, enzymes and transcription factors. Recent results demonstrated that celastrol **1.26** suppressed metastasis-related processes, such as proliferation, invasion and migration of

prostate cancer cells, as well as tumorigenicity and progression in bone tissue in mice [*251*]. The downregulation of C-X-C chemokine receptor type 4 (CXCR4), which is a target that is closely linked with tumour metastasis, was further described in colon and pancreatic cancer cells [*188*]. In melanoma cancer cells, the role of integrin inhibition in this process was also discussed: the inhibition of migration and invasion by celastrol **1.26** was attributed to the regulation of integrin function and cell adhesion, partly via p38 MAPK activation [*208*].

Matrix metalloproteinases (MMPs) are a family of highly homologous protein-degrading zinc-dependent endopeptidases. Among them, MMP-2 and -9 have been closely correlated with tumour invasion and metastasis [*252*]. Several studies revealed that the *NF-κB* gene is an upstream regulator of MMPs and is closely associated with tumour invasion and migration [*253*]. In lung adenocarcinoma cells, it has been shown that celastrol **1.26** inhibits TNF-induced invasive activity, which was correlated with the inhibition of NF-κB-mediated MMP-9 expression [*254*]. Similar results were described for breast cancer cells [*184*, *223*]. Furthermore, it has been shown that, in addition to NF-κB inhibition, celastrol **1.26** also inhibits invasion of hepatocellular carcinoma cells through the reduction of miR-224 expression, by decreasing MMP-2 and -9 protein levels [*255*]. More recently, it was demonstrated that celastrol **1.26** inhibits migration and invasion through the blocking of the NF-κB pathway by inhibiting IκBα phosphorylation and preventing IκBα degradation and p65 accumulation in ovarian cancer cells. Moreover, the expression and activity of the NF-κB target protein MMP-9, but not those of MMP-2, were inhibited by celastrol **1.26** in these cells [*256*]. In addition, the PI3K/Akt pathway is considered to be a significant regulatory factor in NF-κB activation. The activation of Akt has been revealed to be critical for the degradation of the inhibitor of NF-κB and κB (IκB) [*257*]. Notably, celastrol **1.26** negatively regulated the cell invasion and migration ability of human osteosarcoma cells via the downregulation of the PI3K/Akt/NF-κB signalling pathway *in vitro* [*153*].

Inhibition of tumour angiogenesis

Angiogenesis, the formation of new blood vessels, has a crucial function in tumour progression, in which the vascular endothelial growth factor (VEGF) and respective receptors (VEGFR-1 and -2) play an important role as angiogenic regulators [*1*]. Some studies have shown that celastrol **1.26** has antiangiogenic effects both *in vitro* and *in vivo* [*179*, *217*, *258*, *259*]. The inhibitory effect of celastrol **1.26** on angiogenesis seems to be mediated by the suppression of HIF-1α via Hsp90 [*195*] and mTOR/p70S6K/eIF4e pathway inhibition and extracellular signal-regulated kinase 1/2 (ERK1/2) phosphorylation [*217*, *219*]. This inhibition of HIF-1α led to the decrease of its target genes, such as *VEGF*. In another study, celastrol **1.26** was shown to inhibit vasculogenesis by targeting the VEGF/VEGFR2 and Akt/eNOS signalling axes [*260*]. Celastrol **1.26** has also been reported to inhibit LPS-induced angiogenesis, which is involved in the regulation of the toll-like receptor 4 (TLR-4)-mediated NF-κB signalling pathway [*151*].

1.3.3.2. Synergistic anticancer activity of celastrol

Overcoming the inevitable emergence of chemo-resistance to standard anticancer therapies would be crucial to improve the efficacy of the current cancer treatment. Considering the important side effects, the recurrence and the resistance associated with currently approved drugs, a combination therapy of antineoplastic compounds is one of the most rational strategies to achieve improved results [*261*]. Important synergistic anticancer effects of celastrol **1.26** and chemotherapeutics used in clinical settings [*183*, *204*, *214*, *262*, *263*] and in pre-clinical studies [*206*, *215*, *264–266*] have been documented. Celastrol **1.26** acts in concert with other chemotherapeutic agents to exert synergistic effects against a broad range of human cell lines and *in vivo* models (Table 1.9). The observed improved pharmacological effects favour the combination of celastrol **1.26** with these anticancer agents as promising therapeutic strategies for potentially overcoming the limitations of the clinical use of each one of them seprerately. Additionally, celastrol **1.26** induced cisplatin resensitization via the

inhibition of the JNK/ATF2 pathway [*267*], and might be useful to overcome treatment resistance in different types of cancer [*196*, *206*, *238*, *266*, *268*].

Table 1.9 Synergistic anticancer effects of celastrol **1.26** and other anticancer agents.

Agent	Mechanism of action	*In vitro* cell lines	*In vivo* models	Ref.
Paclitaxel	Growth inhibition	Thyroid carcinoma	—	[*204*]
Lapatinib	Growth inhibition; apoptosis induction; downregulation of EGFR	Hepatocellular carcinoma	—	[*262*]
SAHA	NF-κB inhibition; apoptosis induction; regulation of E-cadherin	Ovarian, lung and prostate cancers	95-D cells in xenografts	[*214*]
17-AAG	Hsp90 inhibition; proteotoxic stress	Glioblastoma	—	[*264*]
17-AAG	Growth inhibition	Myelogenous leukaemia	—	[*206*]
Triptolide	Growth inhibition; cell-cycle arrest; apoptosis induction; ROS accumulation	Lung carcinoma and others cancers	H1299 and H157 cells in xenograft	[*215*]
Embelin	XIAP and NF-κB inhibition	Acute myeloid leukaemia	—	[*265*]
Trastuzumab, Lapatinib	Inhibiting of Hsp90, proteasome and NF-κB; induction of ROS	Breast cancer	BT-474 cells in xenograft	[*183*]
ABT-737	Apoptosis; upregulation of NOXA by ER stress	Hepatocellular carcinoma	—	[*266*]
Temozolomide	Regulation of MAPK and NF-κB signalling pathway	Melanoma	—	[*263*]

1.3.3.3. Limitations of celastrol

Despite the huge therapeutic potential of celastrol **1.26**, further clinical application is still limited by its reduced oral bioavailability, narrow therapeutic index and side effects. The low bioavailability of celastrol **1.26** is derived mainly from its poor water solubility. Although it has been used in a clinical trial [*178*], the oral administration of celastrol **1.26** to rats resulted in ineffective absorption into the systemic circulation, with an absolute bioavailability of 17.06% [*269*]. *In vivo* metabolism and/or tissue distribution can also be responsible for the poor bioavailability of celastrol **1.26** [*270*]**.** Although celastrol **1.26** has demonstrated efficacy in various types of cancer, adverse effects have been reported. The toxic effects of celastrol **1.26** were investigated in zebrafish embryos, a valuable model for toxicity assessment in drug toxicology. These results indicated that celastrol

1.26 affected the normal development of zebrafish embryos in micromoalar concentrations [*271*]. Kusy *et al.* investigated the effects of celastrol **1.26** on the adult murine hematopoietic system. It was demonstrated that celastrol **1.26** treatment resulted in multiple defects in mature lineages and in bone-marrow progenitors [*272*]. Another side effect of celastrol **1.26** might be male infertility. One study indicated that inhibition of Ca^{2+} currents could be responsible for the antifertility activity of this compound [*273*]. Depending on the desired therapeutic effect, the concentration range of celastrol **1.26** is also highly variable.

To overcome these physicochemical and pharmacokinetics limitations of celastrol, **1.26** and to reduce its effective dose, several drug-delivery systems of celastrol **1.26** have been prepared and tested; namely, liposomes [*274–276*], exosomes [*277*], nanoencapsulation [*278*], polymeric micelles [*159*, *279*], cell-penetrating peptides-coated nanostructured lipid carriers [*280*], and self-microemulsifying drug-delivery systems [*281*].

1.3.4. Semisynthetic derivatives of celastrol with anticancer activity

Considering the anticancer potential of celastrol **1.26**, some semisynthetic derivatives have been synthesised with the aim of studying its mechanism of action, improve its therapeutic activity and pharmacokinetics properties and decrease its toxicity. Some of these new semisynthetic analogues exhibited improved anticancer activity in several cancer cell lines and animal models compared with the parent compound, as described below.

C(29)-substituted celastrol derivatives

Modifications at the C(29) position of the celastrol **1.26** core are the most commonly reported, namely simple esterification or amidification of the C(29)-carboxyl functional group, while maintaining the QM functional structure intact [*193*, *282–285*].

Despite the various molecular targets attributed to celastrol **1.26**, its mechanism of action remains only partially understood. Therefore, Morimoto and

coworkers designed a family of celastrol analogues to understand its targets. Those authors determined that the conversion of the carboxyl functional group to amides produces bioactive compounds with improved potency (**1.49–1.58**, Figure 1.14). These compounds induced the heat shock response and antioxidant response, and inhibited Hsp90 activity. Subsequently, active biotinylated conjugates of celastrol (**1.59** and **1.60**, Figure 1.14) were synthesised and used as affinity reagents in Panc-1 cell lysates, and identified Annexin II, eEF1A, and β-tubulin as potential cellular targets of celastrol **1.26**. It was also suggested that celastrol **1.26** targets Hsp90 indirectly via a redox imbalance [*107*].

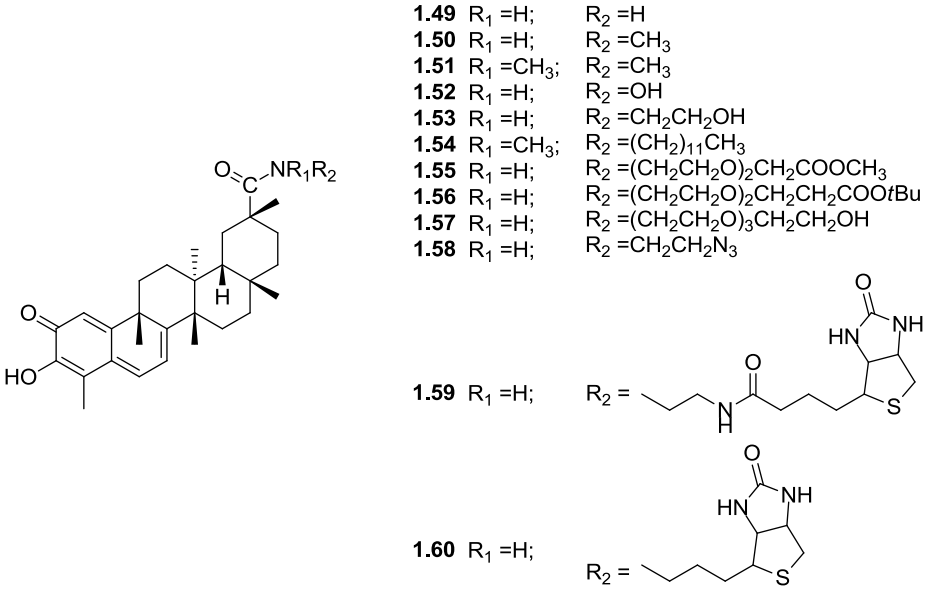

Figure 1.14 Celastrol derivatives **1.49–1.60.**

More recently, other series of celastrol analogues with modifications at the C(29)-carboxyl functional group were synthesised and tested as potential anticancer compounds (**1.61–1.65**, Table 1.10, entries 2–6) [*108*, *286*, *287*].

In this context, Wei *et al.* evaluated the anticancer effect of celastrol **1.26** and two novel derivatives (**1.61** and **1.62**) on hepatocellular carcinoma cells (HepG2, Huh7 and Hep3B) *in vitro*, and on orthotopic xenograft models *in vivo* (Table 1.10, entries 2–3). The results of this study suggest that celastrol **1.26** may be too toxic for clinical use, while celastrol derivatives **1.61** and **1.62** showed lower toxicity. These compounds demonstrated to be valid candidates as Hsp90/Cdc37

antagonists for the treatment of heterogeneous subtypes of hepatocellular carcinoma, either as monotherapy or adjuvant therapy [*286*].

Table 1.10 IC_{50} (μM) values of celastrol **1.26** and derivatives **1.61–1.65** in tumour cell lines.

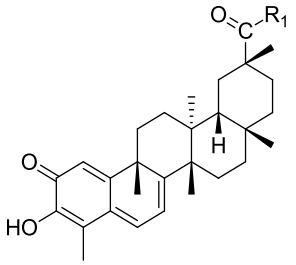

Entry	Comp.	R_1	Cell line/IC_{50} (μM)						Ref.
			HepG2	Huh7	Hep3B	Panc-1	SGC-7901	SMMC-7721	
1	**Celastrol 1.26**	—OH	1.22[a]	1.07[a]	0.30[a]	1.49[b]	0.15[b]	0.58[b]	
2	**1.61**	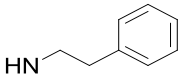	3.58	1.04	1.06	-	-	-	[*286*][a]
3	**1.62**	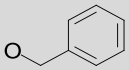	4.26	2.15	2.77	-	-	-	[*286*][a]
4	**1.63**	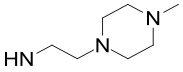	-	-	-	1.12	-	-	[*108*][b]
5	**1.64**	$NHCH_2CH_2OH$	0.61	-	-	-	0.16	0.30	[*287*][b]
6	**1.65**	$NHCH_2CHOHCH_3$	0.28	-	-	-	0.10	0.61	[*287*][b]

[a] Cells were treated with different concentrations of the indicated compounds for 72 h, and the cell viability was determined using the CellTiter-Glo®. [b] Cells were treated with different concentrations of the indicated compounds for 48 h, and the cell viability was determined by the MTT assay.

Jiang *et al.* also synthesised amide celastrol derivatives and investigated their SAR as Hsp90-Cdc37 disruptors. Among the 23 celastrol analogues synthesised, compound **1.63** (Table 1.10, entry 4), with a much more polar group bound to C(29), had improved Hsp90-Cdc37 disruption (IC_{50} = 4.71 μM) and anti-proliferative activities, as well as solubility and permeability, showing better druglikeness properties than celastrol **1.26**. Moreover, compound **1.63** induced the degradation of Hsp90 client proteins (Akt and CDK4), G0/G1 cell-cycle arrest and apoptosis in Panc-1 cells. These results support further studies of celastrol derivatives as Hsp90-Cdc37 disruptors [*108*].

Compounds **1.64** and **1.65**, which carry a β-hydroxyl-alkylamide substituent, exhibited a significant anticancer activity against all the cell lines tested (SGC-7901, SMMC-7721 and HepG2) (Table 1.10, entries 5–6). The best results were achieved for the SGC-7901 cell line and compounds **1.64** and **1.65** (IC_{50} = 0.16 μM and 0.10 μM, respectively). Preliminary studies of their mechanisms of action showed that derivative **1.64** induces apoptosis in SMMC-7721 cells. The telomerase activity assay indicated that telomerase and anti-proliferative inhibitions were directly correlated with this effect; again, compounds **1.64** and **1.65** exhibited the best inhibitory activity (IC_{50} = 0.11 and 0.34 μM, respectively). Furthermore, molecular docking studies revealed that compound **1.64** bound nicely to telomerase hTERT via both hydrogen and van der Waals interactions. These results suggest that optimised celastrol derivatives may be potent anticancer agents that act as telomerase inhibitors [*287*].

C(3)-substituted celastrol derivatives

The structure of the A-ring of celastrol **1.26** comprises a C(3)-hydroxyl group that forms a hydrogen bond with the neighbouring carbonyl group and conjugates with the QM moiety. Therefore, modification at this position may change the activity of the molecule.

In fact, the synthesis of the C(3)-substituted celastrol derivatives **1.66–1.71** (Table 1.11, entries 2–7) generally resulted in an important decrease in cytotoxic activity in rat PC-12 adrenal gland phaeochromocytoma and C-6 glioma cell lines compared with celastrol **1.26**. This suggests that the intact core structure of celastrol **1.26,** including the hydroxyl group at C(3) *ortho* to the ketone group, is crucial for its cytotoxic activity [*285*].

Table 1.11 IC_{50} *(*μM) values of celastrol **1.26** and derivatives **1.66–1.71** in rat cell lines [*285*].

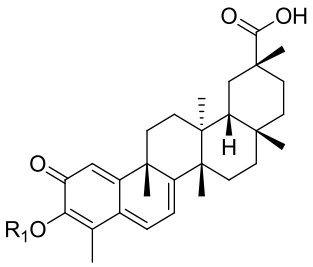

Entry	Comp.	R_1	Cell line/IC_{50} (μM)[a]	
			PC-12	C-6
1	**Celastrol 1.26**	-H	3.15	1.48
2	**1.66**	-$COCH_3$	5.31	2.66
3	**1.67**	-$COCH_2CH_3$	>50	>50
4	**1.68**	-$COCH_2CH_2CH_3$	>50	>50
5	**1.69**	-$COCH(CH_3)CH_3$	>50	>50
6	**1.70**	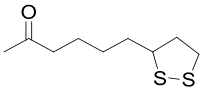	>50	>50
7	**1.71**	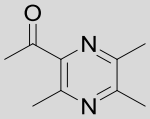	2.37	2.82

[a] Cells were treated with different concentrations of the indicated compounds for 48 h, and the cell viability was determined by the MTT assay.

More recently, Zhan *et al.* synthesised a series of celastrol derivatives, including C(3)-derivatives and evaluated their growth-inhibition activities against several tumour cell lines (**1.72–1.80**, Table 1.12, entries 2–10). Their results revealed that the properties of substituents, as well as the substitution position, had an important impact on the cytotoxic activity. The conversion of the hydroxyl group at the C(3) position into a carbamate introduced nitrogen and oxygen atoms as new hydrogen-bond acceptors, which benefited the solubility and bioavailability of the molecule. The type and size of the carbamate substituents at this position were also important factors for cytotoxic activity *in vitro*: the activity decreased in the case of larger substituents (Table 1.12, entries 2–10). Additionally, preliminary *in vivo* antitumour studies of compound **1.77** — celastrol derivative modified at positions C(3) and C(29) — showed higher inhibition rates and a better safety

profile compared with celastrol **1.26**, suggesting that it might be a promising candidate for the development of new antitumour agents [*288*].

Table 1.12 IC_{50} (μM) values of celastrol **1.26** and derivatives **1.72–1.80** in tumour cell lines [*288*].

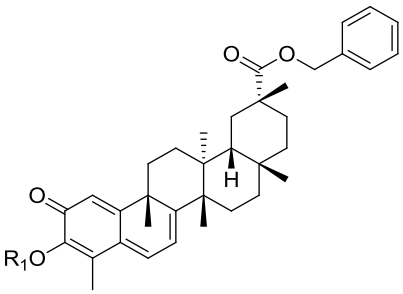

Entry	Comp.	R_1	Cell line/IC_{50} (μM)[a]				
			A549	Bel 7402	SGC 7901	HeLa	HepG2
1	**Celastrol 1.26**	—	2.12	0.44	0.87	0.84	0.58
2	**1.72**	-H	2.33	0.20	0.31	0.46	0.80
3	**1.73**	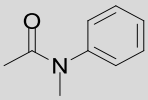	14.85	4.07	4.31	6.36	4.25
4	**1.74**	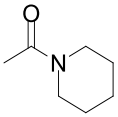	12.07	3.22	3.04	2.82	7.43
5	**1.75**	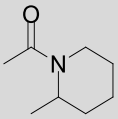	15.03	5.05	4.73	4.27	8.19
6	**1.76**	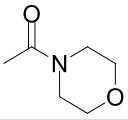	9.35	1.56	1.78	1.55	1.36
7	**1.77**	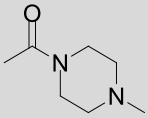	5.18	1.02	1.28	2.31	2.61
8	**1.78**	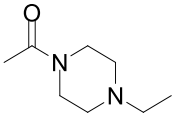	5.91	2.44	2.88	1.59	4.61
9	**1.79**	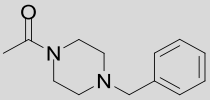	8.85	5.17	11.72	18.01	9.90
10	**1.80**	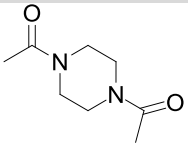	7.20	4.23	3.64	1.35	5.79

[a] Cells were treated with different concentrations of the indicated compounds for 48 h, and the cell viability was determined by the MTT assay.

Celastrol derivatives with modified A/B-rings

Celastrol **1.26** reduction generates dihydrocelastrol **1.81**, a compound that retains the carboxyl group at the C(29) position but exhibits a different topology of the A/B-rings (Figure 1.15). As mentioned above, the intracellular activity of celastrol **1.26** and its analogues has been attributed to the electrophilicity of the QM substructure extending over the A/B-rings. Therefore, this simple rearrangement is very useful to explore the importance of the QM structure of celastrol **1.26** for its biological activity.

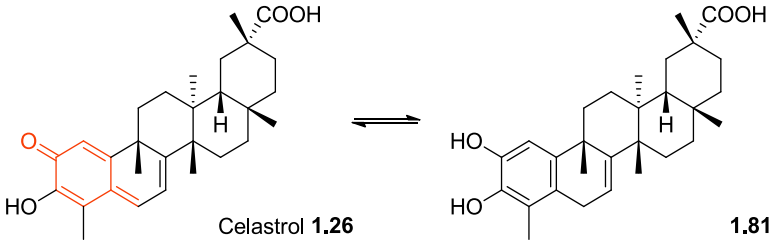

Figure 1.15 Conversion of celastrol **1.26** (*para*-quinonemethide structure indicated in orange) to dihydrocelastrol **1.81.**

It has been shown that this relatively small change in structure has a large impact on the activity of the compound. However, it is not still fully understood whether the differences in activity are caused by changes in the binding to the protein targets, or by differences in stability, absorption, distribution, or metabolism (*i.e.*, pharmacokinetics) [*240*]. In fact, some studies have suggested that reactivity toward thiols is the predominant mode of action of celastrol **1.26**; therefore, dihydrocelastrol **1.81**, which lacks the QM substructure and is not electrophilic, is inactive or much less potent than celastrol **1.26** [*107*, *198*, *282*]. However, a more recent study demonstrated the antitumour potential of dihydrocelastrol **1.81**, *in vitro* and *in vivo,* to inhibit multiple myeloma cell proliferation, and induce apoptosis through different mechanisms, possibly via the IL-6/STAT3 and ERK1/2 pathways [*289*].

Dihydrocelastrol **1.81** is easily converted to dihydrocelastrol diacetate **1.82**, which is another celastrol derivative that lacks the QM substructure (Figure 1.16). The results of studies that compared the activity of celastrol **1.26** with that of dihydrocelastrol diacetate **1.82** are also inconsistent; thus, the importance of the

QM moiety in the cellular mechanism of action of this molecule remains unclear. On the one hand, this structure seems to be important for celastrol **1.26** activity, because dihydrocelastrol diacetate **1.82** showed a significantly weaker effect as a Hsp90 inhibitor [*245*, *290*] and failed to inhibit melanoma cell viability [*282*]. On the other hand, dihydrocelastrol diacetate **1.82** exhibited a similar potency as a heat shock activator [*240*]. However, the activity of both dihydrocelastrol **1.81** and dihydrocelastrol diacetate **1.82** could be related to the instability of these compounds and their propensity to hydrolase and be converted back to parent celastrol **1.26** rather than to the structure of the ring system itself [*107*].

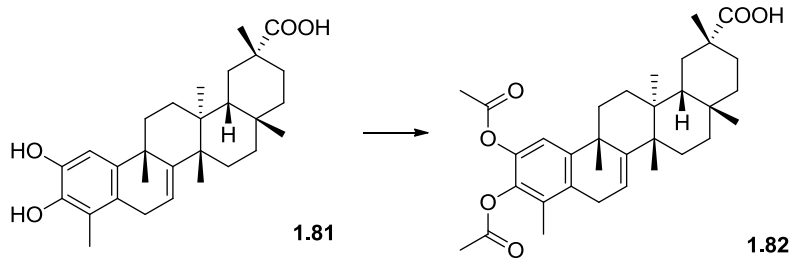

Figure 1.16 Conversion of dihydrocelastrol **1.81** to dihydrocelastrol diacetate **1.82.**

C(6)-substituted celastrol derivatives with modified A/B-rings

The C(6) position is highly susceptible to nucleophilic addition, thus enabling the formation of Michael adducts, namely via reaction with the thiol groups of biomolecules [*110*]. Substitutions at the C(6) position imply the rearrangement of the A/B-rings, thus generating celastrol derivatives that lack the QM moiety.

The activity of these C(6)-celastrol derivatives was explored, and analogues with improved potency were synthesised. Compound **1.83** (Figure 1.17, Table 1.13, entry 2), which is a C(6)-sulfonated analogue, was selected for animal testing. In PC-3 tumour-bearing nude mice, the intraperitoneal administration of 3 mg/kg of compound **1.83** led to good activity and decreased toxicity, compared with celastrol **1.26** [*291*]. These results encouraged Lu and coworkers to explore further the chemical space of this modification site [*292*, *293*].

Initially, three types of C6-modified celastrol derivatives were designed and synthesised: C6-sulfonated (**1.84**), C6-carbonated (**1.85**) and C6-sulfided (**1.86** and **1.87**) derivatives, and their anticancer activity was evaluated against human cancer cell lines (Figure 1.17, Table 1.13, entries 3–6). Most of the derivatives exhibited higher cytotoxicity than did celastrol **1.26** against the cell lines tested with the exception of compound **1.85**, the cytotoxicity potency of which dropped drastically (IC_{50} > 150 μM) (Table 1.13, entry 4). The compound with the best results in *in vitro* studies (**1.84**, Table 1.13, entry 3), was also evaluated in *in vivo* studies, using nude mice bearing Colo 205 xenografts, and showed significant inhibition of tumour growth at low-range concentrations. Therefore, this study suggests that modifications at the C(6) position of celastrol **1.26** might be useful for improving its anticancer activity [*292*].

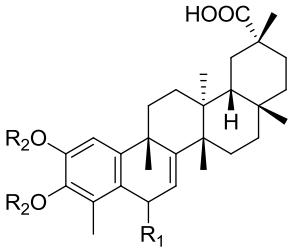

1.83 $R_1 = SO_3Na$; $R_2 = H$
1.84 $R_1 = SO_3Na$; $R_2 = COCH_3$
1.85 $R_1 = CH_2COCH_3$; $R_2 = COCH_3$
1.86 $R_1 = S(p\text{-}C_6H_4)CH_3$; $R_2 = COCH_3$
1.87 $R_1 = S(p\text{-}C_6H_4)NHCOCH_3$; $R_2 = COCH_3$

Figure 1.17 Celastrol derivatives **1.83–1.87.**

Subsequently, a new series of C(6)-modified celastrol analogues was prepared. Compounds **1.88**–**1.93** (Figure 1.18, Table 1.13, entries 7–12), bearing an indole group at C(6), were tested for their cytotoxicity against the human glioblastoma H4 and human hepatocellular carcinoma Bel7402 cell lines. Compounds **1.88**, **1.90** and **1.92** did not show any improvement in the cytotoxic activity against these cell lines (Table 1.13, entries 7, 9 and 11) compared with celastrol **1.26** (IC_{50} = 1.55–2.09 μM). Interestingly, the analogous compounds that were methylated at the phenolic hydroxyl and carboxyl functional groups, **1.89** (IC_{50} = 4.59–0.51 μM), **1.91** (IC_{50} = 7.88–0.02 μM) and **1.93** (IC_{50} = 2.03–0.01 μM) (Table 1.13, entries 8, 10 and 12, respectively), showed good *in vitro* anticancer activity against H4 and Bel7402 cells. These results confirm the previous findings, suggesting that the Michael acceptor system of celastrol **1.26** is not essential for its anticancer activity [*293*]. Subsequently, a new method for the synthesis of these

C(6)-indole celastrol derivatives was developed, affording an experimentally simple, highly efficient Michael-type Friedel-Crafts addition of indoles to the *p*-QM of celastrol **1.26** [*294*].

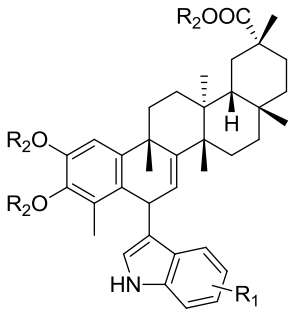

1.88 R_1 = 5-OCH_3; R_2 = H
1.89 R_1 = 5-OCH_3; R_2 = CH_3
1.90 R_1 = 6-CH_3; R_2 = H
1.91 R_1 = 6-CH_3; R_2 = CH_3
1.92 R_1 = 6-Cl; R_2 = H
1.93 R_1 = 6-Cl, *N*-CH_3; R_2 = CH_3

Figure 1.18 Celastrol derivatives **1.88–1.93.**

Table 1.13 IC_{50} (μM) values of celastrol **1.26** and derivatives **1.83–1.93** in tumour cell lines.

Entry	Comp.	Cell line/IC_{50} (μM) [a]								Ref.
		H4	Bel7402	BGC923	H522	Colo205	HepG2	MDA-MB468	BGC823	
1	**Celastrol 1.26**	2.09	1.55	3.73	-	-	-	-	-	[*292*]
2	**1.83**	0.91	1.17	0.77	0.47	0.51	0.68	0.89	0.77	[*292*]
3	**1.84**	1.37	1.73	0.49	0.39	0.06	0.29	0.33	1.53	[*292*]
4	**1.85**	>150	>150	>150	-	-	-	-	-	[*292*]
5	**1.86**	0.37	0.45	0.47	-	-	-	-	-	[*292*]
6	**1.87**	0.35	0.46	0.42	-	-	-	-	-	[*292*]
7	**1.88**	24.39	45.42	-	-	-	-	-	-	[*293*]
8	**1.89**	4.59	0.51	-	-	-	-	-	-	[*293*]
9	**1.90**	6.66	5.52	-	-	-	-	-	-	[*293*]
10	**1.91**	7.88	0.02	-	-	-	-	-	-	[*293*]
11	**1.92**	7.83	6.53	-	-	-	-	-	-	[*293*]
12	**1.93**	2.03	0.01	-	-	-	-	-	-	[*293*]

[a] Cells were treated with different concentrations of the indicated compounds for 72 h, and the cell viability was determined by the MTT assay

As discussed herein, celastrol **1.26** is a promising hit-compound in drug discovery. Moreover, the semisynthesis of celastrol derivatives has proved to be fairly useful in producing novel compounds with improved anticancer activity compared with the parent compound. However, the effects of specific structural modifications of its basic scaffold and the extension by which they can be

optimised are not fully understood. In addition, it should be emphasised that a limited number of synthetic analogues of celastrol **1.26** are reported in the literature, mainly because of its short supply and complex chemical structure. Consequently, further research is warranted to explore additional structural modifications of celastrol **1.26** and to synthesise novel, more effective and selective celastrol derivatives as potential anticancer agents.

CHAPTER II

GENERAL OBJECTIVES

2. CHAPTER II

General objectives

Given the high prevalence of cancer and its profound impact on society, as well as the anticancer potential of natural products, such as celastrol **1.26**, the aim of this thesis is to explore structural modifications of celastrol **1.26** to prepare more effective and safer anticancer agents.

The proposed aim will be accomplished by fulfilling the following general objectives:

- **Preparation of new semisynthetic derivatives of celastrol 1.26**

  The preparation of the new celastrol derivatives will be based on one or more of the following synthetic strategies: modification of the QM structure of celastrol **1.26**; additional A/B-ring modifications, such as the introduction of an α,β-unsaturated carbonyl group at C(6); and conversion of the C(29)-carboxylic acid into nitrogen-containing groups or others groups.

- **Elucidation of the chemical structure of all new semisynthetic derivatives**

  The structures and high purity of the new celastrol derivatives will be elucidated via numerous analytical techniques, such as melting point determination, IR spectroscopy, NMR spectroscopy (^{1}H NMR, ^{13}C NMR and DEPT-135 NMR) and, MS and elemental analyses.

- **Evaluation of the biological activity of new compounds in human cancer cell lines**

  The effect of celastrol **1.26** and its analogues on cancer cell viability will be tested against several human cancer cell lines, and the IC_{50} values will be determined using the MTT assay. The IC_{50} values will be used to establish a SAR study.

- **Assessment of the selectivity of the antiproliferative activity of some relevant compounds**

  The most relevant derivatives of each series will be further tested against the human non-tumour fibroblast cell line BJ.

- **Evaluation of the synergism between some celastrol derivatives and chemotherapeutic agents currently used in the clinic**

  Possible synergistic anticancer effects of the most relevant compounds and approved drugs will be evaluated in cancer cell lines using the Chou and Talalay method.

- **Study of the mechanism underlying the anticancer activity of the most promising analogues**

  Several assays will be used to investigate the anticancer mechanisms of action of these compounds, namely: flow cytometry, to investigate cell-cycle arrest and apoptosis induction; fluorescence microscopy, for morphological analysis; clonogenic assay to assess antiproliferative activity; and western blotting, to detect target proteins and investigate specific cell signalling pathways.

Taken together, the results of these experiments will be used to propose new leads for cancer drug development.

CHAPTER III

NOVEL CELASTROL DERIVATIVES WITH IMPROVED SELECTIVITY AND ENHANCED ANTITUMOUR ACTIVITY: DESIGN, SYNTHESIS AND BIOLOGICAL EVALUATION

Sandra A.C. Figueiredo, Jorge A.R. Salvador, Roldán Cortés, Marta Cascante

Novel celastrol derivatives with improved selectivity and enhanced antitumour activity: design, synthesis and biological evaluation

European Journal of Medicinal Chemistry, 138 (2017) 422–437

http://dx.doi.org/10.1016/j.ejmech.2017.06.029

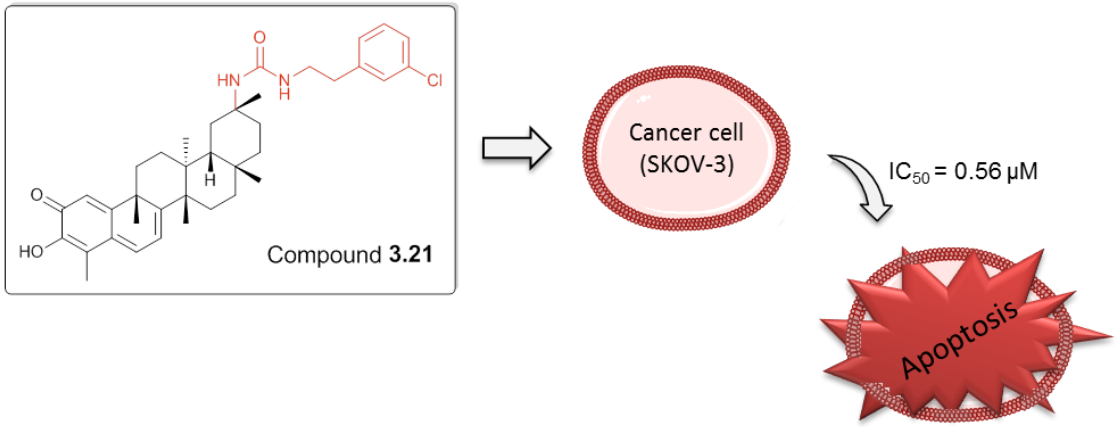

Highlights

- New celastrol derivatives with improved anticancer activity were synthesised.
- Among all the tested derivatives, compound **3.21** was the most active and selective.
- Compound **3.21** induced apoptosis and decrease of dysfunctional p53 in SKOV-3 cells.
- Compound **3.21** may act as an Hsp90 inhibitor and affect the Akt/mTOR pathway.

3. CHAPTER III

Novel celastrol derivatives with improved selectivity and enhanced antitumour activity: design, synthesis and biological evaluation

3.1. INTRODUCTION

The rational drug design for the discovery of new potent anticancer agents with minimal side effects is a major goal of modern medicinal chemistry [*17*]. The development of new chemotherapy options is often aimed at finding new compounds for combination therapies, due to the drug resistance and considerable side effects usually related with monotherapy in cancer [*295*].

Natural products are a unique source for the development of novel effective cytotoxic agents [*296–299*]. Celastrol **1.26** is one of the most active antitumour compounds among the natural triterpenoids [*113*]. It is a chemical substance isolated from the root bark of the Chinese medicinal plant *Tripterygium wilfordii Hook F.*, which belongs to the Celastracea family, an important source of bioactive secondary metabolites [*117*].

Structurally, celastrol **1.26** is a triterpenoid QM that, as implied in its name, bears a structure that is analogous to a quinone with one of the carbonyl oxygens replaced by a methylene group [*106*]. Moreover, it has a hydroxyl group *ortho* to the quinone carbonyl group and extended conjugation at the exocyclic methylene group. The stability of the chemical structure is further influenced by the steric and conformational features of the 5-ring triterpene [*300*, *301*]. The A/B-rings of celastrol **1.26** make the molecule polarised and, thus, extremely reactive. It incorporates a Michael acceptor in which the C(6) position is highly prone to nucleophilic addition [*107*, *108*]. Therefore, celastrol **1.26** has the ability to form covalent Michael adducts by reacting with the nucleophilic thiol groups of the cysteine residues of biomolecules, such as DNA and proteins [*110*]. This seems to be the chief mechanism responsible for the wide range of biological activities associated with celastrol **1.26** [*106*, *110*, *112*, *117*]. Among these pharmacological

activities, its potent antitumour effect has been the most widely investigated [*108*, *185*, *186*, *268*, *302*].

Celastrol **1.26** has been reported to be highly active against a wide variety of human tumour cell lines [*185*, *189*, *197*, *199*, *218*]. Its potential mechanisms of action have also been studied, and it has been revealed that celastrol **1.26** can regulate the survival [*254*], proliferation [*182*], invasion [*195*], angiogenesis [*260*] and metastasis [*251*] of tumour cells via several pathways. Despite the huge potential of celastrol **1.26** as an anticancer agent, it presents some important limitations for clinical application, such as systemic toxicity, poor aqueous solubility and low bioavailability [*269*, *278*]. For this reason, in recent years, an effort has been made to develop and optimise new celastrol derivatives [*108*, *287*, *292*].

Urea-containing derivatives of some chemical products have been recently synthesised, resulting in enhanced compounds with versatile properties that helped to improve their pharmacological and pharmacokinetics profile [*303–305*]. In this article, we report a rational approach to the synthesis and characterization of several new urea-containing derivatives of celastrol **1.26**, resulting in antitumour compounds that are even more effective and less toxic. The most active compound, compound **3.21**, was selected for additional studies aimed at gaining insight into the mechanism of action via which this derivative causes a decrease in the viability of cancer cells.

3.2. RESULTS AND DISCUSSION

3.2.1. Chemistry

The synthetic routes used here for the novel celastrol derivatives are outlined in Scheme 3.1–3.3. The structures and high purity of all compounds were corroborated by melting point (Mp) determination, infrared spectroscopy (IR), nuclear magnetic resonance spectroscopy (^{1}H NMR, ^{13}C NMR and DEPT-135 NMR), mass spectrometry (MS) and elemental analyses.

Celastrol **1.26** contains a hydroxyquinonemethide moiety which can be easily reduced with sodium borohydride to the dihydro derivative **1.81** (Scheme 3.1) [*119*]. This derivative is readily converted back to its parent celastrol **1.26** by aerial oxidation [*306*]. Interestingly, the progress of these reactions can be monitored visually by following changes in the colour of the reaction mixture. The disappearance of the orange-red colour that is characteristic of celastrol **1.26** is linked to the loss of the ortho-quinonoid structure [*155*]. Phenolic hydroxyl groups are highly reactive; in order to avoid the formation of multiple derivatives, the protection of these groups was carried out by preparing the respective diacetate **1.82** using acetic anhydride (Scheme 3.1) [*107*, *240*, *306*, *307*].

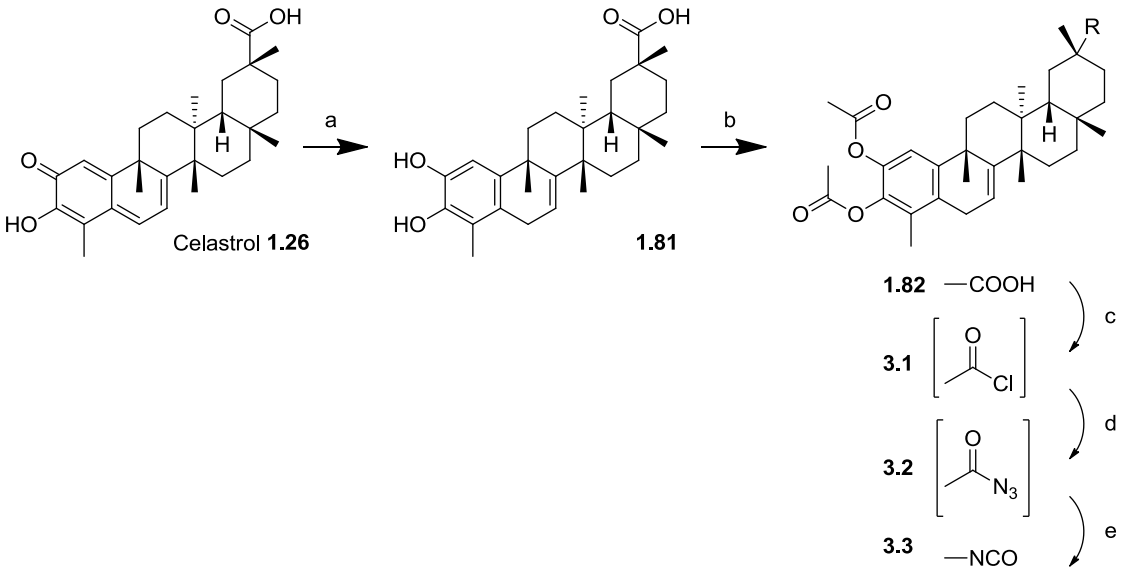

Scheme 3.1 Synthesis of celastrol derivatives **1.81, 1.82** and **3.1–3.3.** *Reagents and conditions:* a) $NaBH_4$, MeOH, R.T., 10 min; b) $(CH_3CO)_2O$, DMAP, THF, R.T., N_2, 4 h; c) $(COCl)_2$, CH_2Cl_2, R.T., N_2, 4 h; d) NaN_3, H_2O, acetone, 0 ºC, 1 h; e) in toluene, reflux, 2 h.

Compound **1.82** was treated with oxalyl chloride in dichloromethane to give directly the acid chloride of dihydrocelastrol diacetate **3.1**, which was further converted to the acid azide **3.2** using sodium azide in aqueous acetone; Curtius rearrangement in toluene after 2 h of reflux gave isocyanate **3.3** (Scheme 3.1) [*304*, *308*], a central intermediate to obtain urea-type compounds. The introduction of an isocyanate function in compound **3.3** was confirmed by the specific IR observation at 2253 cm^{-1} (Figure 3.1), in combination with the observation of a

signal for the quaternary carbon attached to the nitrogen at 120.77 ppm in the ^{13}C NMR spectrum (Figure 3.2).

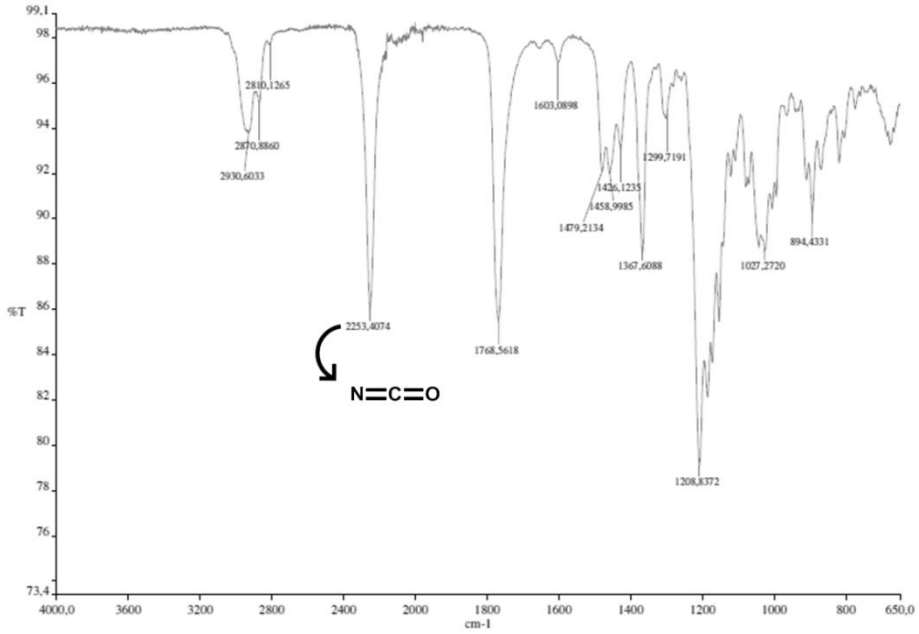

Figure 3.1 IR spectrum of compound **3.3.**

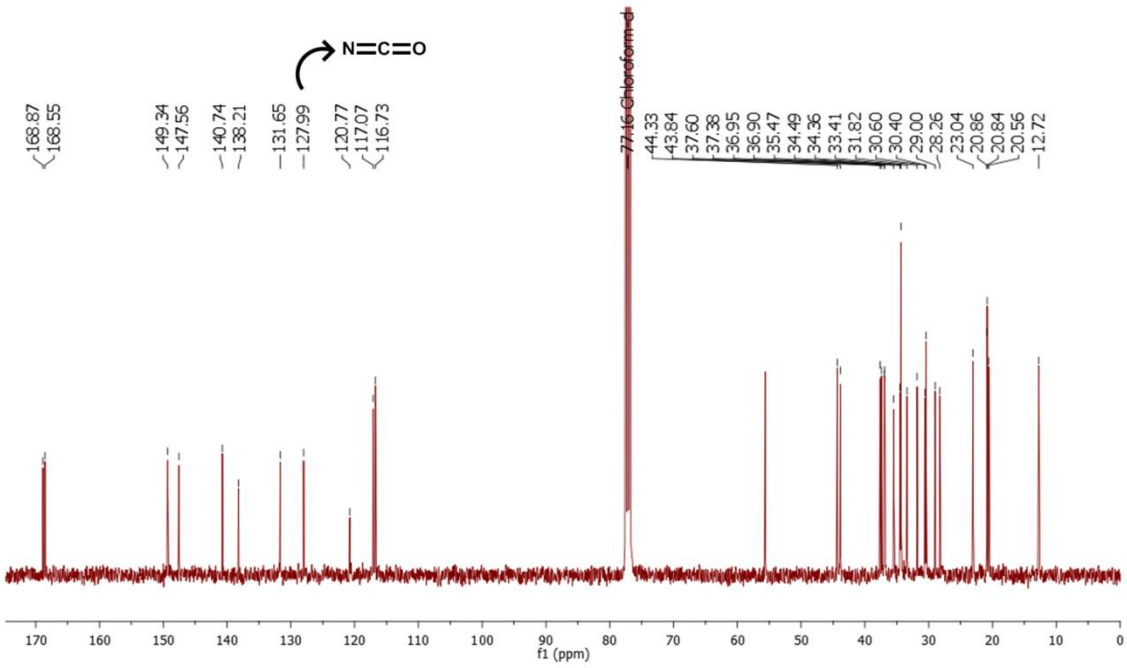

Figure 3.2 ^{13}C NMR spectrum of compound **3.3**

To verify the importance of the QM moiety for the anticancer activity in the urea derivatives of celastrol, some ureas 6-oxo derivatives (Scheme 3.2) were

also synthesised. We adapted a previously described procedure [*309*] for the allylic oxidation of compound **1.82** using *tert*-butyl hydroperoxide in the presence of sodium chlorite in aqueous acetonitrile at room temperature, to give 6-oxo celastrol diacetate **3.4** in good yield (Scheme 3.2). Successful allylic oxidation was confirmed by the observation of an IR band at 1715 cm^{-1}, corresponding to the C=O stretching vibration (Figure 3.3) and of a ^{13}C NMR signal for the α,β-unsaturated carbonyl C(6) at 187.13 ppm (Figure 3.4).

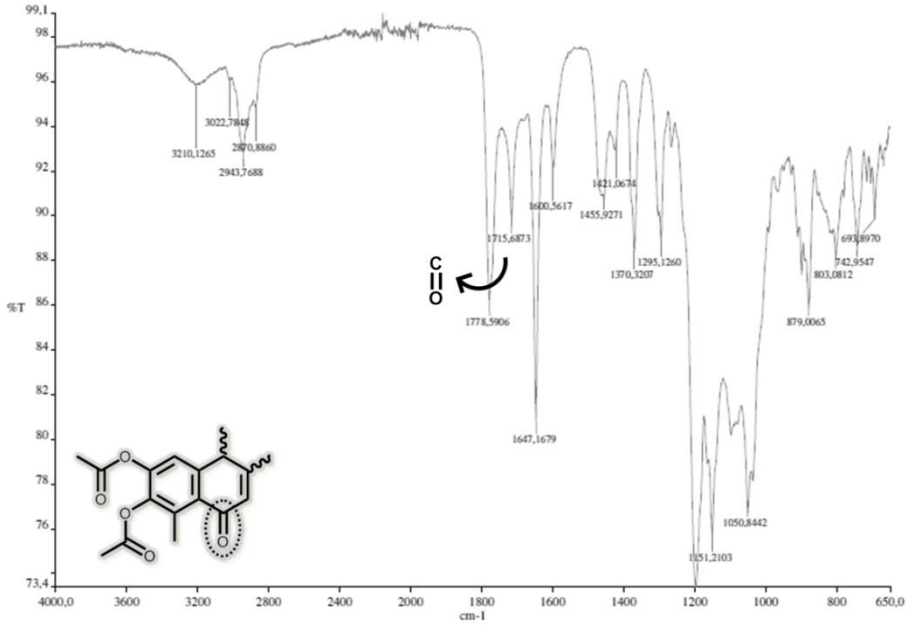

Figure 3.3 IR spectrum of compound **3.4.**

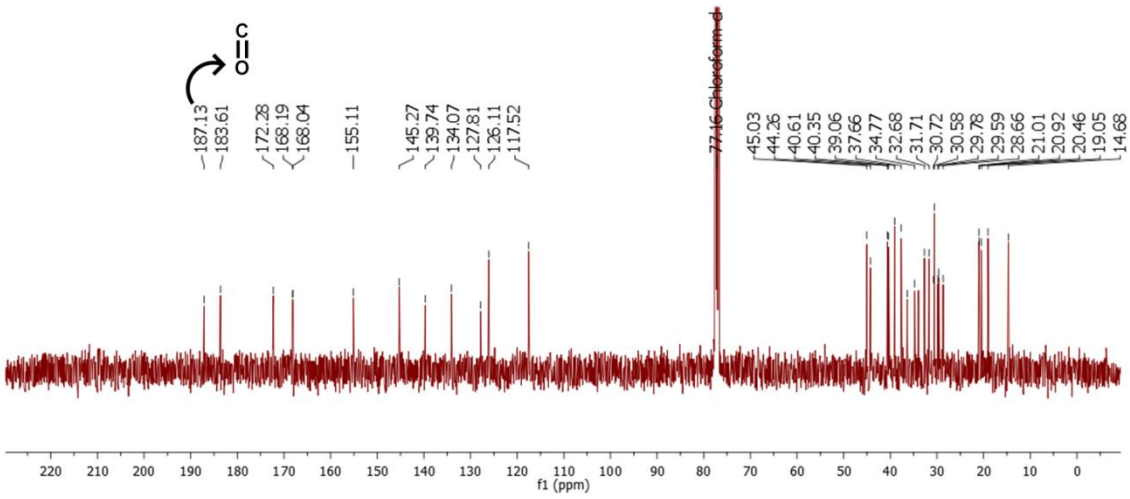

Figure 3.4 ^{13}C NMR spectrum of compound **3.4.**

The treatment of compound **3.4** with ammonium acetate catalysed efficiently the deprotection of the aromatic acetates in aqueous methanol at room temperature, to yield the corresponding diphenol **1.45** (Scheme 3.2) [*310*]. This spectroscopic evidence was consistent with the data reported in the literature, thus confirming that the structure of compound **1.45** corresponds to the natural triterpenoid Wilforol A [*130*]. Compound **3.4** was converted to the corresponding isocyanate **3.5** in a manner similar to that described previously. For the synthesis of urea **3.7** and **3.8**, intermediate isocyanate **3.5** was treated with ammonium acetate and methylamine, respectively. Because of the basic character of these reactions, the deprotection of the aromatic acetates was spontaneous, directly affording the corresponding urea 6-oxo-diphenol derivatives of celastrol. The presence of a urea moiety on the new derivatives **3.7** and **3.8** was supported by the characteristic ^{13}C NMR signal observed at 161.08 and 161.43 ppm, respectively. Furthermore, these compounds did not present any signal relative to the acetates, unlike compound **3.5**, which showed two δ signals on the ^{1}H spectrum, around 2.35 and 2.55 ppm (corresponding to three protons each). Urea **3.8** was structurally diversified using anhydrous potassium carbonate (K_2CO_3) and methyl iodide in dimethylformamide, to give the methyl derivative **3.9** (Scheme 3.2).

For the synthesis of C(29) urea derivatives of celastrol **1.26** with preserved hydroxyquinonemethide moiety **3.11–3.22**, the intermediate **3.3** was used as a starting point (Scheme 3.3).

In the first step, **3.3** was hydrolysed by K_2CO_3 in methanol, to give compound **3.10** with a free QM moiety (Scheme 3.3). Treatment with *N*-methyl-hydroxylamine hydrochloride in the presence of sodium bicarbonate gave urea **3.11**, while treatment with ammonium acetate in the presence of triethylamine (Et_3N) gave urea **3.13**. Similarly, substituted urea compounds **3.12**, **3.14–3.22** were prepared via parallel reactions of isocyanate **3.10** with the respective amines in dichloromethane, in good yields (Scheme 3.3) [*308*]. The successful preparation of compounds **3.11–3.22** was confirmed by the characteristic IR spectra, which showed absorption bands corresponding to the hydroxyl and carbonyl groups of A-

ring and absorption bands corresponding to the amino and carbonyl groups of C(29) urea (Figure 3.5). In the ^{13}C NMR spectra, the signal for the urea carbonyl carbon was observed between 155 and 160 ppm (Figure 3.8).

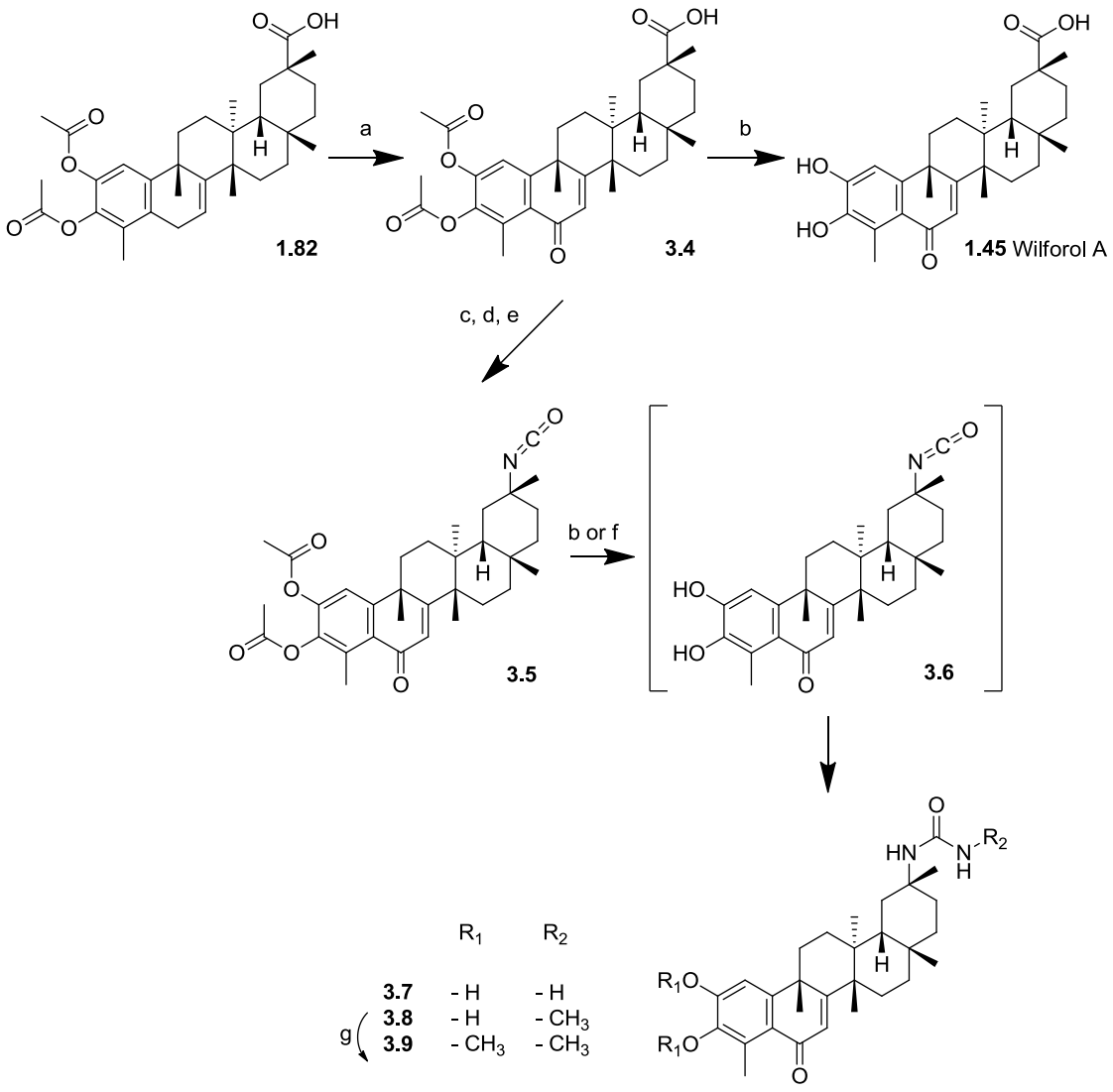

Scheme 3.2 Synthesis of celastrol derivatives **1.45** and **3.4–3.9.** *Reagents and conditions*: a) *t*-BuOOH, $NaClO_2$, aq. CH_3CN 1:3, R.T., 1 h; b) NH_4OAc, Et_3N, aq. MeOH (1:4), R.T., 2 h; c) $(COCl)_2$, CH_2Cl_2, R.T., N_2, 4 h; d) NaN_3, H_2O, acetone, 0 ºC, 1 h; e) in toluene, reflux, 2 h; f) $MeNH_2$, THF, R.T., N_2, 12 h; g) CH_3I, K_2CO_3, DMF, R.T., N_2, 6 h.

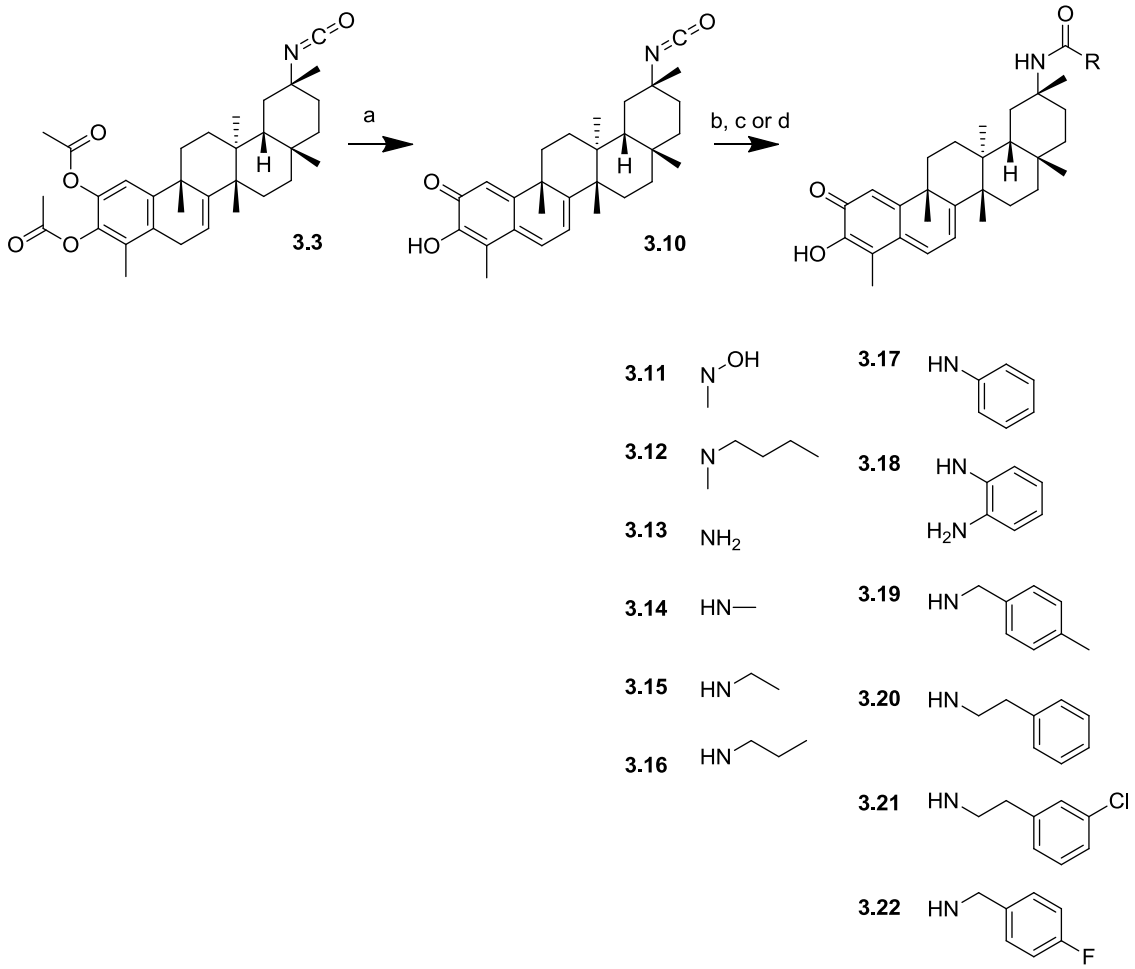

Scheme 3.3 Synthesis of celastrol derivatives **3.10–3.11.** *Reagents and conditions*: a) K_2CO_3, MeOH, 0 ºC, N_2, 15 min; b) $NaHCO_3$, $CH_3NHOH.HCl$ in acetone, CH_2Cl_2, R.T., 0.5 h; c) RNH_2, CH_2Cl_2, R.T., N_2, 4 h; d) NH_4OAc, Et_3N, aq. MeOH (1:4), R.T., 2 h.

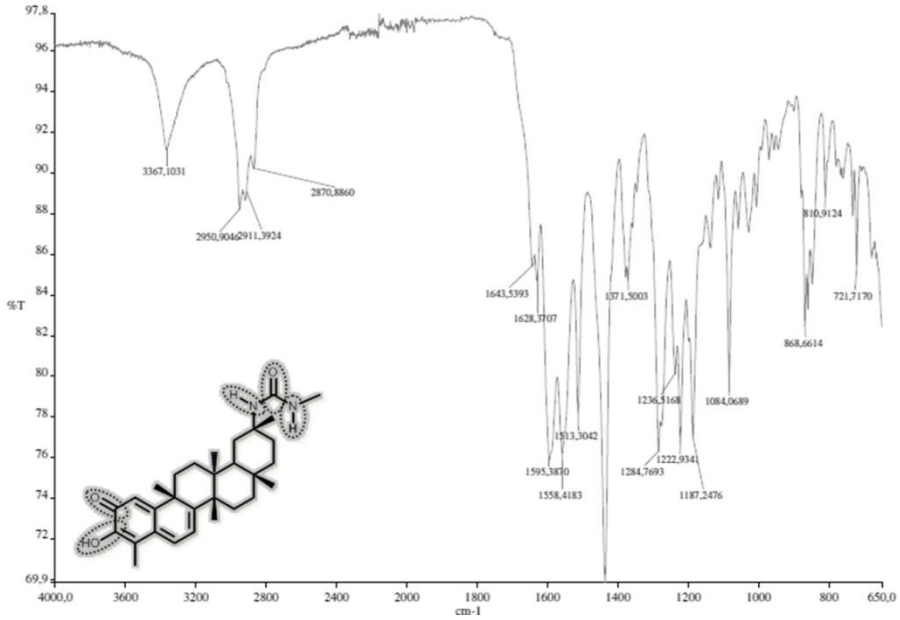

Figure 3.5 IR spectrum of compound **3.14.**

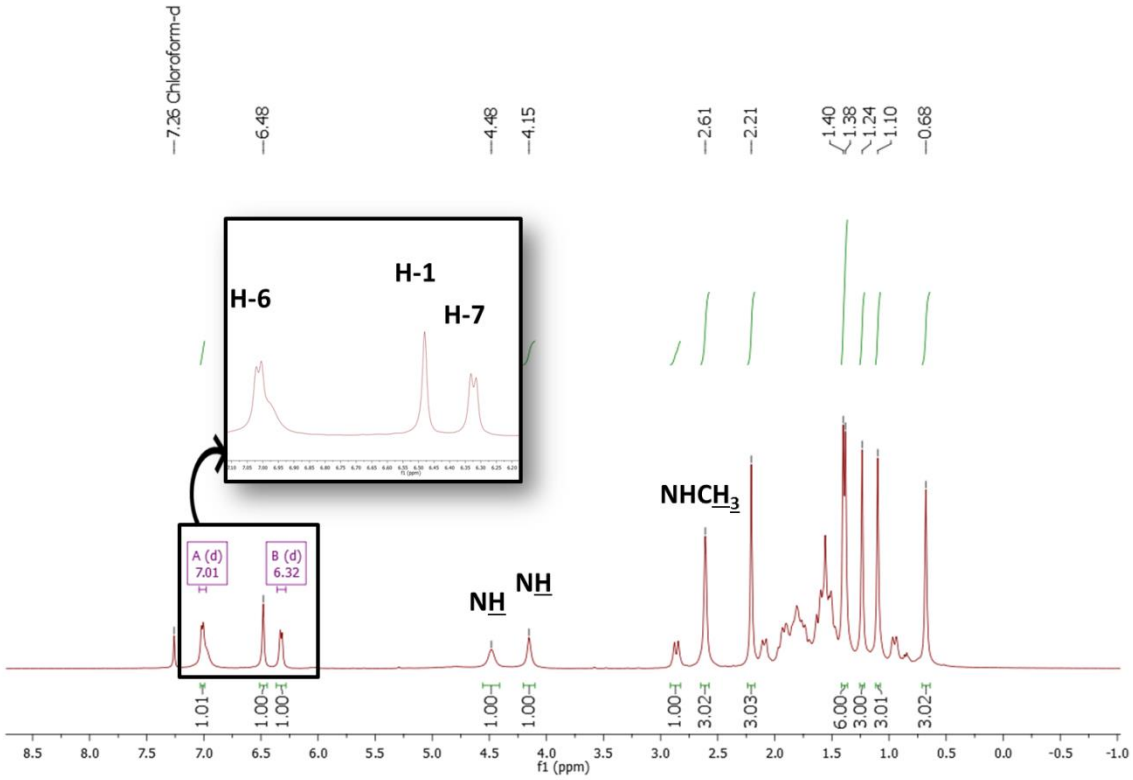

Figure 3.6 ^{1}H NMR spectrum of compound **3.14.**

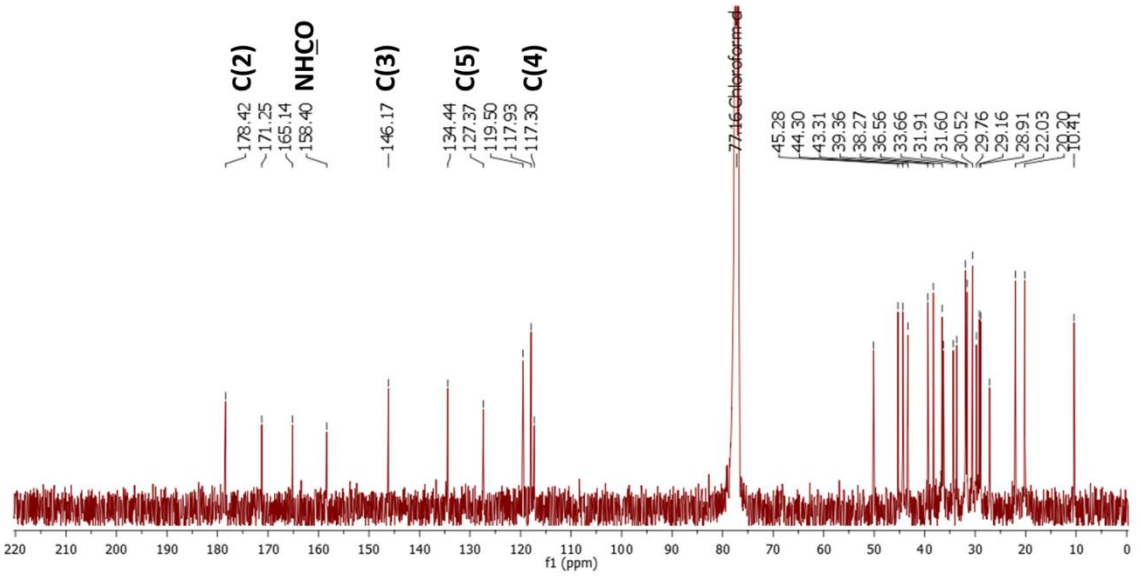

Figure 3.7 ^{13}C NMR spectrum of compound **3.14.**

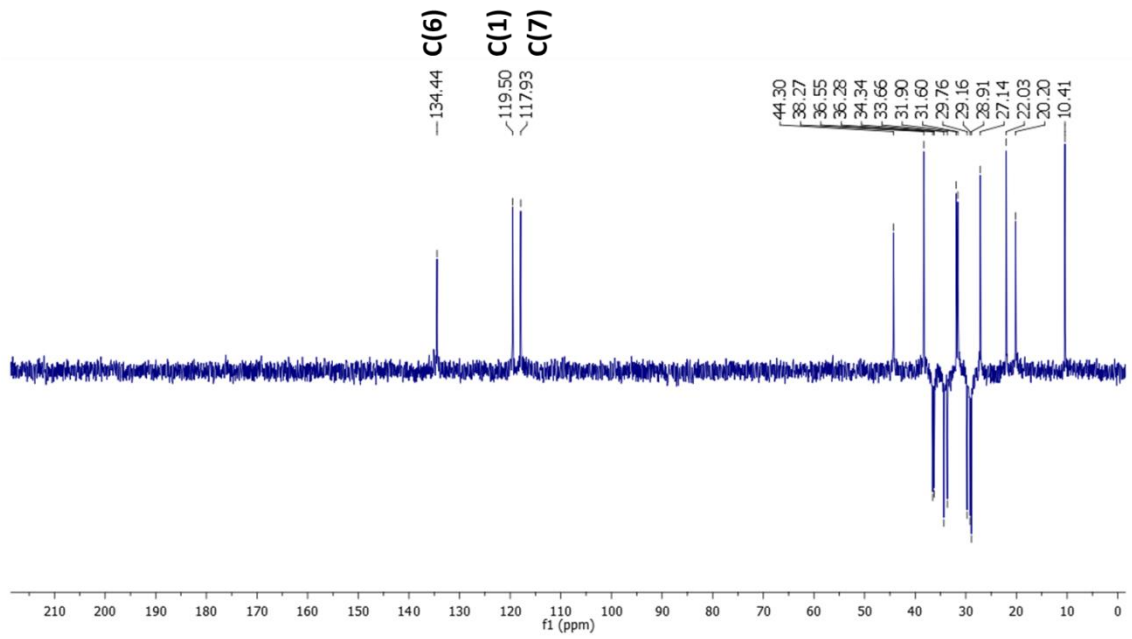

Figure 3.8 DEPT-135 NMR spectrum of compound **3.14.**

3.2.2. Biological activities

3.2.2.1. Evaluation of antiproliferative activity and selectivity

The effect of celastrol **1.26** and its derivatives on tumour cell viability was firstly screened against human lung carcinoma A549 cell line and the human pancreatic carcinoma MIA PaCa-2 cell line. The results, summarised in Table 3.1, are expressed as IC_{50} values (concentration of compound required to reduce 50% of cell viability) and were determined by MTT assay.

As shown in Table 3.1, celastrol **1.26** itself exhibited a potent cytotoxic effect on these cell lines. Intermediates **1.81**, **1.82** and **3.3,** which differ from celastrol **1.26** on their QM moiety, presented less potent antitumour activities, suggesting that these modifications of the A-ring are not favourable to the improvement of cytotoxic activity. To further explore if the intracellular activity of celastrol **1.26** and analogues is dependent on the electrophilicity of the hydroxyquinonemethide substructure extending over the A/B-rings, the activity of the derivatives of celastrol **1.26** bearing a carbonyl group at the C(6) position was assessed. Interestingly, the antiproliferative activity of compounds with this feature

(**3.4**–**3.9)** in these cell lines dropped drastically — more than 10-fold increase in their IC_{50} values compared with celastrol **1.26**.

Table 3.1 Cell viability (IC_{50} values) of celastrol **1.26** and its derivatives against A549 and MIA PaCa-2 tumour cell lines.

Compound	Cell line/IC_{50}[a] (μM ± SEM)	
	A549	MIA PaCa-2
Celastrol **1.26**	1.56±0.08	0.46±0.03
1.81	3.15±0.07	0.72±0.06
1.82	2.21±0.17	0.56±0.02
3.3	2.89±0.14	1.41±0.09
3.4	>15	>5
1.45	>15	>5
3.5	>15	>5
3.7	>15	>5
3.8	>15	>5
3.9	>15	>5
3.10	2.47±0.05	0.53±0.03
3.11	3.50±0.13	0.85±0.03
3.12	1.44±0.07	0.31±0.01
3.13	2.48±0.08	0.63±0.02
3.14	1.45±0.06	0.41±0.12
3.15	1.41±0.18	0.55±0.03
3.16	1.26±0.08	0.66±0.03
3.17	2.27±0.05	0.40±0.02
3.18	2.99±0.08	0.56±0.03
3.19	2.45±0.10	0.45±0.03
3.20	1.66±0.09	0.41±0.02
3.21	1.27±0.05	0.35±0.02
3.22	4.34±0.24	0.56±0.02

IC_{50} values were determined by MTT assay after 72 h-long incubations with different concentrations of each compound, and are expressed as the mean ± SEM of three independent experiments.

[a]IC_{50} is the concentration of compound required to reduce 50% of cell viability.

This loss of activity was independent of modifications in A-ring, as all diacetate compounds (**3.4** and **3.5**), diphenol compounds (**1.45**, **3.7** and **3.8**), and dimethoxyphenyl compounds (**3.9**) exhibited IC_{50} values >15 μM and >5 μM for the A549 and MIA PaCa-2 cell lines, respectively (Table 3.1). Although some recent

studies [*108*, *287*, *292*] reported that C(6)-derivatives of celastrol **1.26** are potential drug candidates for treating cancer, our results did not lead us to reach the same conclusions. In fact, the loss of antitumour effect observed here is consistent with other observations [*107*, *119*, *242*, *311*], which suggest that the reactivity toward thiols is the main mode of action of celastrol **1.26**. This hypothesis is further supported by the direct comparison of the highly active C(29) urea derivatives of celastrol **1.26** bearing the intact QM group (compounds **3.13** and **3.14**) with their low-activity analogues bearing the C(6)-carbonyl group (compounds **3.7** and **3.8**, respectively).

The introduction of a urea group at C(29) of celastrol **1.26** afforded compounds (**3.11**–**3.22**) that strongly inhibited the growth of the cell lines studied and that exhibited an activity that was dependent on the nature of the urea nitrogen. Compared with the hit compound **1.26**, the majority of these derivatives resulted in an improvement of antiproliferative activity against one (**18**, **20**, **22** and **23**) or even both (**3.12**, **3.14** and **3.21**) of the A549 and MIA PaCa-2 cell lines (Table 3.1). As compounds **3.12**, **3.14** and **3.21** were the most active celastrol derivatives against these cancer cell lines, the selectivity of their antiproliferative activity was assessed using the human non-tumour fibroblast cell line BJ (Table 3.2).

Table 3.2 Cell viability (IC_{50} values) of celastrol **1.26** and its derivatives against non-tumour fibroblast cell line BJ and tumour cell lines (SKOV-3, SKBR-3 and MDAMB-231).

Compound	Cell line/IC_{50}[a] (μM ± SEM)			
	BJ	**SKOV-3**	**SKBR-3**	**MDAMB-231**
Celastrol **1.26**	2.74±0.14	1.16±0.03	0.72±0.02	1.32±0.11
3.12	2.12±0.09	ND	ND	ND
3.14	1.96±0.05	ND	ND	ND
3.21	3.29±0.11	0.56±0.01	0.78±0.03	1.15±0.04

IC_{50} values were determined by MTT assay after 72 h-long incubations with different concentrations of each compound, and are expressed as the mean ± SEM of three independent experiments.
ND: Not determined.
[a]IC_{50} is the concentration of compound required to reduce 50% of cell viability.

As depicted in Table 3.3, all of the compounds tested presented a selectivity index (IC_{50} BJ cell line/IC_{50} tumour cell line) superior to 1, which

indicates a selective cytotoxic activity for malignant cells. Moreover, compound **3.21** was 3 to 9 times more active in tumour cell lines than in the non-tumour BJ cell line, which represents an important improvement in selectivity compared with the hit compound **1.26**. These results clearly suggest that structural modifications of the parent structure **1.26** can produce more potent and more selective new derivatives.

Table 3.3 Selectivity index against non-tumour BJ cells of celastrol **1.26** and its derivatives **15, 17** and **3.21.**

Compounds	Selectivity Index (IC_{50} BJ cell line/IC_{50} tumour cell line)		
	A549	**MIA PaCa-2**	**SKOV-3**
Celastrol **1.26**	1.75	5.97	2.34
3.12	1.48	6.94	ND
3.14	1.36	4.72	ND
3.21	2.59	9.31	5.81

ND: Not determined.

To confirm its activity in a wider variety of tumours, the antiproliferative activity of compound **3.21**, the derivative with the most promising results, was further tested in ovarian (SKOV-3) and breast (SKBR-3 and MDAMB-231) cancer cell lines. Compared with celastrol **1.26**, the greatest improvement in the antitumour effect of compound **3.21** was observed for the SKOV-3 cell line (2-fold activity increase) (Table 3.2). Furthermore, the analysis of the selectivity index values (Table 3.3) indicated that compound **3.21** was 6 times more active in SKOV-3 cells than in non-tumour BJ cells, which represents the largest improvement in selectivity (2.5-fold) compared with celastrol **1.26**. Therefore, compound **3.21** was selected for further studies in the SKOV-3 cell line, with the purpose of studying its selective antiproliferative mechanism.

3.2.2.2. Effects on cell-cycle distribution

Failure of the cell-cycle arrest responses is a common trait in tumour cells [*312*]. Thus, the effect of compound **3.21** on the cell-cycle distribution of SKOV-3 cells was analysed. The cell-cycle analysis was performed by fluorescence-

activated cell sorting (FACS) after labelling the cells with propidium iodide (PI), a DNA-binding dye. SKOV-3 cells were treated with the IC_{50} concentration of compound **3.21** for 24, 48 and 72 h, and untreated cells were used as the control. As shown in Figure 3.9**,** the effect of compound **3.21** on the distribution of SKOV-3 cells throughout the different phases of the cell-cycle was minimal, suggesting that cell-cycle arrest does not play a crucial role in the antiproliferative mechanism of the compound.

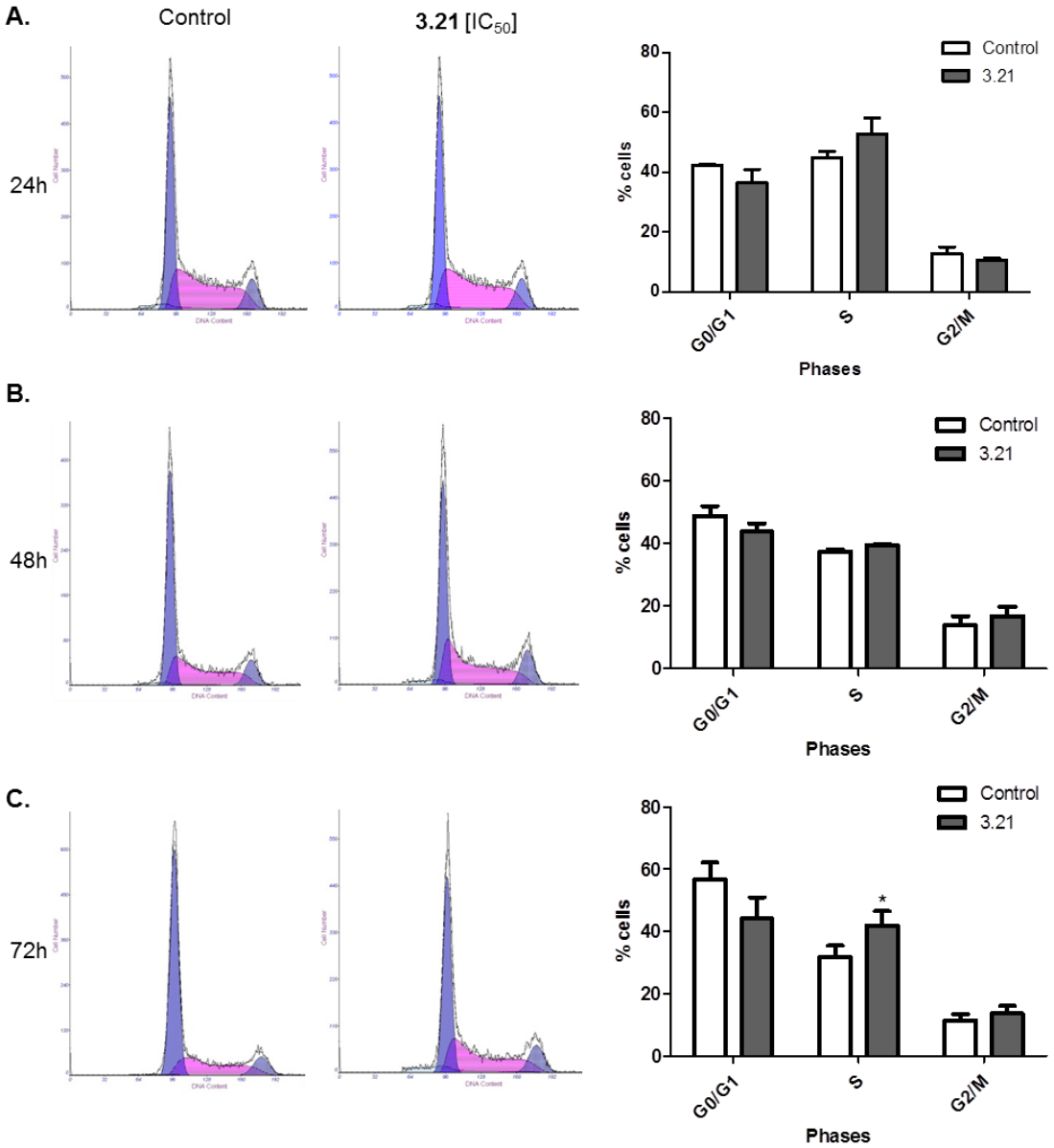

Figure 3.9 Representative histograms and plots showing the proportion of cells in each phase of the cell-cycle. SKOV-3 cells untreated (control condition) or SKOV-3 cells treated with compound **3.21** at its IC_{50} concentration for 24 (A), 48 (B) and 72 (C) hours. Values represent the means ± SD of three independent experiments. * indicates $p < 0.05$ with respect to untreated cells.

3.2.2.3. Annexin V-FTIC/PI flow cytometry assay

Because the effect of compound **3.21** on cell-cycle regulation was shown to be mild at best, it was speculated that the main mechanism underlying the cytotoxic activity of this compound might be the induction of apoptosis. Apoptosis, also known as noninflammatory, programmed cell death, is a continuous physiological process that plays a critical role in the control of cell proliferation [*38*]. The dysregulation of apoptosis can lead to tumorigenesis by disrupting the equilibrium between cell proliferation and death; therefore, compounds that can specifically regulate molecules that are involved in apoptosis are recognised strategies for the development of more effective and less toxic anticancer drugs [*1*, *29*, *313*]. The early stage of apoptosis is characterised by the loss of membrane asymmetry and the translocation of phosphatidylserine (PS) from the inner to the outer cell membrane. The externalised PS can be detected using annexin V-FITC (fluorescein isothiocyanate), a fluorescent active dye that selectively binds with high affinity to PS [*314*]. During the late stage of apoptosis, cell membranes lose their integrity and PI can penetrate cells and bind to DNA. Thus, FACS analysis of annexin V-FITC/PI double-stained cell allows the differentiation of live cells (annexin V−/PI−), early apoptotic cells (annexin V+/PI−) and late apoptotic/necrotic cells (PI+) [*314*]. SKOV-3 cells were incubated with compound **3.21** at the IC_{50} concentration for 24, 48 and 72 h, followed by double staining with annexin V-FITC/PI prior to analysis by FACS. As shown in Figure 3.10, the effect observed after 24 h of treatment with **3.21** was not significant. However, at 48 h, the percentage of cells in early apoptosis increased from 4.5% to 15.0% compared with the control condition. After an even longer incubation time, 72 h, the apoptotic effect was greatly enhanced (from 4.7% in the control condition to 31.8% in treated cells). These results suggest that compound **3.21** induces apoptosis in SKOV-3 cells in a time-dependent manner.

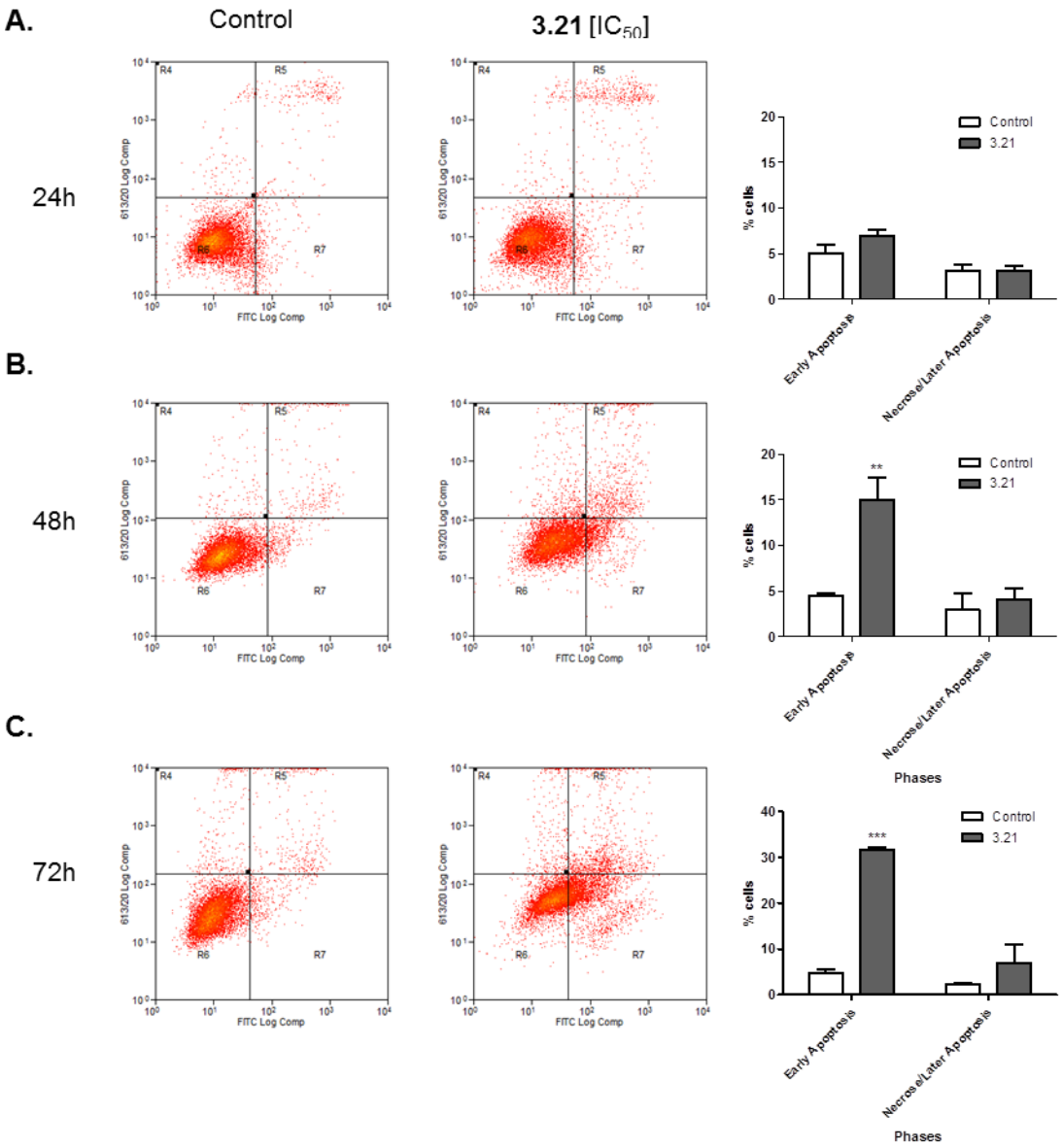

Figure 3.10 Representative histograms and plots showing the proportion of apoptotic/non-apoptotic SKOV-3 cells untreated (control condition) or treated with compound **3.21** at its IC_{50} concentration for 24 (A), 48 (B) and 72 (C) hours. Histograms depict the variation of the percentage of cells which are non-apoptotic (lower left quadrant), early apoptotic (lower right quadrant) and late apoptotic/necrotic (upper left and right quadrants). Graph bar summarises the variation of the percentage of early apoptotic cells and late apoptotic/necrotic cells. Values represent the mean ± SD of three independent experiments. After a Student's t-test, differences between treated and control groups were considered significant when $p < 0.05$ (*), $p<0.01$(**) or $p<0.001$(***), with respect to untreated cells.

3.2.2.4. Morphological analysis by Hoechst 33342 staining

Cells undergoing apoptotic cell death acquire characteristic morphological features, such as cell shrinkage, nuclear fragmentation, chromatin condensation,

zeiosis and apoptotic bodies formation [*27*, *315*]. The morphological changes in SKOV-3 cells after treatment for 48 h with compound **3.21** were assessed. To achieve this, cells were stained with Hoechst 33342, a cell-permeant nuclear fluorescent dye that binds to DNA, and were then observed by fluorescence microscopy.

As depicted in Figure 3.11, the nuclei of control cells were uniformly stained with Hoechst 33342 and did not exhibit morphological changes. In contrast, after 48 h of incubation with compound **3.21** at its IC_{50} concentration, SKOV-3 cells showed typical apoptotic features, such as cell shrinkage, chromatin condensation and formation of apoptotic bodies, together with a reduction in cell density. These morphological changes further support our hypothesis that compound **3.21** induces apoptosis in SKOV-3 cells.

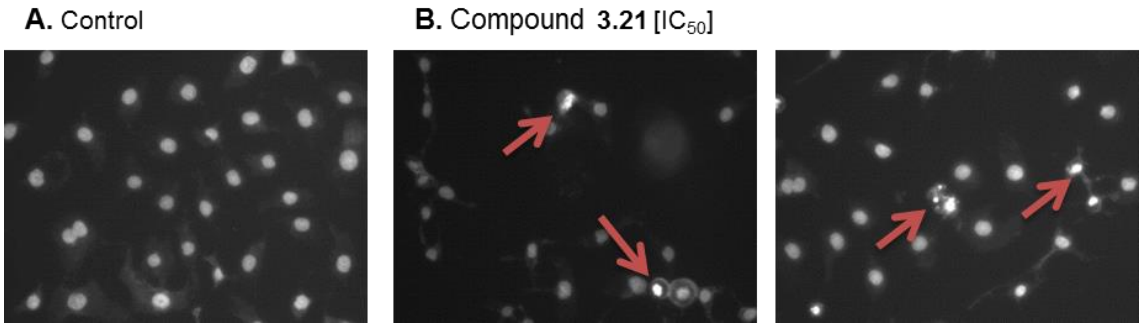

Figure 3.11 Representative fluorescence microscopic images of SKOV-3 cells (A) untreated (control) and (B) treated with compound **3.21** at its IC_{50} concentration for 48 h. Arrows represent apoptotic cells, whose morphological changes — cell shrinkage, chromatin condensation, formation of apoptotic bodies — can be observed after Hoechst 33342 staining.

3.2.2.5. Effects on apoptosis-related proteins

To elucidate the mechanism via which compound **3.21** induces apoptosis in SKOV-3 cells, we investigated its effect on the levels of apoptosis-related proteins via immunoblot analysis. Apoptosis is a highly complex process that involves an intricate cascade of molecular events, among which the activation of caspases is one of the key events in its execution [*27*]. There are two main apoptotic pathways via which caspases can be activated: the extrinsic pathway (death receptor pathway) and the intrinsic pathway (mitochondrial pathway) [*316*].

Stimulation of death receptors can result in the activation of the initiator caspase-8, which can directly cleave downstream effector caspases, such as caspase-3. This effector caspase in turn cleaves several substrates, including Poly (ADP-ribose) polymerase (PARP), generating an 89 KDa fragment that is considered a biomarker of apoptosis [*27*]. As observed in Figure 3.12A, SKOV-3 cells treated with compound **3.21** at its IC_{50} concentration for 72 h simultaneously exhibited lower levels of inactive procaspase-8 and higher levels of active cleaved caspase-8. The levels of procaspase-3 were also decreased and, accordingly, an increase in the cleavage of PARP (as demonstrated by a decrease in the levels of full-length PARP and the concurrent increase in the levels of cleaved PARP) was observed. These results strongly suggest that compound **3.21** induces apoptosis via the extrinsic pathway.

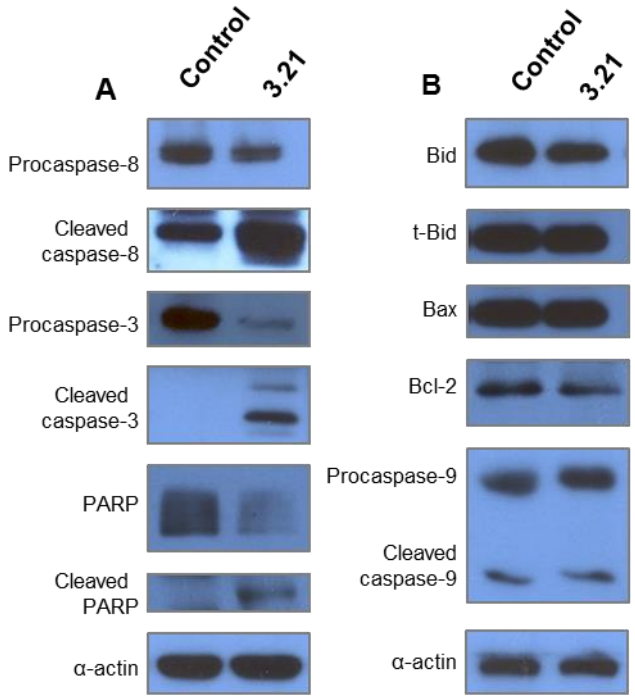

Figure 3.12 Western blot results indicating the levels of apoptosis-related proteins associated with the extrinsic (A) and the intrinsic (B) pathways on SKOV-3 cells untreated (control) and treated with compound **3.21** at its IC_{50} concentration for 72 h. α-actin was used as loading control.

The extrinsic pathway and the mitochondrial pathway are linked at different molecular levels. Active caspase-8 may result in cleavage of Bid, affording proapoptotic truncated tBid, which can in turn interact with Bcl-2 (an antiapoptotic

protein) and Bax (a proapoptotic protein), thus leading to the activation of the mitochondrial pathway [*316*]. Therefore, the effect of compound **3.21** on the levels of these proteins from the Bcl-2 family (Bid, tBid, Bax and Bcl-2) was also investigated. However, the differences in the levels of Bid, tBid, Bcl-2 and Bax proteins were not clear (Figure 3.12B). Moreover, the effect of **3.21** on the mitochondrial-pathway-initiator caspase-9 was examined and, again, the differences between the treated and the control cells were not relevant. Taken together, these findings suggest that compound **3.21** induces apoptosis in SKOV-3 cells through the activation of the extrinsic death receptor pathway, without any concomitant activation of the intrinsic mitochondrial pathway.

The tumour suppressor p53 is a key mediator of apoptosis, which regulates several physiological mechanisms by preventing the accumulation of genomic damage. Mutations in the *p53* gene are very common in human cancers and allow the uncontrolled replication of DNA leading to increased cell proliferation and genomic instability and consequently to tumour progression [*317*]. With this in mind, we tested the expression of p53 in SKOV-3 cells, which possess an established mutation in the *p53* gene [*318*, *319*]. Surprisingly, the levels of the mutant p53 protein in SKOV-3 cells after 72 h of treatment with compound **3.21** at its IC_{50} concentration were decreased, as shown in Figure 3.13A**.** It has recently been demonstrated that mutant p53 proteins do not only lead to the loss of wild-type p53 tumour-suppressor functions, but can also be responsible for an oncogenic gain-of-function. These newly described oncogenic properties of mutant p53 proteins can favour the maintenance, expansion, spread and resistance of tumour cells, thus promoting proliferation of mutant p53-expressing cells [*49*, *50*]. To confirm if the effect of compound **3.21** on the levels of the p53 protein was dependent on whether p53 was mutated, we tested the effect of **3.21** on the p53 wild-type lung cancer cell line A549 [*320*] (this cell line was chosen because, as seen in Table 3.1, compound **3.21** also showed a high antiproliferative activity in A549 cells). In contrast to our findings in SKOV-3 cells, the treatment with **3.21** in A549 cells did not seem to change the levels of the p53 expression (Figure 3.13B). Interestingly, our results indicate not only that the cell growth inhibition effect of **3.21** is observed independently of the p53 status of the cells, but also that the

compound is able both to decrease the protein levels of dysfunctional p53 (which has been described to have an oncogenic effect) and to maintain the levels of wild-type p53 (which acts as a tumour suppressor).

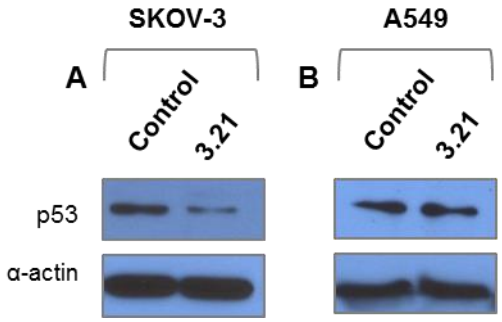

Figure 3.13 Western blot results indicating the levels of p53 protein in p53 mutant SKOV-3 (A) and p53 wild-type A549 (B) cells, untreated (control) and treated with compound **3.21** at its IC_{50} concentration for 72 h. α-actin was used as loading control.

3.2.2.6. Inhibition of Hsp90 and subsequent inhibition of the AKT/mTOR pathway

Hsp90, a member of the heat-shock protein family, acts as a regulator of apoptosis and is an attractive molecular target for developing new anticancer drugs [*57*, *321*, *322*]. Celastrol **1.26** has been heavily studied as an interesting potential Hsp90 inhibitor [*119*, *243*, *290*, *323*]. For these reasons, we investigated the effect of compound **3.21** on the levels of this protein after incubation of SKOV-3 cells with its IC_{50} concentration for 72 h. A clear decrease in the protein levels of Hsp90 was observed in treated cells (Figure 3.14). One of the most important proteins that are regulated by Hsp90 is the protein Akt [*246*], and Hsp90 has been proven to be responsible for the stabilization of its active form, pAkt [*60*]. Akt triggers the downstream mTOR, and the disruption of these pathways plays an important role in the oncogenic process [*246*, *248*]. As depicted in Figure 3.14, the treatment of SKOV-3 cells with compound **3.21** resulted in an appreciable downregulation of the protein levels of pAkt, without an effect on total Akt expression. Similarly, the levels of phosphorylated-mTOR (its active form) were lower in compound **3.21**-treated cells, while no relevant effects on the levels of the total mTOR protein were observed. These results suggest that compound **3.21** is

an Hsp90 inhibitor, and that the Akt/mTOR pathway might be involved in the downstream regulation that leads to the antiproliferative response of SKOV-3.

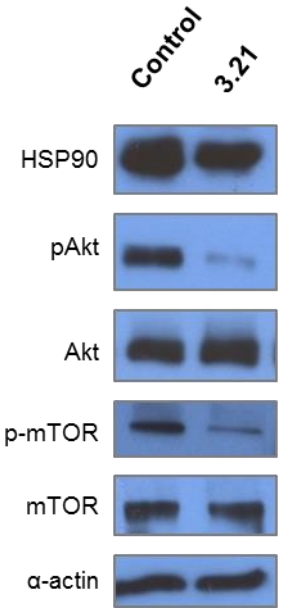

Figure 3.14 Western blot results indicating the levels of Hsp90 and Akt/mTOR pathway proteins on SKOV-3 cells untreated (control) and treated with compound **3.21** at its IC_{50} concentration for 72 hours. α-actin was used as loading control.

3.2.2.7. Evaluation of synergism

Overcoming the inevitable emergence of chemo-resistance to standard platinum-based therapy could be crucial to improve current cancer treatment efficacy [*324*, *325*]. Cisplatin is a platinum-based antineoplastic drug that is used as a chemotherapy medication to treat different types of cancer, including ovarian cancer [*326*, *327*]. Considering the important side effects and the recurrence of resistance associated with this drug, a combination therapy of cisplatin with other antineoplastic compounds is the most rational strategy to achieve improved results [*328*]. To evaluate quantitatively the combination effect of cisplatin and compound **3.21** on the growth rates of SKOV-3 cells, the combination index (CI) values between those two compounds were calculated based on the equation of Chou and Talalay [*261*, *329*]. SKOV-3 cells were treated for 72 h with both compounds (**3.21** or cisplatin) at different concentrations, separately and in combination. The combined experiments were carried out at a constant equipotency combination

ratio of $[IC_{50}]_{\mathbf{3.21}}$:$[IC_{50}]_{cisplatin}$ (1:6.7) (data not shown). Although a slight synergistic effect was observed under these conditions, extended studies at different combination ratios were performed in order to find out which ratio improved synergy the most, as proposed by Chou [*261*]. The equipotent **3.21**:cisplatin 1:3 dose ratio yielded clear synergistic effects, as seen in Table 3.4 (CI values lower than 1 indicate a synergistic effect, which is stronger the closer the value is to 0). When considering this synergistic effect between compound **3.21** and cisplatin in the inhibition of SKOV-3 proliferation, we may infer that the combination of compound **3.21** and cisplatin may be a valid strategy to increase the therapeutic efficacy of the latter.

Table 3.4 CI values for combinations of compound **3.21** and cisplatin, at a constant ratio of 1:3, in SKOV-3 cells after 72 h incubation. CI values were calculated using CompuSyn software.

3.21 (μM)	Cisplatin (μM)	1-Viability	CI
0.15	0.45	0.108	1.04695
0.3	0.9	0.166	1.37381
0.6	1.8	0.307	1.44019
1.2	3.6	0.756	0.68548
2.4	7.2	0.918	0.57503
4.8	14.4	0.959	0.71023

3.3. CONCLUSIONS

Celastrol **1.26** was used as a hit compound and a starting point for the synthesis of new celastrol derivatives. Some compounds, mainly urea derivatives, were more cytotoxic than celastrol **1.26** against tumour cell lines. Compound **3.21** proved to be a derivative with both improved antiproliferative activity and improved selectivity compared with celastrol **1.26**, and its mechanism of action was further investigated in the SKOV-3 cell line. The preliminary studies of its mechanism of action showed that compound **3.21** induced apoptosis via the extrinsic pathway, which involves the activation of caspase-8 and caspase-3 and the cleavage of PARP. Compound **3.21** also induced the downregulation of p53 in the SKOV-3 cell line, a p53-mutant cell line. The results also suggest that compound **3.21** may be an Hsp90 inhibitor and that the Akt/mTOR pathway might be involved in the

downstream signalling that leads to a decrease in SKOV-3 cell viability. Furthermore, a synergistic inhibitory effect on the proliferation of SKOV-3 cells was observed between compound **3.21** and cisplatin. Taken together, these results indicate that compound **3.21** might be a promising lead compound for anticancer drug development.

3.4. EXPERIMENTAL SECTION

3.4.1. Chemistry

3.4.1.1. General

Celastrol **1.26** and all reagents were purchased from Sigma-Aldrich. The solvents were obtained from VWR Portugal and were dried according to usual procedures. Thin layer chromatography (TLC) analyses were performed on aluminium TLC plate, silica gel coated with fluorescent indicator F_{254} (Merck, detection by UV absorption). For preparative TLC was used preparative layer plates silica gel 60 F_{254}, 1 mm (Merck, detection by UV absorption). Melting points are uncorrected and were determined on a Büchi® melting point apparatus (Model B-540). IR spectra were determined on a Fourier transform IR spectrometer. Nuclear magnetic resonance (NMR) spectra were recorded using the Bruker digital FT-NMR-Avance 400 MHz spectrometer in $CDCl_3$ or CD_3OD with tetramethylsilane (TMS) as the internal standard. Elucidation of the chemical structures was based on ^{1}H, ^{13}C and DEPT-135 NMR experiments. The chemical shifts values (δ) are given in parts per million (ppm) and the coupling constants (*J*) are presented in hertz (Hz). MS were taken on a Thermo Scientific Finnigan LXQ Mass Spectrometer, with a direct insertion probe using electrospray ionisation mass spectrometry. Elemental analysis was performed by chromatographic combustion using the Carlo Erba EA 1108 Elemental Analyser.

Derivative 1.81 — 2,3-Dihydroxy-24-nor-friedela-1,3,5(10),7-tetraen-29-oic acid

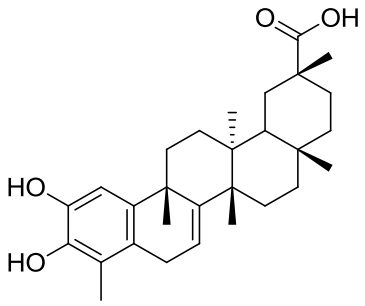

Figure 3.15 Chemical structure of compound **1.81.**

Compound **1.81** was prepared according to the literature [*119*] from celastrol **1.26** to give a white solid (91%). Mp: 267.3-269.7 °C. IR (neat) $_{vmax}$: 3426, 2924, 1695, 1451, 1376, 1283 cm^{-1}. ^{1}H NMR (400 MHz, $CDCl_3$): δ 6.72 (s, 1H, H-1), 5.68 (d, *J* = 4.9 Hz, 1H, H-7), 3.27 (dd, *J* = 20.5, 5.9 Hz, 1H, H-6b), 2.98 (d, *J* = 20.6 Hz, 1H, H-6a), 2.40 (d, *J* = 15.7 Hz, 1H), 2.16 (s, 3H, H-23), 1.27 (s, 3H), 1.18 (s, 3H), 1.14 (s, 3H), 1.04 (s, 3H), 0.60 (s, 3H) ppm; ^{13}C NMR (100 MHz, $CDCl_3$): δ 184.64 (C29), 149.98 (ArC bridge), 141.70 (ArC-OH), 141.52 (ArC-OH), 139.82 (ArC bridge), 125.87 (C4), 120.58 (C8), 117.79 (C7), 108.79 (C1), 44.27, 43.77, 40.44, 37.55, 36.81, 34.58, 34.50, 34.00, 32.91, 31.68, 30.76, 30.64, 30.22, 29.65, 28.89, 27.92, 23.03, 19.10, 11.66 ppm.

Derivative 1.82 — 2,3-Diacetoxy-24-nor-friedela-1,3,5(10),7-tetraen-29-oic acid

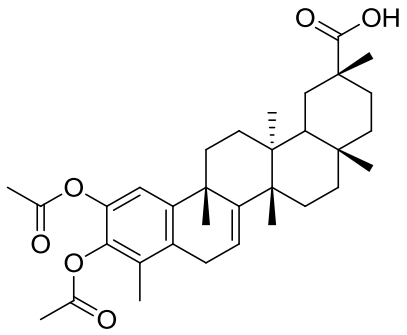

Figure 3.16 Chemical structure of compound **1.82.**

To a stirred solution of **1.81** (300.0 mg, 0.66 mmol) in dry THF (20 mL) in the presence of 4-dimethylaminopyridine (DMAP) was added acetic anhydride (0.3 mL, 3.3 mmol). The mixture was stirred for 4 h at room temperature and N_2 atmosphere. The reaction mixture was evaporated under reduced pressure to remove THF. The obtained crude was diluted with EtOAc (100 mL) and washed with water (3 × 50 mL) and brine (50 mL). The obtained organic phase was dried over anhydrous Na_2SO_4. Filtration and evaporation of solvent at reduced pressure gave a whitish solid, which was purified by preparative TLC (CH_2Cl_2/MeOH 20:1), to yield **1.82** (257.3 mg, 72%) as a white solid. Mp: 221.3-224.2 °C. IR (neat) $_{vmax}$: 3314, 2942, 1770, 1742, 1696, 1462, 1370 cm^{-1}. ^{1}H NMR (400 MHz, $CDCl_3$): δ 6.99 (s, 1H, H-1), 5.72 (d, *J* = 4.6 Hz, 1H, H-7), 3.32 (dd, *J* = 20.9, 5.9 Hz, 1H, H-6b), 3.05 (d, *J* = 20.9 Hz, 1H, H-6a), 2.38 (d, *J* = 15.6 Hz, 1H, H-19), 2.30 (s, 3H, C$\underline{H_3}$CO), 2.27 (s, 3H, C$\underline{H_3}$CO), 2.05 (s, 3H, H-23), 1.33 (s, 3H), 1.20 (s, 3H), 1.11 (s, 3H), 1.05 (s, 3H), 0.67 (s, 3H) ppm; ^{13}C NMR (100 MHz, $CDCl_3$): δ 184.20 (C29), 168.84 ($CH_3\underline{C}OO$), 168.51 ($CH_3\underline{C}OO$), 149.48, 147.65, 140.71, 138.17, 131.64, 127.91, 117.11, 116.69, 44.33, 43.87, 40.35, 37.63, 37.34, 36.84, 34.72, 34.51, 34.26, 32.80, 31.69, 30.69, 30.62, 30.21, 29.65, 28.98, 28.24, 23.06, 20.83, 20.56, 18.83, 12.72 ppm. MS (DI-ESI) (*m/z*): 559.5 $[M+Na]^+$. Anal. Calcd. for $C_{33}H_{44}O_6$: C, 73.85; H, 8.26. Found: C, 73.69; H, 8.00.

Derivative 3.3 — 20α-Isocyanato-24-nor-friedela-1,3,5(10),7-tetraen-2,3-di-yl diacetate

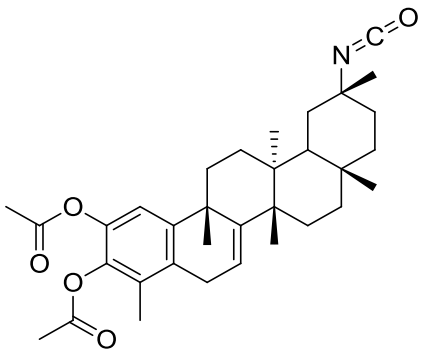

Figure 3.17 Chemical structure of compound **3.3.**

To a solution of **1.82** (200.0 mg, 0.37 mmol) in dry CH_2Cl_2 (20 mL) was added oxalyl chloride (0.19 mL, 2.24 mmol) and stirred for 4 h at room temperature and N_2 atmosphere. The mixture was concentrated to dryness under reduced pressure to yield crude **3.1**. The resulting residue **3.1** was taken up in acetone (20 mL) and transferred dropwise to a stirring aqueous solution (0.4 M) of sodium azide (60.6 mg, 0.93 mmol) for 1 h at 0 ºC. The mixture was concentrated to remove the organic solvent under reduced pressure to yield crude **3.2**. The resulting residue **3.2** was re-dissolved in toluene (10 mL) and refluxed for 2 h. The solvent was evaporated under reduced pressure to obtain the crude product that was purified by preparative TLC (PE/EtOAc 2:1), to yield **3.3** (148.4 mg, 75%) as a pale yellow solid. Mp: 191.6-193.8 °C. IR (neat) $_{vmax}$: 2930, 2253, 1769, 1459, 1368, 1209 cm^{-1}. ^1H NMR (400 MHz, $CDCl_3$): δ 7.01 (s, 1H, H-1), 5.77 (d, *J* = 4.8 Hz, 1H, H-7), 3.34 (dd, *J* = 20.9, 6.0 Hz, 1H, H-6b), 3.08 (d, *J* = 20.9 Hz, 1H H-6a), 2.31 (s, 3H, $C\underline{H_3}CO$), 2.27 (s, 3H, $C\underline{H_3}CO$), 2.07 (s, 3H, H-23), 1.41 (s, 3H), 1.36 (s, 3H), 1.23 (s, 3H), 1.05 (s, 3H), 0.99 (s, 3H) ppm; ^{13}C NMR (100 MHz, $CDCl_3$): δ 168.87 ($CH_3\underline{C}OO$), 168.55 ($CH_3\underline{C}OO$), 149.34, 147.56, 140.74, 138.21, 131.65, 127.99, 120.77 ($N\underline{C}O$), 117.07, 116.73, 55.63, 44.33, 43.84, 37.60, 37.38, 36.95, 36.90, 35.47, 34.49, 34.36, 33.41, 31.82, 30.60, 30.40, 29.00, 28.26, 23.04, 20.86, 20.84, 20.56, 12.72 ppm. MS (DI-ESI) (*m/z*): 556.4 $[M+H]^+$. Anal. Calcd. for $C_{33}H_{43}NO_5$: C, 74.27; H, 8.12; N, 2.62. Found: C, 74.05; H, 7.73; N, 2.27.

Derivative 3.4 — 2,3-Diacetoxy-6-oxo-24-nor-friedela-1,3,5(10),7-tetraen-29-oic acid

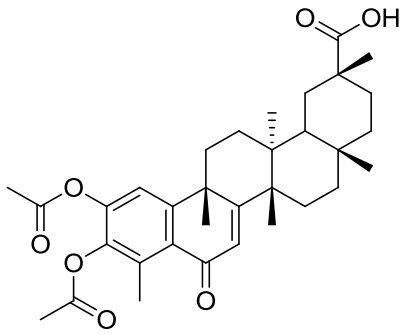

Figure 3.18 Chemical structure of compound **3.4.**

To a solution of **1.82** (550.0 mg, 1.0 mmol) in aqueous acetonitrile (1:3) (20 mL), was added $NaClO_2$ (222.6 mg, 2.0 mmol, technical grade, 80%) and *tert*-butyl hydroperoxide (0.9 mL, 5 mmol, 5.0–6.0 M solution in decane). After 1 h under stirring at room temperature, the solution was poured into sulphite solution (10% aqueous) and extracted with EtOAc (3 × 100 mL). The extract was washed with aqueous saturated solution of $NaHCO_3$ (50 mL), water (50 mL) and brine (50 mL). The obtained organic phase was dried over anhydrous Na_2SO_4, filtrated and evaporated at reduced pressure to give a yellow solid, which was purified by preparative TLC (CH_2Cl_2/MeOH 15:1), to yield **3.4** (460.7 mg, 82%) as a pale yellow solid. Mp: 275.7-277.5 °C. IR (neat) $_{vmax}$: 3210, 2943, 1778, 1715, 1647, 1456, 1370 cm^{-1}. ^{1}H NMR (400 MHz, $CDCl_3$): δ 7.21 (s, 1H, H-1), 6.28 (s, 1H, H-7), 2.54 (s, 3H, C<u>H</u>$_3$CO), 2.34 (s, 3H, C<u>H</u>$_3$CO), 2.30 (s, 3H, H-23), 1.55 (s, 3H), 1.28 (s, 3H), 1.12 (s, 3H), 1.07 (s, 3H), 0.67 (s, 3H) ppm; ^{13}C NMR (100 MHz, $CDCl_3$): δ 187.13 (C6), 183.61 (C29), 172.28, 168.19 (CH$_3$<u>C</u>OO), 168.04 (CH$_3$<u>C</u>OO), 155.11, 145.27 (Ar<u>C</u>-Ac), 139.74 (Ar<u>C</u>-Ac), 134.07, 127.81, 126.11, 117.52, 45.03, 44.26, 40.61, 40.35, 39.06, 37.66, 36.37, 34.77, 33.98, 32.68, 31.71, 30.72, 30.58, 29.78, 29.59, 28.66, 21.01, 20.92, 20.46, 19.05, 14.68 ppm. MS (DI-ESI) (*m/z*): 573.4 $[M+Na]^+$. Anal. Calcd. for $C_{33}H_{42}O_7$: C, 71.98; H, 7.69. Found: C, 71.83; H, 7.36.

Derivative 1.45 — 2,3-Dihydroxy-6-oxo-24-nor-friedela-1,3,5(10),7-tetraen-29-oic acid

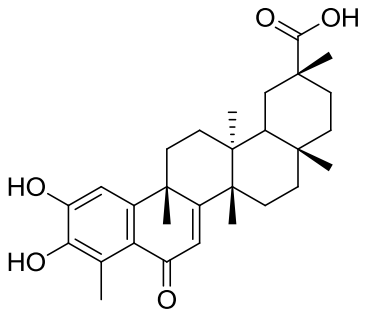

Figure 3.19 Chemical structure of compound **1.45.**

To a solution of **3.4** (55.0 mg, 0.1 mmol) in aqueous MeOH (1:4, 3 mL) and Et_3N (0.3 mL), NH_4OAc (38.5 mg, 0.5 mmol) was added. The resulting mixture was stirred at room temperature. After 2 h the mixture was concentrated and the residue was extracted with AcOEt (3 × 40 mL). The extract was washed with HCl 5% (20 mL), aqueous saturated solution of $NaHCO_3$ (20 mL), water (20 mL) and brine (20 mL). The obtained organic phase was dried over anhydrous Na_2SO_4, filtrated and evaporated at reduced pressure to give a yellow solid, which was purified by preparative TLC (CH_2Cl_2/MeOH 7:1), to yield **1.45** (23.2 mg, 50%) as a yellow solid. Mp: 332.1-333.7 °C. IR (neat) $_{vmax}$: 3181, 2941, 1697, 1633, 1571, 1455, 1378 cm^{-1}. ^1H NMR (400 MHz, $CDCl_3$, CD_3OD): δ 6.72 (s, 1H, H-1), 6.10 (s, 1H, H-7), 2.49 (s, 3H, H-23), 1.41 (s, 3H), 1.19 (s, 3H), 1.09 (s, 3H), 1.00 (s, 3H), 0.60 (s, 3H) ppm; ^{13}C NMR (100 MHz, $CDCl_3$, CD_3OD): δ 188.37 (C6), 181.46 (C29), 172.49, 151.24, 148.77 (ArC-OH), 141.41 (ArC-OH), 125.85, 125.68, 121.94, 108.27, 48.88, 44.63, 44.22, 40.10, 39.07, 37.47, 36.32, 34.76, 33.95, 32.67, 31.46, 30.68, 30.46, 29.75, 29.69, 28.49, 20.77, 18.38, 13.48 ppm. MS (DI-ESI) (*m/z*): 467.4 $[M+H]^+$. Anal. Calcd. for $C_{29}H_{38}O_5$: C, 74.65; H, 8.21. Found: C, 74.4; H, 8.00.

Derivative 3.5 — 20α-isocyanato-6-oxo-24-nor-friedela-1,3,5(10),7-tetraen-2,3-di-yl diacetate

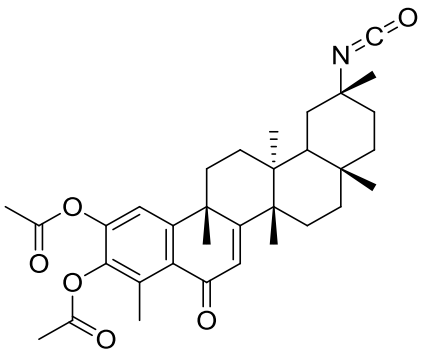

Figure 3.20 Chemical structure of compound **3.5**

Compound **3.5** was prepared from **3.4** (400.0 mg, 0.72 mmol) according to the method previously described to prepare compound **3.3** from **1.82**. The obtained residue was purified by preparative TLC (CH_2Cl_2/MeOH 10:1), to yield **3.5** (215.3 mg, 54%) as a yellow solid. Mp: 350.2-352.2 °C. IR (neat) $_{vmax}$: 2929, 2260, 1771, 1647, 1454, 1370 cm^{-1}. ^{1}H NMR (400 MHz, $CDCl_3$): δ 7.23 (s, 1H, H-1), 6.32 (s, 1H, H-7), 2.55 (s, 3H, CH_3CO), 2.35 (s, 3H, CH_3CO), 2.30 (s, 3H, H-23), 1.58 (s, 3H), 1.42 (s, 3H), 1.32 (s, 3H), 1.07 (s, 3H), 1.00 (s, 3H) ppm; ^{13}C NMR (100 MHz, $CDCl_3$): δ 187.13 (C6), 172.02, 168.22 (CH_3COO), 168.07 (CH_3COO), 154.98, 145.28 (ArC-Ac), 139.76 (ArC-Ac), 134.06, 127.91, 126.05, 121.04 (NCO), 117.52, 55.56, 44.95, 44.25, 40.61, 38.99, 37.77, 36.86, 36.41, 35.40, 34.37, 33.96, 33.55, 31.84, 30.37, 30.17, 28.67, 21.06, 20.99, 20.93, 20.45, 14.66 ppm. MS (DI-ESI) (*m/z*): 570.4 $[M+Na]^+$. Anal. Calcd. for $C_{33}H_{41}NO_6$: C, 72.37; H, 7.55; N, 2.56. Found: C, 72.63; H, 7.38; N, 2.31.

Derivative 3.7 — *N*-[2,3-Dihydroxy-6-oxo-24-nor-friedela-1,3,5(10),7-tetraen-20-yl] urea

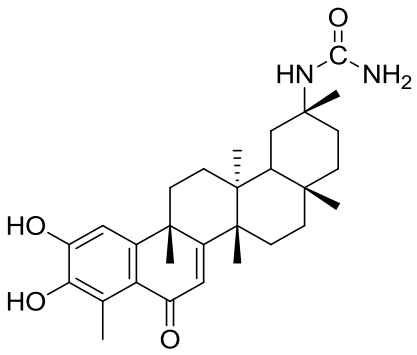

Figure 3.21 Chemical structure of compound **3.7**

Compound **3.7** was prepared from **3.5** (100.0 mg, 0.18 mmol) according to the method previously described to prepare compound **1.45** from **3.4**. The obtained residue was purified by preparative TLC (CH_2Cl_2/MeOH 10:1), to yield **3.7** (73.2 mg, 83%) as a yellow solid. Mp: 321.7-324.0 °C. IR (neat) $_{vmax}$: 3484, 3356, 3190, 2942, 1635, 1569, 1454, 1312 cm^{-1}. ^{1}H NMR (400 MHz, CD_3OD): δ 6.84 (s, 1H, H-1), 6.18 (s, 1H, H-7), 2.56 (s, 3H, H-23), 1.52 (s, 3H), 1.36 (s, 3H), 1.33 (s, 3H), 1.14 (s, 3H), 0.85 (s, 3H) ppm; ^{13}C NMR (100 MHz, CD_3OD): δ 189.81 (C6), 174.96, 161.43 ($NH\underline{C}ONH_2$), 152.65, 151.50 (ArC-OH), 143.51 (ArC-OH), 126.80, 126.33, 122.33, 109.55, 50.63, 45.90, 45.67, 41.54, 40.19, 38.34, 37.66, 37.11, 35.36, 35.04, 32.20, 31.69, 31.45, 31.00, 29.97, 29.58, 21.65, 20.69, 14.08 ppm. MS (DI-ESI) (*m/z*): 481.4 $[M+H]^+$. Anal. Calcd. for $C_{29}H_{40}N_2O_4$: C, 72.47; H, 8.39; N, 5.83. Found: C, 72.75; H, 8.49; N, 6.01.

Derivative 3.8 — *N'*-(Methyl)-*N*-[2,3-dihydroxy-6-oxo-24-nor-friedela-1,3,5(10),7-tetraen-20-yl] urea

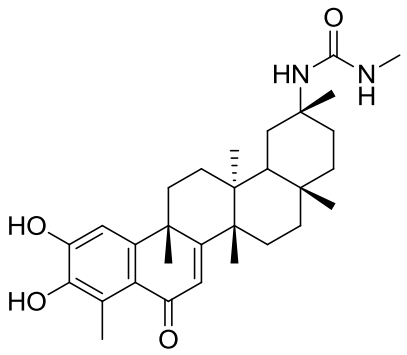

Figure 3.22 Chemical structure of compound **3.8.**

To a solution of **3.5** (100.0 mg, 0.18 mmol) in dry THF (10 mL), methylamine solution 2.0 M in THF (0.36 mL, 0.73 mmol) was added and the reaction mixture was stirred at room temperature, under an inert atmosphere. After 12 h the mixture was concentrated and the residue was extracted with AcOEt (3 × 50 mL). The extract was washed with HCl 5% (25 mL), water (25 mL) and brine (25 mL). The obtained organic phase was dried over anhydrous Na_2SO_4, filtrated and evaporated at reduced pressure to give a yellow solid, which was purified by preparative TLC (CH_2Cl_2/MeOH 10:1), to yield **3.8** (67.2 mg, 74%) as a light yellow solid. Mp: 318.2-319.6 °C. IR (neat) $_{vmax}$: 3332, 2931, 1637, 1567, 1452, 1312 cm^{-1}. ^{1}H NMR (400 MHz, CD_3OD): δ 6.81 (s, 1H, H-1), 6.16 (s, 1H, H-7), 2.56 (s, 6H, H-23, C<u>H</u>$_3$N), 1.51 (s, 3H), 1.35 (s, 3H), 1.32 (s, 3H), 1.14 (s, 3H), 0.80 (s, 3H) ppm; ^{13}C NMR (100 MHz, CD_3OD): δ 189.67 (C6), 174.68, 161.06 (NH<u>C</u>ONH), 153.36, 153.00 (ArC-OH), 144.07 (ArC-OH), 126.35, 125.99, 121.46, 108.89, 50.68, 45.85, 45.70, 41.53, 40.19, 38.32, 37.69, 37.12, 35.41, 35.13, 32.22, 31.91, 31.45, 31.03, 30.00, 29.85, 26.57, 21.69, 20.78, 14.16 ppm. MS (DI-ESI) (*m/z*): 495.4 $[M+H]^+$. Anal. Calcd. for $C_{30}H_{42}N_2O_4$: C, 72.84; H, 8.56; N, 5.66. Found: C, 72.99; H, 8.79; N, 5.84.

Derivative 3.9 — *N'*-(Methyl)-*N*-[2,3-dimethoxy-6-oxo-24-nor-friedela-1,3,5(10),7-tetraen-20-yl] urea

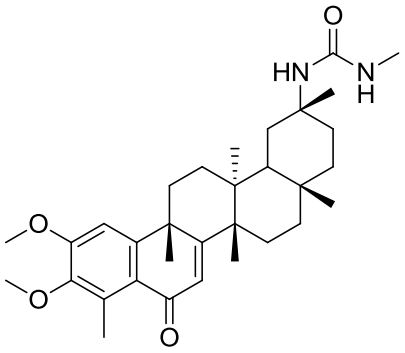

Figure 3.23 Chemical structure of compound **3.9.**

Compound **3.9** was prepared according to the literature [*330*] from **3.8** (50 mg, 0,1 mmol). The obtained crude was purified by preparative TLC (CH_2Cl_2/MeOH 20:1), to yield **3.9** (31.6 mg, 60%) as a yellow solid. Mp: 254.0-256.1 °C. IR (neat) $_{vmax}$: 3374, 2937, 1640, 1579, 1449, 1294, 1089 cm^{-1}. ^{1}H NMR (400 MHz, $CDCl_3$): δ 6.82 (s, 1H, H-1), 6.21 (s, 1H, H-7), 3.90 (s, 3H, C$\underline{H_3}$O), 3.74 (s, 3H, C$\underline{H_3}$O), 2.62 (s, 3H, H-23), 2.60 (d, *J* = 4.8 Hz, 3H, C$\underline{H_3}$N), 1.49 (s, 3H), 1.40 (s, 3H), 1.27 (s, 3H), 1.11 (s, 3H), 0.78 (s, 3H) ppm; ^{13}C NMR (100 MHz, $CDCl_3$): δ 187.47 (C6), 172.07, 158.53 (NH$\underline{C}$ONH), 155.88, 154.74, 145.94, 133.68, 125.99, 123.04, 105.67, 60.45 ($\underline{C}H_3O$), 55.73 ($\underline{C}H_3O$), 50.10, 44.89, 44.32, 40.81, 39.05, 37.51, 36.69, 36.62, 34.67, 34.31, 31.85, 31.69, 30.57, 30.08, 28.92, 28.73, 27.08, 21.03, 20.11, 14.18 ppm. MS (DI-ESI) (*m/z*): 523.5 $[M+H]^+$. Anal. Calcd. for $C_{32}H_{46}N_2O_4$: C, 75.53; H, 8.87; N, 5.36. Found: C, 75.36; H, 8.70; N, 5.44.

Derivative 3.10 — 3-Hydroxy-2-oxo-24-nor-friedela-1(10),3,5,7-tetraen-20-isocyanate

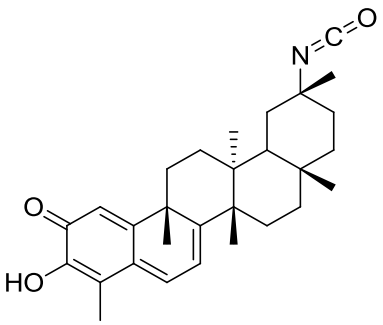

Figure 3.24 Chemical structure of compound **3.10.**

To a stirred solution of **3.3** (1.0 g, 1.9 mmol) in MeOH (100 mL) was added potassium carbonate (259.1 mg, 1.9 mmol). The mixture was stirred for 15 min in ice and N_2 atmosphere. The reaction mixture was evaporated under reduced pressure to remove MeOH. The obtained crude was diluted with AcOEt (500 mL) and washed with HCl 5% (250 mL), water (250 mL) and brine (250 mL). The obtained organic phase was dried over anhydrous Na_2SO_4. Filtration and evaporation of solvent at reduced pressure gave a dark orange solid, which was purified by preparative TLC (CH_2Cl_2/MeOH 30:1), to yield **3.10** (587.8 mg, 70%) as an orange solid. Mp: 187.5-189.2 °C. IR (neat) $_{vmax}$: 3316, 2924, 2252, 1593, 1436 cm^{-1}. ^{1}H NMR (400 MHz, $CDCl_3$): δ 7.03 (d, *J* = 6.3 Hz, 1H, H-6), 6.54 (s, 1H, H-1), 6.37 (d, *J* = 7.2 Hz, 1H, H-7), 2.22 (s, 3H, H-23), 1.45 (s, 3H), 1.42 (s, 3H), 1.27 (s, 3H), 1.07 (s, 3H), 0.95 (s, 3H) ppm; ^{13}C NMR (100 MHz, $CDCl_3$): δ 178.53 (C2), 169.98, 164.85, 146.12 (C3), 134.20 (C6), 127.59 (C5), 120.88 (N<u>C</u>O), 119.69 (C1), 118.18 (C7), 117.24 (C4), 55.63, 45.12, 44.27, 43.10, 39.45, 38.45, 36.97, 36.46, 35.33, 34.40, 33.60, 33.51, 31.86, 30.37, 30.05, 28.73, 21.84, 20.98, 10.43 ppm. MS (DI-ESI) (*m/z*): 448.3 $[M+H]^+$. Anal. Calcd. for $C_{29}H_{37}NO_3$: C, 77.82; H, 8.33; N, 3.13. Found: C, 77.99; H, 8.53; N, 3.38.

Derivative 3.11 — *N'*-Hydroxy-*N'*-methyl-*N*-[3-hydroxy-2-oxo-24-nor-friedela-1(10),3,5,7-tetraen-20-yl] urea

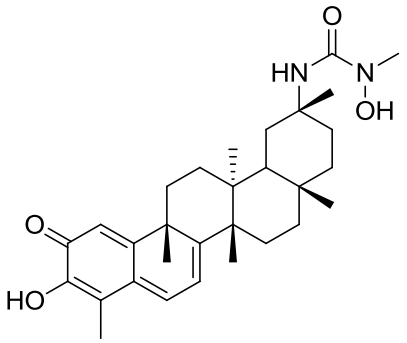

Figure 3.25 Chemical structure of compound **3.11.**

To a suspension of $NaHCO_3$ (15.0 mg, 0.18 mmol) in 5 mL acetone was added *N*-methyl-hydroxylamine hydrochloride (11.2 mg, 0.13 mmol). The reaction mixture was stirred at room temperature and a solution of compound **3.10** (40.0 mg, 0.09 mmol) in 5 mL of CH_2Cl_2 was added drop by drop. The reaction mixture was stirred for 0.5 h at room temperature diluted with water and extracted with CH_2Cl_2 (3 × 40 mL). The combined organic layer was washed with HCl 5% (20 mL), water (20 mL) and brine (20 mL). The separated organic layer was dried over anhydrous Na_2SO_4, filtered and evaporated at reduced pressure to give an orange solid. Purification of the residue on preparative TLC (CH_2Cl_2/MeOH 20:1) yielded **3.11** (37.2 mg, 84%) as an orange solid. Mp: 295.7-297.0 °C. IR (neat) $_{vmax}$: 3407, 2921, 1646, 1588, 1512, 1436 cm^{-1}. ^1H NMR (400 MHz, $CDCl_3$): δ 7.00 (d, *J* = 5.8 Hz, 1H, H-6), 6.48 (s, 1H, H-1), 6.33 (d, *J* = 6.1 Hz, 1H, H-7), 5.82 (s, 1H, N<u>H</u>), 3.01 (s, 3H, C<u>H</u>$_3$N), 2.19 (s, 3H, H-23), 1.41 (s, 3H), 1.38 (s, 3H), 1.25 (s, 3H), 1.11 (s, 3H), 0.69 (s, 3H) ppm; ^{13}C NMR (100 MHz, $CDCl_3$): δ 178.38 (C2), 171.53, 165.23, 161.06 (NH<u>C</u>O), 146.13 (C3), 134.85 (C6), 127.31 (C5), 119.45 (C1), 118.10 (C7), 117.59 (C4), 50.21, 45.34, 44.21, 43.39, 39.50, 39.42, 38.33, 36.54, 35.53, 34.33, 33.59, 31.95, 31.17, 30.48, 29.85, 29.19, 28.91, 22.02, 20.46, 10.41 ppm. MS (DI-ESI) (*m/z*): 495.3 $[M+H]^+$. Anal. Calcd. for $C_{30}H_{42}N_2O_4$: C, 72.84; H, 8.56; N, 5.66. Found: C, 72.61; H, 8.42; N, 5.89.

Synthesis of urea (3.12, 3.14–3.22) — general procedure

To a solution of **3.10** (40.0 mg, 0.09 mmol) in 5 mL of CH_2Cl_2 was added the respective amine and the reaction mixture was stirred for 4 h at room temperature and N_2 atmosphere. Water (20 mL) was added to the reaction mixture and the layers were separated. The aqueous layer was extracted with CH_2Cl_2 (3 × 40 mL), the combined CH_2Cl_2 layers were washed with water (30 mL), dried over anhydrous Na_2SO_4, filtered and the solvent was removed under vacuum to get the crude product that was purified by preparative TLC (CH_2Cl_2/MeOH 20:1) to give the urea product.

Derivative 3.12 — *N'*-Butyl-*N'*-methyl-*N*-[3-hydroxy-2-oxo-24-nor-friedela-1(10),3,5,7-tetraen-20-yl] urea

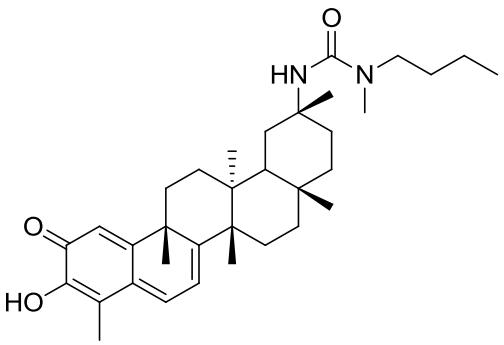

Figure 3.26 Chemical structure of compound **3.12**

Prepared according to general procedure from **3.10** (40.0 mg, 0.09 mmol) and *N*-butylmethylamine (0.02 mL, 0.18 mmol) to yield **3.12** (37.5 mg, 78%) as a dark orange powder. Mp: 267.5-269.3 °C. IR (neat) $_{vmax}$: 3351, 2926, 1639, 1591, 1514, 1436 cm^{-1}. ^{1}H NMR (400 MHz, $CDCl_3$): δ 7.01 (d, *J* = 7.0 Hz, 1H, H-6), 6.52 (s, 1H, H-1), 6.35 (d, *J* = 7.1 Hz, 1H, H-7), 3.93 (s, 1H, N<u>H</u>), 2.69 (s, 3H, C<u>H</u>$_3$N), 2.20 (s, 3H, H-23), 1.43 (s, 3H), 1.40 (s, 3H), 1.26 (s, 3H), 1.11 (s, 3H), 0.85 (t, *J* = 7.3 Hz, 3H), 0.72 (s, 3H) ppm; ^{13}C NMR (100 MHz, $CDCl_3$): δ 178.46 (C2), 170.88, 164.92, 157.13 (NH<u>C</u>O), 146.15 (C3), 134.09 (C6), 127.49 (C5), 119.69 (C1), 117.97 (C7), 117.08 (C4), 50.39, 48.46, 45.18, 44.17, 43.23, 39.45, 38.32, 36.82, 36.52, 34.42, 34.37, 33.59, 31.89, 31.70, 30.64, 30.46, 29.68, 28.99, 28.50, 22.10,

20.15, 14.08, 10.41 ppm. MS (DI-ESI) (*m/z*): 535.3 $[M+H]^+$. Anal. Calcd. for $C_{34}H_{50}N_2O_3$: C, 76.36; H, 9.42; N, 5.24. Found: C, 75.99; H, 9.28; N, 5.01.

Derivative 3.13 — *N*-[3-Hydroxy-2-oxo-24-nor-friedela-1(10),3,5,7-tetraen-20-yl] urea

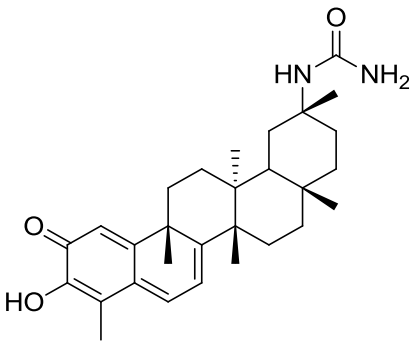

Figure 3.27 Chemical structure of compound **3.13**

Compound **3.13** was prepared from **3.10** (40.0 mg, 0.09 mmol) according to the method previously described to prepare compound **1.45** from **3.4**. The obtained residue was purified by preparative TLC (CH_2Cl_2/MeOH 20:1), to yield **3.13** (31.2 mg, 75%) as an orange solid. Mp: 246.8-248.8 °C. IR (neat) $_{vmax}$: 3478, 3335, 2922, 1654, 1578, 1433 cm^{-1}. ^{1}H NMR (400 MHz, $CDCl_3$): δ 7.01 (d, *J* = 4.8 Hz, 1H, H-6), 6.61 (s, 1H, H-1), 6.18 (d, *J* = 5.0 Hz, 1H, H-7), 5.06 (s, 2H, N<u>H</u>$_2$), 4.93 (s, 1H, N<u>H</u>), 2.26 (s, 3H, H-23), 1.33 (s, 3H), 1.30 (s, 3H), 1.15 (s, 3H), 1.03 (s, 3H), 0.51 (s, 3H) ppm; ^{13}C NMR (100 MHz, $CDCl_3$): δ 178.54 (C2), 172.15, 165.38, 159.35 (NH<u>C</u>O), 146.42 (C3), 134.78 (C6), 127.13 (C5), 119.33 (C1), 117.64 (C7), 117.57 (C4), 49.94, 45.35, 44.26, 43.42, 39.28, 38.16, 36.37, 36.16, 34.23, 33.44, 31.93, 31.34, 30.31, 29.53, 28.84, 28.71, 21.87, 20.43, 10.52 ppm. MS (DI-ESI) (*m/z*): 465.3 $[M+H]^+$. Anal. Calcd. for $C_{29}H_{40}N_2O_3$: C, 74.96; H, 8.68; N, 6.03. Found: C, 75.19; H, 8.52; N, 6.27.

Derivative 3.14 — *N'*-Methyl-*N*-[3-hydroxy-2-oxo-24-nor-friedela-1(10),3,5,7-tetraen-20-yl] urea

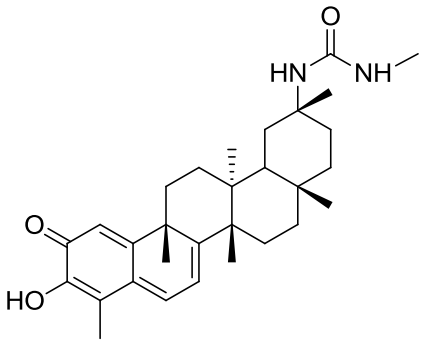

Figure 3.28 Chemical structure of compound **3.14**

Prepared according to general procedure from **3.10** (40.0 mg, 0.09 mmol) and methylamine 2 M in THF (0.18 mL, 0.36 mmol) to yield **3.14** (36.9 mg, 86%) as a dark orange powder. Mp: 256.9-260.1 °C. IR (neat) $_{vmax}$: 3367, 2950, 1628, 1595, 1558, 1438 cm^{-1}. ^{1}H NMR (400 MHz, $CDCl_3$): δ 7.01 (d, *J* = 6.3 Hz, 1H, H-6), 6.48 (s, 1H, H-1), 6.32 (d, *J* = 6.5 Hz, 1H, H-7), 4.48 (s, 1H, NH), 4.15 (s, 1H, NH), 2.61 (s, 3H, CH_3NH), 2.21 (s, 3H, H-23), 1.40 (s, 3H), 1.38 (s, 3H), 1.24 (s, 3H), 1.10 (s, 3H), 0.68 (s, 3H) ppm; ^{13}C NMR (100 MHz, $CDCl_3$): δ 178.42 (C2), 171.25, 165.14, 158.40 (NHCO), 146.17 (C3), 134.44 (C6), 127.37 (C5), 119.50 (C1), 117.93 (C7), 117.30 (C4), 50.11, 45.28, 44.30, 43.31, 39.36, 38.27, 36.56, 36.28, 34.34, 33.66, 31.91, 31.60, 30.52, 29.76, 29.16, 28.91, 27.14, 22.03, 20.20, 10.41 ppm. MS (DI-ESI) (*m/z*): 479.3 $[M+H]^+$. Anal. Calcd. for $C_{30}H_{42}N_2O_3$: C, 75.28; H, 8.84; N, 5.85. Found: C, 75.15; H, 8.50; N, 5.68.

Derivative 3.15 — *N'*-Ethyl-*N*-[3-hydroxy-2-oxo-24-nor-friedela-1(10),3,5,7-tetraen-20-yl] urea

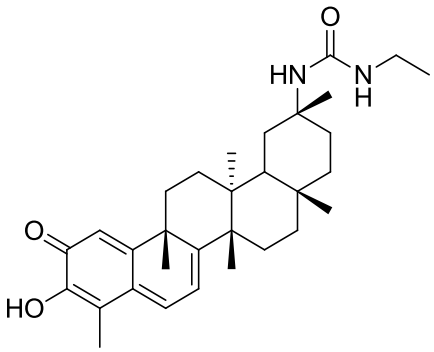

Figure 3.29 Chemical structure of compound **3.15**

Prepared according to general procedure from **3.10** (40.0 mg, 0.09 mmol) and ethylamine 2 M in THF (0.18 mL, 0.36 mmol) to yield **3.15** (33.1 mg, 75%) as a brownish powder. Mp: 209.7-212.1 °C. IR (neat) $_{vmax}$: 3356, 2946, 1642, 1587, 1547, 1512, 1436 cm^{-1}. ^{1}H NMR (400 MHz, $CDCl_3$): δ 7.02 (d, *J* = 6.6 Hz, 1H, H-6), 6.49 (s, 1H, H-1), 6.34 (d, *J* = 7.0 Hz, 1H, H-7), 4.31 (s, 1H, NH), 4.08 (s, 1H, NH), 2.20 (s, 3H, H-23), 1.41 (s, 3H), 1.39 (s, 3H), 1.25 (s, 3H), 1.10 (s, 3H), 1.02-0.97 (m, 3H, $NHCH_2CH_3$), 0.72 (s, 3H) ppm; ^{13}C NMR (100 MHz, $CDCl_3$): δ 178.47 (C2), 171.12, 165.11, 157.53 (NHCO), 146.16 (C3), 134.38 (C6), 127.43 (C5), 119.52 (C1), 117.94 (C7), 117.29 (C4), 50.11, 45.29, 44.29, 43.33, 39.40, 38.27, 36.56, 36.37, 35.18, 34.34, 33.57, 31.90, 31.60, 30.56, 29.76, 29.14, 28.95, 22.10, 20.24, 15.76, 10.42 ppm. MS (DI-ESI) (*m/z*): 493.33 $[M+H]^+$. Anal. Calcd. for $C_{31}H_{44}N_2O_3$: C, 75.57; H, 9.00; N, 5.69. Found: C, 75.39; H, 8.89; N, 5.91.

Derivative 3.16 — *N'*-Propyl-*N*-[3-hydroxy-2-oxo-24-nor-friedela-1(10),3,5,7-tetraen-20-yl] urea

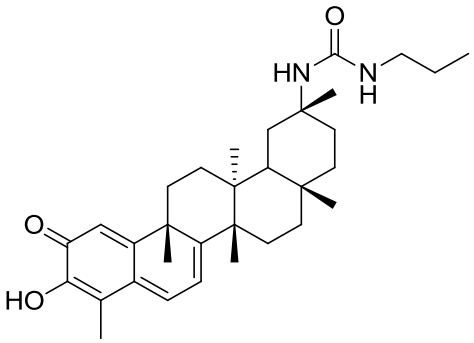

Figure 3.30 Chemical structure of compound **3.16**

Prepared according to general procedure from **3.10** (40.0 mg, 0.09 mmol) and propylamine (0.03 mL, 0.36 mmol) to yield **3.16** (18.6 mg, 41%) as an orange powder. Mp: 216.4-217.9 °C. IR (neat) $_{vmax}$: 3315, 2922, 1639, 1589, 1549, 1512, 1436 cm^{-1}. ^{1}H NMR (400 MHz, $CDCl_3$): δ 7.02 (d, *J* = 7.0 Hz, 1H, H-6), 6.52 (s, 1H, H-1), 6.35 (d, *J* = 7.2 Hz, 1H, H-7), 4.10 (s, 1H, NH), 3.91 (s, 1H, NH), 2.21 (s, 3H, H-23), 1.43 (s, 3H), 1.40 (s, 3H), 1.26 (s, 3H), 1.11 (s, 3H), 0.83 (t, *J* = 7.2 Hz, 3H, $NHCH_2CH_2\underline{CH_3}$), 0.77 (s, 3H) ppm; ^{13}C NMR (100 MHz, $CDCl_3$): δ 178.45 (C2), 171.07, 165.10, 157.64 (NH<u>C</u>O), 146.14 (C3), 134.37 (C6), 127.46 (C5), 119.53 (C1), 118.00 (C7), 117.29 (C4), 50.19, 45.28, 44.27, 43.32, 42.26, 39.41, 38.30, 36.56, 36.35, 34.34, 33.58, 31.91, 31.63, 30.58, 29.77, 29.19, 28.98, 23.60, 22.14, 20.31, 11.53, 10.41 ppm. MS (DI-ESI) (*m/z*): 507.3 $[M+H]^+$. Anal. Calcd. for $C_{32}H_{46}N_2O_3$: C, 75.85; H, 9.15; N, 5.53. Found: C, 75.66; H, 8.99; N, 5.84.

Derivative 3.17 — *N'*-Phenyl-*N*-[3-hydroxy-2-oxo-24-nor-friedela-1(10),3,5,7-tetraen-20-yl] urea

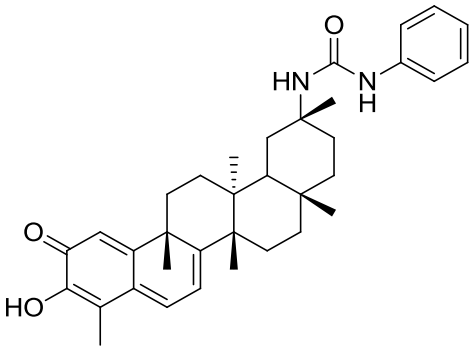

Figure 3.31 Chemical structure of compound **3.17**

Prepared according to general procedure from **3.10** (40.0 mg, 0.09 mmol) and aniline (0.02 mL, 0.22 mmol) to yield **3.17** (35.1 mg, 73%) as an orange powder. Mp: 288.0-291.2 °C. IR (neat) $_{vmax}$: 3344, 2942, 1653, 1595, 1542, 1499, 1441 cm^{-1}. ^{1}H NMR (400 MHz, $CDCl_3$): δ 7.30 (t, *J* = 7.0 Hz, 2H, Ar-H), 7.23 (d, *J* = 7.2 Hz, 2H, Ar-H), 7.01 (t-like, 2H, H-6, Ar-H), 6.33 (s, 1H, H-1), 6.26 (d, *J* = 7.0 Hz, 1H, H-7), 4.69 (s, 1H, NH), 2.22 (s, 3H, H-23), 1.42 (s, 3H), 1.29 (s, 3H), 1.17 (s, 3H), 1.09 (s, 3H), 0.46 (s, 3H) ppm; ^{13}C NMR (100 MHz, $CDCl_3$): δ 178.61 (C2), 171.84, 165.24, 155.01 (NHCO), 146.20 (C3), 139.14 (NHArC), 134.99 (C6), 129.48 (2 × ArC), 127.15 (C5), 123.39 (ArC), 120.60 (2 × ArC), 119.59 (C1), 117.73 (C7), 117.39 (C4), 50.38, 45.33, 44.43, 43.50, 39.66, 37.93, 36.58, 36.16, 34.50, 33.06, 32.01, 31.19, 30.27, 29.88, 29.08, 28.69, 21.93, 20.01, 10.46 ppm. MS (DI-ESI) (*m/z*): 541.3 $[M+H]^+$. Anal. Calcd. for $C_{35}H_{44}N_2O_3$: C, 77.74; H, 8.20; N, 5.18. Found: C, 77.48; H, 8.33; N, 5.41.

Derivative 3.18 — *N'*-(2-Amino-phenyl)-*N*-[3-hydroxy-2-oxo-24-nor-friedela-1(10),3,5,7-tetraen-20-yl] urea

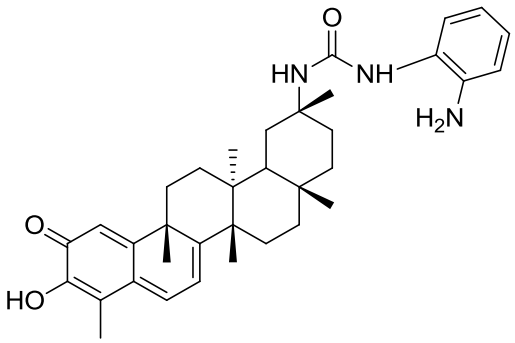

Figure 3.32 Chemical structure of compound **3.18**

Prepared according to general procedure from **3.10** (40.0 mg, 0.09 mmol) and o-phenylenediamine (19.3 mg, 0.18 mmol) to yield **3.18** (34.4 mg, 69%) as a dark orange powder. Mp: 302.6-303.9 °C. IR (neat) $_{vmax}$: 3341, 2920, 1646, 1581, 1542, 1502, 1437 cm^{-1}. ^{1}H NMR (400 MHz, $CDCl_3$): δ 7.02 (d, *J* = 6.9 Hz, 1H, Ar-H), 6.96 (d, *J* = 7.8 Hz, 1H, Ar-H), 6.73–6.64 (m, 3H, H-6, 2 × Ar-H), 6.48 (s, 1H, H-1), 6.33 (d, *J* = 7.1 Hz, 1H, H-7), 4.50 (s, 1H, NH), 3.86 (s, 2H, NH_2), 3.39 (s, 1H, NH), 2.21 (s, 3H, H-23), 1.41 (s, 3H), 1.40 (s, 3H), 1.23 (s, 3H), 1.08 (s, 3H), 0.67 (s, 3H) ppm; ^{13}C NMR (100 MHz, $CDCl_3$): δ 178.53 (C2), 170.74, 164.98, 156.55 (NHCO), 146.22 (C3), 134.86 (NHArC), 134.30 (C6), 123.42 (C5), 120.41 (2 × ArC), 119.65, 119.26, 118.02, 117.33 (C4), 116.89, 116.72, 50.57, 45.22, 44.27, 43.24, 39.37, 38.24, 36.51, 35.64, 34.31, 33.40, 31.90, 31.21, 30.44, 29.87, 29.58, 28.89, 22.07, 20.38, 10.43 ppm. MS (DI-ESI) (*m/z*): 556.3 $[M+H]^+$. Anal. Calcd. for $C_{35}H_{45}N_3O_3$: C, 75.64; H, 8.16; N, 7.56. Found: C, 75.78; H, 8.37; N, 7.65.

Derivative 3.19 — *N'*-(4-Methyl-benzyl)-*N*-[3-hydroxy-2-oxo-24-nor-friedela-1(10),3,5,7-tetraen-20-yl] urea

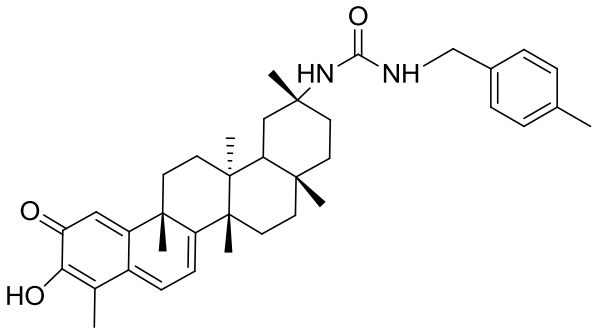

Figure 3.33 Chemical structure of compound **3.19**

Prepared according to general procedure from **3.10** (40.0 mg, 0.09 mmol) and 4-methylbenzylamine (0.05 mL, 0.36 mmol) to yield **3.19** (19.2 mg, 38%) as a brownish powder. 296.8-298.7 °C. IR (neat) $_{vmax}$: 3377, 2920, 1636, 1592, 1550, 1513, 1437 cm^{-1}. ^{1}H NMR (400 MHz, $CDCl_3$): δ 7.07–6.94 (m, 5H, 4 × Ar-H, H-6), 6.53 (s, 1H, H-1), 6.33 (d, *J* = 7.2 Hz, 1H, H-7), 4.62 (s, 1H, NH), 2.21 (s, 3H, Ar-CH_3), 2.20 (s, 3H, H-23), 1.42 (s, 3H), 1.39 (s, 3H), 1.25, (s, 3H), 1.09 (s, 3H), 0.71 (s, 3H) ppm; ^{13}C NMR (100 MHz, $CDCl_3$): δ 178.43 (C2), 170.99, 165.07, 157.51 (NHCO), 146.16 (C3), 136.95 (ArC), 136.64 (ArC), 134.32 (C6), 129.33 (2 × ArC), 127.46 (2 × ArC), 127.42 (C5), 119.64 (C1), 117.99 (C7), 117.15 (C4), 50.27, 45.20, 44.26, 44.03, 43.27, 39.47, 38.30, 36.57, 36.37, 34.24, 33.74, 31.88, 31.62, 30.56, 29.81, 29.15, 28.93, 22.02, 21.04, 20.48, 10.41 ppm. MS (DI-ESI) (*m/z*): 569.3 $[M+H]^+$. Anal. Calcd. for $C_{37}H_{48}N_2O_3$: C, 78.13; H, 8.51; N, 4.93. Found: C, 78.40; H, 8.32; N, 4.78.

Derivative 3.20 — *N'*-(2-Phenylethyl)-*N*-[3-hydroxy-2-oxo-24-nor-friedela-1(10),3,5,7-tetraen-20-yl] urea

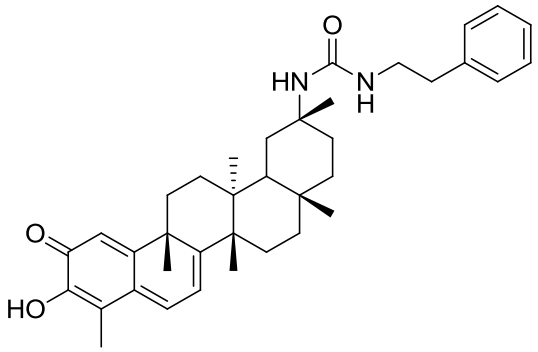

Figure 3.34 Chemical structure of compound **3.20.**

Prepared according to general procedure from **3.10** (40.0 mg, 0.09 mmol) and phenethylamine (0.05 mL, 0.36 mmol) to yield **3.20** (29.7 mg, 58%) as a brownish powder. Mp: 276.8-280.1 °C. IR (neat) $_{vmax}$: 3367, 2922, 1638, 1590, 1550, 1512, 1433 cm^{-1}. ^{1}H NMR (400 MHz, $CDCl_3$): δ 7.21-7.07 (m, 5H, Ar-H), 7.03 (d, *J* = 7.0 Hz, 1H, H-6), 6.52 (s, 1H, H-1), 6.35 (d, *J* = 7.2 Hz, 1H, H-7), 4.10 (s, 1H, NH), 2.22 (s, 3H, H-23), 1.43 (s, 3H), 1.37 (s, 3H), 1.26 (s, 3H), 1.10 (s, 3H), 0.70 (s, 3H) ppm; ^{13}C NMR (100 MHz, $CDCl_3$): δ 178.47 (C2), 170.85, 164.97, 157.32 (NHCO), 146.16 (C3), 139.25 (ArC), 134.24 (C6), 128.85 (2 × ArC), 128.65 (2 × ArC), 127.49 (C5), 126.46 (ArC), 119.69 (C1), 118.03 (C7), 117.15 (C4), 50.29, 45.24, 44.25, 43.27, 41.51, 39.42, 38.29, 36.54, 36.47, 36.18, 34.33, 33.69, 31.92, 31.52, 30.54, 29.80, 29.30, 28.99, 22.12, 20.32, 10.41 ppm. MS (DI-ESI) (*m/z*): 569.4 $[M+H]^+$. Anal. Calcd. for $C_{37}H_{48}N_2O_3$: C, 78.13; H, 8.51; N, 4.93. Found: C, 78.39; H, 8.12; N, 4.80.

Derivative 3.21 — *N'*-[2-(3-Chlorophenyl)-ethyl]-*N*-[3-hydroxy-2-oxo-24-nor-friedela-1(10),3,5,7-tetraen-20-yl] urea

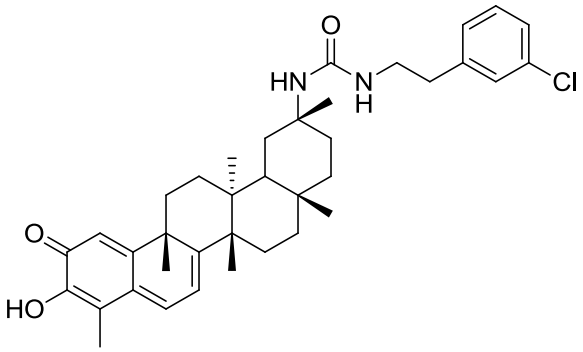

Figure 3.35 Chemical structure of compound **3.21.**

Prepared according to general procedure from **3.10** (40.0 mg, 0.09 mmol) and 2-(3-chlorophenyl)ethylamine (0.05 mL, 0.36 mmol) to yield **3.21** (21.2 mg, 40%) as a dark orange powder. Mp: 201.6-203.0 °C. IR (neat) $_{vmax}$: 3355, 2923, 1640, 1588, 1549, 1513, 1436 cm^{-1}. ^{1}H NMR (400 MHz, $CDCl_3$): δ 7.14–7.00 (m, 4H, Ar-H), 6.98 (d, *J* = 6.4 Hz, 1H, H-6), 6.50 (s, 1H, H-1), 6.35 (d, *J* = 6.9 Hz, 1H, H-7), 4.14 (s, 1H, NH), 2.21 (s, 3H, H-23), 1.43 (s, 3H), 1.37 (s, 3H), 1.25 (s, 3H), 1.10 (s, 3H), 0.69 (s, 3H) ppm; ^{13}C NMR (100 MHz, $CDCl_3$): δ 178.47 (C2), 170.84, 165.02, 157.23 (NHCO), 146.15 (C3), 141.45 (ArC), 134.38 (C6), 134.28 (ArC-Cl), 129.93 (ArC), 128.99 (ArC), 127.50 (C5), 127.10 (ArC), 126.62 (ArC), 119.63 (C1), 118.08 (C7), 117.23 (C4), 50.34, 45.25, 44.26, 43.27, 41.21, 39.44, 38.26, 36.54, 36.22, 36.14, 34.34, 33.72, 31.92, 31.50, 30.52, 29.83, 29.33, 28.97, 22.09, 20.32, 10.42 ppm. MS (DI-ESI) (*m/z*): 603.3 $[M+H]^+$. Anal. Calcd. for $C_{37}H_{47}ClN_2O_3$: C, 73.67; H, 7.85; N, 4.64. Found: C, 73.53; H, 7.68; N, 4.53.

Derivative 3.22 — *N'*-(4-Fluoro-benzyl)-*N*-[3-hydroxy-2-oxo-24-nor-friedela-1(10),3,5,7-tetraen-20-yl] urea

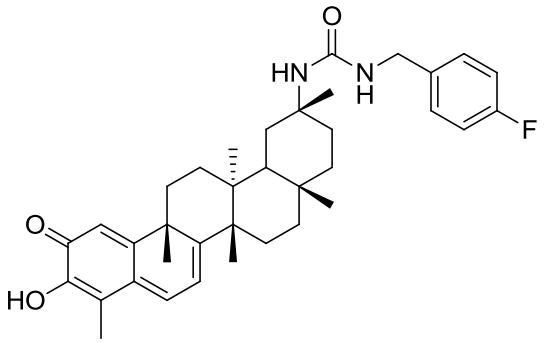

Figure 3.36 Chemical structure of compound **3.22**

Prepared according to general procedure from **3.10** (40.0 mg, 0.09 mmol) and 4-fluorobenzylamine (0.04 mL, 0.36 mmol) to yield **3.22** (42.0 mg, 82%) as an orange powder. Mp: 217.6-219.7 °C. IR (neat) $_{vmax}$: 3366, 2922, 1639, 1588, 1550, 1437, 1437 cm^{-1}. ^{1}H NMR (400 MHz, $CDCl_3$): δ 7.17–7.10 (m, 2H, Ar-H), 7.02 (d, *J* = 6.8 Hz, 1H, H-6), 6.87 (t, *J* = 8.3 Hz, 2H, Ar-H), 6.48 (s, 1H, H-1), 6.33 (d, *J* = 7.0 Hz, 1H, H-7), 4.72 (s, 1H, N<u>H</u>), 4.21-4.12 (m, 3H, N<u>H</u>, NHC<u>H</u>$_2$), 2.21 (s, 3H, H-23), 1.41 (s, 3H), 1.38 (s, 3H), 1.24 (s, 3H), 1.09 (s, 3H), 0.68 (s, 3H) ppm, ^{13}C NMR (100 MHz, $CDCl_3$): δ 178.44 (C2), 170.86, 165.03, 163.27 (ArC-F), 160.83 (ArC-F), 157.39 (NH<u>C</u>O), 146.17 (C3), 135.41 (ArC), 134.36 (C6), 129.16 (ArC), 129.08 (ArC), 127.45 (C5), 119.57 (C1), 118.04 (C7), 117.28 (C4), 115.56 (ArC), 115.34 (ArC), 50.38, 45.21, 44.24, 43.64, 43.24, 39.41, 38.29, 36.54, 36.25, 34.29, 33.66, 31.89, 31.54, 30.53, 29.78, 29.24, 28.92, 22.05, 20.40, 10.42 ppm. MS (DI-ESI) (*m/z*): 573.3 $[M+H]^+$. Anal. Calcd. for $C_{36}H_{45}FN_2O_3$: C, 75.49; H, 7.92; N, 4.89. Found: C, 75.81; H, 8.01; N, 5.06.

3.4.2. Biology

3.4.2.1. Reagents and cells

All cell lines were obtained from the American Type Culture Collection (ATCC, USA). Dulbecco's Modified Eagle's Medium (DMEM) High Glucose with L-Glutamine, Phosphate buffered saline (PBS) and L-glutamine were purchased from Biowest. DMEM, no glucose, no glutamine, no phenol red; Penicillin (10.000 units/mL)/Streptomycin (10.000 µg/mL) (P/S) Solution, MEM-EAGLE Non Essential Aminoacids 100 ×, Fetal bovine serum (FBS), protease inhibitor cocktail, phosphatase inhibitor cocktail and Pierce™ BCA Protein Assay Kit were obtained from Thermo Fisher Scientific. 3-(4,5-Dimethylthiazol-2-yl)-2,5-diphenyltetrazolium bromide (MTT) powder was obtained from Applichem Panreac. DMSO, Hoechst 33342, Propidium Iodide (PI), sodium bicarbonate solution 7.5%, glucose solution 45%, Igepal® CA-630, Trizma Base, Ethylenediaminetetraacetic acid (EDTA), Triton X-100, Sodium Deoxycholate and Tween-20® were purchased from Sigma-Aldrich Co. Human insulin solution 10 mg/mL was obtained from SantaCruz Biotechnology. Sodium pyruvate solution 100 mM, ECL Western Blotting Detection Kit Reagent and Trypsin/EDTA (0.05%/0.02%) were obtained from Biological Industries. Annexin V-FITC was purchased from Bender MedSystems. Hydrophobic Polyvinylidene Fluoride (PVDF) and Western Blotting Detection Kit Reagent (Millipore) were purchased from Merck Millipore.

Primary antibody against α-actin was purchased from MP Biomedicals. Primary antibodies against caspase-3, cleaved caspase-3, caspase-8, caspase-9, Hsp90, mTOR, p-mTOR, Akt and pAkt were obtained from Cell Signalling Technology. Primary antibodies against Bax, Bcl-2, p-JNK, p-JNK, were purchased from SantaCruz Biotechnology. Primary antibodies against PARP, Bid and cytochrome c were obtained from BD Pharmingen, and primary antibody against p53 was obtained from Merck Millipore. Secondary antibody HRP-conjugated anti-mouse was obtained from Dako and secondary antibody HRP-conjugated anti-rabbit were obtained from Amersham Biosciences.

3.4.2.2. Compounds

Celastrol **1.26** and its derivatives were stored at -20 ºC as stock solutions of 10 mM in DMSO. The stock solutions were diluted in culture medium just before the start of each experiment in order to obtain the working solutions with the final concentrations of the compounds. Final concentration of DMSO was lower than 0.5% in all conditions assayed. Cisplatin was obtained from Sigma Aldrich.

3.4.2.3. Cell culture

A549, MDAMB-231, MIA PaCa-2, SKBR-3 and SKOV-3 cells were grown in DMEM High Glucose with L-Glutamine supplemented with 10% (V/V) FBS and 1% (V/V) P/S solution. MCF-7 cells were maintained in DMEM without phenol red supplemented with 10% (V/V) FBS, 0.1% (V/V) P/S solution, 2 mM L-glutamine, 1 mM sodium pyruvate, 10 mM glucose, MEM-EAGLE Non Essential Aminoacids 1 × and 0.01 mg/mL Human Insulin. BJ cells were cultured in DMEM High Glucose supplemented with 10% (V/V) FBS, 1% (V/V) P/S solution, 2 mM L-Glutamine and 1 mM Sodium Pyruvate. All cells were routinely maintained as a monolayer culture and incubated under standard culture conditions (humidified atmosphere with 5% CO_2 at 37 °C).

3.4.2.4. Cell viability assay

The viability of all cell lines in the presence of different concentrations of the compounds was determined by the MTT assay. For this assay, 2×10^3 A549, MIA PaCa-2, SKOV-3 cells or 10×10^3 BJ, SKBR-3, MDAMB-231 cells per well were seeded in 96 well plates and allowed to attach for 24 h. Then, growth medium was changed in every well and the compounds were added at increasing concentrations in triplicate. After 72 h of incubation, the supernatant in each well was replaced by 100 µL of filtered MTT solution (0.5 mg/mL of growth medium), and the plates were incubated again for 1 h at 37 ºC. The MTT solution was then removed, and the formazan crystals formed were dissolved in 100 µL of DMSO. The absorbance at 550 nm in all wells was immediately read on an ELISA plate

reader (Tecan Sunrise MR20-301, TECAN) as an indicator of the cell viability. Subsequently, the IC_{50} values were calculated by non-linear regression using Graphpad Prism 5 software. To obtain the mean ± standard error of mean (SEM) values of IC_{50}, three independent experiments were performed.

3.4.2.5. Cell-cycle assay

SKOV-3 cells were seeded with 2 mL of medium at a density of 4×10^4 cells per well in 6 well plates, and incubated at 37 ºC for 24 h. Cells were then treated with compound **3.21** at the specified concentrations for 24, 48 and 72 h. Following the respective period of incubation, cells were harvested by mild trypsinization, washed twice with PBS, collected by centrifugation and resuspended with Tris-Buffered Saline (TBS) containing 50 mg/mL PI, 10 mg/mL DNase-free RNase and 0.1% Igepal® CA-630. In order to stain the cells with the PI, this suspension was incubated for 1 h at 4 ºC and protected from the light. Subsequently the PI content in each cell was assessed by flow cytometry using a Fluorescence-Activated Cell Sorter (FACS). FACS analysis was carried out at 488 nm in an Epics XL flow cytometer (Coulter Corporation, Hialeah, FL). Data from 1×10^4 cells were collected and analysed using the multicycle software (Phoenix Flow Systems, San Diego, CA). Experiments were repeated three times with two replicates per experiment.

3.4.2.6. Apoptosis assay

SKOV-3 cells were seeded, treated, incubated and harvested as described above for the cell-cycle analysis assay. After centrifugation, the cells were resuspended in 95µL of binding buffer (10 mM HEPES/NaOH, pH 7.4, 140 mM NaCl, 2.5 mM $CaCl_2$). 3 µL of Annexin-V FITC conjugate (1 mg/mL) was then added to the cell suspension, which was then incubated for 30 min protected from the light. Shortly before FACS analysis, 500 µL more of binding buffer and 20 µL of PI solution (1 mg/mL) were added to each cell suspension. FACS analysis was performed at 488 nm in an Epics XL flow cytometer (coulter Corporation, Hialeah, FL). Data from 1×10^4 cells were collected and analysed using the multicycle

software (Phoenix Flow Systems, San Diego, CA). Experiments were repeated three times with two replicates per experiment.

3.4.2.7. Hoechst 33342 staining

SKOV3 cells were seeded at a density of 4×10^4 cells per well in 6-well plates, and incubated at 37 ºC for 24 h. Cells were then treated with compound **3.21** at its IC_{50} concentration for 48 h. The culture medium was removed and cells were washed twice with PBS. The cells were then stained with 500 µL of Hoechst 33342 solution (1 µg/mL in PBS) for 10 min at 37 ºC and protected from light. The morphological modifications were analysed by fluorescence microscopy using a fluorescence microscope (DMRB Leica Microssystems, Weltzar Germany) with a DAPI filter.

3.4.2.8. Preparation of total protein extract

SKOV-3 cells (4×10^4 cells/well) were seed in 6-well plates with 2 mL of medium, and incubated at 37 ºC for 24 h prior to the addition of the compound **3.21** at its IC_{50} concentration. After 72 h of incubation, the cell monolayer was washed twice with ice-cold PBS. The cells were then incubated for 30 min in ice-cold lysis buffer (20 mM Trizma Base pH 7.5, 1 mM dithriothreitol, 1 mM EDTA, 0.0002% Triton X-100, 0.5 mM sodium deoxycholate, 0.4 mM PMSF, 1% protease inhibitor cocktail and 1% phosphatase inhibitor cocktail). Subsequently, the cells were scraped, and the resulting cell extracts were sonicated and centrifuged at 16000 g for 10 min at 4 ºC. Supernatants were kept and their protein content was quantified by the BCA assay kit.

3.4.2.9. Western blot analysis

A volume of protein extract corresponding to 30 µg of protein was loaded on 8% or 15% sodium dodecyl sulfate (SDS)-polyacrylamide gels. The proteins were then separated through electrophoresis, transferred to PVDF membranes and blocked with PBS containing 0.1% Tween-20® (PBST 0.1%) and 5% non-fat milk

during 1 h at room temperature. Afterwards, the membranes were blotted with primary specific antibodies for 1 h at room temperature (α-actin) or overnight at 4 ºC (all the remaining primary antibodies). Then, the membranes were washed with PBST 0.1% and incubated with the appropriate secondary antibody (anti-mouse or anti-rabbit) for 1 h at room temperature. Following this incubation, the membranes were washed again with PBST 0.1%. Blots were developed using a chemiluminescence Western Blotting Detection Kit and autoradiography film.

3.4.2.10. Synergy study

SKOV-3 cells were seeded in 96-well plates as described above for cell viability assays. After 24 h, the cells were treated with **3.21**, cisplatin, or both compounds at the same time at different concentrations with a constant ratio between them. After 72 h of incubation the cell viability was assessed using the MTT assay following the above-mentioned procedure. The CompuSyn software (ComboSyn, Inc., Paramus, NJ, USA) was used to analyse the effect of compound **3.21**, cisplatin and a combination of both. The synergy between both compounds was quantified by determining the Combination Index (CI). CI values below 1, equal to 1 and above 1 represent synergism, additivity and antagonism, respectively.

3.4.2.11. Data analysis and statistical methods

All conditions were performed at least in triplicate. Statistical analyses were performed using Graphpad Prism 5 software. Control and treated conditions were compared using two-tailed independent sample Student's t-tests. Results were considered statistically significant if $p < 0.05$ (*), $p < 0.01$ (**) or $p < 0.001$ (***).

CHAPTER IV

DESIGN, SYNTHESIS AND BIOLOGICAL EVALUATION OF NOVEL C(29) CARBAMATE CELASTROL DERIVATIVES AS POTENT AND SELECTIVE CYTOTOXIC COMPOUNDS

Sandra A.C. Figueiredo, Jorge A.R. Salvador, Roldán Cortés, Marta Cascante

Design, synthesis and biological evaluation of novel C(29) carbamate celastrol derivatives as potent and selective cytotoxic compounds

European Journal of Medicinal Chemistry, 2017, *Article in press*

http://dx.doi.org/10.1016/j.ejmech.2017.08.058

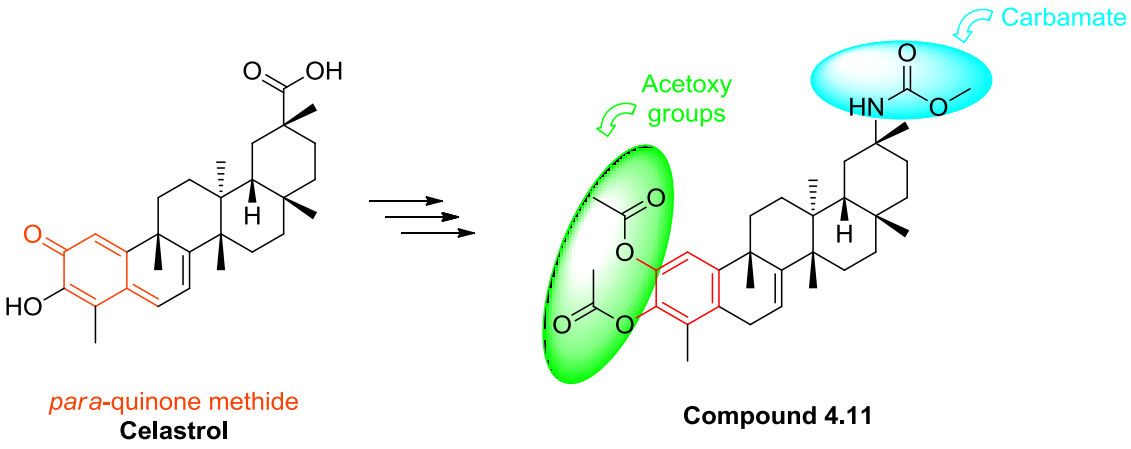

Highlights

- A series of novel C(29) carbamate celastrol derivatives was designed and synthesised.
- Some of the carbamate derivatives showed potent anticancer activity against tumour cell lines.
- A carbamate diacetate derivative, compound **4.11**, was the most active and selective.
- Compound **4.11** induced apoptosis via the extrinsic pathway in ovarian cancer cells.
- Derivative **4.11** is a potential new agent for combinatorial drug therapy for ovarian cancer.

4. CHAPTER IV

Design, synthesis and biological evaluation of novel C(29) carbamate celastrol derivatives as potent and selective cytotoxic compounds

4.1. INTRODUCTION

Triterpenoids comprise a large and structurally diverse class of secondary metabolites that are distributed ubiquitously in plants [*331*, *332*]. The success of these natural products in cancer drug discovery is increasing continuously, as reflected by the exponential growth of scientific publications and patents in this field [*297–299*, *333–338*]. Celastrol **1.26** is a natural QM triterpenoid that was isolated from the traditional Chinese medicinal plant *Tripterygium wilfordii Hook F*., the extracts of which have been used in the treatment of autoimmune, inflammatory and neurodegenerative diseases, as well as in the treatment of many types of cancer [*339–341*]. Although celastrol **1.26** itself has a remarkable anticancer activity on various cancer cells [*235*, *239*, *342*], its pharmacological properties can be further optimised through the generation of more potent derivatives, as demonstrated in other studies [*113*, *287*].

Recently, we synthesised a C(29) urea derivative of celastrol with an intact QM moiety that displayed both increased cytotoxicity and improved selectivity in a variety of human tumour cell lines [*343*]. Thus, modifications of celastrol at C(29) seem to be a valid strategy for obtaining highly active and tumour-cell-selective derivatives. However, while some of the articles on this subject reported to date consider the reactive QM group of celastrol **1.26** as the active moiety [*107*, *119*, *242*], others consider that modifications on the A/B-rings produce celastrol derivatives that are better candidate drugs for treating cancer [*108*, *287*, *292*, *294*]. Therefore, further research on the role of the QM group in the anticancer activity of the derivatives is warranted. Moreover, there is a growing interest in carbamate derivatives because of their application in medicinal chemistry. The carbamate functionality is normally associated with chemical stability and increased permeability across cellular membranes [*344*]. These properties have been

exploited in drug design, which made the carbamate group the key structural element of several approved drugs (e.g., entinostat [*345*], mitomycin C [*346*], irinotecan [*347*] and capecitabine [*348*]).

In this study, we designed, synthesised and evaluated a series of novel carbamate derivatives of celastrol as part of our continued effort to identify natural product derivatives with more potent anticancer activities and higher selectivity. In addition, we established a more consistent SAR study on the effect of the A/B-ring modifications of celastrol derivatives on anticancer activity. The most active compound according to viability assays was further evaluated to study its effect on colony formation capacity, cell-cycle progression, induction of apoptosis and the expression levels of apoptosis-related proteins. Possible synergistic antitumour effects of the compound and carboplatin were also evaluated in ovarian cancer cells.

4.2. RESULTS AND DISCUSSION

4.2.1. Chemistry

The synthetic routes of celastrol derivatives are outlined in Scheme 4.1–4.3. Nuclear magnetic resonance (NMR) was used to elucidate the chemical structures based on ^{1}H, ^{13}C and DEPT-135 NMR experiments. The structures and high purity of all compounds were confirmed by determination of the melting point (Mp), infrared spectroscopy (IR), mass spectrometry (MS) and elemental analyses.

In a previous work, we described an efficient method for the synthesis of the isocyanate compounds **3.3**, **3.10** and **3.5** [*343*]. In the present study, to improve the activity of celastrol **1.26**, we synthesised new carbamate derivatives from isocyanates. The carbamate group is also a key structural motif because of its ability to form hydrogen bonds as both a hydrogen bond donor and acceptor with water, thus contributing to the overall water solubility and bioavailability. Therefore, the novel C(29) carbamate celastrol derivatives **4.1–4.6** (Scheme 4.1), **4.7**, **4.8** (Scheme 4.2) and **4.11** (Scheme 4.3) were prepared by nucleophilic addition of

alcohols to isocyanates catalysed by a base (trimethylamine), in good yields (77%–88%).

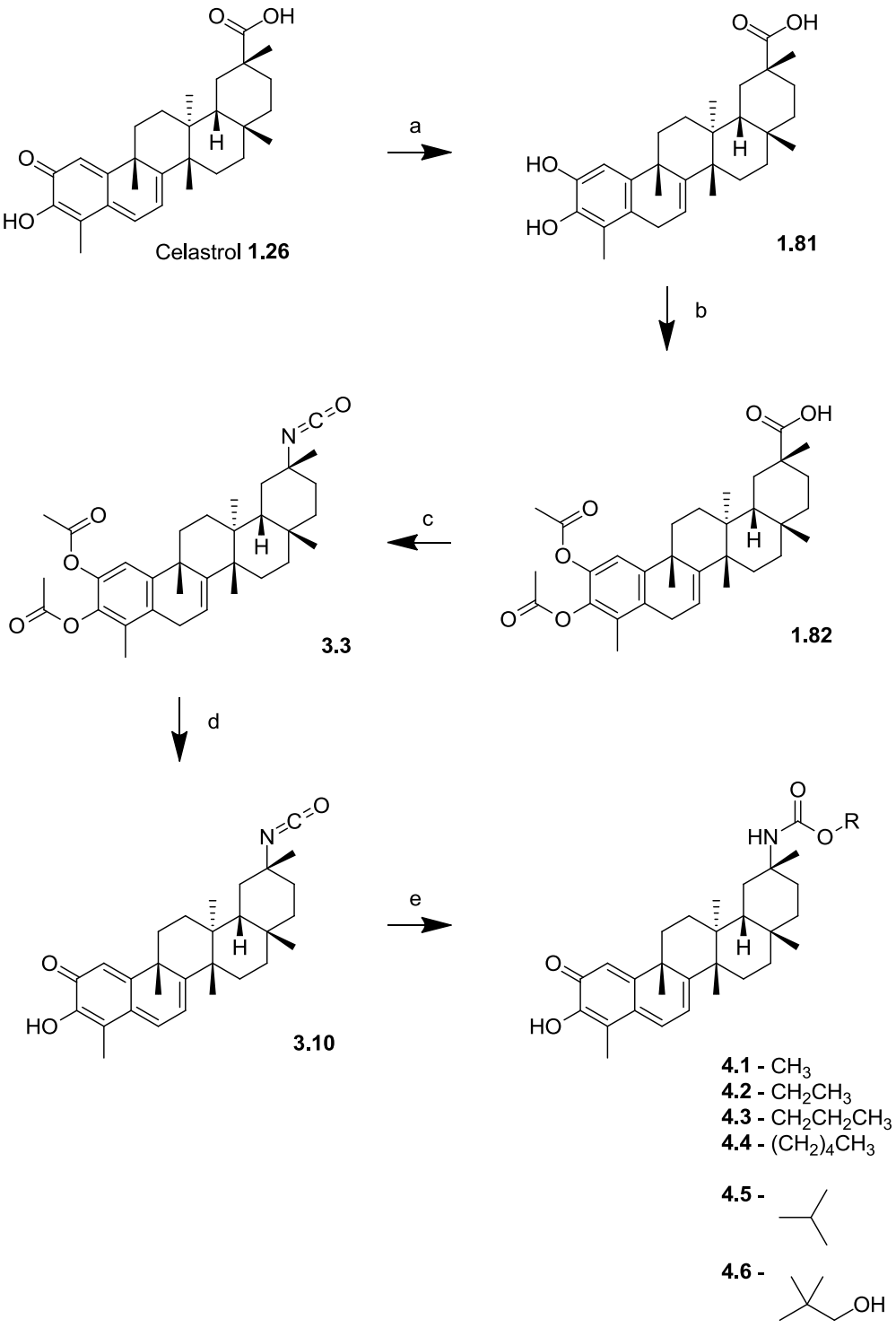

Scheme 4.1 Synthesis of celastrol derivatives **4.1–4.6.** *Reagents and conditions:* a) $NaBH_4$, MeOH, R.T., 10 min; b) $(CH_3CO)_2O$, DMAP, THF, R.T., N_2, 4 h; c) $(COCl)_2$, CH_2Cl_2, R.T., N_2, 4 h; NaN_3, H_2O, acetone, 0 ºC, 1 h; in toluene, reflux, 2 h; d) K_2CO_3, MeOH, 0 ºC, N_2, 15 min; e) ROH, Et_3N, R.T., N_2, 12 **h.**

The introduction of the carbamate function in compounds **4.1–4.11** was confirmed by the specific signal for the proton on nitrogen, a singlet around 4.40 ppm observed in the ^{1}H NMR spectra (Figure 4.1), and for the carbamate carbonyl carbon around 155 ppm observed in the ^{13}C NMR spectra (Figure 4.2). The remaining spectra signals for the series of carbamate derivatives **4.1–4.6** (Scheme 4.1 and Figure 4.2) were similar to those of the parent celastrol **1.26** [*154*].

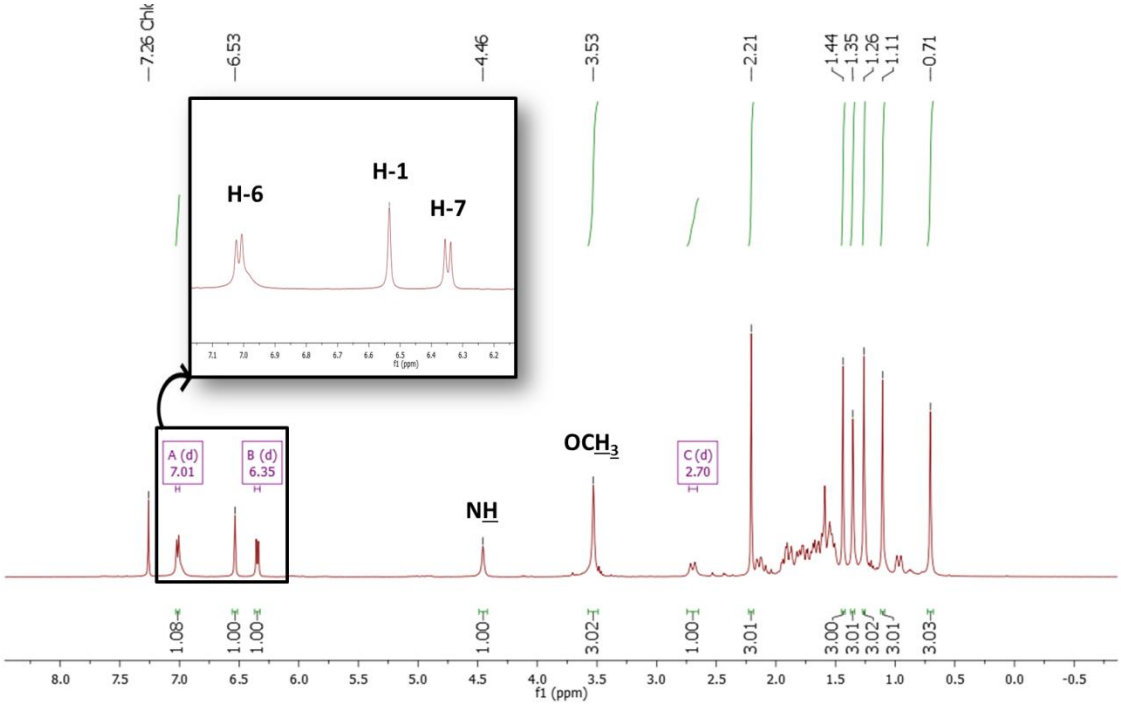

Figure 4.1 ^{1}H NMR spectrum of compound **4.1.**

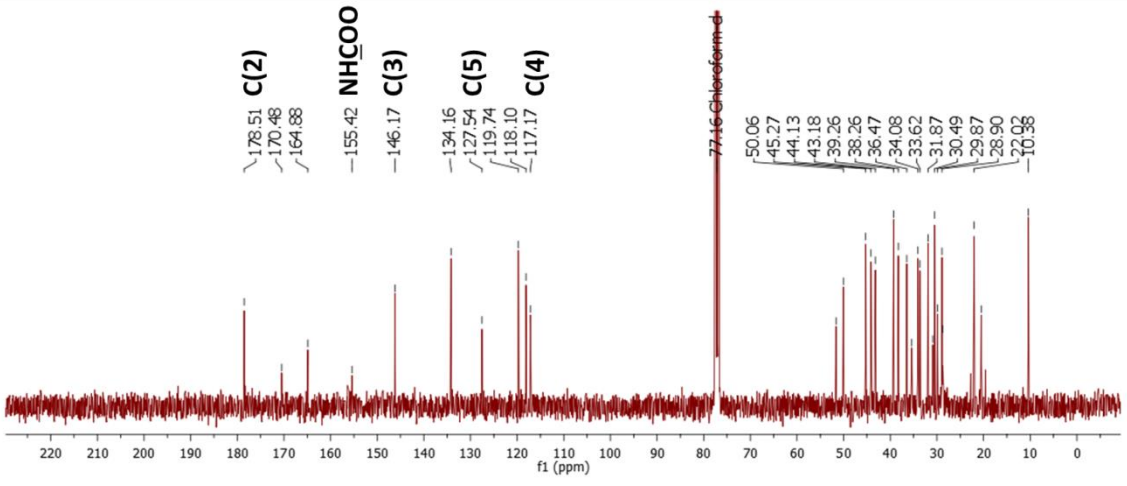

Figure 4.2 ^{13}C NMR spectrum of compound **4.1.**

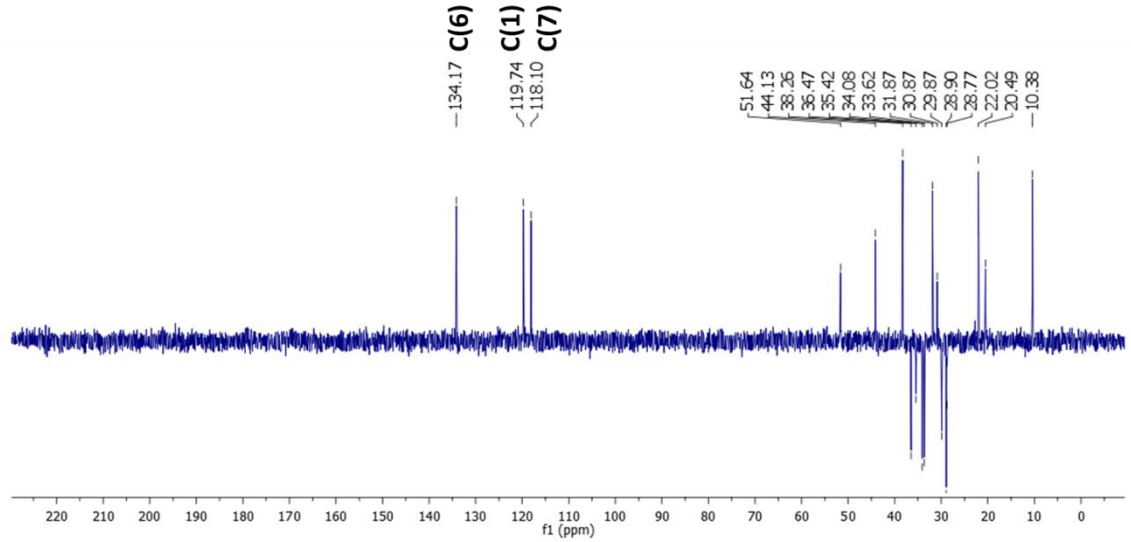

Figure 4.3 DEPT-135 NMR spectrum of compound **4.1.**

Compounds **4.7** and **4.8** (Scheme 4.2) were structurally diversified by methylation in the presence of anhydrous potassium carbonate and methyl iodide, and afforded celastrol analogues **4.9** and **4.10**.

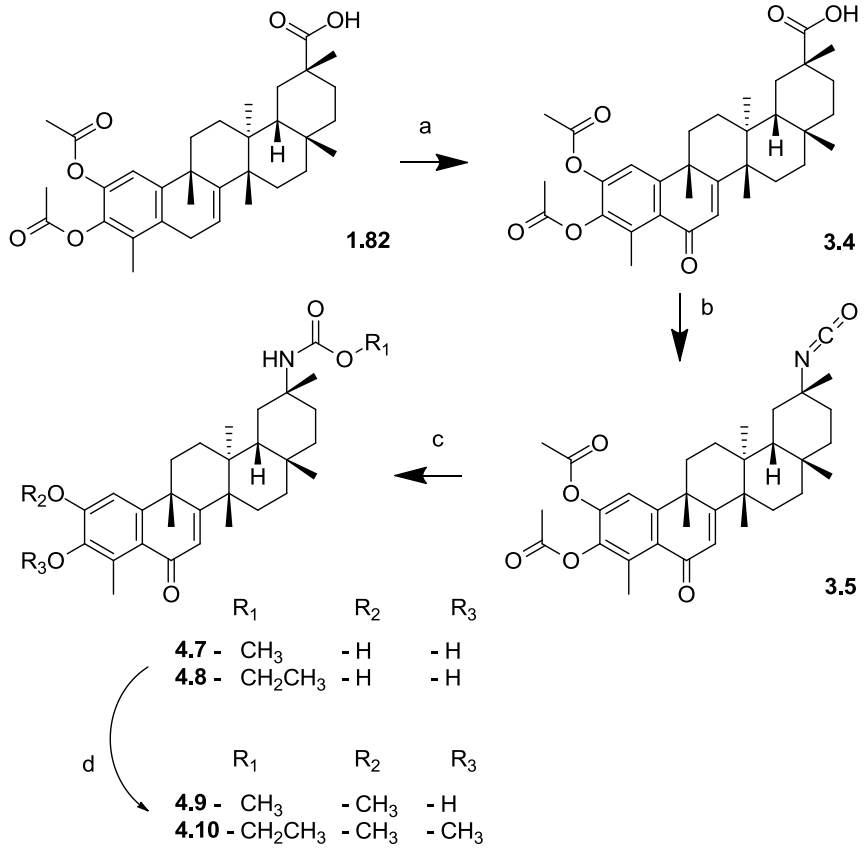

Scheme 4.2 Synthesis of celastrol derivatives **4.7–4.10**. *Reagents and conditions*: a) *t*-BuOOH, $NaClO_2$, aq. CH_3CN 1:3, R.T., 1 h; b) $(COCl)_2$, CH_2Cl_2, R.T., N_2, 4 h; NaN_3, H_2O, acetone, 0 ºC, 1 h; in toluene, reflux, 2 h; c) ROH, Et_3N, R.T., N_2, 12 h; d) CH_3I, K_2CO_3, DMF, R.T., N_2, 6 h.

The spectra signals for the triterpenoic skeleton in the series of compounds **4.7–4.10** were similar to those of the 6-oxo derivatives (Figure 4.4 and Figure 4.5) [*343*].

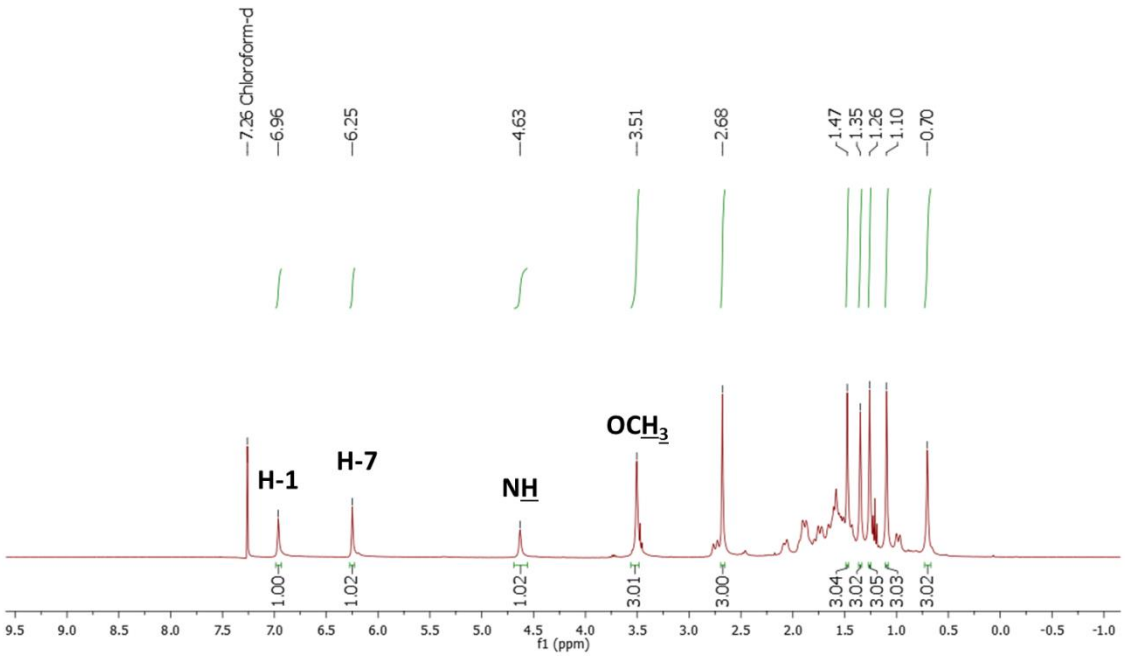

Figure 4.4 ^{1}H NMR spectrum of compound **4.7.**

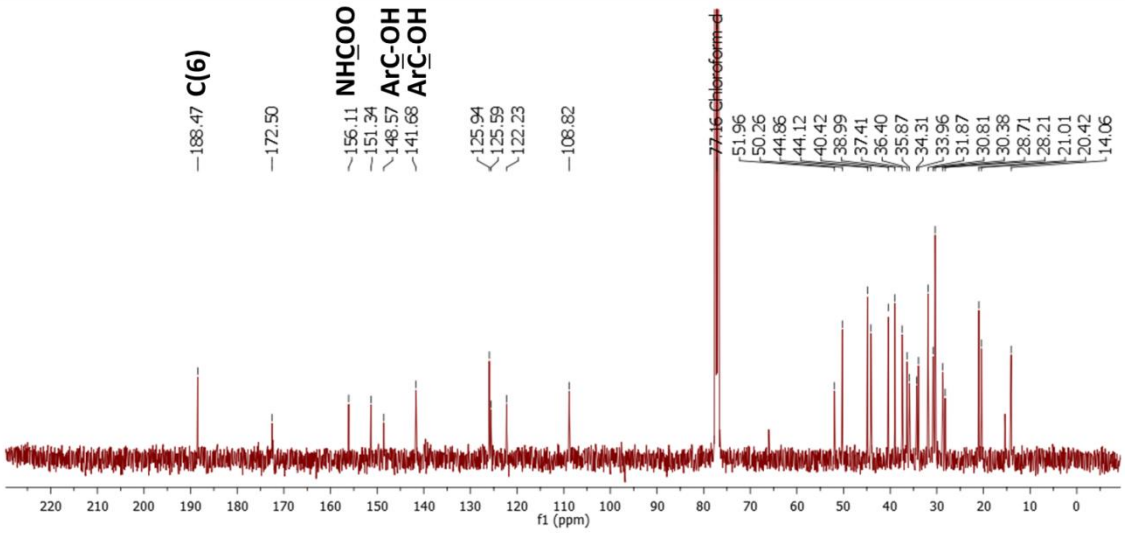

Figure 4.5 ^{13}C NMR spectrum of compound **4.7.**

Additionally, a carbamate diacetate celastrol derivative was synthesised (derivative **4.11**, Scheme 4.3).

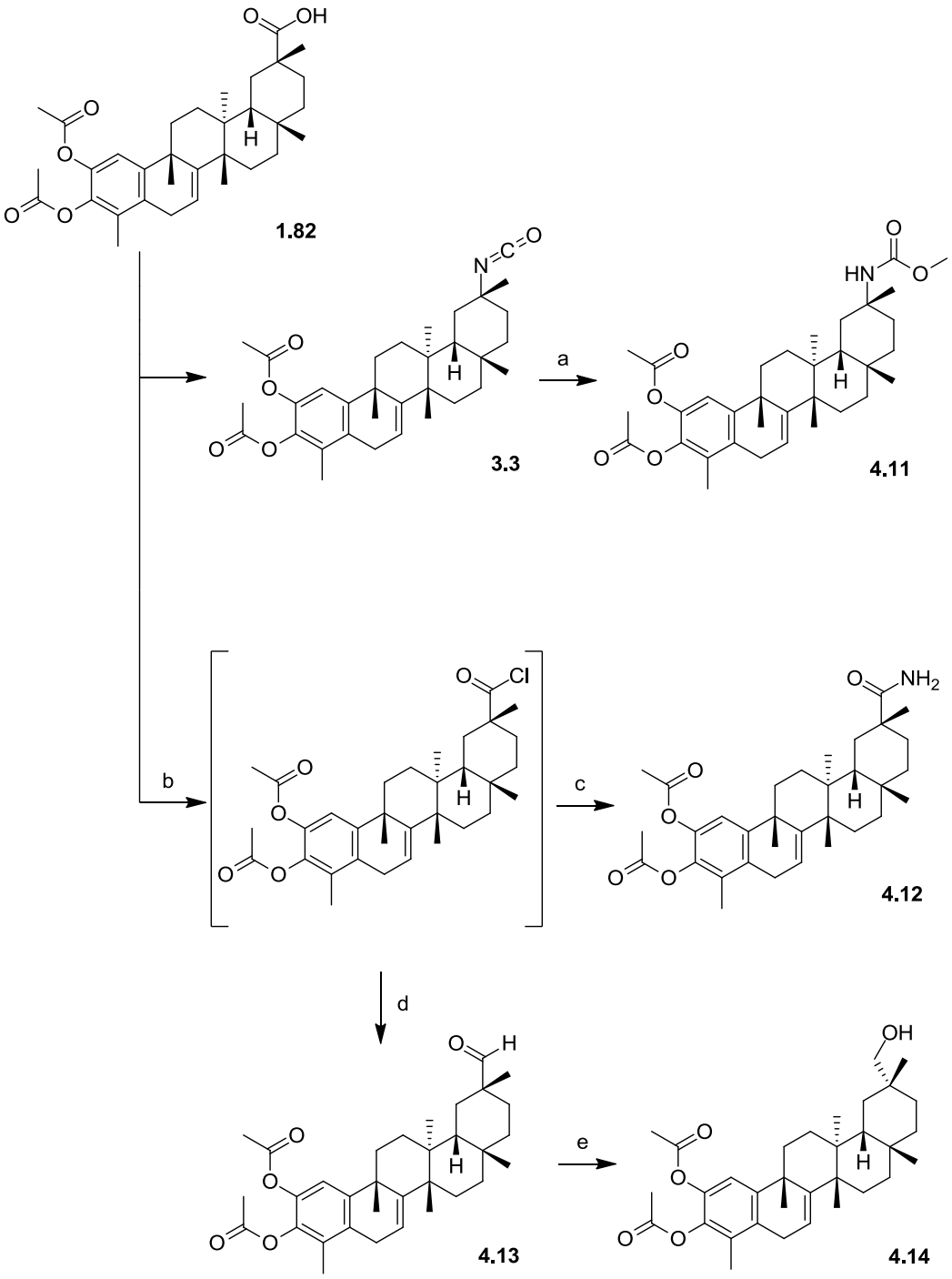

Scheme 4.3 Synthesis of celastrol derivatives **4.11–4.14**. *Reagents and conditions*: a) MeOH, Et_3N, R.T., N_2, 12 h; b) $(COCl)_2$, CH_2Cl_2, R.T., N_2, 4 h; c) conc. ammonia, toluene, 0 ºC, 1 h; d) LTBA, THF, 0 ºC, 1h; e) $NaBH_4$, EtOH, R.T., 1 h.

To confirm the role of the carbamate function at C(29) in the biological activity of the diacetate celastrol derivatives, we synthesised other diacetate derivatives with different functional groups at C(29) (Scheme 4.3), namely a primary amide (derivative **4.12**), an aldehyde (derivative **4.13**) and a primary

alcohol (derivative **4.14**). The spectra signals for the triterpenoic skeleton in the series of compounds **4.11–4.14** were similar to those of the diacetate celastrol derivatives (Figure 4.6 and Figure 4.7) [*343*].

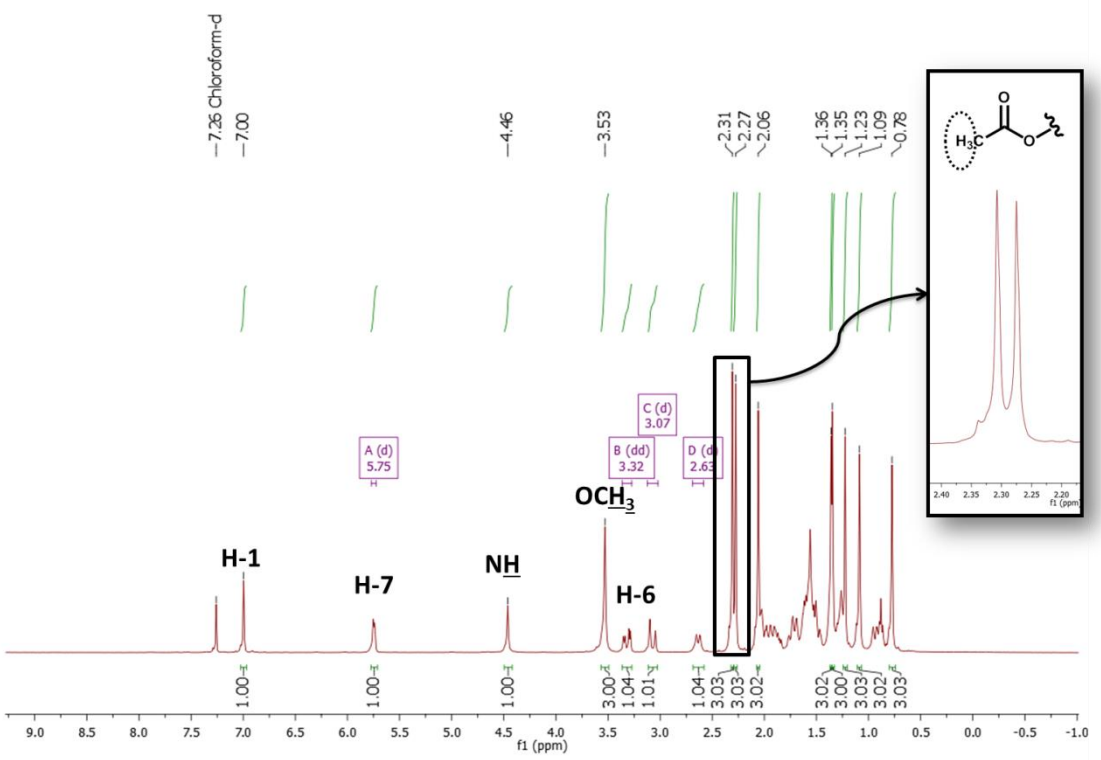

Figure 4.6 ^{1}H NMR spectrum of compound **4.11.**

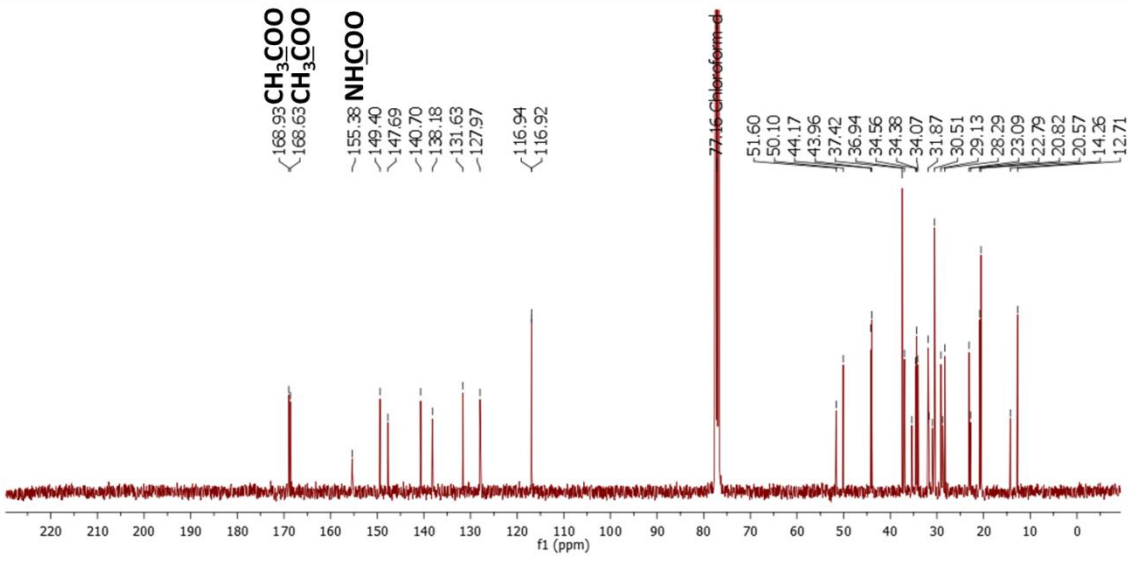

Figure 4.7 ^{13}C NMR spectrum of compound **4.11.**

In addition, the successful synthesis of compounds **4.12–4.14** was confirmed by the characteristic ^{1}H NMR spectra, which showed specific chemical shifts influenced by: the primary amide (singlet at 5.67 ppm, for derivative **4.12**), the aldehyde (doublet ranging from 9.29 to 9.31 ppm, with a coupling constant of 1.3 Hz, for derivative **4.13**) and the primary alcohol (two doublets ranging from 3.43 to 3.39 ppm and from 3.24 to 3.19 ppm, with a coupling constant of around 10.5 Hz, for derivative **4.14**) (Figure 4.8); in combination with the observation of ^{13}C NMR signals at 181.48 ppm, 205.28 ppm and 71.86 ppm, respectively.

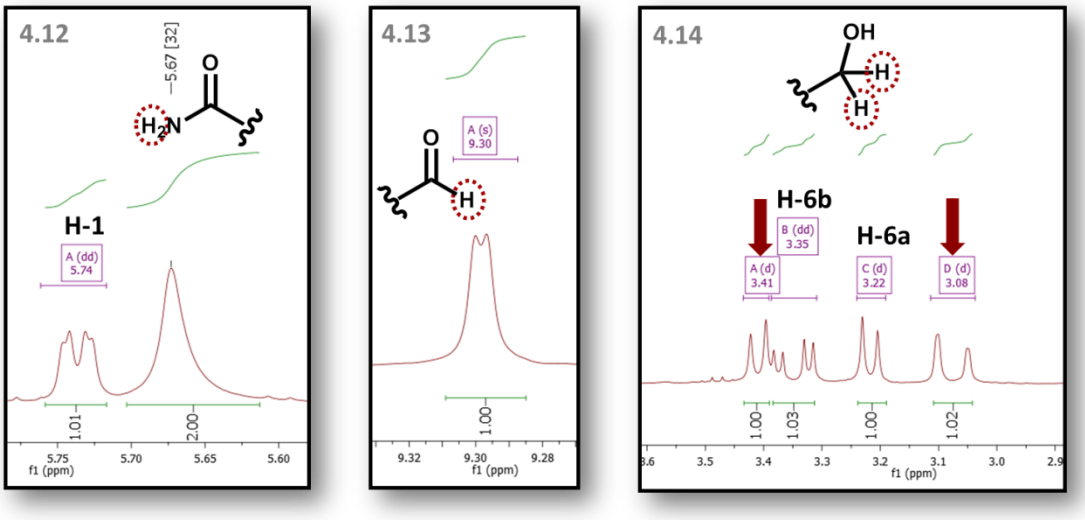

Figure 4.8 Portions of ^{1}H NMR spectra of compound **4.12–4.14**.

4.2.2. Biological evaluation

4.2.2.1. Cytotoxic activity and selectivity of celastrol derivatives

The activity of the celastrol **1.26** and its derivatives (**1.81–4.1**) on the viability of cancer cells was initially evaluated in two human tumour cell lines (lung carcinoma A549 and pancreatic carcinoma MIA PaCa-2 cells) using the well-established 3-[4,5-dimethylthiazol-2-yl]-2,5-diphenyl tetrazolium bromide (MTT) colorimetric assay [*349*]. The results of these assays, expressed as IC_{50} values (the concentration needed to inhibit 50% of cell viability compared with the control condition), are summarised in Table 4.1.

Table 4.1 IC_{50} values of celastrol **1.26** and its derivatives against lung carcinoma A549 and pancreatic carcinoma MIA PaCa-2 cell lines.

Compound	Cell line/IC_{50}[a] (μM ± SEM)	
	A549	MIA PaCa-2
Celastrol **1.26**	1.56±0.08	0.46±0.03
1.81	3.15±0.07	0.72±0.06
1.82	2.21±0.17	0.56±0.02
3.3	2.89±0.14	1.41±0.09
3.10	2.47±0.05	0.53±0.03
4.1	1.74±0.05	0.58±0.05
4.2	1.93±0.04	0.78±0.03
4.3	1.00±0.02	0.40±0.01
4.4	1.05±0.02	0.32±0.01
4.5	2.23±0.02	0.80±0.08
4.6	1.58±0.08	1.00±0.04
3.4	>10	>10
3.5	>10	>10
4.7	6.53±0.43	6.50±0.49
4.8	>10	>10
4.9	>10	>10
4.10	>10	>10
4.11	0.88±0.04	0.33±0.02
4.12	1.27±0.06	0.36±0.01
4.13	2.77±0.22	0.38±0.03
4.14	1.87±0.13	0.48±0.02

[a] Cells were treated with increasing concentrations of the indicated compounds for 72 h. Their effect on cell viability was determined by MTT assay and the IC_{50} values are expressed as the mean ± SEM of three independent experiments.

The conversion of parent celastrol **1.26** into C(29) carbamate derivatives (**4.1–4.6**, Scheme 4.1) resulted in some potent anticancer compounds against the tested tumour cell lines. The IC_{50} values were in the low micromolar range, which was comparable to the values obtained for celastrol **1.26** (Table 4.1). In particular, compound **4.4**, the hydroxyquinonemethide carbamate bearing the longer saturated linear chain (*n*-pentyl), showed the best cytotoxic activity in this series, which might be related with the improvement in membrane permeability caused by the side chain.

To better understand the potential of the C(29) carbamate derivatives, we also tested the cytotoxic activity of analogues with further modifications in the A/B-rings (compounds **4.7–4.10**, Scheme 4.2). Although it has been recently reported that some C(6) functionalised celastrol derivatives displayed increased *in vitro* cytotoxic activities against the tumour cell lines tested [*108*, *287*, *292*], the results obtained here for compounds **4.7–4.10** demonstrated a considerable decrease in their activities (Table 4.1). This seems to confirm that the improvements in the anticancer activity of celastrol derivatives associated with modifications at the C(6) position are highly dependent on the nature of the substituent group.

Considering that substitutions of positions C(2) and C(3) in the A-ring have been reported without entailing loss of activity — as shown for the diacetate compounds **1.82** and **3.3** — we synthesised compound **4.11**, a carbamate diacetate celastrol derivative (Scheme 4.3), and evaluated its effect on the viability of cancer cells (Table 4.1). The anticancer activity of other diacetate celastrol derivatives (compounds **4.12–4.14**, Scheme 4.3) was also assessed and compared with that of compound **4.11** (Table 4.1). Once more, the results confirmed that the remarkable anticancer activity of celastrol **1.26** and its derivatives was not exclusively caused by the electrophilicity of the integral hydroxyquinonemethide substructure of the A/B-rings. In fact, with the exception of compound **4.14**, all the diacetate derivatives exhibited a higher cytotoxic activity against the MIA PaCa-2 cell line compared with the parent compound celastrol **1.26**, and the carbamate derivative **4.11** was the most active among them. Furthermore, the most active of all tested compounds against the cell lines studied were two C(29) carbamates (compounds **4.4** and **4.11**) bearing different substructures of the A/B-rings.

According to these results, derivatives **4.4** and **4.11** were selected to study the selectivity of their effect on cancer cell lines. Thus, additional viability assays were performed on different malignant cells (colorectal adenocarcinoma HT-29, ovarian carcinoma SKOV-3 and breast cancer MCF-7 and MDAMB-231 cells) and on non-malignant human cells (BJ fibroblasts). As observed in Table 4.2, both compounds **4.4** and **4.11** proved to be very potent against all the tumour cell lines,

but only compound **4.11** exhibited an interesting increase in selectivity between tumour cells and non-tumour human BJ cells. Moreover, SKOV-3 cells were more sensitive to compound **4.11** than the other tested cancer cell lines and showed a seven-fold increase in tumour-to-non-tumour sensitivity, which was an important improvement in selectivity compared with the parent compound celastrol **1.26** (Figure 4.9).

Table 4.2 IC_{50} values of celastrol **1.26** and its derivatives against non-tumour fibroblast cell line BJ and tumour cell lines HT-29, SKOV-3, MCF-7 and MDAMB-231.

Compound	Cell line/IC_{50}[a] (μM ± SEM)				
	BJ	HT-29	SKOV-3	MCF-7	MDAMB-231
Celastrol **1.26**	2.74±0.14	1.28±0.05	1.16±0.03	1.35±0.05	1.32±0.11
4.4	0.88±0.03	1.02±0.02	0.45±0.02	0.59±0.04	0.52±0.04
4.7	> 30	ND	7.98±0.39	ND	ND
4.11	3.68±0.20	1.54±0.05	0.54±0.02	1.68±0.13	1.35±0.06

[a] Cells were treated with increasing concentrations of the indicated compounds for 72 h. Their effect on cell viability was determined by MTT assay and the IC_{50} values are expressed as the mean ± SEM of three independent experiments. ND: not determined.

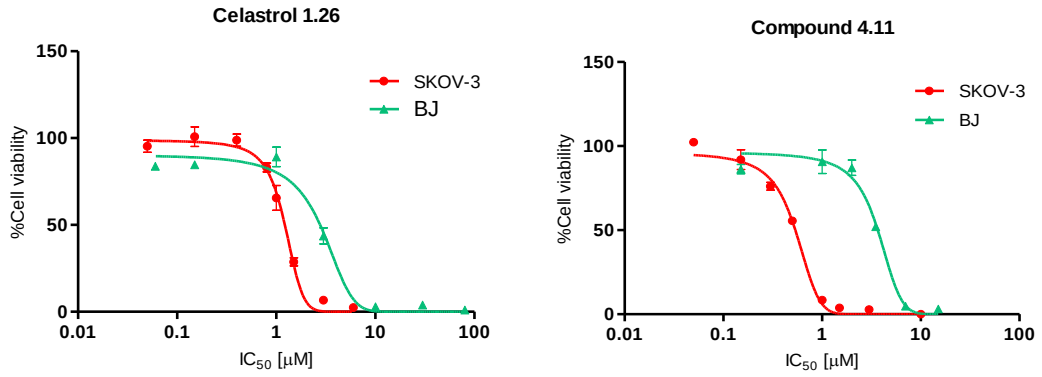

Figure 4.9 Dose-dependent effect of celastrol **1.26** and derivative **4.11** on SKOV-3 and BJ cells viability. The activity on cell viability was determined by MTT assay and the graphs were obtained based on three independent experiments using Graphpad Prism 5 software and expressed as mean ± SEM.

The results of a preliminary SAR study of compounds **4.1**, **4.7**, **4.9** and **4.11** against the A549, MIA PaCa-2 and BJ cell lines, based on their IC_{50} values, are summarised in Table 4.3.

Table 4.3 Schematic representation of the SAR study for the cytotoxic activity of some derivatives of celastrol **1.26** against A549, MIA PaCa-2 and BJ cell lines, based on the IC_{50} values.

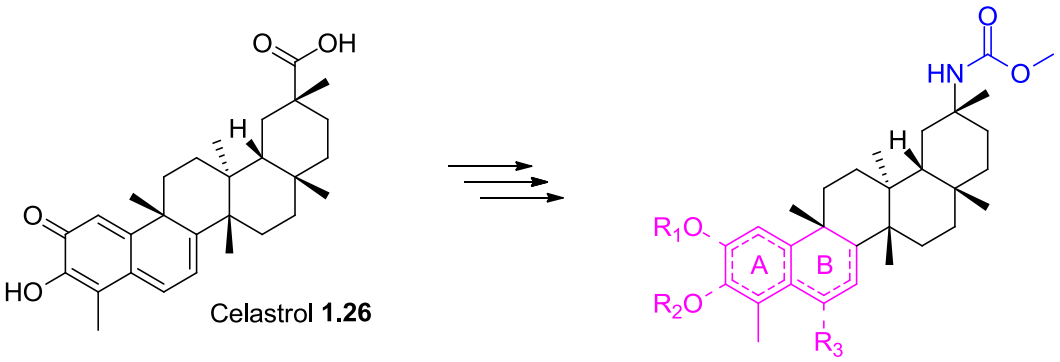

Compound	A/B-rings	SAR for the activity over cell viability and tumour-to-non-tumour selectivity
4.1	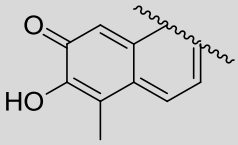	↓ Antitumour activity
4.7	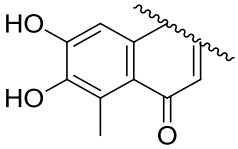	↓↓ Antitumour activity ↑↑↑ Tumour-to-non-tumour selectivity
4.9	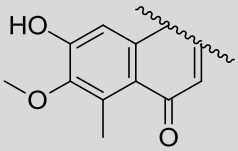	↓↓↓ Antitumour activity
4.11	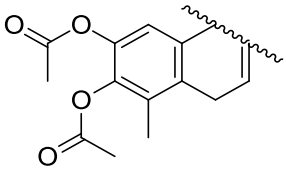	↑↑↑ Antitumour activity ↑↑↑ Tumour-to-non-tumour selectivity

The conversion of the carboxylic acid to a methyl carbamate at the C(29) position (compound **4.1**) had only a minor impact on the anticancer activity. Allylic oxidation at the C(6) position and consequent rearrangement in the A/B-rings (compound **4.7**), on the other hand, appeared to decrease the activity of the compounds (IC_{50} values of 6.5 μM for both A549 and MIA PaCa-2 cell lines), while simultaneously increasing the tumour-to-non-tumour selectivity dramatically (IC_{50} value for BJ cells > 30 μM) (Table 4.2). Methylation of the C(2) hydroxyl group (compound **4.9**) led to an even greater drop in the activity on cell viability. Finally, compound **4.11** — a C(2), C(3) diacetate compound obtained from **4.1** —

simultaneously showed the best cytotoxicity combined with the best selectivity between malignant cells and non-malignant fibroblasts.

4.2.2.1. Antiproliferative activity of derivative 4.11

Based on the IC_{50} values at 72 h shown in Table 4.2, it was found that the SKOV-3 cell line was especially sensitive to derivative **4.11**. These results obtained using short-term MTT assays were complemented with a longer-term *in vitro* cell survival assay — the colony formation assay. This assay determined the ability of single cells to survive and grow into cell colonies after treatment with compound **4.11**. As shown in Figure 4.10, compound **4.11** weakened the colony-formation capacity of SKOV-3 cells in a dose-dependent manner compared with the untreated cells (control). In fact, after exposing the SKOV-3 cells to compound **4.11** at twice its IC_{50} concentration for 24 h, only an insignificant fraction of seeded cells retained the ability to produce colonies. These observations suggest that derivative **4.11** has not only a cytotoxic effect, but also an antiproliferative effect on SKOV-3 cells.

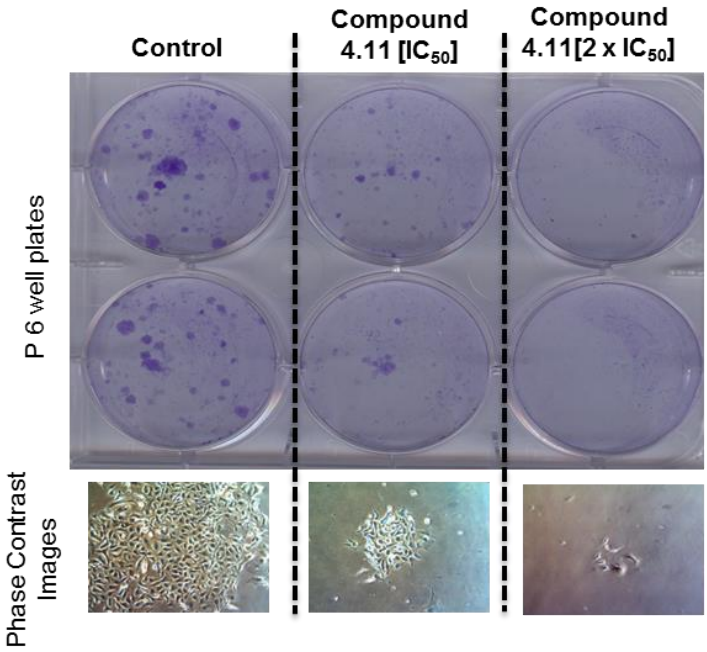

Figure 4.10 Images from the clonogenic assay of SKOV-3 cells untreated (control) and after being exposed to compound **4.11** at concentrations of [IC_{50}] and 2 × [IC_{50}] for 24 h and then allowed to grow in drug-free medium in 6-well plates for another 12 days. (A) Images of P6 plates after staining with 1% crystal violet (in methanol) for 4 h. (B) Phase contrast images of SKOV-3 cells forming colonies.

4.2.2.1. Effects of derivative 4.11 on cell-cycle distribution and apoptosis

It has been reported that celastrol **1.26** induces cell-cycle arrest and apoptosis in different cancer cell lines [*146*, *201*, *205*]. Therefore, compound **4.11** was also selected for the characterisation of its effect on cell-cycle distribution and apoptosis. SKOV-3 cells were treated with compound **4.11** at its IC_{50} concentration for 24, 48 and 72 h and were analysed by flow cytometry using a Fluorescence-Activated Cell Sorter (FACS). To evaluate the possible role of cell-cycle arrest in the anticancer effect of compound **4.11**, SKOV-3 cells were labelled with propidium iodide (PI), a red-fluorescent DNA-binding counter-stain, after treatment with compound **4.11**. This analysis indicated that compound **4.11** had a negligible effect on the cell-cycle distribution of SKOV-3 cells compared with the control conditions (Figure 4.11).

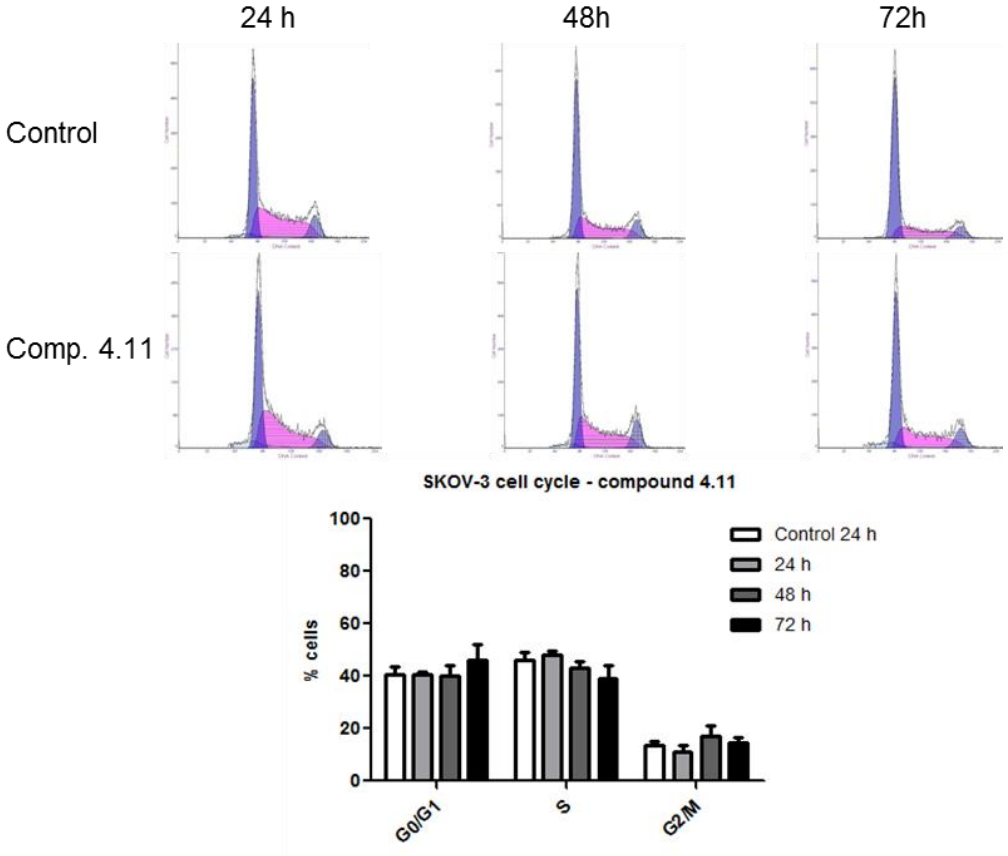

Figure 4.11 Cell-cycle analysis of compound **4.11** in SKOV-3 cells. Cells were treated with compound **4.11** at its IC_{50} concentration for 24, 48 and 72 h and analysed by flow cytometry. The figures are representative of three independent experiments and the values are expressed as means ± SD.

An apoptosis analysis was subsequently performed to examine whether compound **4.11** was able to induce physiological apoptosis in cancer cells. SKOV-3 cells treated with compound **4.11** were analysed after annexin V-FITC/PI double-staining. This analysis distinguishes and quantifies viable cells (annexin V−, PI−), early apoptotic cells (annexin V+, PI−) and late apoptotic/necrotic cells (PI+) [11]. We observed that compound **4.11** significantly induced apoptosis against SKOV-3 cells in a time-dependent manner (Figure 4.12). The greatest effect was registered at 72 h of incubation with an increase from 4.5% (control condition) to 29.9% (treated cells) in early apoptotic cells. In general, these results suggest that the potent antitumour activity of compound **4.11** in SKOV-3 cells is mainly mediated by induction of apoptosis.

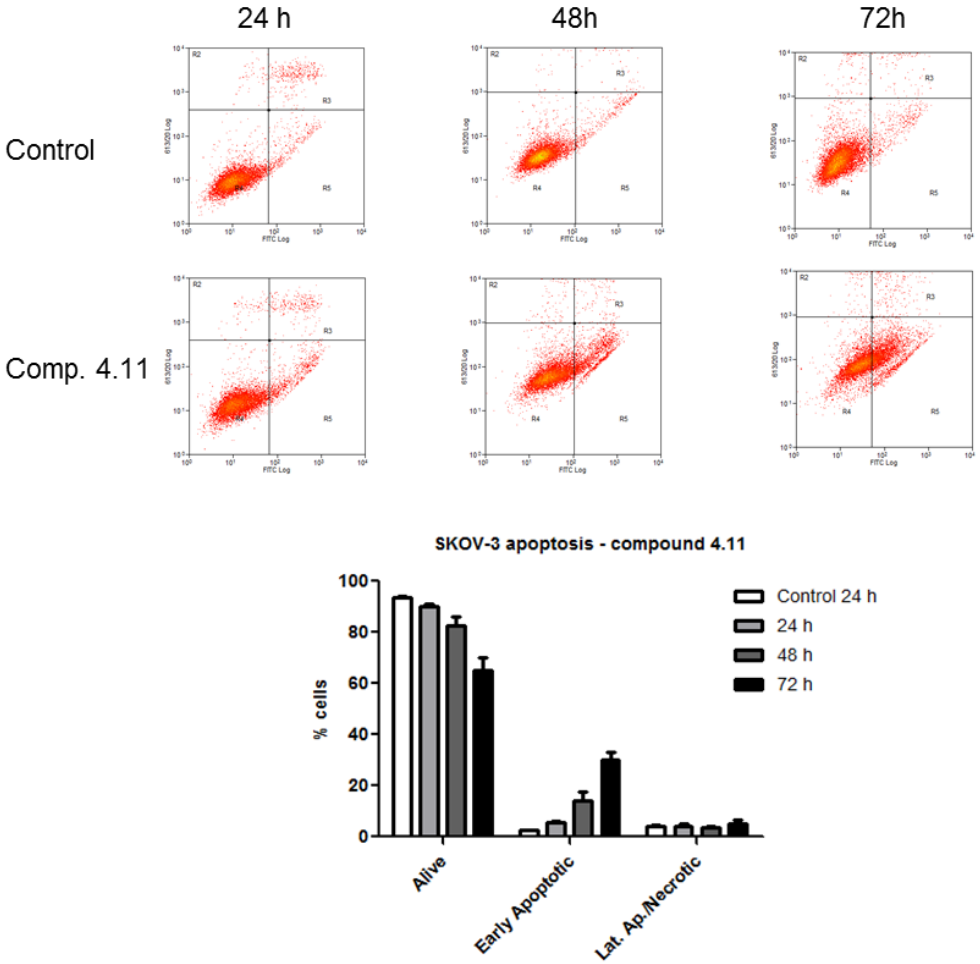

Figure 4.12 Apoptosis analysis of compound **4.11** in SKOV-3 cells. Cells were treated with compound **4.11** at its IC_{50} concentration for 24, 48 and 72 h and analysed by flow cytometry. The figures are representative of three independent experiments and the values are expressed as means ± SD.

4.2.2.1. Morphological characteristics of SKOV-3 cells treated with derivative 4.11

To confirm that apoptosis induction was the main mechanism underlying the biological activity of compound **4.11**, a morphological analysis of cell death by apoptosis was performed using fluorescence microscopy after staining nuclear DNA with the Hoechst 33342 fluorescent dye. As shown in Figure 4.13, SKOV-3 cells treated for 48 h with compound **4.11** at its IC_{50} concentration exhibited nuclear condensation and fragmentation, cell shrinkage and fragmentation into apoptotic bodies, which are all typical morphological characteristics of apoptotic cells. These cytological observations further corroborated the apoptosis-induced effect of compound **4.11** on SKOV-3 cells.

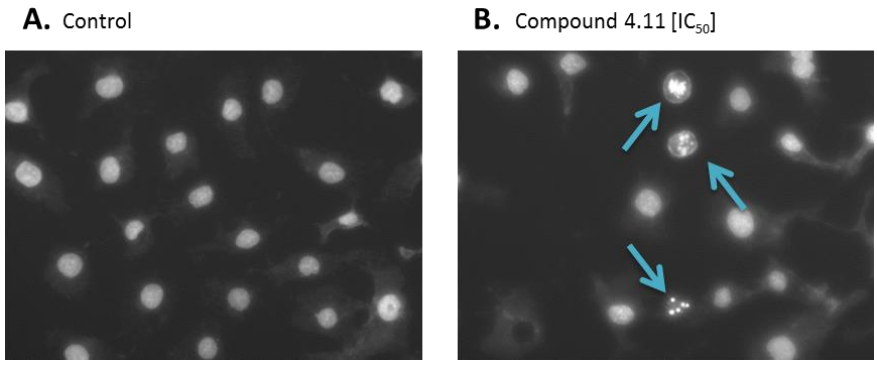

Figure 4.13 Representative fluorescence microscopy images after staining nuclear DNA with Hoechst 33342 fluorescent dye. (A) Control — untreated SKOV-3 cells. (B) SKOV-3 cells treated with compound **4.11** at its IC_{50} concentration for 48 h. Arrows indicate morphological characteristics of apoptotic cells.

4.2.2.2. Effects of derivative 4.11 on the expression levels of apoptosis-related proteins

To further explore the mechanism of action via which compound **4.11** induces apoptosis, its effects on the expression levels of apoptosis-related proteins were also analysed. It is widely known that apoptosis is mediated by a group of cysteine proteases called *caspases*, whose inactive form (procaspase) is activated by proteolytic cleavage. The numerous mechanisms for activating procaspases can be grouped into two main signalling pathways: the extrinsic and the intrinsic pathway [*53*].

Caspase-8 and caspase-9 are key initiators in the extrinsic and intrinsic apoptotic pathways, respectively. While caspase-8 is activated in response to extracellular apoptosis-inducing ligands, caspase-9 is activated in response to several intrinsic stimuli. Caspase-3, a downstream effector caspase, amplifies the initiation signals of both caspase-8 and caspase-9, and, therefore, plays a key role in both pathways [*350*]. In this study, we showed that SKOV-3 cells treated for 72 h with compound **4.11** at its IC_{50} concentration exhibited a great decrease in the expression levels of procaspase-8 and procaspase-3, with a concomitant increase in the levels of the corresponding cleaved (activated) caspases. Differences in the expression levels of caspase-9, in contrast, were not so apparent (Figure 4.14A).

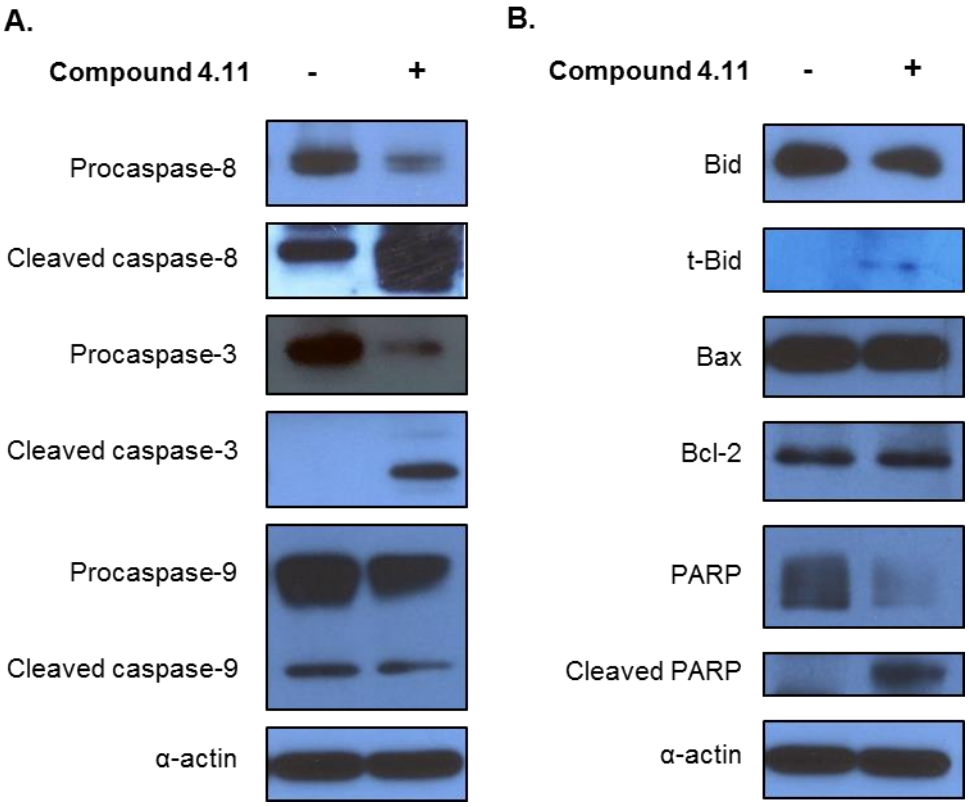

Figure 4.14 Western blot analysis showing the expression levels of apoptosis-related proteins in SKOV-3 ovarian cancer cells after 72 h treatment with compound **4.11** at its IC_{50} concentration. α-actin was used as loading control.

The caspase cascade induces the cleavage of other specific protein targets, such as PARP, the cleaved form of which is considered to be a hallmark of apoptosis [*351*]. Moreover, caspase-8 can cleave Bid into its truncated active form, tBid, a proapoptotic protein that regulates mitochondria-mediated (intrinsic)

apoptosis by activating Bax directly. Consequently, we sought to explore the effect of compound **4.11** on the levels of these proteins [*352*]. As shown in Figure 4.14B, treatment of SKOV-3 cells with compound **4.11** induced a simultaneous decrease in the levels of full-length PARP and an increase in the expression levels of cleaved PARP, while no pronounced effect was observed on the expression of Bcl-2-family proteins (Bid, Bax and Bcl-2 proteins).

These findings further suggest that compound **4.11** is able to activate the extrinsic apoptotic pathway in SKOV-3 cells, with the intrinsic apoptotic pathway not playing a relevant role in its cytotoxic effect.

4.2.2.3. Synergistic effect of carboplatin and derivative 4.11

Ovarian cancer is the most common cause of death from gynaecological malignancy [*353*] and is the seventh most common type of cancer in women [*354*]. The therapeutic management of ovarian cancer normally involves the use of platinum-based antineoplastic drugs (carboplatin or cisplatin) and, in the case of more aggressive tumours, combinations of chemotherapy regimens (e.g., paclitaxel [*355*], docetaxel [*356*] and doxorubicin [*357*]) are generally preferred [*276*]. Therefore, the synergistic combinatorial effect of carboplatin and celastrol derivatives with improved antitumour activity may provide an interesting novel alternative for the treatment of ovarian cancer. Consequently, we tested the effects of a combined treatment using compound **4.11** and carboplatin, which was chosen over cisplatin because of its lower renal toxicity [*358*]. The combination effect of carboplatin and compound **4.11** on SKOV-3 cells was determined using the Chou and Talalay method. The combination index (CI) values indicate whether the combination effect of the two compounds is greater (CI < 1), lesser (CI > 1) or equal (CI = 1) to the expected additive effect [*261*, *329*]. As seen in Table 4.4, combined incubation of SKOV-3 cells for 72 h with different concentrations of carboplatin and compound **4.11** at a constant equipotency ratio of 1:64 ($[IC_{50}]_{\mathbf{4.11}}$:$[IC_{50}]_{\mathbf{carboplatin}}$) resulted in a synergistic effect between them (CI < 1, indicated in bold). These data demonstrate the potential of derivative **4.11** as a new agent for combined treatment with carboplatin in ovarian cancer therapy.

Table 4.4 Results of the synergistic study of compound **4.11** and **carboplatin** at a constant equipotency ratio of 1:64 ($[IC_{50}]_{\mathbf{4.11}}$:$[IC_{50}]_{\mathbf{carboplatin}}$) in SKOV-3 cells.

Compound 4.11 (μM)	Carboplatin (μM)	1-Viability	CI
0.125	8	0.26832	1.11196
0.25	16	0.55877	0.92853
0.5	32	0.85743	0.62735
1	64	0.92209	0.78627
2	128	0.95362	1.07597

CI values were calculated using CompuSyn software.
Bold rows show CI values below 1, which are indicative of a synergic effect.

4.3. CONCLUSIONS

In this work, we reported the design and synthesis of a novel series of C(29) carbamate celastrol derivatives. Some of these compounds showed improved anticancer activity against the tested cancer cell lines compared with celastrol **1.26**. The SAR was discussed and the preliminary results showed the effect of A/B-ring modifications of celastrol analogues on anticancer activity. Among all the synthesised derivatives, compound **4.11** was the most potent, being highly active on all tested tumour cell lines. Mechanistic studies showed that compound **4.11** exerts an antiproliferative effect on SKOV-3 human ovarian cancer cells via extrinsic apoptotic pathway. Simultaneously, compound **4.11** demonstrated an important increase in tumour selectivity compared with the parent compound celastrol **1.26**. Furthermore, our results established the potential of compound **4.11** for use in combination therapy with carboplatin in ovarian cancer. Taken together, our results suggest that compound **4.11** may be used as a promising lead candidate for cancer treatment.

4.4. EXPERIMENTAL SECTION

4.4.1. Chemistry

General

All the reagents and celastrol **1.26** were obtained from Sigma-Aldrich. Derivatives **1.81**, **1.82**, **3.3–3.5** and **3.10** were prepared according as described in

Chapter 3 [*343*]. The solvents were purchased from VWR Portugal and were dried according to usual procedures. Thin layer chromatography (TLC) analyses were performed on aluminium TLC plate, silica gel coated with fluorescent indicator F_{254} (Merck, detection by UV absorption). Preparative TLCs were performed on layer plates of silica gel 60 F_{254}, 1 mm (Merck, detection by UV absorption). General melting points are uncorrected (Büchi® melting point apparatus — Model B-540). IR spectra were determined on a Fourier transform IR spectrometer. NMR was used to elucidate the chemical structures based on ^{1}H, ^{13}C and DEPT-135 NMR experiments. NMR spectra were recorded using the Bruker digital FT-NMR-Avance 400 MHz spectrometer in $CDCl_3$ or CD_3OD, with tetramethylsilane (TMS) as the internal standard. MS were performed on a Thermo Scientific Finnigan LXQ Mass Spectrometer with a direct insertion probe, using electrospray ionisation mass spectrometry. Elemental analysis was performed by chromatographic combustion using the Carlo Erba EA 1108 Elemental Analyser.

General procedure for the synthesis of carbamates (4.1–4.5, 4.7, 4.8 and 4.11)

Isocyanates **3.3, 3.5** and **3.10** (40.0 mg) were dissolved in a mixture of the respective alcohol (4 mL) and triethylamine (0.1 mL, 0.90 mmol). The mixture was stirred for 12 h at room temperature under nitrogen atmosphere. The resulting mixture was then concentrated in vacuo and purified by preparative TLC (CH_2Cl_2/MeOH 20:1) to give the carbamate product.

Derivative 4.1 — Methyl N-[3-hydroxy-2-oxo-24-nor-friedela-1(10),3,5,7-tetraen-20α-yl] carbamate

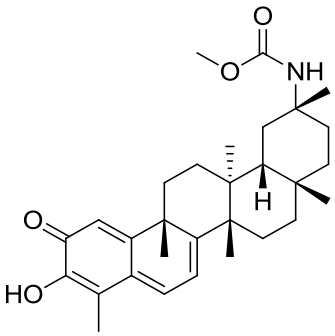

Figure 4.15 Chemical structure of compound **4.1.**

Starting from compound **3.10** (40.0 mg, 0.09 mmol) in dry methanol (4 mL), compound **4.1** (36.1 mg, 84%) was obtained as an orange solid according to the above-mentioned procedure. Mp: 241.7–244.6 °C. IR (neat) $_{vmax}$: 3344, 2943, 2869, 1721, 1589, 1514, 1437, 1222 cm^{-1}. ^{1}H NMR (400 MHz, $CDCl_3$) δ 7.01 (d, *J* = 6.9 Hz, 1H, H-6), 6.53 (s, 1H, H-1), 6.35 (d, *J* = 7.1 Hz, 1H, H-7), 4.46 (s, 1H, NH), 3.53 (s, 3H, OCH_3), 2.21 (s, 3H, H-23), 1.44 (s, 3H), 1.35 (s, 3H), 1.26 (s, 3H), 1.11 (s, 3H), 0.71 (s, 3H) ppm.^{13}C NMR (100 MHz, $CDCl_3$) δ 178.51 (C2), 170.48, 164.88, 155.42 (NHCOO), 146.17 (C3), 134.16 (C6), 127.54 (C5), 119.74 (C1), 118.10 (C7), 117.17 (C4), 51.63, 50.06, 45.27, 44.13, 43.18, 39.26, 38.26, 36.47, 35.40, 34.08, 33.62, 31.87, 30.88, 30.49, 29.87, 28.90, 28.78, 22.02, 20.49, 10.38 ppm. MS (DI-ESI) (*m/z*): 480.2 $[M+H]^+$. Anal. Calcd for $C_{30}H_{41}NO_4$: C, 75.12; H, 8.62; N, 2.92; Found: C, 75.05; H, 8.94; N, 2.96.

Derivative 4.2 — Ethyl N-[3-hydroxy-2-oxo-24-nor-friedela-1(10),3,5,7-tetraen-20α-yl] carbamate

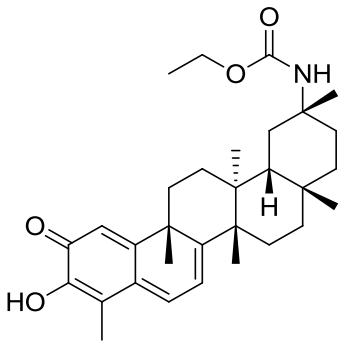

Figure 4.16 Chemical structure of compound **4.2.**

Starting from compound **3.10** (40.0 mg, 0.09 mmol) in dry ethanol (4 mL), compound **4.2** (39.6 mg, 80%) was obtained as an orange solid according to the above-mentioned procedure. Mp: 261.8–264.1 °C. IR (neat) $_{vmax}$: 3341, 2928, 2866, 1715, 1589, 1514, 1437, 1221 cm^{-1}. ^{1}H NMR (400 MHz, $CDCl_3$) δ 7.02 (d, *J* = 6.8 Hz, 1H, H-6), 6.52 (s, 1H, H-1), 6.36 (d, *J* = 7.0 Hz, 1H, H-7), 4.40 (s, 1H, N<u>H</u>), 4.06–3.90 (m, 2H, OC<u>H</u>$_2$$CH_3$), 2.20 (s, 3H, H-23), 1.44 (s, 3H), 1.36 (s, 3H), 1.26 (s, 3H), 1.13 (m, 3H, OCH_2C<u>H</u>$_3$), 1.11 (s, 3H), 0.74 (s, 3H) ppm. ^{13}C NMR (100 MHz, $CDCl_3$) δ 178.52 (C2), 170.51, 164.89, 155.02 (NH<u>C</u>OO), 146.17 (C3), 134.21 (C6), 127.55 (C5), 119.68 (C1), 118.10 (C7), 117.21 (C4), 60.17 (NHCOO<u>C</u>H_2), 49.98, 45.28, 44.11, 43.20, 39.28, 38.25, 36.46, 35.55, 34.07, 33.57, 31.88, 30.89, 30.52, 29.83, 28.93, 28.69, 22.07, 20.44, 14.90, 10.39 ppm. MS (DI-ESI) (*m/z*): 494.3 $[M+H]^+$. Anal. Calcd for $C_{31}H_{43}NO_4$: C, 75.42; H, 8.78; N, 2.84; Found: C, 75.13; H, 9.01; N, 3.25.

Derivative 4.3 — Propyl N-[3-hydroxy-2-oxo-24-nor-friedela-1(10),3,5,7-tetraen-20α-yl] carbamate

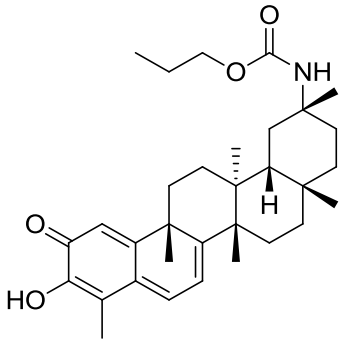

Figure 4.17 Chemical structure of compound **4.3.**

Starting from compound **3.10** (40.0 mg, 0.09 mmol) in 1-propanol (4 mL), compound **4.3** (35.0 mg, 77%) was obtained as a red-orange solid according to the above-mentioned procedure. Mp: 252.2–253.5 °C. IR (neat) $_{vmax}$: 3334, 2936, 2871, 1715, 1589, 1514, 1434, 1221 cm^{-1}. ^{1}H NMR (400 MHz, $CDCl_3$) δ 7.01 (d, *J* = 7.0 Hz, 1H, H-6), 6.52 (s, 1H, H-1), 6.35 (d, *J* = 7.1 Hz, 1H, H-7), 4.40 (s, 1H, N<u>H</u>), 3.92–3.85 (m, 2H, OC<u>H$_2$</u>CH_2), 2.21 (s, 3H, H-23), 1.44 (s, 3H), 1.36 (s, 3H), 1.27 (s, 3H), 1.11 (s, 3H), 0.87–0.82 (m, 3H, OCH_2CH_2C<u>H$_3$</u>), 0.75 (s, 3H) ppm. ^{13}C NMR (100 MHz, $CDCl_3$) δ 178.52 (C2), 170.46, 164.89, 155.14 (NH<u>C</u>OO), 146.16 (C3), 134.16 (C6), 127.56 (C5), 119.65 (C1), 118.10 (C7), 117.19 (C4), 65.91 (NHCOO<u>C</u>H_2), 49.97, 45.27, 44.11, 43.19, 39.26, 38.26, 36.47, 35.52, 34.09, 33.53, 31.88, 30.90, 30.53, 29.83, 28.94, 28.72, 22.53, 22.10, 20.44, 10.46, 10.39 ppm. MS (DI-ESI) (*m/z*): 508.3 $[M+H]^+$. Anal. Calcd for $C_{32}H_{45}NO_4$: C, 75.70; H, 8.93; N, 2.76; Found: C, 75.63; H, 8.87; N, 2.51.

Derivative 4.4 — Pentyl N-[3-hydroxy-2-oxo-24-nor-friedela-1(10),3,5,7-tetraen-20α-yl] carbamate

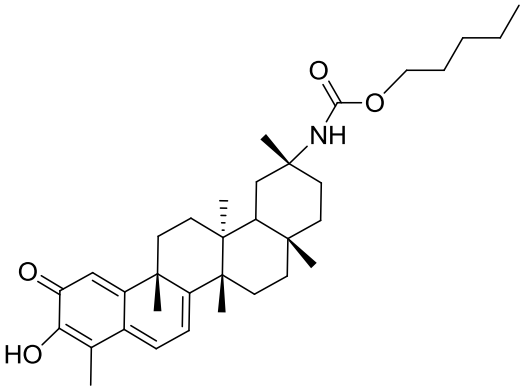

Figure 4.18 Chemical structure of compound **4.4.**

Starting from compound **3.10** (40.0 mg, 0.09 mmol) in 1-pentanol (4 mL), compound **4.4** (40.8 mg, 85%) was obtained as an orange solid according to the above-mentioned procedure. Mp: 225.6–228.7 °C. IR (neat) $_{vmax}$: 3282, 2947, 2870, 1699, 1579, 1508, 1433, 1223 cm^{-1}. ^{1}H NMR (400 MHz, $CDCl_3$) δ 7.01 (d, *J* = 6.9 Hz, 1H, H-6), 6.52 (s, 1H, H-1), 6.36 (d, *J* = 7.0 Hz, 1H, H-7), 4.39 (s, 1H, N<u>H</u>), 4.01–3.81 (m, 2H, OC<u>H</u>$_2$CH$_2$), 2.20 (s, 3H, H-23), 1.44 (s, 3H), 1.36 (s, 3H), 1.27 (s, 3H), 1.11 (s, 3H), 1.24–1.19 (m, 3H, O(CH$_2$)$_4$C<u>H</u>$_3$), 0.74 (s, 3H) ppm. ^{13}C NMR (100 MHz, $CDCl_3$) δ 178.49 (C2), 170.45, 164.83, 155.14 (NH<u>C</u>OO), 146.15 (C3), 134.11 (C6), 127.55 (C5), 119.71 (C1), 118.11 (C7), 117.14 (C4), 64.43 (NHCOO<u>C</u>H$_2$), 49.98, 45.26, 44.12, 43.18, 39.29, 38.29, 36.49, 35.62, 34.06, 33.63, 31.88, 30.91, 30.54, 29.85, 28.95, 28.67, 28.11, 22.49, 22.05, 20.50, 14.03, 10.39 ppm. MS (DI-ESI) (*m/z*): 536.3 $[M+H]^+$. Anal. Calcd for $C_{34}H_{49}NO_4$: C, 76.22; H, 9.22; N, 2.61; Found: C, 75.88; H, 8.97; N, 2.41.

Derivative 4.5 — 2-Methyl-propyl N-[3-hydroxy-2-oxo-24-nor-friedela-1(10),3,5,7-tetraen-20α-yl] carbamate

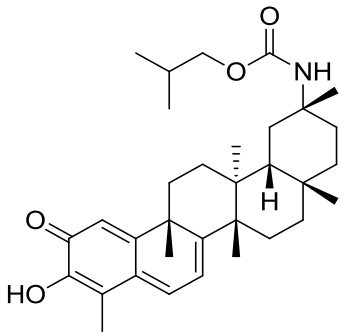

Figure 4.19 Chemical structure of compound **4.5.**

Starting from compound **3.10** (40.0 mg, 0.09 mmol) in 2-methylpropan-1-ol (4 mL), compound **4.5** (37.7 mg, 81%) was obtained as a dark orange solid according to the above-mentioned procedure. Mp: 255.3–257.3 °C. IR (neat) $_{vmax}$: 3339, 2928, 2870, 1715, 1590, 1513, 1437, 1220 cm^{-1}. ^{1}H NMR (400 MHz, $CDCl_3$) δ 7.01 (d, *J* = 6.9 Hz, 1H, H-6), 6.52 (s, 1H, H-1), 6.35 (d, *J* = 7.1 Hz, 1H, H-7), 4.41 (s, 1H, N<u>H</u>), 3.71 (d, *J* = 5.0 Hz, 2H, OC<u>H_2</u>), 2.21 (s, 3H, H-23), 1.44 (s, 3H), 1.36 (s, 3H), 1.27 (s, 3H), 1.11 (s, 3H), 0.83 (d, *J* = 4.5 Hz, 6H, $OCH_2(C\underline{H}_3)_2$), 0.75 (s, 3H) ppm. ^{13}C NMR (100 MHz, $CDCl_3$) δ 178.54 (C2), 170.42, 164.90, 155.17 (NH<u>C</u>OO), 146.16 (C3), 134.16 (C6), 127.58 (C5), 119.64 (C1), 118.11 (C7), 117.21 (C4), 70.50 (NHCOO<u>C</u>H_2), 49.98, 45.27, 44.12, 43.20, 39.26, 38.28, 36.48, 35.50, 34.12, 33.50, 31.89, 30.90, 30.54, 29.84, 28.95, 28.79, 28.15, 22.15, 20.46, 19.57, 19.19, 10.40 ppm. MS (DI-ESI) (*m/z*): 522.3 $[M+H]^+$. Anal. Calcd for $C_{33}H_{47}NO_4$: C, 75.97; H, 9.08; N, 2.68; Found: C, 75.84; H, 8.86; N, 2.52.

Derivative 4.6 — 3-Hydroxy-2,2-dimethyl-propyl N-[3-hydroxy-2-oxo-24-nor-friedela-1(10),3,5,7-tetraen-20α-yl] carbamate

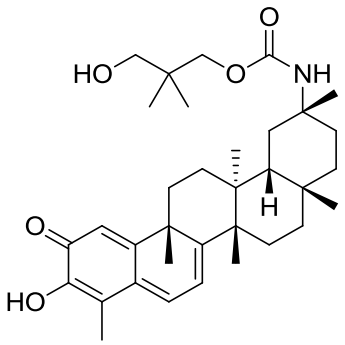

Figure 4.20 Chemical structure of compound **4.6.**

Isocyanate **3.10** (40.0 mg, 0.09 mmol) was dissolved in a mixture of toluene (4 mL), neopentyl glycol (37.3 mg, 0.36 mmol) and triethylamine (0.1 mL, 0.90 mmol). The mixture was stirred for 12 h at room temperature under nitrogen atmosphere. The resulting mixture was then concentrated in vacuo and purified by preparative TLC (CH_2Cl_2/MeOH 20:1) to give compound **4.6** (39.4 mg, 80%). Mp: 272.9–275.5 °C. IR (neat) $_{vmax}$: 3433, 3343, 2942, 2871, 1695, 1588, 1512, 1437, 1221 cm^{-1}. ^{1}H NMR (400 MHz, $CDCl_3$) δ 7.01 (d, *J* = 6.6 Hz, 1H, H-6), 6.53 (s, 1H, H-1), 6.35 (d, *J* = 6.9 Hz, 1H, H-7), 4.55 (s, 1H, N<u>H</u>), 3.78 (dd, *J* = 80.8, 11.2 Hz, 2H, OC<u>H$_2$</u>), 3.17 (s, 2H, <u>CH$_2$</u>OH), 2.21 (s, 3H, H-23), 1.44 (s, 3H), 1.37 (s, 3H), 1.27 (s, 3H), 1.11 (s, 3H), 0.81 (d, *J* = 4.5 Hz, 6H, $OCH_2C(C\underline{H_3})_2$), 0.75 (s, 3H) ppm. ^{13}C NMR (100 MHz, $CDCl_3$) δ 178.53 (C2), 170.14, 164.83, 155.93 (NH<u>C</u>OO), 146.17 (C3), 134.07 (C6), 127.63 (C5), 119.67 (C1), 118.14 (C7), 117.20 (C4), 69.08 (O<u>C</u>H$_2$), 67.88 (O<u>C</u>H$_2$), 50.26, 45.23, 44.05, 43.16, 39.26, 38.26, 36.97, 36.43, 35.23, 34.04, 33.45, 31.84, 30.76, 30.53, 29.87, 28.92, 22.14, 21.68, 21.54, 20.56, 10.40 ppm. MS (DI-ESI) (*m/z*): 552.3 $[M+H]^+$. Anal. Calcd for $C_{34}H_{49}NO_5$: C, 74.01; H, 8.95; N, 2.54; Found: C, 73.98; H, 9.09; N, 2.64.

Derivative 4.7 — Methyl N-[2,3-dihydroxy-6-oxo-24-nor-friedela-1,3,5(10),7-tetraen-20α-yl] carbamate

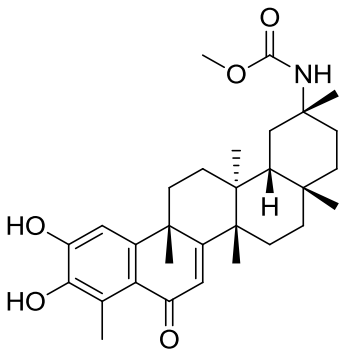

Figure 4.21 Chemical structure of compound **4.7.**

Starting from compound **3.5** (40.0 mg, 0.07 mmol) in dry methanol (4 mL), compound **4.7** (31.2 mg, 86%) was obtained as an orange solid according to the above-mentioned procedure. Mp: 280.7–282.4 °C. IR (neat) $_{vmax}$: 3306, 2943, 2871, 1696, 1637, 1578, 1506, 1452, 1312 cm^{-1}. ^{1}H NMR (400 MHz, $CDCl_3$) δ 6.96 (s, 1H, H-1), 6.25 (s, 1H, H-7), 4.63 (s, 1H, NH), 3.51 (s, 3H, $COOCH_3$), 2.68 (s, 3H, H-23), 1.47 (s, 3H), 1.35 (s, 3H), 1.26 (s, 3H), 1.10 (s, 3H), 0.70 (s, 3H) ppm. ^{13}C NMR (100 MHz, $CDCl_3$) δ 188.47 (C6), 172.50, 156.11 (NHCOO), 151.34, 148.57 (ArC-OH), 141.68 (ArC-OH), 125.94, 125.59, 122.23, 108.82, 51.96, 50.26, 44.86, 44.12, 40.42, 38.99, 37.41, 36.40, 35.87, 34.31, 33.96, 31.87, 30.81, 30.38, 28.71, 28.21, 21.01, 20.42, 14.06 ppm. MS (DI-ESI) (*m/z*): 496.5 $[M+H]^+$. Anal. Calcd for $C_{30}H_{41}NO_5$: C, 72.70; H, 8.34; N, 2.83; Found: C, 72.41; H, 7.98; N, 2.48.

Derivative 4.8 — Ethyl N-[2,3-dihydroxy-6-oxo-24-nor-friedela-1,3,5(10),7-tetraen-20α-yl] carbamate

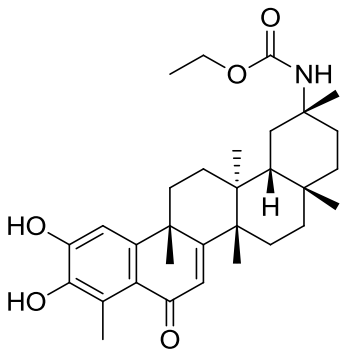

Figure 4.22 Chemical structure of compound **4.8.**

Starting from compound **3.5** (40.0 mg, 0.07 mmol) in dry ethanol (4 mL), compound **4.8** (32.7 mg, 88%) was obtained as an orange solid according to the above-mentioned procedure. Mp: 258.9–261.0 °C. IR (neat) $_{vmax}$: 3322, 2936, 2866, 1694, 1636, 1582, 1507, 1452, 1309 cm^{-1}. ^{1}H NMR (400 MHz, CD_3OD) δ 6.82 (s, 1H, H-1), 6.18 (s, 1H, H-7), 3.94 (dd, *J* = 17.5, 7.1 Hz, 2H, $OC\underline{H_2}CH_3$), 2.57 (s, 3H, H-23), 1.53 (s, 3H), 1.34 (s, 3H), 1.32 (s, 3H), 1.14 (s, 3H, $OCH_2C\underline{H_3}$), 1.11 (s, 3H), 0.80 (s, 3H) ppm. ^{13}C NMR (100 MHz, CD_3OD) δ 189.66 (C6), 174.48, 157.47 ($NH\underline{C}OO$), 157.47, 152.79 (ArC-OH), 143.91 (ArC-OH), 126.43, 126.33, 121.76, 109.76, 60.79 ($NHCOO\underline{C}H_2$), 50.73, 45.91, 45.54, 41.52, 40.12, 38.19, 37.60, 36.01, 35.34, 35.05, 32.19, 31.40, 31.23, 31.10, 29.99, 29.04, 21.71, 20.90, 15.19, 14.13 ppm. MS (DI-ESI) (*m/z*): 510.5 $[M+H]^+$. Anal. Calcd for $C_{31}H_{43}NO_5$: C, 73.05; H, 8.50; N, 2.75; Found: C, 72.93; H, 8.22; N, 2.65.

Derivative 4.9 — Methyl N-[2-hydroxy-3-methoxy-6-oxo-24-nor-friedela-1,3,5(10),7-tetraen-20α-yl] carbamate

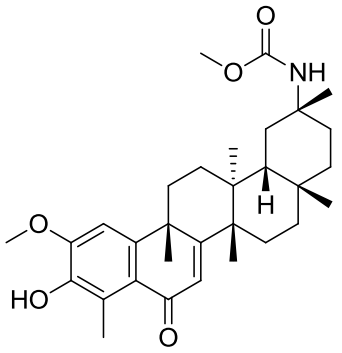

Figure 4.23 Chemical structure of compound **4.9.**

Compound **4.9** was prepared according to the literature [*330*] from compound **4.7** (25.0 mg, 0.05 mmol). The obtained crude was purified by preparative TLC (CH_2Cl_2/MeOH 20:1), to yield compound **4.9** (16.7 mg, 65%) as a yellowish solid. Mp: 251.8–255.0 °C. IR (neat) $_{vmax}$: 3342, 2942, 2870, 1714, 1641, 1595, 1489, 1447, 1307 cm^{-1}. ^{1}H NMR (400 MHz, $CDCl_3$) δ 6.81 (s, 1H, H-1), 6.26 (s, 1H, H-7), 4.45 (s, 1H, NH), 3.96 (s, 3H, ArOCH_3) 3.50 (s, 3H, COOCH_3), 2.64 (s, 3H, H-23), 1.54 (s, 3H), 1.36 (s, 3H), 1.30 (s, 3H), 1.11 (s, 3H), 0.75 (s, 3H) ppm. ^{13}C NMR (100 MHz, $CDCl_3$) δ 187.73 (C6), 171.33, 155.54 (NHCOO), 150.11, 149.33 (ArC-OH), 142.37 (ArC-OH), 126.29, 124.70, 123.55, 103.89, 56.01, 51.53, 50.08, 44.85, 44.15, 40.46, 38.89, 37.60, 36.50, 35.75, 34.57, 34.04, 31.89, 30.88, 30.46, 30.17, 28.77, 28.46, 21.09, 20.34, 13.46 ppm. MS (DI-ESI) (*m/z*): 510.5 $[M+H]^+$. Anal. Calcd for $C_{31}H_{43}NO_5$: C, 73.05; H, 8.50; N, 2.75; Found: C, 73.25; H, 8.48; N, 2.56.

Derivative 4.10 — Ethyl N-[2,3-dimethoxy-6-oxo-24-nor-friedela-1,3,5(10),7-tetraen-20α-yl] carbamate

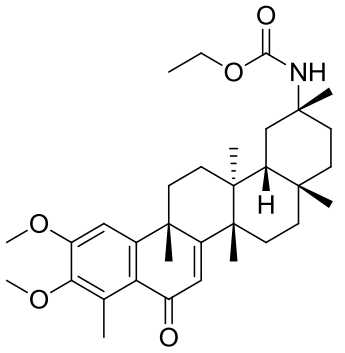

Figure 4.24 Chemical structure of compound **4.10.**

Compound **4.10** was prepared according to the literature [*330*] from compound **4.8** (25.0 mg, 0.05 mmol). The obtained crude was purified by preparative TLC (CH_2Cl_2/MeOH 20:1), to yield compound **4.10** (17.1 mg, 67%) as a yellowish solid. Mp: 220.4–221.9 °C. IR (neat) $_{vmax}$: 3340, 2936, 2869, 1715, 1644, 1584, 1483, 1449, 1294 cm^{-1}. ^{1}H NMR (400 MHz, $CDCl_3$, CD_3OD) δ 6.83 (s, 1H, H-1), 6.26 (s, 1H, H-7), 4.41 (s, 1H, N<u>H</u>), 3.92 (s, 3H, ArOC<u>H</u>$_3$), 3.77 (s, 3H, ArOC<u>H</u>$_3$), 2.65 (s, 3H, H-23), 1.55 (s, 3H), 1.36 (s, 3H), 1.31 (s, 3H), 1.11 (s, 6H, OCH_2C<u>H</u>$_3$), 0.78 (s, 3H) ppm. ^{13}C NMR (100 MHz, CD_3OD) δ 187.42 (C6), 171.21, 155.81 (NH<u>C</u>OO), 155.17, 154.27 (ArC-OH), 146.03 (ArC-OH), 133.81, 126.26, 123.36, 105.57, 60.47, 30.11, 28.80, 28.46, 21.25, 20.30, 14.81, 14.14 ppm. MS (DI-ESI) (*m/z*): 538.5 $[M+H]^+$. Anal. Calcd for $C_{33}H_{47}NO_5$: C, 73.71; H, 8.81; N, 2.60; Found: C, 73.62; H, 8.59; N, 2.43.

Derivative 4.11 — Methyl N-[2,3-Diacetoxy-24-nor-friedela-1,3,5(10),7-tetraen-20α-yl] carbamate

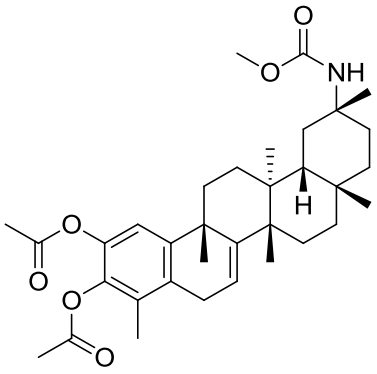

Figure 4.25 Chemical structure of compound **4.11.**

Starting from compound **3.3** (40.0 mg, 0.08 mmol) in dry methanol (4 mL), compound **4.11** was obtained as a white solid according to the above-mentioned general procedure for the synthesis of carbamates. Compound **4.11** was purified by flash column chromatography (PE/AcOEt, 6:1→5:1), to yield compound **4.11** (33.1 mg, 78%) as a white solid. Mp: 231.3–233.5 °C. IR (neat) $_{vmax}$: 3357, 2942, 2865, 1768, 1724, 1452, 1369, 1215 cm^{-1}. ^{1}H NMR (400 MHz, $CDCl_3$) δ 7.00 (s, 1H, H-1), 5.75 (d, *J* = 4.5 Hz, 1H, H-7), 4.46 (s, 1H, NH), 3.53 (s, 3H, OCH_3), 3.32 (dd, *J* = 21.0, 5.9 Hz, 1H, H-6b), 3.07 (d, *J* = 21.0 Hz, 1H, H-6a), 2.31 (s, 3H, CH_3CO), 2.27 (s, 3H, CH_3CO), 2.06 (s, 3H, H-23), 1.36 (s, 3H), 1.35 (s, 3H), 1.23 (s, 3H), 1.09 (s, 3H), 0.78 (s, 3H) ppm. ^{13}C NMR (100 MHz, $CDCl_3$) δ 168.93 (CH_3COO), 168.63 (CH_3COO), 155.38 ($NHCOO$), 149.40, 147.69, 140.70, 138.18, 131.63, 127.97, 116.94, 116.92, 51.60, 50.10, 44.17, 43.96, 37.42, 36.94, 35.38, 34.56, 34.38, 34.07, 31.87, 31.73, 30.93, 30.51, 29.13, 28.73, 28.29, 23.09, 22.79, 20.82, 20.57, 14.26, 12.71 ppm. MS (DI-ESI) (*m/z*): 588.5 $[M+Na]^+$. Anal. Calcd for $C_{34}H_{47}NO_6$: C, 72.18; H, 8.37; N, 2.48; Found: C, 72.57; H, 8.15; N, 2.32.

Derivative 4.12 — 20α-Amido-24-nor-friedela-1,3,5(10),7-tetraen-2,3-di-yl diacetate

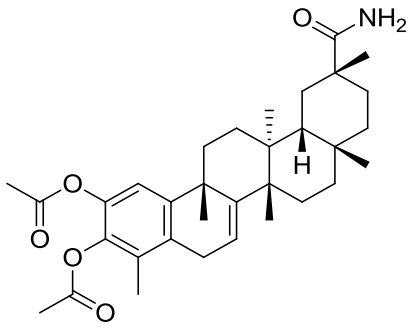

Figure 4.26 Chemical structure of compound **4.12.**

Oxalyl chloride (0.04 mL, 0.45 mmol) was added to a solution of compound **1.82** (40.0 mg, 0.07 mmol) in dry dichloromethane (4 mL), and the resulting mixture was stirred for 4 h at room temperature and N_2 atmosphere. The mixture was concentrated to dryness under reduced pressure and the residue was dissolved in dry toluene (4 mL). A concentrated solution of ammonia (0.5 mL) was added at 0 ºC, and the mixture was stirred for 1 h. The mixture was then extracted with dichloromethane (3 × 20 mL), the combined extracts were washed with an aqueous saturated solution of $NaHCO_3$ (20mL), water (20 mL), and brine (20 mL), and dried over anhydrous Na_2SO_4. Finally, it was filtered and concentrated under vacuo to afford a yellowish powder, which was purified by preparative TLC (PE/AcOEt 1:1) to yield compound **4.12** (25.7 mg, 64%) as a white solid. Mp: 221.0–222.8°C. IR (neat) $_{vmax}$: 3483, 3372, 3183, 2926, 2865, 1769, 1663, 1460, 1369, 1221 cm^{-1}. ^1H NMR (400 MHz, $CDCl_3$) δ 6.98 (s, 1H, H-1), 5.74 (dd, *J* = 6.0, 1.7 Hz, 1H, H-7), 5.67 (s, 2H, $N\underline{H_2}$), 3.32 (dd, *J* = 20.9, 6.1 Hz, 1H, H-6b), 3.06 (d, *J* = 20.9 Hz, 1H, H-6a), 2.30 (s, 3H, $C\underline{H_3}CO$), 2.26 (s, 3H, $C\underline{H_3}CO$), 2.06 (s, 3H, H-23), 1.32 (s, 3H), 1.22 (s, 3H), 1.18 (s, 3H), 1.09 (s, 3H), 0.75 (s, 3H) ppm. ^{13}C NMR (100 MHz, $CDCl_3$) δ 181.48 ($\underline{C}ONH_2$), 168.86 ($CH_3\underline{C}OO$), 168.55 ($CH_3\underline{C}OO$),149.69, 147.65, 140.69, 138.17, 131.70, 127.90, 117.08, 116.71, 77.16, 44.42, 43.83, 40.57, 37.61, 37.35, 36.86, 34.94, 34.44, 34.15, 33.94, 31.67, 30.99, 30.93, 30.57, 30.13, 29.06, 28.27, 23.21, 20.84, 20.56, 18.80, 12.73 ppm. MS (DI-ESI) (*m/z*): 558.5 $[M+Na]^+$. Anal. Calcd for $C_{33}H_{45}NO_5$: C, 73.99; H, 8.47; N, 2.61; Found: C, 74.31; H, 8.38; N, 2.31.

Derivative 4.13 — 20α-Formyl-24-nor-friedela-1,3,5(10),7-tetraen-2,3-di-yl diacetate

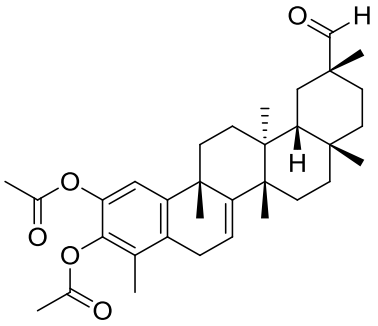

Figure 4.27 Chemical structure of compound **4.13.**

Oxalyl chloride (0.04 mL, 0.45 mmol) was added to a solution of compound **1.82** (40.0 mg, 0.07 mmol) in dry dichloromethane (4 mL), and the resulting mixture was stirred for 4 h at room temperature and N_2 atmosphere. The mixture was concentrated to dryness under reduced pressure and the residue was dissolved in dry tetrahydrofuran (4 mL). Lithium tri-*tert*-butoxyaluminum hydride (LTBA) (22.8 mg, 0.09 mmol) was added at 0 ºC, and the mixture was stirred for 1 h. The reaction mixture was evaporated under reduced pressure to remove tetrahydrofuran. The obtained crude was then diluted with ethyl acetate (3 × 20 mL), and the combined extracts were washed with a sulfite solution (10% aq) (20mL), water (20 mL), and brine (20 mL), and dried over anhydrous Na_2SO_4. Finally, it was filtered and concentrated under vacuo to afford a whitish powder, which was purified by preparative TLC (PE/AcOEt 4:1) to yield compound **4.13** (24.3 mg, 63%) as a white solid. Mp: 257.7–260.1 °C. IR (neat) $_{vmax}$: 3544, 2941, 2865, 1778, 1479, 1456, 1369, 1211 cm^{-1}. ^{1}H NMR (400 MHz, $CDCl_3$) δ 9.30 (d, *J* = 1.3 Hz, 1H, CO<u>H</u>), 6.99 (s, 1H, H-1), 5.74 (dd, *J* = 6.0, 1.8 Hz, 1H, H-7), 3.32 (dd, *J* = 20.9, 6.1 Hz, 1H, H-6b), 3.05 (d, *J* = 21.0 Hz, 1H, H-6a), 2.30 (s, 3H, C<u>H</u>$_3$CO), 2.26 (s, 3H, C<u>H</u>$_3$CO), 2.06 (s, 3H, H-23), 1.35 (s, 3H), 1.22 (s, 3H), 1.09 (s, 3H), 0.93 (s, 3H), 0.58 (s, 3H) ppm. ^{13}C NMR (100 MHz, $CDCl_3$) δ 205.28 (C=O), 168.86 (CH$_3$<u>C</u>OO), 168.54 (CH$_3$<u>C</u>OO), 148.91, 147.50, 140.72, 138.18, 131.62, 128.01, 117.38, 116.67, 44.64, 43.97, 43.85, 37.88, 37.31, 36.90, 34.62, 34.52, 34.38, 31.61, 30.88, 30.62, 29.38, 28.83, 28.22, 27.68, 26.49, 22.92, 20.84,

20.54, 20.16, 12.71 ppm. MS (DI-ESI) (*m/z*): 543.5 $[M+Na]^+$. Anal. Calcd for $C_{33}H_{44}O_5$: C, 76.12; H, 8.52; Found: C, 75.71; H, 8.15.

Derivative 4.14 — 20α-Hydroxy-24-nor-friedela-1,3,5(10),7-tetraen-2,3-di-yl diacetate

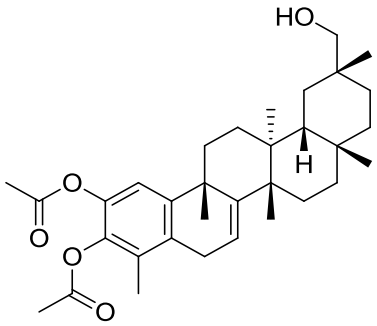

Figure 4.28 Chemical structure of compound **4.14.**

Compound **4.13** (20.0 mg, 0.04 mmol) was dissolved in ethanol (2 mL) and was treated with sodium borohydride (2.2 mg, 0.06 mmol), and the resulting mixture was stirred for 1 h at 0 ºC. Excess reagent sodium borohydride was decomposed with acetone (2 mL) at 0 ºC. The resulting mixture was evaporated under reduced pressure to dryness, to afford a white residue. The residue was subjected to preparative TLC (PE/AcOEt 3:1) to afford compound **4.14** (13.7 mg, 68%) as a white solid. Mp: 214.3–215.9 °C. IR (neat) $_{vmax}$: 3565, 2941, 2869, 1586, 1438, 1456, 1375, 1286 cm^{-1}. ^1H NMR (400 MHz, $CDCl_3$) δ 6.99 (s, 1H, H-1), 5.78 (dd, *J* = 6.1, 1.7 Hz, 1H, H-7), 3.41 (d, *J* = 10.4 Hz, 1H, C$\underline{H_2}$OH), 3.35 (dd, *J* = 20.9, 6.2 Hz, 1H, H-6b), 3.22 (d, *J* = 10.5 Hz, 1H, C$\underline{H_2}$OH), 3.08 (d, *J* = 20.0 Hz, 1H, H-6a), 2.31 (s, 3H, C$\underline{H_3}$CO), 2.27 (s, 3H, C$\underline{H_3}$CO), 2.07 (s, 3H, H-23), 1.33 (s, 3H), 1.32 (s, 3H), 1.17 (s, 3H), 0.99 (s, 3H), 0.82 (s, 3H) ppm. ^{13}C NMR (100 MHz, $CDCl_3$) δ 168.92 ($CH_3\underline{C}OO$), 168.59 ($CH_3\underline{C}OO$), 150.97, 147.65, 140.68, 138.18, 132.01, 127.99, 117.54, 116.52, 71.86 ($\underline{C}H_2OH$), 43.31, 43.16, 37.80, 37.48, 37.12, 36.67, 34.26, 33.72, 33.04, 32.30, 30.61, 30.56, 30.46, 29.47, 28.89, 28.28, 28.24, 25.85, 20.83, 20.56, 19.47, 12.74 ppm. MS (DI-ESI) (*m/z*): 545.5 $[M+Na]^+$. Anal. Calcd for $C_{33}H_{46}O_5$: C, 75.83; H, 8.87; Found: C, 75.87; H, 8.99.

4.4.2. Biological activity assays

4.4.2.1. Reagents

Dulbecco's Modified Eagle's Medium (DMEM) — no glucose, no glutamine, no phenol red, Penicillin-Streptomycin (100 ×) (P/S) solution, MEM-Eagle non-essential aminoacids (100 ×), and Fetal Bovine Serum (FBS) were purchased from Thermo Fisher Scientific. DMEM — high glucose with L-glutamine, Phosphate Buffered Saline (PBS), and L-glutamine were obtained from Biowest. MTT powder was purchased from Applichem. DMSO, Hoechst 33342, and PI were purchased from Sigma-Aldrich. Hydrophobic Polyvinylidene Fluoride (PVDF) and western blotting detection kit reagent were purchased from Merck Millipore.

Primary antibodies against caspase-3, cleaved caspase-3, caspase-8, caspase-9, Hsp90, mTOR, p-mTOR, Akt, and pAkt were purchased from Cell Signalling Technology. Primary antibodies against PARP, Bid, and cytochrome c were obtained from BD Pharmingen. Primary antibodies against Bax, Bcl-2, p-JNK, and p-JNK were obtained from SantaCruz Biotechnology. Primary antibody against p53 was purchased from Merck Millipore and the antibody against α-actin was purchased from MP Biomedicals. Secondary antibody HRP-conjugated anti-mouse was obtained from Dako, and the anti-rabbit antibody was obtained from Amersham Biosciences.

4.4.2.2. Compounds

Stock solutions were prepared at a concentration of 10 mM by dissolving celastrol **1.26** and its derivatives in DMSO, and subsequently stored at -20 ºC. To obtain the working solutions at the final desired concentration, the stock solutions were further diluted in culture medium just before each experiment. The final concentration of DMSO was always lower than 0.5% for all working solutions.

4.4.2.3. Cell culture

A549, HT-29, MCF-7, MDAMB-231, MIA PaCa-2, SKOV-3, and BJ cell lines were obtained from American Type Culture Collection (ATCC). A549, MDAMB-231, MIA PaCa-2, SKBR-3, and SKOV-3 cells were routinely maintained in DMEM — high glucose with L-glutamine, supplemented with 10% (V/V) FBS and P/S solution (1 ×). BJ cells were cultured in DMEM — high glucose, supplemented with 10% (V/V) FBS and P/S solution (1 ×), 2 mM L-glutamine, and 1 mM sodium pyruvate. MCF-7 cells were grown in DMEM — no phenol red, supplemented with 10% (V/V) FBS, P/S solution (1 ×), MEM-Eagle non-essential aminoacids (1 ×), 2 mM L-glutamine, 10 mM glucose, 1 mM sodium pyruvate, and 0.01 mg/mL human insulin. All cells were incubated in a humidified incubator at 37°C in 5% CO_2.

4.4.2.4. MTT assay

The effect of the compounds at different concentrations on the viability of the cell lines was determined using the MTT assay. A549, MIA PaCa-2, SKOV-3 (2×10^3 cells/well), and HT-29 cells (4×10^3 cells/well), and BJ, MDAMB-231 and MCF-7 cells (10×10^3 cells/well) were seeded in 96-well plates and pre-incubated for 24 h. Cells were then treated with increasing concentrations of each compound, in triplicate. After 72 h of incubation at 37 ºC, the supernatant was removed and replaced by 100 µL of filtered MTT solution (0.5 mg/mL in growth medium) in each well, and the plates were incubated for an additional 1 h. Then the MTT solution was removed and 100 µL of DMSO was added in each well to dissolve the formazan crystals formed. The absorbance values were immediately measured using an ELISA plate reader (Tecan Sunrise MR20-301) at 550 nm. The IC_{50} values were calculated based on three independent experiments using Graphpad Prism 5 software and expressed as mean ± standard error of mean (SEM).

4.4.2.5. Cell-cycle and apoptosis assay

Cell-cycle distribution and apoptosis were measured by flow cytometry using a Fluorescence-Activated Cell Sorter (FACS). SKOV-3 cells (4×10^4 cells/well) were seeded in 6-well plates, and pre-incubated at 37 ºC for 24 h. Then cells were further incubated with fresh growth medium (control) or compound **4.11** at its IC_{50} concentration for 24, 48 or 72 h. After the respective period of incubation, cells were harvested by mild trypsinization, washed with PBS, and collected by centrifugation. For cell-cycle analysis, the cells were resuspended in Tris-Buffered Saline (TBS) containing 50 mg/mL PI, 10 mg/mL DNase-free RNase, and 0.1% Igepal CA-630, incubated at 4 ºC for 1h, and protected from the light. For apoptosis analysis, after centrifugation, the cells were resuspended in 95 µL of binding buffer and 3 µL of Annexin-V FITC conjugate (1 mg/mL), incubated for 30 min, and protected from the light, and 500 µL of binding buffer and 20 µL of PI solution (1 mg/mL) were added to the cell suspension just before FACS analysis. FACS analysis was performed using an Epics XL flow cytometer at 488 nm. The data was collected from 1×10^4 cells and analysed using the multicycle software (Phoenix Flow Systems). Each condition had two replicates and the experiments were repeated three times.

4.4.2.6. Fluorescence microscopy imaging

SKOV-3 cells (4×10^4 cells/well) were seeded in 6-well plates, and pre-incubated at 37 ºC for 24 h. Then cells were incubated with fresh culture medium (control) or compound **4.11** at its IC_{50} concentration for 48 h. After removing the culture medium and washing with PBS 500 µL of Hoechst 33342 solution (1 µg/mL in PBS) was added to each well, and the plates were incubated for 10 min at 37 ºC protected from the light. The cells were then imaged on a fluorescence microscope (DMRB Leica Microsystems) with a DAPI filter to detect the differences on the morphological features of SKOV-3 cells.

4.4.2.7. Western blot analysis

Protein extracts of SKOV-3 cells untreated (control) and treated with compound **4.11** at its IC_{50} concentration for 72 h were prepared with lysis buffer (20 mM trizma base pH 7.5, 1 mM dithriothreitol, 1 mM EDTA, 0.0002% triton X-100, 0.5 mM sodium deoxycholate, 0.4 mM PMSF, 1% protease inhibitor cocktail, and 1% phosphatase inhibitor cocktail), and the protein concentration was subsequently quantified by the BCA assay kit. The extracted proteins were separated on 8% or 15% sodium dodecyl sulphate (SDS)-polyacrylamide gels by electrophoresis and transferred to PVDF membranes. After blocking the membranes with PBS containing 0.1% Tween-20® (PBST 0.1%) and 5% non-fat milk for 1 h, the membranes were incubated with the primary specific antibodies overnight at 4 ºC, with the exception of α-actin (incubated only for 1 h at room temperature). The membranes were then washed with PBST 0.1% and incubated for 1 h with the appropriate secondary antibody (anti-mouse or anti-rabbit). After incubation, the membranes were washed again with PBST 0.1%, and the immunocomplexes were visualised using a chemiluminescence western blotting detection kit and autoradiography film.

4.4.2.8. Clonogenic assay

Briefly, 1000 SKOV-3 cells per well were seeded in 6-well plates and incubated for 24 h. Then the cells were treated with compound **4.11** at its IC_{50} concentration or twice its IC_{50} concentration for 24 h. The cells were then allowed to grow in drug-free medium in 6-well plates for an additional 12 days. Afterwards, the medium was removed and the resulting colonies were fixed and stained with 1% crystal violet in methanol for 4 h. After washing with PBS, the colonies were observed under an inverted phase contrast microscope (Olympus IMT-2) with an objective of 40 ×, and photographed with a digital camera Fujifilm A2O5S.

4.4.2.9. Synergy study

SKOV-3 cells were incubated in 96-well plates following the above-mentioned procedure for the MTT assay. After 24 h, the cells were treated with increasing concentrations of compound **4.11**, carboplatin, or the combination of both with a constant ratio of concentrations. After 72 h of incubation, the relative cell viability was analysed as described above for the MTT assay. The effect of compound **4.11**, carboplatin or the combination of both was analysed using the CompuSyn software, which determined the Combination Index (CI) values. CI values below 1, equal to 1, and above 1 indicate synergy, additivity, and antagonism, respectively.

CHAPTER V

STRUCTURAL DIVERSIFICATION OF THE CELASTROL DERIVATIVES AND THEIR IMPACT ON ANTITUMOUR ACTIVITY

Sandra A.C. Figueiredo, Jorge A.R. Salvador, Roldán Cortés, Marta Cascante

Structural diversification of the celastrol derivatives and their impact on antitumour activity

Article in preparation

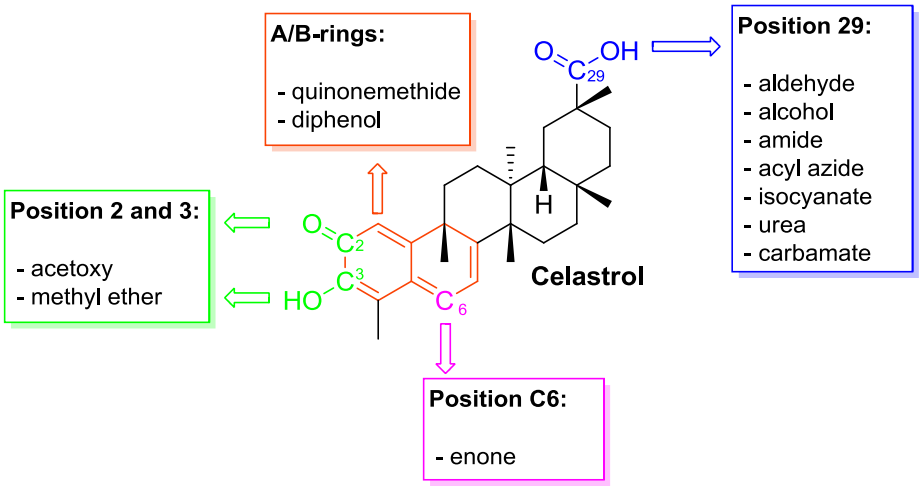

Highlights

- Synthesis of new celastrol derivatives with anticancer activity.
- Structural diversification through different chemical modifications and structural elucidation of novel derivatives.
- Study of structure-activity relationship of new anticancer compounds.

5. CHAPTER V

Structural diversification of the celastrol derivatives and their impact on antitumour activity

5.1. INTRODUCTION

Our previous results (**Chapter 3** and **4**) showed that some celastrol derivatives, such as ureas and carbamates at the C(29) position, presented a remarkable activity against tumour cell lines, while closely related structures turned out to be almost inactive. Given the biological importance of celastrol **1.26**, any additional structural modifications to its backbone would be most informative. Thus, this analysis enables the determination of the chemical groups responsible for its activity, especially for the anticancer activity studied here.

Therefore, in this chapter we describe further structural diversification through new chemical modification, as well as structural elucidation of celastrol derivatives and new insight of previous prepared celastrol analogues. This allowed us a deeper understanding of structure-activity relationship, chemical reactivity and stability. To determine their anticancer potential, the activity of all synthesised analogues on the viability of cancer cells was evaluated against two human tumour cell lines (lung carcinoma A549 and pancreatic carcinoma MIA PaCa-2), using the MTT assay.

5.2. RESULTS AND DISCUSSION

5.2.1. Protecting groups

As indicated previously, celastrol **1.26** is a natural QT, whose *p*-QM substructure consists of a cyclohexadiene moiety in *para*-conjugation with a carbonyl group and an exo-methylene component. *p*-QMs are formally neutral molecules, which zwitterionic aromatic valence bond resonance structures make an important contribution to their structure (Figure 5.1) [*359*].

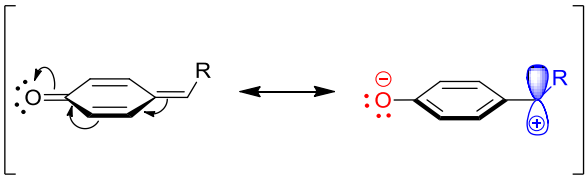

Figure 5.1 Zwitterionic structure of *p*-quinonemethide.

Unlike simple *p*-QM, the terpenoid structure of celastrol **1.26** has a hydroxyl group in the *ortho* position relative to the carbonyl oxygen, which enhances its reactivity through an intramolecular hydrogen bond, and an extended conjugation at the exocyclic methylene group that counteracts this activation (Figure 5.2). This combination of neutral and zwitterionic valence bond structures confers a distinctive chemical reactivity to celastrol **1.26**, which makes it a highly reactive chemical molecule [*360*]. Therefore, in order to carry out selective reactions and have greater control over the chemistry used, these reactive sites should be temporarily protected.

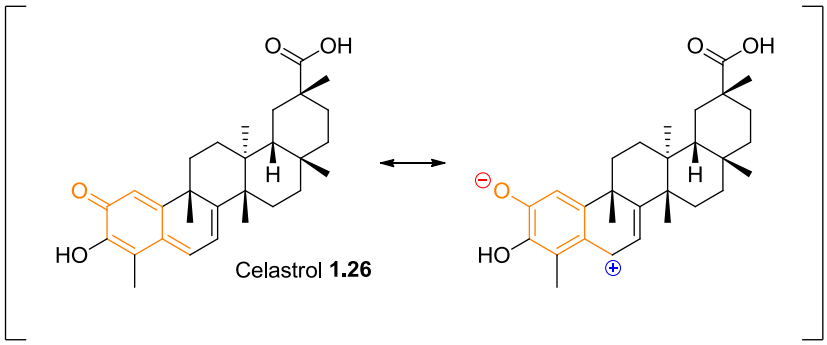

Figure 5.2 Zwitterionic form of celastrol **1.26**.

The strategy used to protect the *p*-QM structure, has been shown previously and, consisted in firstly reducing celastrol **1.26** to dihydrocelastrol **1.81** using $NaBH_4$ in ethanol (Scheme 5.1). *p*-QMs triterpenoids are readily reduced by a variety of reagents (e.g., $NaBH_4$ and $LiAlH_4$), resulting in a simple nucleophilic addition of a hydride to the C(6) position of B-ring, leading to aromatization of A-ring. Notably, this quick reaction is accompanied by complete discoloration of the reaction solution, which is characteristic of the reduction of the chromophore that extends over the A/B-rings responsible for the red-orange colour. After isolation,

the dihydrocelastrol **1.81** product is very unstable and undergoes rapid reoxidation back to starting compound **1.26**. Therefore we did not isolate it and proceeded to direct acetylation after quenching and evaporating the solvent [*119*]. The method of choice for protection was the conversion to dihydrocelastrol diacetate **1.82**, since the formation and subsequent cleavage can be achieved under mild conditions. The reaction was performed by using acetic anhydride in the presence of the base triethylamine and DMAP as cocatalyst (Scheme 5.1). Besides the protecting function, it should be reemphasised that the compound dihydrocelastrol diacetate **1.82** was found to have potency comparable to the parent compound **1.26** [*240*].

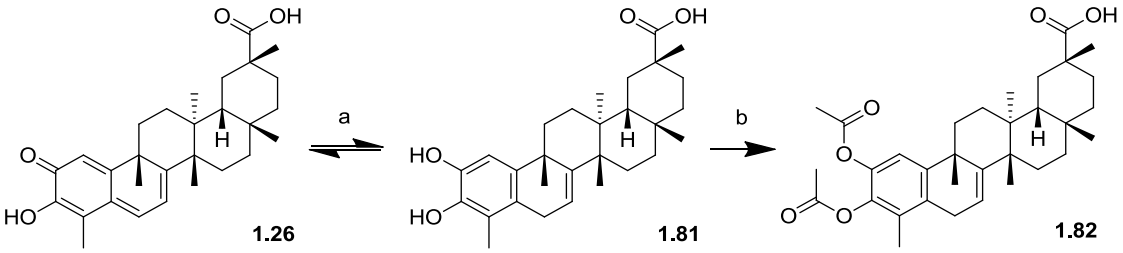

Scheme 5.1 Synthesis of dihydrocelastrol diacetate **1.82**. *Reagents and conditions*: a) $NaBH_4$, MeOH, R.T., 10 min; b) $(CH_3CO)_2O$, DMAP, THF, R.T., N_2, 4 h.

Deprotection of aromatic acetates can classically be carried out under acidic or basic conditions. However, these deprotection methods may affect the sensitive functional groups present in the molecules [*361*]. Therefore, we used a simple, green, mild and highly efficient protocol with remarkable selectivity for deprotection of aromatic acetates. This method uses ammonium acetate as a neutral catalyst in aqueous methanol under neutral conditions at room temperature [*310*]. Thus, the deprotection of the acetyl protecting groups of compound **1.82** led to the formation of dihydrocelastrol **1.81** and further aerial oxidation back to the parent compound **1.26** (Scheme 5.2). Afterwards we verified that a small amount of triethylamine, a weak base, accelerated considerably the reaction without influencing the chemical stability of these molecules.

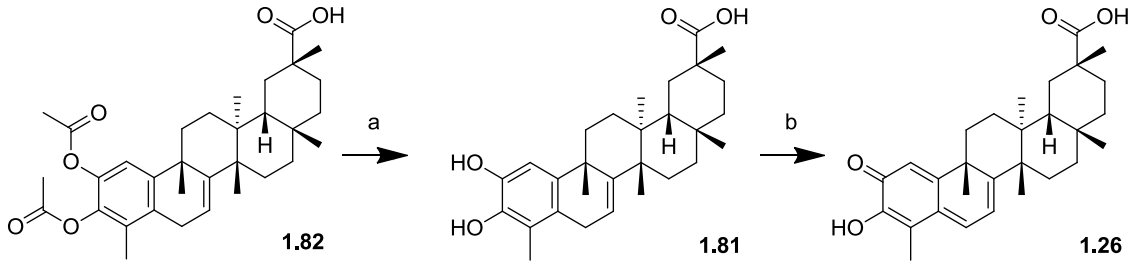

Scheme 5.2 Deprotection of dihydrocelastrol diacetate **1.82**. *Reagents and conditions:* a) NH_4OAc, Et_3N, aq. MeOH (1:4), R.T., 1 h; b) atmospheric air

The modifications in the A/B-rings from *p*-QM (e.g., compound **1.26**) to aromatic substructures (e.g., compound **1.81** and **1.82**) were confirmed by NMR. In celastrol **1.26** ^{1}H NMR spectrum, it was observed two doublets at 7.06 ppm with a coupling constant of 6.9 Hz and at 6.32 ppm with a coupling constant of 7.2 Hz, typical of the conjugated dienes (H-6 and H-7, respectively) (Figure 5.3). After protection, the high H-6 signal disappeared, and the chemical shift of alkene H-7 was observed as a doublet at 5.72 ppm with a coupling constant of 4.6 Hz in derivative **1.82**; additionally, it was observed two singlets at 2.30 and 2.27 ppm corresponded to the acetate protons (Figure 5.4). Moreover, in the ^{13}C NMR spectrum of diacetate celastrol **1.82**, the signals for quaternary carbonyl carbons were observed at 168.84 and 168.51 ppm. These data were constant for all the diacetate derivatives of celastrol.

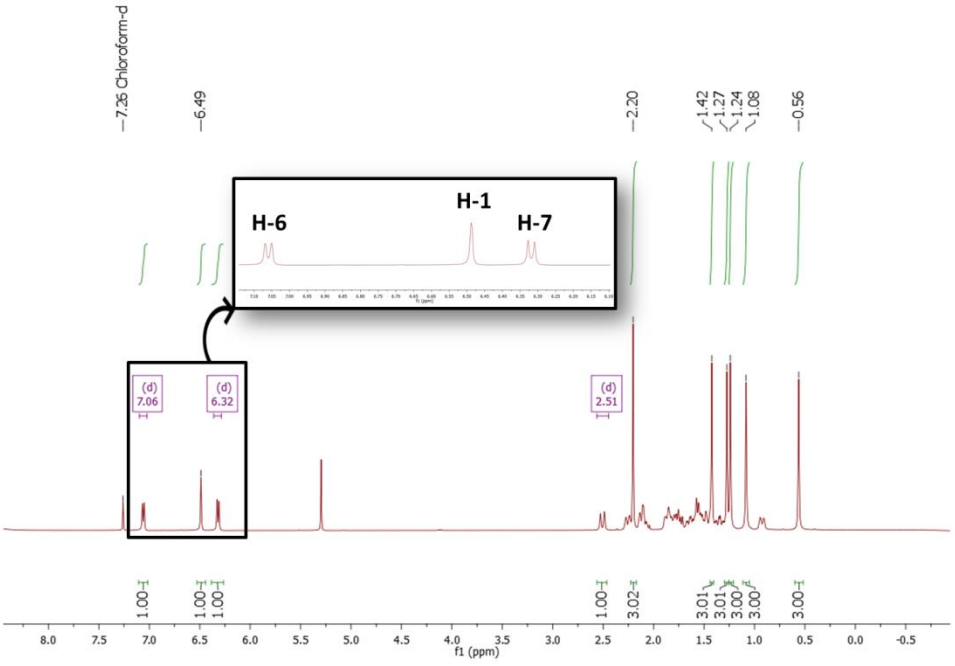

Figure 5.3 ^{1}H NMR spectrum of celastrol**1.26**.

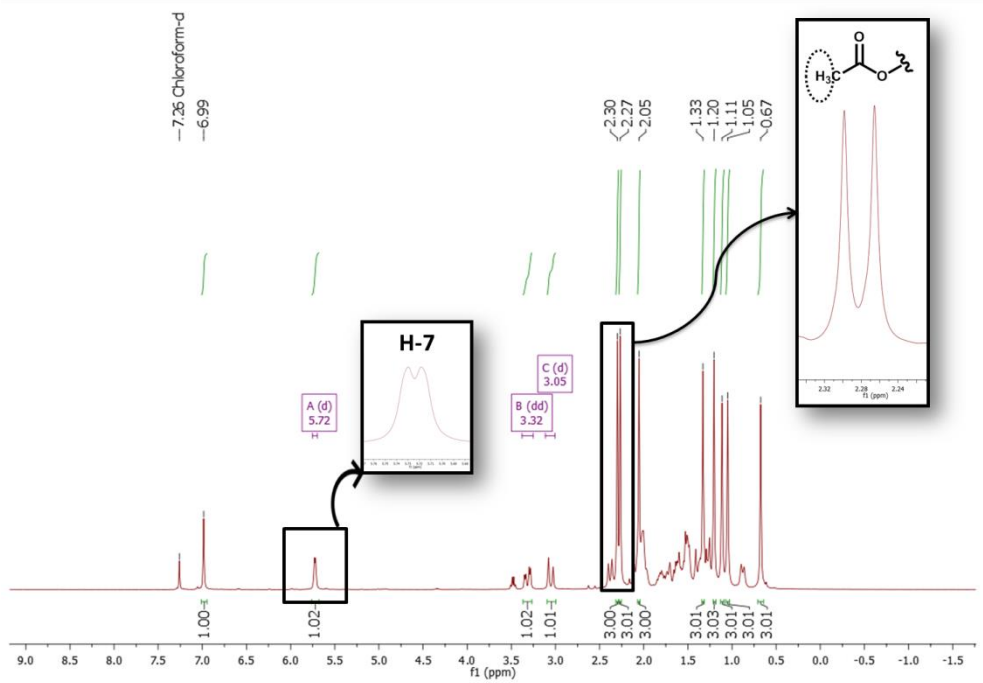

Figure 5.4 ^{1}H NMR spectrum of diacetate celastrol **1.82**.

5.2.2. C(29)-derivatives

Modifications at the C(29) position are the most common among the literature of celastrol derivatives. Simple modifications, such as esterification and amidification, afforded compound with similar or better anticancer activity than the parent compound **1.26** [*107*, *108*, *286*, *287*]. However, far more strategies can be applied to obtain new compounds with improved biological and pharmacokinetics properties.

5.2.2.1. Reduction reactions

Herein, we investigated the importance of the carboxylic functionality of celastrol **1.26** with simultaneous retention of hydrogen donor properties, affording aldehyde **5.1** and alcohol **5.2**. Since the direct attempts to selectively reduce the carboxylic group of celastrol **1.26** resulted in complete recovery of the starting material, we used the strategy of protection/deprotection of the A/B-rings as described in the previous subsection. Then, we treated dihydrocelastrol diacetate **1.82** with oxalyl chloride in dichloromethane to give the acid chloride of dihydrocelastrol diacetate **3.1** (Scheme 5.3).

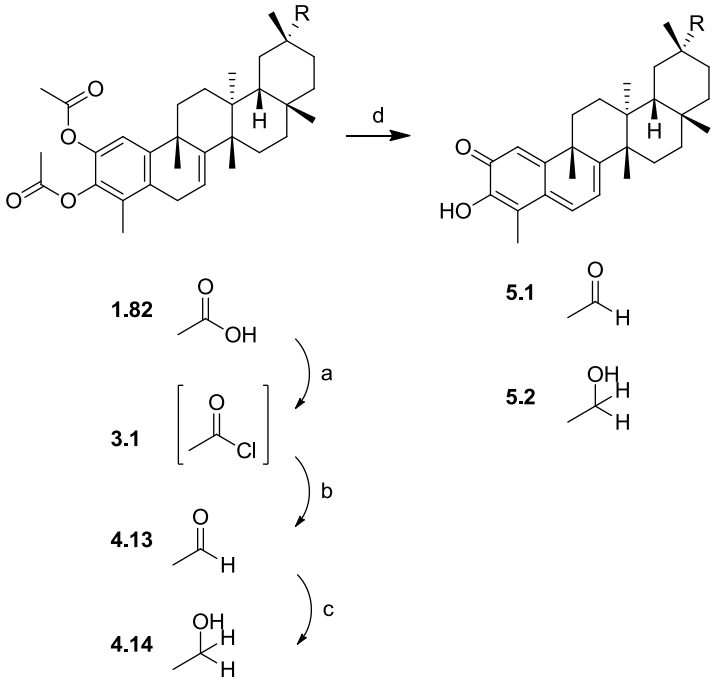

Scheme 5.3 Synthesis of aldehyde **5.1** and alcohol **5.2**. *Reagents and conditions:* a) $(COCl)_2$, CH_2Cl_2, R.T., N_2, 4 h; b) LTBA, THF, 0ºC, 1h; c) $NaBH_4$, EtOH, R.T., 1 h; d) NH_4OAc, Et_3N, aq. MeOH (1:4), R.T., 1 h.

Acid chlorides can be selectively converted to aldehydes using lithium tri-*tert*-butoxyaluminum hydride (LTBA). LTBA has a unique reactivity profile and reduces aldehydes and ketones selectively in the presence of esters, with which it reacts extremely slowly (Figure 5.5) [*362*]. Acid chloride **3.1** is highly activated, so it still reacts with LTBA, the hydride source, at 0 ºC, yielding compound **5.1**; the formed aldehyde will react slowly, allowing its isolation. Additional reduction of aldehyde **5.1** with sodium tetrahydroborate afforded primary alcohol **5.2** (Scheme 5.3) [*363*].

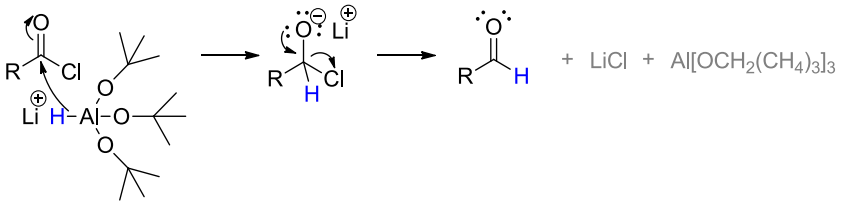

Figure 5.5 Reduction of acyl chloride to give aldehyde with LTBA.

The presence of the aldehyde functional group in compound **5.1** was confirmed by the presence in the ^{1}H NMR spectrum of a signal at 9.32 ppm,

corresponding to the CHO proton. The signal corresponding to the tertiary carbons CHO was found at 205.24 ppm in the ^{13}C NMR spectrum. The presence of the primary alcohol of compound **5.2** was also confirmed by the two doublets in the ^{1}H NMR spectrum at 3.42 ppm and 3.21 ppm, with a coupling constant of J = 10.5 Hz. The ^{13}C NMR signal observed at 71.48 ppm corresponded to a secondary carbon, as this signal was inverted in the DEPT spectrum, and was attributed to the carbon CH_2OH.

Both aldehyde **5.1** and alcohol **5.2** exhibited high anticancer activity on human lung carcinoma A549 and the human pancreatic carcinoma MIA PaCa-2 cell lines; however, the activity slightly decreased with the decreasing of oxidation state of the derivatives (Table 5.1).

Table 5.1 IC_{50} (µM) values of celastrol **1.26** and derivatives **5.1** and **5.2** in tumour cell lines and respective oxidation state.

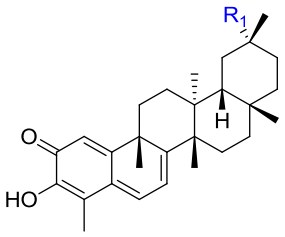

Compounds	R_1	Oxidation state	IC_{50} (µM ± SEM) A549	IC_{50} (µM ± SEM) MIA PaCa-2
Celastrol **1.26**	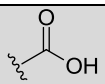		1.56±0.08	0.46±0.03
5.1			1.83±0.04	0.57±0.03
5.2			2.17±0.04	0.68±0.02

5.2.2.2. Nitrogen compounds

Nitrogen is one of the most interesting elements in medicinal chemistry, as numerous nitrogen-containing molecules are found in natural and/or biologically active products. Carbon-nitrogen bonds are polarised towards nitrogen and are involved in many organic functions groups, such as amides ($RCONR_2$), acyl azides

($RCON_3$), isocyanates (RNCO), nitriles (RCN), carbamates (RNCOOR') and ureas (RNCONR') [*364*]. A wide variety of nitrogen-containing quinones and QM have been reported to show anticancer effect [*365–369*]. The versatility of these compounds and their potential to be selectively toxic to cancer cells offer a great opportunity to antitumour therapy [*370*]. Taking this into account, we investigated the effect of different nitrogen functional groups at the C(29) position on the antitumour activity of celastrol **1.26**.

Curtius rearrangement is a synthetic strategy that has been developed to address the preparation of nitrogen-containing molecules. This rearrangement involves the thermal decomposition of an acyl azide into an isocyanate with loss of a nitrogen gas (Figure 5.6) [*371*]. The synthesis of a variety of carbamates and ureas using such strategy is possible by the subsequent nucleophilic attack of alcohols and amines, respectively [*372*].

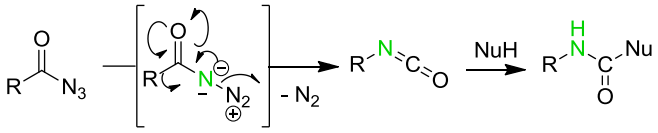

Figure 5.6 Curtius rearrangement.

To prepare these type of derivatives, we firstly treated the dihydrocelastrol diacetate **1.82** with oxalyl chloride in dichloromethane. Compound **3.1** was further converted to the acyl azide **3.2** using sodium azide in aqueous acetone; Curtius rearrangement in toluene after 2 h of reflux gave isocyanate **3.3**, in excellent overall yield (Scheme 5.4) [*304*, *308*]. Compound **3.3** was the central intermediate to obtain carbamate- and urea-type compounds.

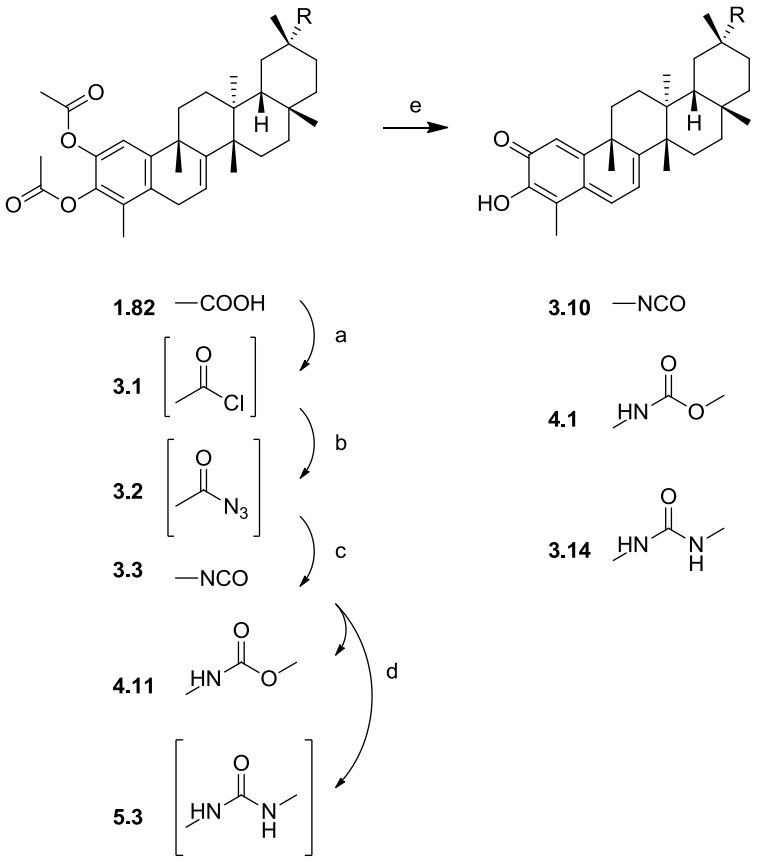

Scheme 5.4 Synthesis of nitrogen-containing derivatives of celastrol **1.26**. *Reagents and conditions:* a) $(COCl)_2$, CH_2Cl_2, R.T., N_2, 4 h; b) NaN_3, H_2O, acetone, 0 ºC, 1 h; c) in toluene, reflux, 2 h, d) ROH, Et_3N, R.T., N_2, 12 h or RNH_2, CH_2Cl_2, R.T., N_2, 4 h ; e) NH_4OAc, Et_3N, aq. MeOH (1:4), R.T., 1 h.

Other interesting compounds with carbon-nitrogen bonds are the nitrile-containing derivatives. The over 30 nitrile-containing approved pharmaceuticals and additional leads in clinical development, attest to the biocompatibility of these functionality [*373*]. Therefore, we reasoned the synthesis of nitrile celastrol derivatives, as part of our investigation. To prepare derivatives with the nitrile group at the C(29) position we started with the synthesis of compound **3.1** followed by the addition of a solution of concentrated ammonia that gave the amide **4.12**. Refluxing of compound **4.12** in thionyl chloride yielded the diacetate nitrile **5.4** that after deprotection gave the *p*-QM nitrile **5.5** (Scheme 5.5).

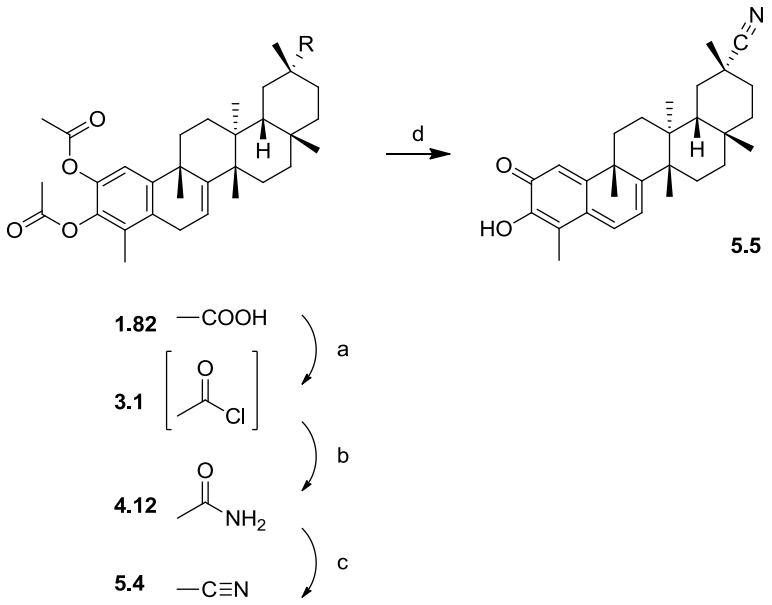

Scheme 5.5 Synthesis of nitrile-containing derivatives of celastrol **1.26**. *Reagents and conditions:* a) $(COCl)_2$, CH_2Cl_2, R.T., N_2, 4 h; b) conc. ammonia, toluene, 0 ºC, 1 h; c) $SOCl_2$, $CHCl_3$, reflux, 3 h; e) NH_4OAc, Et_3N, aq. MeOH (1:4), R.T., 1 h.

The conversion of primary amide into nitrile was confirmed by the IR absorption band for C≡N stretching vibration observed at 2228 cm^{-1}. In the ^{13}C NMR spectrum, the signal for the CN carbon appeared at around 127 ppm (Figure 5.7). These structural data were consistent for both nitrile containing derivatives **5.4** and **5.5**.

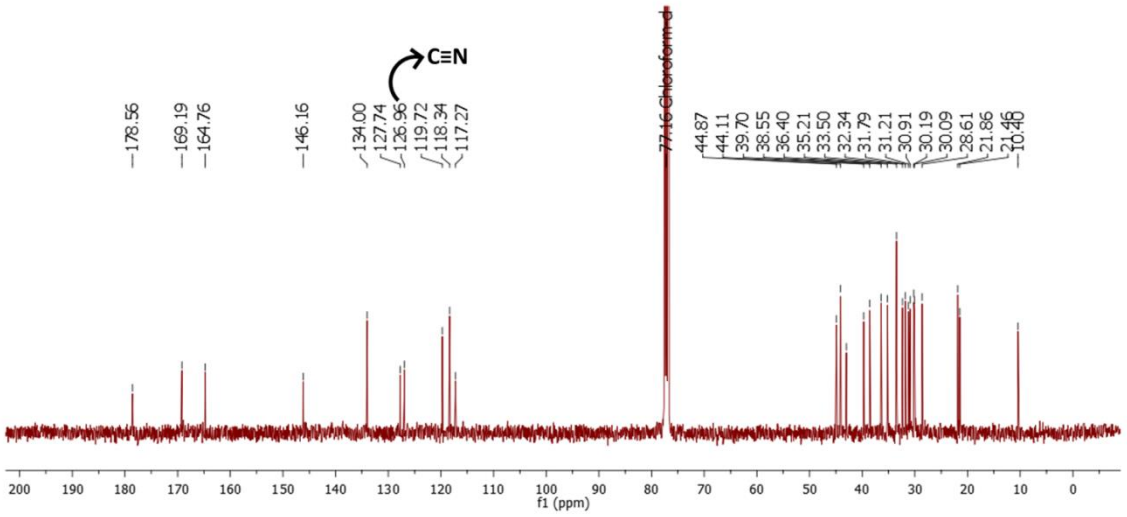

Figure 5.7 ^{13}C NMR spectrum of compound **5.5**.

As we can observe from the Table 5.2, all the nitrogen-containing derivatives from celastrol **1.26** bearing intact *p*-QM structure presented a significant decrease of viability of the studied cancer cells; however, only the urea celastrol derivative **3.14** showed improved anticancer activity on these cell lines compared with celastrol **1.26**.

Table 5.2 IC_{50} (μM) values of celastrol **1.26** and nitrogen-containing derivatives in tumour cell lines.

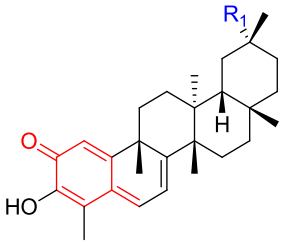

Comp.	Nitrogen group at C(29)	R1	IC50 (μM ± SEM)	
			A549	MIA PaCa-2
Celastrol **1.26**	—	—	1.56±0.08	0.46±0.03
3.10	Isocyanate	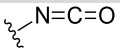	2.47±0.05	0.53±0.03
4.1	Carbamate	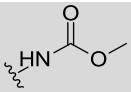	1.74±0.05	0.58±0.05
3.14	Urea	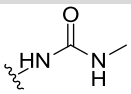	1.45±0.06	0.41±0.12
5.5	Nitrile		3.15±0.10	0.84±0.09

Carbamates and ureas could be further optimised through modifications of the side chain, as seen in **Chapter 3** and **4**.

5.2.3. A/B-ring modifications

QM, in general, are much more reactive than simple enones (e.g., α, β-unsaturated ketones) since nucleophilc attack on a QM produces an aromatic alcohol, with aromatization of the ring being a major driving force (Figure 5.1) [*374*]. As a result of the intrinsic electrophilic reactivity of QMs, highly reactive transient *p*-QM species generated *in situ* are implicated in many chemical, medicinal and biological processes, such as enzyme inhibition and DNA alkylation and cross-linking [*360*]. The reactivity and selectivity of QM with biological

nucleophiles are highly sensitive to structural modifications and to the protonation of the carbonyl moiety [*375*]. Herein, we explored this reactivity, using different celastrol derivatives with the same substituents at the C(29) position and different A/B-rings structures.

5.2.3.1. Aldehyde

Aldehydes are common among natural isolates and very versatile as a functional intermediate because of the high reactivity of the formyl group. Thus, we synthesised different C(29)-aldehydes celastrol derivatives and compared their activity.

After preparing the diacetate aldehyde celastrol **4.13** the acetoxy groups were successfully converted to the corresponding enol-hydroxyl group **5.1** as described above (Scheme 5.3). The possibility of masking the interfering enol by converting the hydroxyl group into methyl ether was explored, and compound **5.6** was successfully prepared using anhydrous potassium carbonate and methyl iodide in DMF (Scheme 5.6).

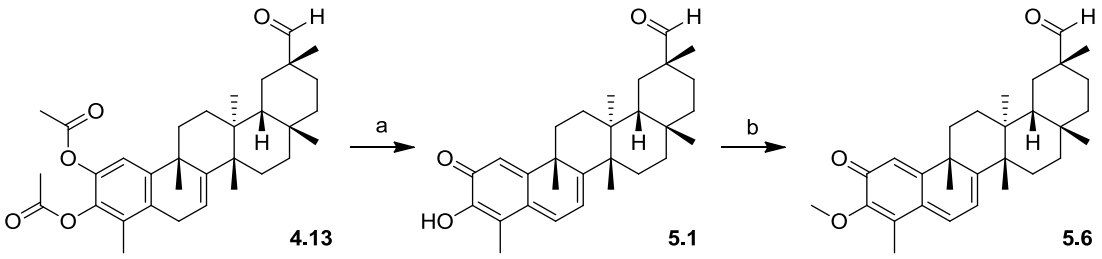

Scheme 5.6 Synthesis of aldehydes derivatives of celastrol **1.26**. *Reagents and conditions:* a) NH_4OAc, Et_3N, aq. MeOH (1:4), R.T., 1 h; atmospheric air; b) CH_3I, K_2CO_3, DMF, R.T., N_2, 6 h.

The preparation of the derivative **5.6** was confirmed by a signal at 3.54 ppm in the ^{1}H NMR spectrum, corresponding to the methyl protons of the methoxy group (Figure 5.8). In the ^{13}C NMR spectrum of compound **5.6**, the signal of methoxy carbon was observed at 51.7, a tertiary carbon, as this signal appeared in the DEPT-135 spectrum (Figure 5.9).

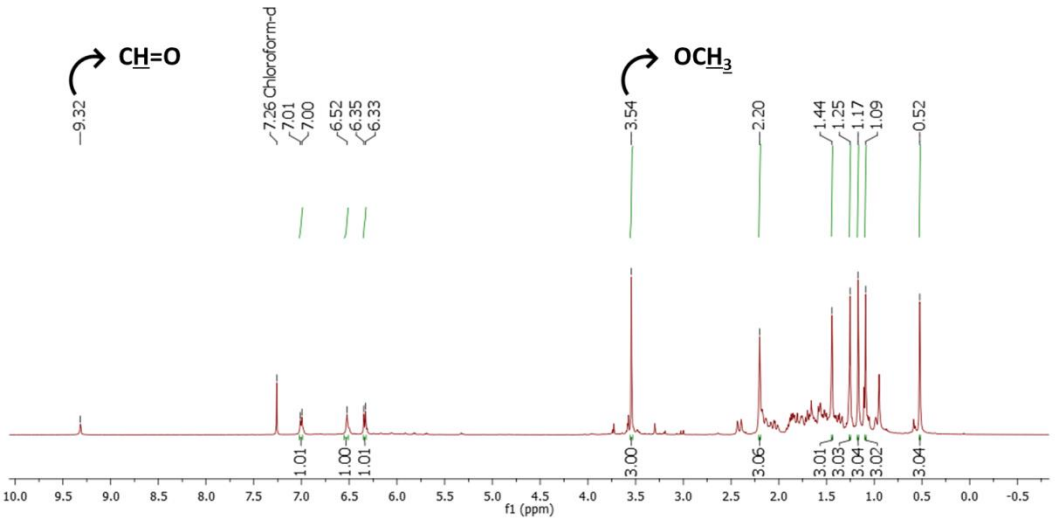

Figure 5.8 ^{1}H NMR spectrum of compound **5.6.**

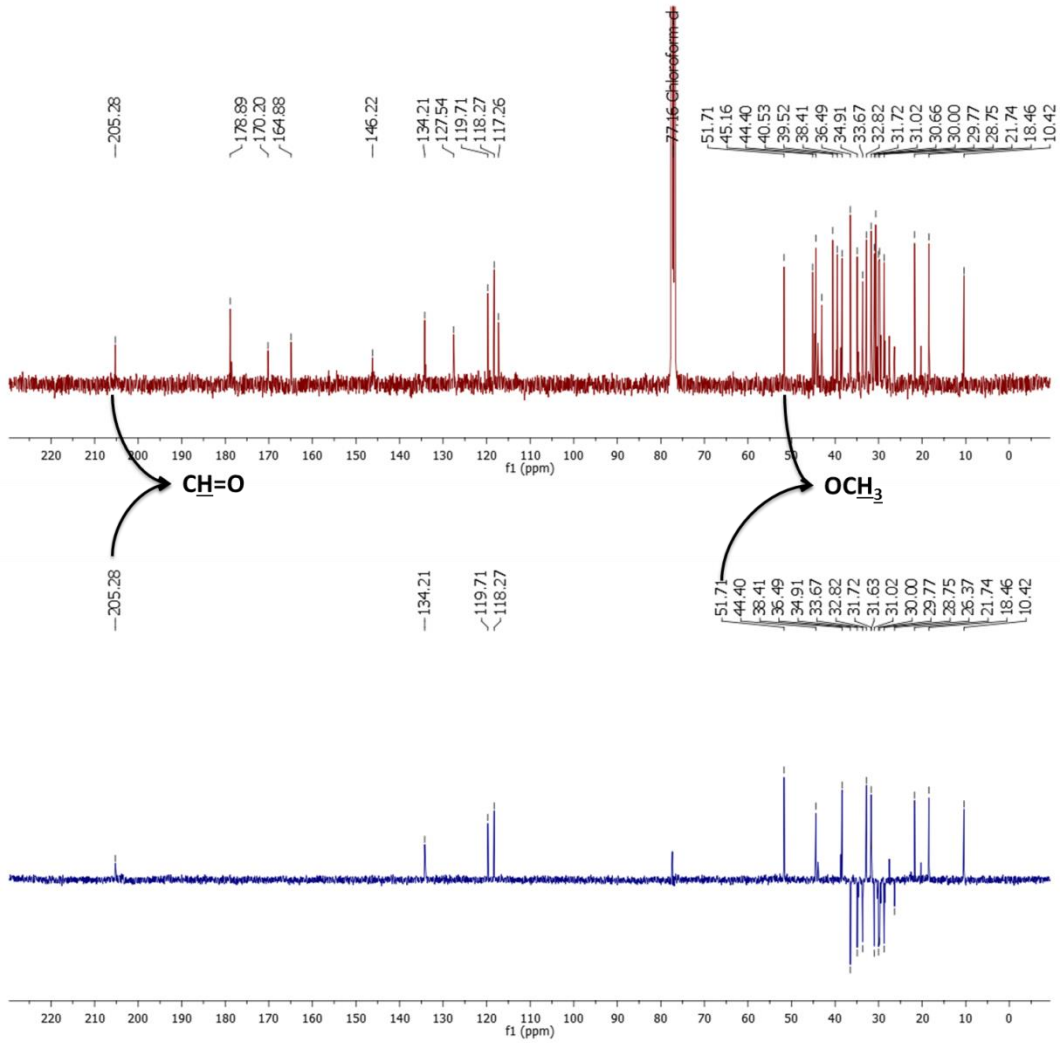

Figure 5.9 ^{13}C and DEPT-135 NMR spectrum of compound **5.6.**

The aldehyde derivatives of celastrol (compounds **4.13**, **5.1** and **5.6**) retained a high level of activity in tumour cells despite A/B-ring modifications. The *p*-QM **5.1** was the most active against the lung cancer cell line A549, while the diacetate **4.13** was the most active against pancreas cancer cell line MIA PaCa-2 (Table 5.3).

Table 5.3 IC_{50} (μM) values of aldehyde derivatives in tumour cell lines.

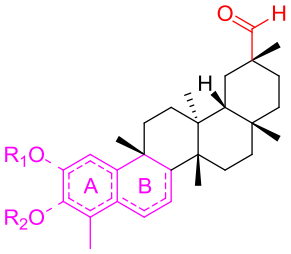

Compounds	A/B-rings	IC_{50} (μM ± SEM)	
		A549	MIA PaCa-2
4.13	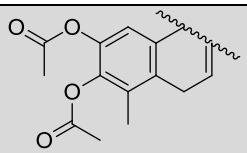	2.77±0.22	0.38±0.03
5.1	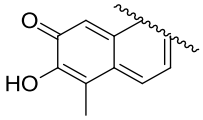	1.83±0.04	0.57±0.03
5.6	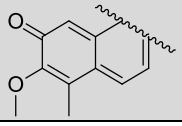	1.99±0.14	0.78±0.03

These data demonstrate (in addition to our findings described in **Chapter 4**) that acetylated celastrol derivatives are not only useful to protect functional groups but also to provide active compounds. Moreover, these data suggest that it is not just the topology of the ring that is responsible for the observed activity, but also the electronic properties of the A/B-rings system that are important for the anticancer activity.

5.2.3.2. C(6)-derivatives

Celastrol **1.26** and *p*-QM celastrol derivatives contain electrophilic sites within the A/B-rings of QM structure in positions C(2) and C(6) and they can react with the nucleophilic thiol groups of cysteine residues and form covalent Michael adducts (Figure 5.10A). On the other hand, enone celastrol derivatives (6-oxo-celastrol derivatives) kept the elecrophilic centre at C(6) blocked, as shown in Figure 5.10B.

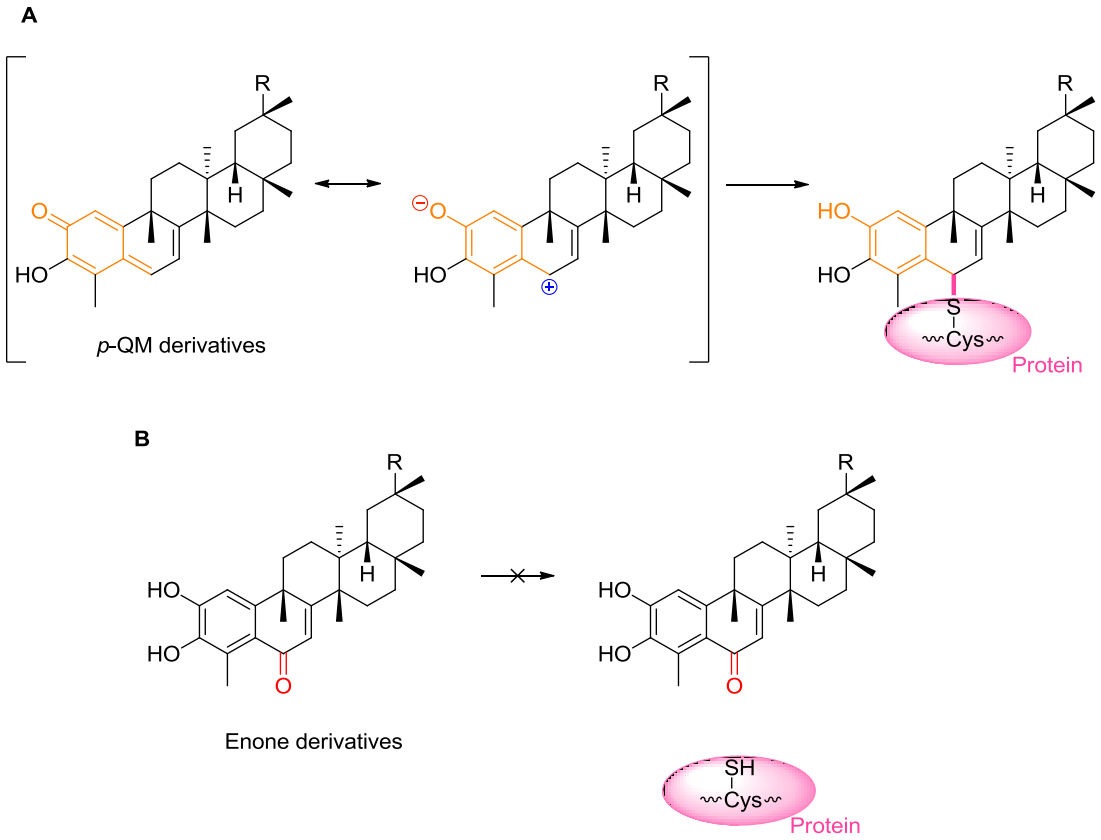

Figure 5.10 Molecular mechanism for **(A)** the addition of *p*-QM celastrol derivatives to the thiol group of proteins and **(B)** the blockage of elecrophilic centre at C(6) of enone celastrol derivatives. Adapted from [*242*].

Despite their lack of anticancer activity, in **Chapter 3** and **4** these α,β-unsaturated carbonyl derivatives have proved to be useful for directly compare the importance of the *p*-QM functionality on the observed biological properties of different celastrol derivatives. Thus, we decided to further explore these compounds, preparing enone celastrol derivatives with similar nitrogen-containing groups at C(29) — methyl ureas and ethyl ureas — methylated or not on A-ring.

Firstly we prepared the 6-oxo celastrol derivatives by allylic oxidation, which consists of a direct insertion of oxygen into an allylic carbon–hydrogen bond. For that purpose, we used *tert*-butyl hydroperoxide in combination with sodium chlorite, under mild, transition-metal free conditions (Scheme 5.7) [*376*].

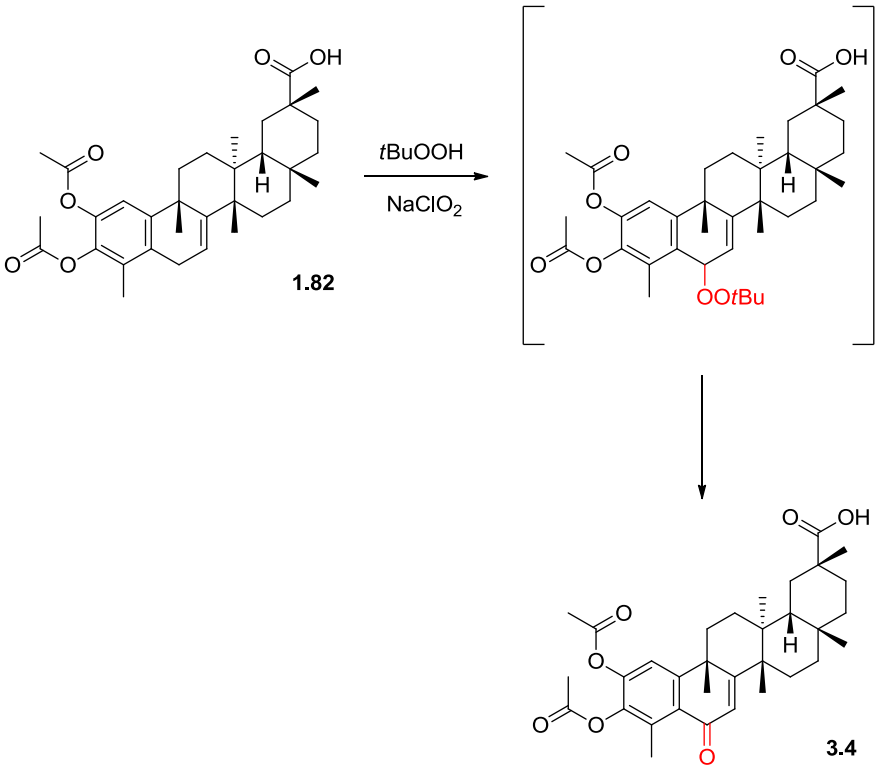

Scheme 5.7 Allylic oxidation reaction with *tert*-butyl hydroperoxide and sodium chlorite.

To synthesise methyl amide **5.7** we added methylamine to the previews prepared acid chloride of 6-oxo dihydrocelastrol. Because of the basic character of these reactions, the deprotection of the aromatic acetates was spontaneous, directly affording the corresponding amide 6-oxo-diphenol derivative **5.7**. Then, compound **5.7** was structurally diversified using anhydrous potassium carbonate and methyl iodide in DMF, to give the methyl derivative **5.8** (Scheme 5.8). Methyl ureas **3.8** and **3.9** were prepared as mentioned in **Chapter 3**.

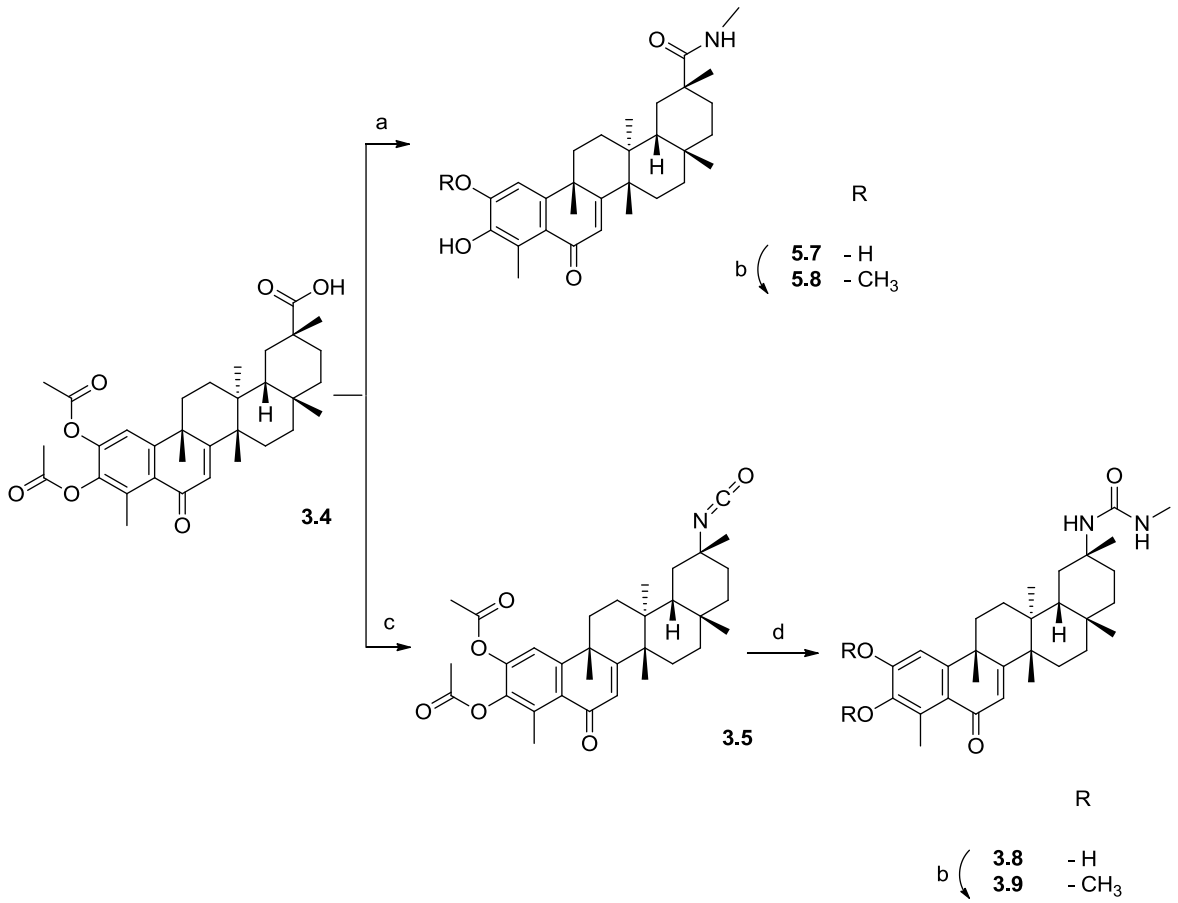

Scheme 5.8 Synthesis of methyl amides and methyl ureas derivatives of 6-oxo-celastrol **1.26**. *Reagents and conditions:* a) $(COCl)_2$, CH_2Cl_2, R.T., N_2, 4 h; CH_3NH_2, Et_3N, CH_2Cl_2, R.T., N_2, 10h; b) CH_3I, K_2CO_3, DMF, R.T., N_2, 6 h; c) $(COCl)_2$, CH_2Cl_2, R.T., N_2, 4 h; NaN_3, H_2O, acetone, 0 ºC, 1 h; in toluene, reflux, 2 h; d) CH_3NH_2, THF, R.T., N_2, 12 h.

In the IR spectrum, the secondary amide derivatives **5.7** and **5.8** presented a band corresponding to the carbonyl stretching vibration of the amide at around 1635 cm^{-1} and a N–H stretching band at around 3360 cm^{-1} (Figure 5.11).

In the ^{1}H NMR spectrum of compound **5.7** and **5.8**, the signals for the $NH\underline{CH_3}$ protons were found at 2.57 and 2.64 ppm, respectively (Figure 5.12). The ^{13}C NMR signal for the C(29) carbonyl carbon of the amide in compounds **5.7** and **5.8** was observed at 181.41 and 178.65 ppm, respectively (Figure 5.13).

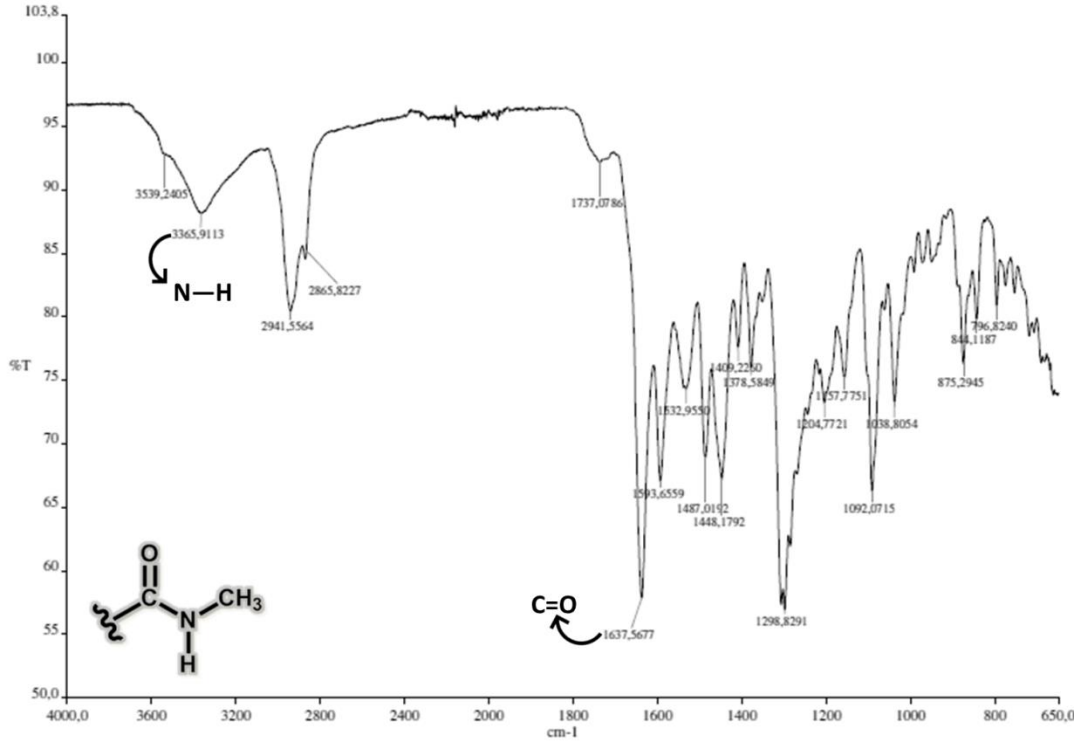

Figure 5.11 IR spectrum of compound **5.8.**

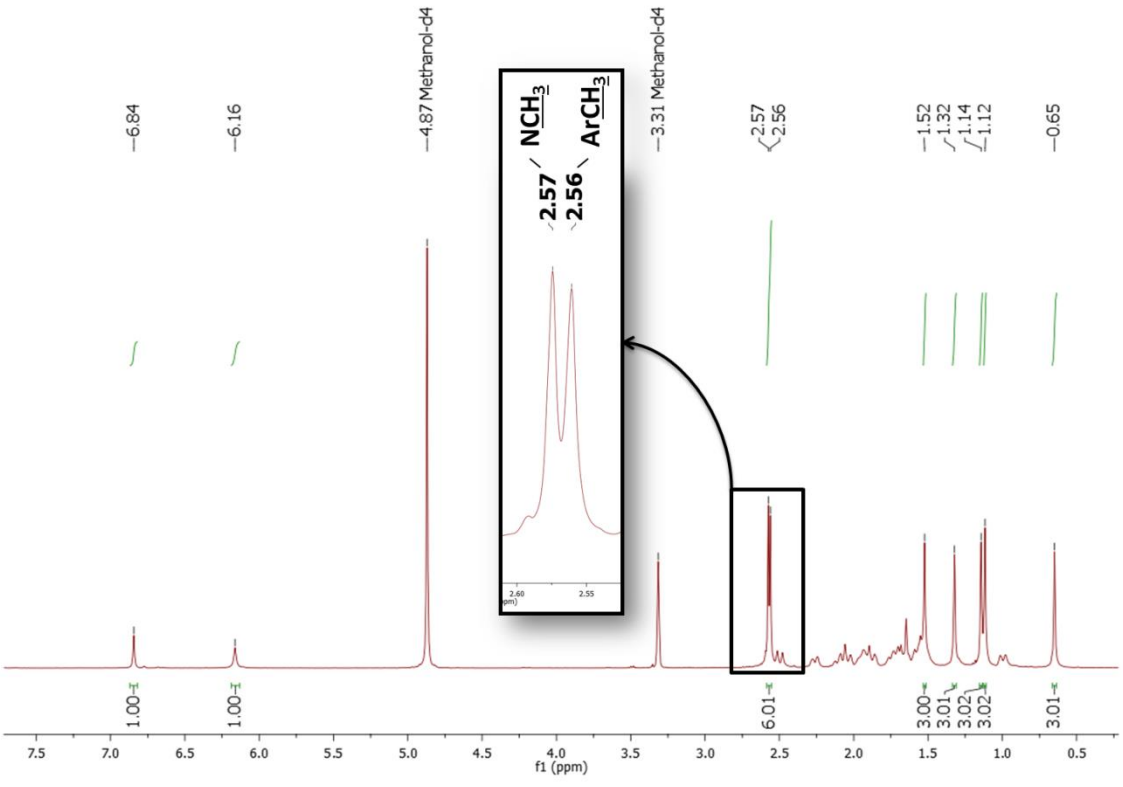

Figure 5.12 ^{1}H NMR spectrum of compound **5.7.**

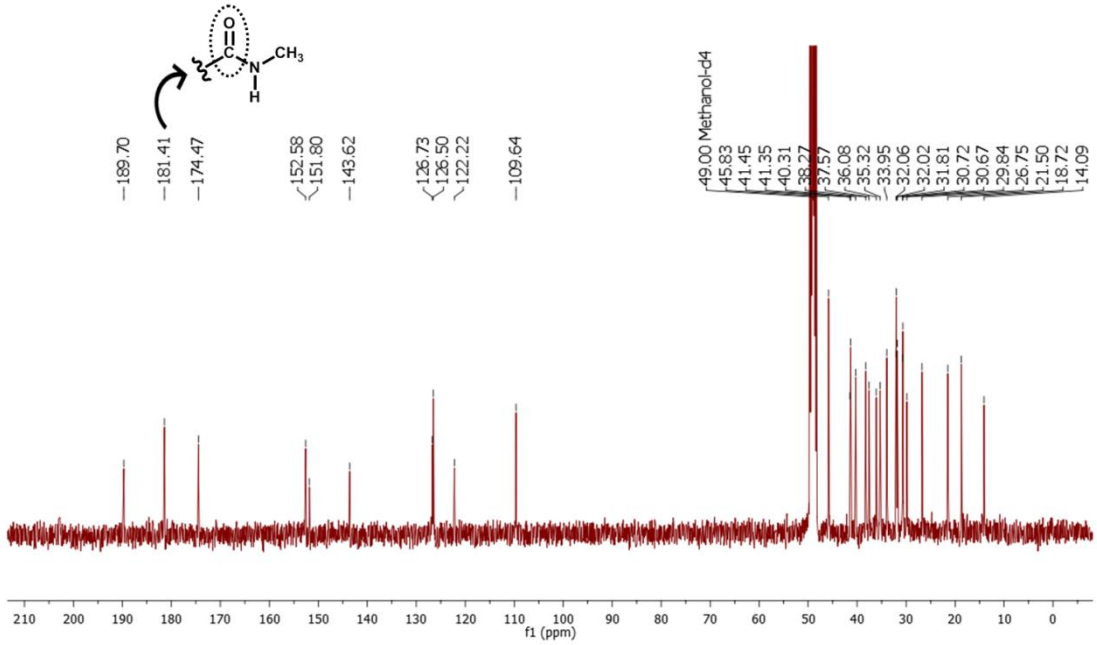

Figure 5.13 ^{13}C NMR spectrum of compound **5.7.**

As shown in Table 5.4, enone celastrol derivatives reduced drastically the ability to decrease the tumour cell viability in approximately tenfold the IC_{50} values of celastrol **1.26**. Moreover, this lack of activity occurred independently of the nitrogen-containing group at C(29), which is in accordance with the results obtained previously.

Table 5.4 IC_{50} (μM) values of enone celastrol derivatives (methyl amides and methyl ureas) in tumour cell lines.

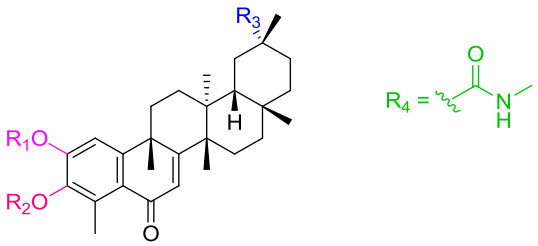

Compounds	R_1	R_2	R_3	IC_{50} (μM)	
				A549	MIA PaCa-2
5.7	- H	- H	= R_4	>15	>5
5.8	- CH_3	- H	= R_4	>15	>5
3.8	- H	- H		>15	>5
3.9	- CH_3	- CH_3		>15	>5

5.3. CONCLUSIONS

In this chapter, we successfully synthesised new celastrol derivatives and explored their potential by comparing their anticancer activity with other celastrol analogues prepared in the previews chapters. Modifications at the C(29) position can be favourable, namely the insertion of some nitrogen-containing groups, while reductions at this position seemed to be unfavourable for the anticancer activity. Moreover, A/B-ring modifications can be crucial for the anticancer activity of celastrol derivatives, because they influence the topology, electronic properties and reactivity of these molecules. In general, this study allowed us a deeper understanding of structure-activity relationship and chemical reactivity of celastrol derivatives.

5.4. EXPERIMENTAL SECTION

5.4.1. Chemistry

5.4.1.1. General

Celastrol **1** and all reagents were purchased from Sigma-Aldrich. Derivatives **1.45**, **1.81**, **1.82**, **3.1–3.10**, **3.14**, **4.1**, **4.11–4.14** were prepared according to **Chapter 3** and **4**. The solvents were obtained from VWR Portugal and were dried according to usual procedures. TLC analyses were performed on aluminium TLC plate, silica gel coated with fluorescent indicator F_{254} (Merck, detection by UV absorption). For preparative TLC was used preparative layer plates silica gel 60 F_{254}, 1 mm (Merck, detection by UV absorption). NMR spectra were recorded using the Bruker digital FT-NMR-Avance 400 MHz spectrometer in $CDCl_3$ or CD_3OD with TMS as the internal standard. Elucidation of the chemical structures was based on ^{1}H, ^{13}C and DEPT-135 NMR experiments. The chemical shifts values (δ) are given in parts per million (ppm) and the coupling constants (*J*) are presented in hertz (Hz).

Derivative 5.1 — 3-Hydroxy-2-oxo-24-nor-friedela-1(10),3,5,7-tetraen-20α-carbaldehyde

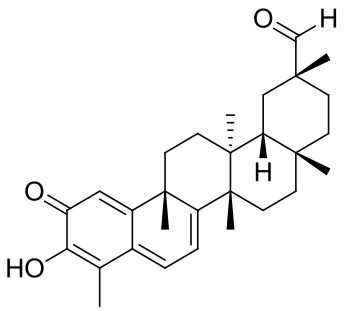

Figure 5.14 Chemical structure of compound **5.1**.

To a solution of **4.13** (55.0 mg, 0.1 mmol) in aqueous MeOH (1:4, 3 mL) and Et_3N (0.3 mL), NH_4OAc (38.5 mg, 0.5 mmol) was added. The resulting mixture was stirred at room temperature. After 2 h the mixture was concentrated and the residue was extracted with AcOEt (3 × 40 mL). The extract was washed with HCl 5% (20 mL), aqueous saturated solution of $NaHCO_3$ (20 mL), water (20 mL) and brine (20 mL). The obtained organic phase was dried over anhydrous Na_2SO_4, filtrated and evaporated at reduced pressure to give a dark orange solid, which was purified by preparative TLC (CH_2Cl_2/MeOH 20:1), to yield **5.1** (35.8 mg, 78%) as an orange solid. Mp: 243.1–244.9 °C. IR (neat) $_{vmax}$: 3306, 2925, 2866, 2689, 1720, 1592, 1515, 1436 cm^{-1}. ^1H NMR (400 MHz, $CDCl_3$) δ 9.32 (d, *J* = 1.3 Hz, 1H, CO<u>H</u>), 7.00 (d, *J* = 6.1 Hz, 1H, H-6), 6.51 (s, 1H, H-1), 6.33 (d, *J* = 7.1 Hz, 1H, H-7), 2.20 (s, 3H, H-23), 1.45 (s, 3H), 1.27 (s, 3H), 1.11 (s, 3H), 0.95 (s, 3H), 0.52 (s, 3H) ppm; ^{13}C NMR (100 MHz, $CDCl_3$) δ 205.24 (C=O), 178.55 (C2), 169.28, 164.79, 146.18 (C3), 133.99 (C6), 127.70 (C5), 119.73 (C1), 118.37 (C7), 117.25 (C4), 45.13, 44.69, 43.98, 42.98, 39.73, 38.68, 36.52, 34.70, 33.60, 31.64, 30.62, 30.38, 29.51, 28.60, 27.56, 26.42, 21.74, 20.31, 10.40 ppm.

Derivative 5.2 — 3,29-Dihydroxy -24-nor-friedela-1(10),3,5,7-tetraen-2-anone

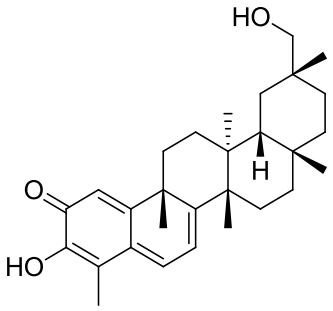

Figure 5.15 Chemical structure of compound **5.2.**

To a solution of **4.14** (55.0 mg, 0.1 mmol) in aqueous MeOH (1:4, 3 mL) and Et_3N (0.3 mL), NH_4OAc (38.5 mg, 0.5 mmol) was added. The resulting mixture was stirred at room temperature. After 2 h the mixture was concentrated and the residue was extracted with AcOEt (3 × 40 mL). The extract was washed with HCl 5% (20 mL), aqueous saturated solution of $NaHCO_3$ (20 mL), water (20 mL) and brine (20 mL). The obtained organic phase was dried over anhydrous Na_2SO_4, filtrated and evaporated at reduced pressure to give an orange solid, which was purified by preparative TLC (CH_2Cl_2/MeOH 20:1), to yield **5.2** (28.1 mg, 61%) as an orange solid. Mp: 266.8–269.0 °C. IR (neat) $_{vmax}$: 3366, 2941, 2870, 1586, 1511, 1437 cm^{-1}. ^1H NMR (400 MHz, $CDCl_3$) δ 7.02 (d, *J* = 7.0 Hz, 1H H-6), 6.52 (s, 1H, H-1), 6.37 (d, *J* = 7.2 Hz, 1H, H-7), 3.42 (d, *J* = 10.5 Hz, 1H, C$\underline{H}_2$OH), 3.21 (d, *J* = 10.5 Hz, 1H, C$\underline{H}_2$OH), 2.21 (s, 3H, H-23), 1.44 (s, 3H), 1.35 (s, 3H), 1.18 (s, 3H), 0.99 (s, 3H), 0.79 (s, 3H) ppm; ^{13}C NMR (100 MHz, $CDCl_3$) δ 178.50 (C2), 171.55, 164.75, 146.18 (C3), 134.23 (C6), 127.49 (C5), 119.50 (C1), 118.48 (C7), 117.34 (C4), 71.48 (C$\underline{H}_2$OH), 44.55, 43.43, 43.41, 39.50, 38.46, 36.97, 36.44, 33.23, 32.98, 32.41, 30.56, 30.04, 29.99, 29.54, 29.14, 28.18, 24.34, 19.41, 10.41 ppm.

Derivative 5.4 — 20α-Nitrile-24-nor-friedela-1,3,5(10),7-tetraen-2,3-di-yl diacetate

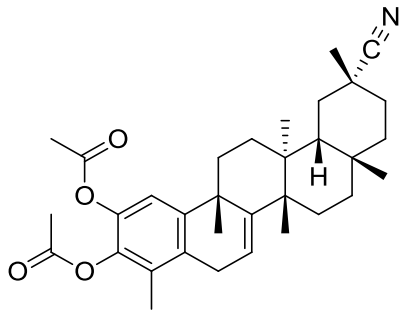

Figure 5.16 Chemical structure of compound **5.4.**

Compound **4.12** (55 mg, 0.1 mmol) was dissolved in chloroform (4 mL) and thionyl chloride (1.3 mL) and the solution was heated under reflux for 3 h. The solvents were removed under reduced pressure; the residue was extracted with AcOEt (3 × 40 mL). The extract was washed with water (20 mL) and brine (20 mL). The obtained organic phase was dried over anhydrous Na_2SO_4, filtrated and evaporated at reduced pressure to give a yellowish solid, which was purified by preparative TLC (PE/AcOEt 2:1), to yield **5.4** (42.7 mg, 80%) as a white solid. Mp: 225.4–227.7 °C. ^{1}H NMR (400 MHz, $CDCl_3$) δ 7.00 (s, 1H, H-1), 5.78 (d, *J* = 4.3 Hz, 1H, H-7), 3.35 (dd, *J* = 20.9, 6.0 Hz, 1H, H-6b), 3.08 (d, *J* = 20.7 Hz, 1H, H-6a), 2.30 (s, 3H, C$\underline{H_3}$CO), 2.27 (s, 3H, C$\underline{H_3}$CO), 2.07 (s, 3H, H-23), 1.43 (s, 3H), 1.36 (s, 3H), 1.24 (s, 3H), 1.07 (s, 3H), 0.85 (s, 3H) ppm. ^{13}C NMR (100 MHz, $CDCl_3$) δ 168.84 ($CH_3\underline{C}OO$), 168.53 ($CH_3\underline{C}OO$), 148.98, 147.45, 140.76, 138.24, 131.59, 128.00, 127.07 ($\underline{C}$≡N), 117.39, 116.69, 44.12, 43.61, 37.91, 37.35, 36.81, 35.12, 34.45, 34.37, 33.57, 32.57, 31.74, 31.02, 30.88, 30.62, 30.22, 28.85, 28.26, 23.09, 21.37, 20.84, 20.55, 12.73 ppm.

Derivative 5.5 — 3-Hydroxy-2-oxo-24-nor-friedela-1(10),3,5,7-tetraen-20 α – nitrile

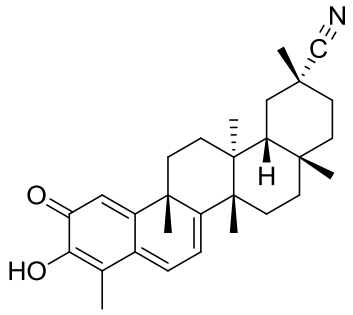

Figure 5.17 Chemical structure of compound **5.5.**

To a solution of **5.4** (52.0 mg, 0.1 mmol) in aqueous MeOH (1:4, 3 mL) and Et_3N (0.3 mL), NH_4OAc (38.5 mg, 0.5 mmol) was added. The resulting mixture was stirred at room temperature. After 2 h the mixture was concentrated and the residue was extracted with AcOEt (3 × 40 mL). The extract was washed with HCl 5% (20 mL), aqueous saturated solution of $NaHCO_3$ (20 mL), water (20 mL) and brine (20 mL). The obtained organic phase was dried over anhydrous Na_2SO_4, filtrated and evaporated at reduced pressure to give a dark orange solid, which was purified by preparative TLC (CH_2Cl_2/MeOH 20:1), to yield **5.5** (36.2 mg, 84%) as an orange solid. Mp: 231.1–234.0 °C. IR (neat) $_{vmax}$: 3312, 2945, 2876, 2228, 1583, 1520, 1439 cm^{-1}. ^1H NMR (400 MHz, $CDCl_3$) δ 7.02 (d, *J* = 7.0 Hz, 1H, H-6), 6.53 (s, 1H, H-1), 6.37 (d, *J* = 7.1 Hz, 1H, H-7), 2.21 (s, 3H, H-23), 1.46 (s, 3H), 1.44 (s, 3H), 1.28 (s, 3H), 1.08 (s, 3H), 1.03 (s, 3H) ppm; ^{13}C NMR (100 MHz, $CDCl_3$) δ 178.56 (C2), 169.19, 164.76, 146.16 (C3), 134.00 (C6), 127.74 (C5), 126.96 (C≡N), 119.72 (C1), 118.34 (C7), 117.27 (C4), 44.87, 44.11, 43.02, 39.70, 38.55, 36.40, 35.21, 33.50, 32.34, 31.79, 31.21, 30.91, 30.19, 30.09, 28.61, 21.86, 21.46, 10.40 ppm.

Derivative 5.6 — 3-Methoxy-2-oxo-24-nor-friedela-1(10),3,5,7-tetraen-20α-carbaldehyde

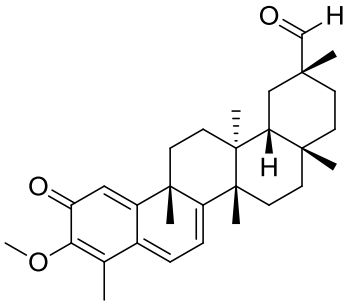

Figure 5.18 Chemical structure of compound **5.6.**

Compound **5.6** was prepared according to the literature [*330*] from **5.1** (45 mg, 0,1 mmol). The obtained crude was purified by preparative TLC (CH_2Cl_2/MeOH 20:1), to yield **5.6** (28.7 mg, 64%) as an orange solid. Mp: 244.7–246.8 °C. ^{1}H NMR (400 MHz, $CDCl_3$) δ 9.32 (s, 1H, CO<u>H</u>), 7.00 (d, *J* = 6.7 Hz, 1H, H-6), 6.52 (s, 1H, H-1), 6.34 (d, *J* = 7.1 Hz, 1H, H-7), 3.54 (s, 3H, OC<u>H</u>$_3$), 2.20 (s, 3H, H-23), 1.44 (s, 3H), 1.25 (s, 3H), 1.17 (s, 3H), 1.09 (s, 3H), 0.52 (s, 3H) ppm; ^{13}C NMR (100 MHz, $CDCl_3$) δ 205.28 (C=O), 178.89 (C2), 170.20, 164.88, 146.22 (C3), 134.21 (C6), 127.54 (C5), 119.71 (C1), 118.27 (C7), 117.26 (C4), 51.71 (O<u>C</u>H$_3$), 45.16, 44.40, 43.05, 40.53, 39.52, 38.41, 36.49, 34.91, 33.67, 32.82, 31.72, 31.02, 30.66, 30.00, 29.77, 28.75, 21.74, 18.46, 10.42 ppm.

Derivative 5.7 — N-Methyl 2,3-dihydroxy-6-oxo-24-nor-friedela-1,3,5(10),7-tetraen-29-amide

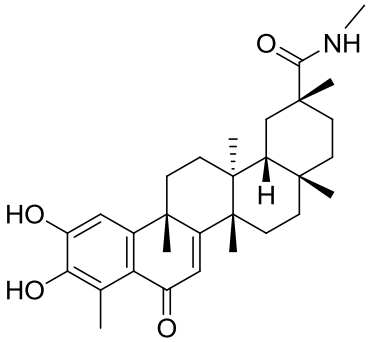

Figure 5.19 Chemical structure of compound **5.7.**

To a solution of **3.4** (55.0 mg, 0.1 mmol) in dry CH_2Cl_2 (5 mL) was added oxalyl chloride (0.04 mL, 1 mmol) and stirred for 4 h at room temperature and N_2 atmosphere. The mixture was concentrated to dryness under reduced pressure. The resulting residue was taken up in dry CH_2Cl_2 (5 mL) and was added triethylamine (0.1 mL, 0.90 mmol) and methylamine solution 2.0 M in THF (0.1 mL, 0.02 mmol). The reaction mixture was stirred at room temperature, under an inert atmosphere. After 10 h the mixture was concentrated and the residue was extracted with AcOEt (3 × 40 mL). The extract was washed with HCl 5% (20 mL), aqueous saturated solution of $NaHCO_3$ (20 mL), water (20 mL) and brine (20 mL). The obtained organic phase was dried over anhydrous Na_2SO_4, filtrated and evaporated at reduced pressure to give a yellow solid, which was purified by preparative TLC (CH_2Cl_2/MeOH 20:1), to yield **5.7** (41.1 mg, 86%) as an yellow solid. Mp: 290.5–292.2 °C. IR (neat) $_{vmax}$: 3357, 2942, 2866, 1722, 1635, 1577, 1456, 1312 cm^{-1}. ^1H NMR (400 MHz, CD_3OD) δ 6.84 (s, 1H, H-1), 6.16 (s, 1H, H-7), 2.57 (s, 3H, NH$\underline{CH_3}$) 2.56 (s, 3H, H-23), 1.52 (s, 3H), 1.32 (s, 3H), 1.14 (s, 3H), 1.12 (s, 3H), 0.65 (s, 3H) ppm; ^{13}C NMR (100 MHz, CD_3OD) δ 189.70 (C6), 181.41 ($\underline{C}$ONH), 174.47, 152.58, 151.80 (ArC-OH), 143.62 (ArC-OH), 126.73, 126.50, 122.22, 109.64, 45.83, 41.45, 41.35, 40.31, 38.27, 37.57, 36.08, 35.32, 33.95, 32.06, 32.02, 31.81, 30.72, 30.67, 29.84, 26.75, 21.50, 18.72, 14.09 ppm.

Derivative 5.8 — N-Methyl 3-hydroxy-2-metoxy-6-oxo-24-nor-friedela-1,3,5(10),7-tetraen-29-amide

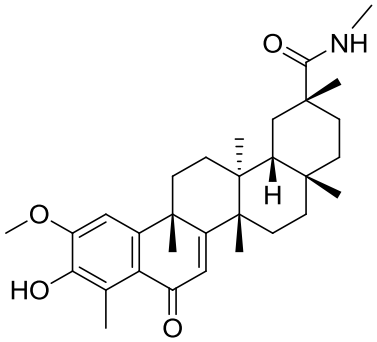

Figure 5.20 Chemical structure of compound **5.8.**

Compound **5.8** was prepared according to the literature [*330*] from **5.7** (50 mg, 0,1 mmol). The obtained crude was purified by preparative TLC (CH_2Cl_2/MeOH 20:1), to yield **5.8** (33.5 mg, 65%) as a yellow solid. Mp: 281.8–283.1 °C. IR (neat) $_{vmax}$: 3366, 2942, 2866, 1737, 1638, 1594, 1487, 1448, 1299 cm^{-1}. ^{1}H NMR (400 MHz, $CDCl_3$) δ 6.80 (s, 1H, H-1), 6.23 (s, 1H, H-7), 5.84 (d, *J* = 3.7 Hz, 1H, N<u>H</u>CH_3), 3.95 (s, 3H, ArOC<u>H_3</u>), 2.64 (s, 3H, NH<u>CH_3</u>), 2.63 (s, 3H, H-23), 1.52 (s, 3H), 1.28 (s, 3H), 1.14 (s, 3H), 1.12 (s, 3H), 0.64 (s, 3H) ppm. ^{13}C NMR (100 MHz, $CDCl_3$) δ 187.85 (C6), 178.65 (<u>C</u>ONH), 171.71, 150.16, 149.31 (ArC-OH), 142.34 (ArC-OH), 126.24, 124.65, 123.55, 103.86, 56.01 (NH<u>C</u>H_3), 44.77, 44.38, 40.56, 40.37, 39.01, 37.98, 36.49, 34.99, 34.45, 33.82, 31.64, 31.11, 30.94, 30.33, 29.63, 28.67, 26.57, 21.01, 18.19, 13.45 ppm.

5.4.2. Biology

5.4.2.1. Reagents and cells

DMEM — no glucose, no glutamine, no phenol red, Penicillin-Streptomycin (100 ×) (P/S) solution and FBS were purchased from Thermo Fisher Scientific. PBS was obtained from Biowest. MTT powder was obtained from Applichem.

5.4.2.2. Compounds

Stock solutions were prepared at a concentration of 10 mM by dissolving celastrol **1** and its derivatives in DMSO, and subsequently stored at -20 ºC. To obtain the working solutions at the final desired concentration, the stock solutions were further diluted in culture medium just before each experiment. The final concentration of DMSO was always lower than 0.5% for all working solutions.

5.4.2.3. Cell culture

A549 and MIA PaCa-2 cell lines were obtained from ATCC and were routinely maintained in DMEM — high glucose with L-glutamine, supplemented with 10% (V/V) FBS and P/S solution (1 ×). All cells were incubated in a humidified incubator at 37°C in 5% CO_2.

5.4.2.4. Cell viability assay

The viability of all cell lines in the presence of different concentrations of the compounds was determined by the MTT assay. For this assay, 2×10^3 A549 and MIA PaCa-2 cells per well were seeded in 96 well plates and allowed to attach for 24 h. Then, growth medium was changed in every well and the compounds were added at increasing concentrations in triplicate. After 72 h of incubation, the supernatant in each well was replaced by 100 µL of filtered MTT solution (0.5 mg/mL of growth medium), and the plates were incubated again for 1 h at 37 ºC. The MTT solution was then removed, and the formazan crystals formed were dissolved in 100 µL of DMSO. The absorbance at 550 nm in all wells was

immediately read on an ELISA plate reader (Tecan Sunrise MR20-301, TECAN) as an indicator of the cell viability. Subsequently, the IC_{50} values were calculated by non-linear regression using Graphpad Prism 5 software. To obtain the mean ± SEM values of IC_{50}, three independent experiments were performed.

CHAPTER VI

CONCLUDING REMARKS

6. CHAPTER VI

Concluding remarks

Cancer is a highly complex disease with a poor prognosis and a massive impact on society. Although chemotherapy is crucial to the clinical management of cancer, in many cases it only offers a modest therapeutic benefit because of its lack of selectivity for cancer cells. For these reasons, the development of optimised anticancer drugs remains one of the most important fields of medicinal chemistry.

There is an increasing interest in natural products, particularly in PTs, for the development of new antineoplastic drugs. Among them, celastrol **1.26** is one of the most active antitumour natural compounds. Despite its outstanding anticancer activity, the pharmacological properties of celastrol **1.26** can be further optimised through the generation of more potent and safer derivatives.

In this work, we successfully designed and synthesised several new celastrol derivatives. First, selective protection by acetylation and deprotection with ammonium acetate of the QM structure of celastrol **1.26** was explored, to carry out selective reactions and achieve greater control over the chemical reactions (**Chapters 3–5**). Additionally, *tert*-butyl hydroperoxide was used under mild, transition-metal free conditions to synthesise C(6)-substituted celastrol derivatives bearing an α,β-unsaturated carbonyl group (6-oxo-celastrol derivatives) by allylic oxidation (**Chapters 3–5**). Moreover, we synthesised several C(29)-derivatives: for instance, urea (**Chapter 3**) and carbamate (**Chapter 4**) derivatives were prepared in good yields from key isocyanate intermediates. Some of these compounds exhibited a remarkable anticancer activity. Other C(29)-derivatives were also synthesised, namely primary amide, aldehyde, primary alcohol (**Chapter 4**) and nitrile (**Chapter 5**) derivatives. Other strategies of semisynthesis allowed the preparation of further diversified celastrol derivatives, by converting the hydroxyl groups into methyl ether, and subsequently masking the interfering enols by methylation with methyl iodide (**Chapters 3–5**).

The structures of all new celastrol derivatives were elucidated by numerous analytical techniques, including IR spectroscopy, NMR spectroscopy (^{1}H NMR, ^{13}C NMR and DEPT-135 NMR) and MS and elemental analyses.

These new celastrol derivatives were tested for their cytotoxicity against human cell lines, and some of them showed an improved antiproliferative profile compared with the parent compound. The IC_{50} values determined using the MTT assay were used to establish a preliminary SAR study. Modifications at the C(29) position were shown to be favourable, namely by inserting some nitrogen-containing groups (e.g., urea and carbamate). Furthermore, A/B-ring modifications can be crucial for the anticancer activity of celastrol derivatives, because they influence the topology, electronic properties and reactivity of these molecules. In particular, allylic oxidation, which blocked the electrophilic centre at the C(6) position, and the consequent rearrangement in the A/B-rings appeared to decrease the anticancer activity of these compounds drastically.

The most relevant derivatives of each panel were further tested against the human non-tumour fibroblast cell line BJ, to assess the selectivity of their antiproliferative activities. Compounds **3.29** and **4.11** exhibited a lower toxicity toward non-tumour BJ cells than they did toward cancer cells, and an improved selectivity compared with celastrol **1.26**. The synergistic anticancer effects of these compounds together with approved anticancer drugs were evaluated using an ovarian cancer cell line (SKOV-3). An evident synergistic anticancer effect of compound **3.29** combined with cisplatin was observed, as well as for compound **4.11** combined with carboplatin. Finally, the mechanism underlying the anticancer activity of the most promising derivatives was studied in SKOV-3 cells. It was shown that compound **3.21** induced apoptosis via the extrinsic pathway, which involved the activation of caspase-8 and caspase-3 and the cleavage of PARP. Compound **3.21** also induced the downregulation of p53 in a p53-mutant cell line. Moreover, the results suggested that compound **3.21** might be an Hsp90 inhibitor and that the Akt/mTOR pathway might be involved in the downstream signalling that leads to a decrease in SKOV-3 cell viability. Similarly, preliminary mechanistic

studies showed that compound **4.11** exerted an antiproliferative effect on SKOV-3 cells via the extrinsic apoptotic pathway.

Although this work provides valuable insights into the mechanism of action of the most relevant derivatives of celastrol **3.29** and **4.11**, additional studies of their anticancer molecular pathways are needed. It would also be important to explore further the potential effects and mechanisms of the anticancer synergy of derivatives **3.29** and **4.11,** with the tested drugs (cisplatin and carboplatin), as well as other chemotherapeutic agents. Additionally, pharmacogenomics and pharmacokinetics studies are warranted to demonstrate fully their potential effectiveness.

In conclusion, this thesis demonstrates the remarkable anticancer potential of celastrol derivatives as promising lead candidates for anticancer drug development.

CHAPTER VII

REFERENCES

7. CHAPTER VII

References

[1] Hanahan, D.; Weinberg, R. A. Hallmarks of cancer: the next generation. *Cell* **2011**, *144*, 646–674.

[2] Connolly, J. L.; Schnitt, S. J.; Wang, H. H.; Dvorak, A. M.; Dvorak, H. F. Principles of Cancer Pathology. In *Holland-Frei Cancer Medicine*; Kufe DW, Pollock RE, W. R., Ed.; ISBN: 1-55009-213-8: Hamilton, **2000**.

[3] Ferlay J, Soerjomataram I, Ervik M, Dikshit R, Eser S, M. C. GLOBOCAN 2012, Cancer Incidence and Mortality Worldwide: IARC CancerBase No. 11 **2012**.

[4] WHO. http://www.who.int/mediacentre/factsheets/fs297/en/ (accessed March 21, 2017).

[5] Siegel, R.; Miller, K.; Jemal, A. Cancer statistics, 2017. *CA Cancer J. Clin.* **2017**, *67*, 7–30.

[6] Stewart, B. W.; Wild, C. P. World cancer report 2014. *WHO* **2014**, 1–2.

[7] Bradbury, R. H. *Cancer*; Springer Berlin Heidelberg; **2007**; Vol. 1.

[8] Sawyers, C. Targeted cancer therapy. *Nature* **2004**, *432*, 294–297.

[9] Lauren, P. Molecular Biology of Cancer: Mechanisms, targets, and therapeutics. *Oxford Univ. Press* **2012**, 1–342.

[10] Hanahan, D.; Weinberg, R. A. The Hallmarks of Cancer. *Cell* **2000**, *100*, 57–70.

[11] Ross JS, Schenkein DP, Pietrusko R, Rolfe M, Linette GP, Stec J, Stagliano NE, Ginsburg GS, Symmans WF, Pusztai L, H. G. Targeted therapies for cancer 2004. *Am. J. Clin. Pathol.* **2004**, *122*, 598–609.

[12] Ferrara, N.; Hillan, K. J.; Gerber, H.-P.; Novotny, W. Discovery and development of bevacizumab, an anti-VEGF antibody for treating cancer. *Nat. Rev. Drug Discov.* **2004**, *3*, 391–400.

[13] Montagut, C.; Rovira, a; Albanell, J. The proteasome: a novel target for anticancer therapy. *Clin. Transl. Oncol.* **2006**, *8*, 313–7.

[14] Raymond, E.; Faivre, S.; Armand, J. P. Epidermal growth factor receptor tyrosine kinase as a target for anticancer therapy. *Drugs* **2000**, *60 Suppl 1*, 15-23-42.

[15] Lydon, N. B.; Druker, B. J. Lessons learned from the development of imatinib. *Leuk. Res.* **2004**, *28*.

[16] Maloney, D. G.; Smith, B.; Rose, A. Rituximab: Mechanism of action and resistance. *Semin. Oncol.* **2002**, *29*, 2–9.

[17] Lombardino, J. G.; Lowe, J. A. The role of the medicinal chemist in drug discovery-then and now. *Nat. Rev. Drug Discov.* **2004**, *3*, 853–862.

[18] Barouch-bentov, R.; Che, J.; Lee, C. C.; Yang, Y.; Jia, Y.; Velentza, A.; Watson, J.; Sternberg, L.; Ziaee, N.; Miller, A.; Jackson, C.; Fujimoto, M.; Young, M.; Batalov, S.; Liu, Y.; Warmuth, M.; Wiltshire, T.; Cooke, M. P. A conserved salt bridge in the G-loop of multiple protein kinases is important for catalysis and for in vivo lyn function. *Mol. Cell* **2009**, *33*, 43–52.

[19] Capdeville, R.; Buchdunger, E.; Zimmermann, J.; Matter, A. Glivec (STI571, imatinib), a rationally developed, targeted anticancer drug. *Nat. Rev. Drug Discov.* **2002**, *1*, 493–502.

[20] Schindler, T.; Bornmann, W.; Pellicena, P.; Miller, W. T.; Clarkson, B.; Kuriyan, J.; Schindler, T.; Bornmann, W.; Pellicena, P.; Miller, W. T.; Clarkson, B.; Kuriyan, J. Structural mechanism for STI-571 inhibition of abelson tyrosine kinase. *Science* **2000**, *289*, 1938–1942.

[21] Yuan, H.; Wang, Z.; Gao, C.; Chen, W.; Huang, Q.; Yee, J.-K.; Bhatia, R.; Chen, W. BCR-ABL gene expression is required for its mutations in a novel KCL-22 cell culture model for acquired resistance of chronic myelogenous leukemia. *J. Biol. Chem.* **2010**, *285*, 5085–5096.

[22] National Cancer Institute. https://www.cancer.gov/about-cancer/treatment/types/targeted-therapies/targeted-therapies-fact-sheet (accessed August 13, 2017).

[23] Cotter, T. G. Apoptosis and cancer: the genesis of a research field. *Nat. Rev. Cancer* **2009**, *9*, 501–507.

[24] Baig, S.; Seevasant, I.; Mohamad, J.; Mukheem, A.; Huri, H. Z.; Kamarul, T. Potential of apoptotic pathway-targeted cancer therapeutic research: Where do we stand? *Cell Death Dis.* **2016**, *7*, e2058.

[25] Czabotar, P. E.; Lessene, G.; Strasser, A.; Adams, J. M. Control of apoptosis by the BCL-2 protein family: implications for physiology and therapy. *Nat. Rev. Mol. Cell Biol.* **2013**, *15*, 49–63.

[26] Labi, V.; Erlacher, M. How cell death shapes cancer. *Cell Death Dis.* **2015**, *6*, e1675.

[27] Ziegler, U.; Groscurth, P. Morphological features of cell death. *News Physiol. Sci.* **2004**, *19*, 124–128.

[28] Fulda, S. Tumor resistance to apoptosis. *Int. J. Cancer* **2009**, *124*, 511–515.

[29] Hassan, M.; Watari, H.; Abualmaaty, A.; Ohba, Y.; Sakuragi, N. Apoptosis and molecular targeting therapy in cancer. *Biomed. Res. Int.* **2014**, 150845.

[30] Walsh, C. M. Grand challenges in cell death and survival: apoptosis vs. necroptosis. *Front. cell Dev. Biol.* **2014**, *2*, 3.

[31] Igney, F. H.; Krammer, P. H. Death and anti-death: tumour resistance to apoptosis. *Nat. Rev. Cancer* **2002**, *2*, 277–288.

[32] Zamzami, N.; Kroemer, G. The mitochondrion in apoptosis: how Pandora's box opens. *Nat. Rev. Mol. Cell Biol.* **2001**, *2*, 67–71.

[33] Kluck, R. M.; Bossy-Wetzel, E.; Green, D. R.; Newmeyer, D. D. The release of cytochrome c from mitochondria: a primary site for Bcl-2 regulation of apoptosis. *Science* **1997**, *275*, 1132–6.

[34] Hakem, R.; Hakem, A.; Duncan, G. S.; Henderson, J. T.; Woo, M.; Soengas, M. S.; Elia, A.; de la Pompa, J. L.; Kagi, D.; Khoo, W.; Potter, J.; Yoshida, R.; Kaufman, S. A.; Lowe, S. W.; Penninger, J. M.; Mak, T. W. Differential requirement for caspase 9 in apoptotic pathways in vivo. *Cell* **1998**, *94*, 339–52.

[35] Vasilikos, L.; Spilgies, L. M.; Knop, J.; Wong, W. W.-L. Regulating the balance between necroptosis, apoptosis and inflammation by inhibitors of apoptosis proteins. *Immunol. Cell Biol.* **2017**, *95*, 160–165.

[36] Thomas, S.; Quinn, B. A.; Das, S. K.; Dash, R.; Emdad, L.; Dasgupta, S.; Wang, X.-Y.; Dent, P.; Reed, J. C.; Pellecchia, M.; Sarkar, D.; Fisher, P. B. Targeting the Bcl-2 family for cancer therapy. *Expert Opin. Ther. Targets* **2013**, *17*, 61–75.

[37] Croce, C. M.; Reed, J. C. Finally, an apoptosis-targeting therapeutic for cancer. *Cancer Res.* **2016**, *76*, 5914–5920.

[38] Schultz, D. R.; Harrington, W. J. Apoptosis: programmed cell death at a molecular level. *Semin. Arthritis Rheum.* **2003**, *32*, 345–369.

[39] Elmore, S. Apoptosis: a review of programmed cell death. *Toxicol. Pathol.* **2007**, *35*, 495–516.

[40] Green, D. R.; Reed, J. C. Mitochondria and apoptosis. *Science* **1998**, *281*, 1309–12.

[41] Ashkenazi, A.; Pai, R. C.; Fong, S.; Leung, S.; Lawrence, D. A.; Marsters, S. A.; Blackie, C.; Chang, L.; McMurtrey, A. E.; Hebert, A.; DeForge, L.; Koumenis, I. L.; Lewis, D.; Harris, L.; Bussiere, J.; Koeppen, H.; Shahrokh, Z.; Schwall, R. H. Safety and antitumor activity of recombinant soluble Apo2 ligand. *J. Clin. Invest.* **1999**, *104*, 155–162.

[42] de Miguel, D.; Lemke, J.; Anel, A.; Walczak, H.; Martinez-Lostao, L. Onto better TRAILs for cancer treatment. *Cell Death Differ.* **2016**, *23*, 733–47.

[43] Wang, Y.; Tjandra, N. Structural insights of tBid, the caspase-8-activated Bid, and its BH3 domain. *J. Biol. Chem.* **2013**, *288*, 35840–51.

[44] Parrales, A.; Iwakuma, T. Targeting oncogenic mutant p53 for cancer therapy. *Front. Oncol.* **2015**, *5*, 288.

[45] Rodier, F.; Campisi, J.; Bhaumik, D. Two faces of p53: aging and tumor suppression. *Nucleic Acids Res.* **2007**, *35*, 7475–84.

[46] Yu, J.; Zhang, L. PUMA, a potent killer with or without p53. *Oncogene* **2008**, *27 Suppl 1*, S71-83.

[47] Chipuk, J. E.; Kuwana, T.; Bouchier-Hayes, L.; Droin, N. M.; Newmeyer, D. D.; Schuler, M.; Green, D. R. Direct activation of Bax by p53 mediates mitochondrial membrane permeabilization and apoptosis. *Science* **2004**, *303*, 1010–1014.

[48] Wang, Z.; Sun, Y. Targeting p53 for novel anticancer therapy. *Transl. Oncol.* **2010**, *3*, 1–12.

[49] Strano, S.; Dell'Orso, S.; Di Agostino, S.; Fontemaggi, G.; Sacchi, A.; Blandino, G. Mutant p53: an oncogenic transcription factor. *Oncogene* **2007**, *26*, 2212–2219.

[50] Kim, E.; Deppert, W. Transcriptional activities of mutant p53: When mutations are more than a loss. *J. Cell. Biochem.* **2004**, *93*, 878–886.

[51] Chen, G.-X.; Zhang, S.; He, X.-H.; Liu, S.-Y.; Ma, C.; Zou, X.-P. Clinical utility of recombinant adenoviral human p53 gene therapy: current perspectives. *Onco. Targets. Ther.* **2014**, *7*, 1901–9.

[52] Arcaro, A.; Guerreiro, A. S. The phosphoinositide 3-kinase pathway in human cancer: genetic alterations and therapeutic implications. *Curr. Genomics* **2007**, *8*, 271–306.

[53] Reed, J. C. Apoptosis-targeted therapies for cancer. *Cancer Cell* **2003**, *3*, 17–22.

[54] LoPiccolo, J.; Blumenthal, G. M.; Bernstein, W. B.; Dennis, P. A. Targeting the PI3K/Akt/mTOR pathway: Effective combinations and clinical considerations. *Drug Resist. Updat.* **2008**, *11*, 32–50.

[55] Porta, C.; Paglino, C.; Mosca, A. Targeting PI3K/Akt/mTOR signaling in cancer. *Front. Oncol.* **2014**, *4*, 64.

[56] Richter, K.; Haslbeck, M.; Buchner, J. The Heat Shock Response: Life on the verge of death. *Mol. Cell* **2010**, *40*, 253–266.

[57] Takayama, S.; Reed, J. C.; Homma, S. Heat-shock proteins as regulators of apoptosis. *Oncogene* **2003**, *22*, 9041–9047.

[58] Neckers, L. Hsp90 inhibitors as novel cancer chemotherapeutic agents. *Trends Mol. Med.* **2002**, *8*, S55-61.

[59] Zuehlke, A.; Johnson, J. L. Hsp90 and co-chaperones twist the functions of

diverse client proteins. *Biopolymers* **2010**, *93*, 211–7.

[60] Sato, S.; Fujita, N.; Tsuruo, T. Modulation of Akt kinase activity by binding to Hsp90. *Proc. Natl. Acad. Sci.* **2000**, *97*, 10832–10837.

[61] Modi, S.; Stopeck, A.; Linden, H.; Solit, D.; Chandarlapaty, S.; Rosen, N.; D'Andrea, G.; Dickler, M.; Moynahan, M. E.; Sugarman, S.; Ma, W.; Patil, S.; Norton, L.; Hannah, A. L.; Hudis, C. Hsp90 inhibition is effective in breast cancer: a phase II trial of tanespimycin (17-AAG) plus trastuzumab in patients with HER2-positive metastatic breast cancer progressing on trastuzumab. *Clin. Cancer Res.* **2011**, *17*.

[62] Zhang, C.; Zhai, S.; Li, X.; Zhang, Q.; Wu, L.; Liu, Y.; Jiang, C.; Zhou, H.; Li, F.; Zhang, S.; Su, G.; Zhang, B.; Yan, B. Synergistic action by multi-targeting compounds produces a potent compound combination for human NSCLC both in vitro and in vivo. *Cell Death Dis.* **2014**, *5*, e1138.

[63] Weinstein, I. B.; Joe, A. K. Mechanisms of disease: Oncogene addiction-a rationale for molecular targeting in cancer therapy. *Nat. Clin. Pract. Oncol.* **2006**, *3*, 448–57.

[64] Payne, S.; Miles, D. Mechanisms of anticancer drugs. In *Scott-Brown's Otorhinolaryngology: Head and Neck Surgery*; ISBN: 9780340808931, **2008**; pp. 34–46.

[65] Willis, K. J.; Bachman, S. The state of the world's plants report. *R. Bot. Gard. Kew* **2016**, 24–27.

[66] Vuorelaa, P.; Leinonenb, M.; Saikkuc, P.; Tammelaa, P.; Rauhad, J.-P.; Wennberge, T.; Vuorela, H. Natural products in the process of finding new drug candidates. *Curr. Med. Chem.* **2004**, *11*, 1375–89.

[67] Hassan, H. M. a. A short history of the use of plants as medicines from ancient times. *Chim. Int. J. Chem.* **2015**, *69*, 622–623.

[68] Pan, S. Y.; Pan, S.; Yu, Z.-L.; Ma, D.-L.; Chen, S.-B.; Fong, W.-F.; Han, Y.-F.; Ko, K.-M. New perspectives on innovative drug discovery: an overview. *J. Pharm. Pharm. Sci.* **2010**, *13*, 450–71.

[69] Hounsome, N.; Hounsome, B.; Tomos, D.; Edwards-Jones, G. Plant metabolites and nutritional quality of vegetables. *J. Food Sci.* **2008**, *73*, R48-65.

[70] Li, J. W.-H.; Vederas, J. C. Drug discovery and natural products: end of an era or an endless frontier? *Science* **2009**, *325*, 161–5.

[71] Atanasov, A. G.; Waltenberger, B.; Pferschy-Wenzig, E.-M.; Linder, T.; Wawrosch, C.; Uhrin, P.; Temml, V.; Wang, L.; Schwaiger, S.; Heiss, E. H.; Rollinger, J. M.; Schuster, D.; Breuss, J. M.; Bochkov, V.; Mihovilovic, M. D.; Kopp, B.; Bauer, R.; Dirsch, V. M.; Stuppner, H. Discovery and resupply of pharmacologically active plant-derived natural products: A review.

Biotechnol. Adv. **2015**, *33*, 1582–614.

[72] Mukherjee, A. K.; Basu, S.; Sarkar, N.; Ghosh, A. C. Advances in cancer therapy with plant based natural products. *Curr. Med. Chem.* **2001**, *8*, 1467–86.

[73] WHO Traditional Medicine Strategy 2014-2023. *WHO Libr. Cat. Data* **2013**, 1–76.

[74] Newman, D. J.; Cragg, G. M. Natural products as sources of new drugs from 1981 to 2014. *J. Nat. Prod.* **2016**, *79*, 629–661.

[75] Briskin, D. P. Medicinal plants and phytomedicines. Linking plant biochemistry and physiology to human health. *Plant Physiol.* **2000**, *124*, 507–514.

[76] Ji, H.-F.; Li, X.-J.; Zhang, H.-Y. Natural products and drug discovery. Can thousands of years of ancient medical knowledge lead us to new and powerful drug combinations in the fight against cancer and dementia? *EMBO Rep.* **2009**, *10*, 194–200.

[77] Newman, D. J.; Cragg, G. M. Natural products as sources of new drugs over the 30 years from 1981 to 2010. *J. Nat. Prod.* **2012**, *75*, 311–35.

[78] Cragg, G. M.; Newman, D. J. Natural products: a continuing source of novel drug leads. *Biochim. Biophys. Acta* **2013**, *1830*, 3670–95.

[79] Yu, X.; Che, Z.; Xu, H. Recent advances in the chemistry and biology of podophyllotoxins. *Chem. A Eur. J.* **2017**, *23*.

[80] Gordaliza, M. Natural products as leads to anticancer drugs. *Clin. Transl. Oncol.* **2007**, *9*, 767–776.

[81] Xu, H.; Lv, M.; Tian, X. A review on hemisynthesis, biosynthesis, biological activities, mode of action, and structure-activity relationship of podophyllotoxins: 2003-2007. *Curr. Med. Chem.* **2009**, *16*, 327–49.

[82] You, Y. Podophyllotoxin derivatives: current synthetic approaches for new anticancer agents. *Curr. Pharm. Des.* **2005**, *11*, 1695–1717.

[83] Liu, Y.-Q.; Tian, J.; Qian, K.; Zhao, X.-B.; Morris-Natschke, S. L.; Yang, L.; Nan, X.; Tian, X.; Lee, K.-H. Recent progress on C-4-modified podophyllotoxin analogs as potent antitumor agents. *Med. Res. Rev.* **2015**, *35*, 1–62.

[84] Keglevich, P.; Hazai, L.; Kalaus, G.; Szántay, C. Modifications on the basic skeletons of vinblastine and vincristine. *Molecules* **2012**, *17*, 5893–5914.

[85] Moudi, M.; Go, R.; Yien, C. Y. S.; Nazre, M. Vinca alkaloids. *Int. J. Prev. Med.* **2013**, *4*, 1231–5.

[86] Attaoua, C.; Vincent, L.-A.; Abdel Jaoued, A.; Hadj-Kaddour, K.; Baï, Q.; De

Vos, J.; Vian, L.; Cuq, P. Differential involvement of glutathione S-transferase mu 1 and multidrug resistance protein 1 in melanoma acquired resistance to vinca alkaloids. *Fundam. Clin. Pharmacol.* **2015**, *29*, 62–71.

[87] Zhou, X. J.; Rahmani, R. Preclinical and clinical pharmacology of vinca alkaloids. *Drugs* **1992**, *44 Suppl 4*, 1–16.

[88] Gershenzon, J.; Dudareva, N. The function of terpene natural products in the natural world. *Nat. Chem. Biol.* **2007**, *3*, 408–414.

[89] Jansen, D. J.; Shenvi, R. A. Synthesis of medicinally relevant terpenes: reducing the cost and time of drug discovery. *Future Med. Chem.* **2014**, *6*, 1127–48.

[90] Dewick, P. M. *Medicinal natural products: A biosynthetic approach*; 3rd ed.; John Wiley & Sons; ISBN: 0470741686: New York; **2009**.

[91] Hill, R. A.; Connolly, J. D. Triterpenoids. *Nat. Prod. Rep.* **2012**, *29*, 780–818.

[92] Masullo, M.; Pizza, C.; Piacente, S. Oleanane derivatives for pharmaceutical use: a patent review (2000-2016). *Expert Opin. Ther. Pat.* **2017**, *27*, 237–255.

[93] Hill, R. A.; Connolly, J. D. Triterpenoids. *Nat. Prod. Rep.* **2017**.

[94] Hussain, H.; Al-Harrasi, A.; Csuk, R.; Shamraiz, U.; Green, I. R.; Ahmed, I.; Khan, I. A.; Ali, Z. Therapeutic potential of boswellic acids: a patent review (1990-2015). *Expert Opin. Ther. Pat.* **2017**, *27*, 81–90.

[95] Sheng, H.; Sun, H. Synthesis, biology and clinical significance of pentacyclic triterpenes: a multi-target approach to prevention and treatment of metabolic and vascular diseases. *Nat. Prod. Rep.* **2010**, *28*, 543–593.

[96] Alqahtani, A.; Hamid, K.; Kam, A.; Wong, K. H.; Abdelhak, Z.; Razmovski-Naumovski, V.; Chan, K.; Li, K. M.; Groundwater, P. W.; Li, G. Q. The pentacyclic triterpenoids in herbal medicines and their pharmacological activities in diabetes and diabetic complications. *Curr. Med. Chem.* **2013**, *20*, 908–31.

[97] Laszczyk, M. N. Pentacyclic triterpenes of the lupane, oleanane and ursane group as tools in cancer therapy. *Planta Med.* **2009**, *75*, 1549–60.

[98] Salvador, J. A. R. *Pentacyclic Triterpenes as Promising Agents in Cancer*; 1st ed.; Nova Science Publishers, Inc.; ISBN: 978-1-61122-835-9; **2010**.

[99] Yuan, R. Traditional Chinese medicine an approach to scientific proof and clinical validation. *Pharmacol. Ther.* **2000**, *86*, 191–198.

[100] Singh, B.; Sharma, R. A. Plant terpenes: defense responses, phylogenetic analysis, regulation and clinical applications. *3 Biotech* **2015**, *5*, 129–151.

[101] Phillips, M. A.; Bohlmann, J.; Gershenzon, J. Molecular Regulation of

Induced Terpenoid Biosynthesis in Conifers. *Phytochem. Rev.* **2006**, *5*, 179–189.

[102] James, J. T.; Dubery, I. A. Pentacyclic triterpenoids from the medicinal herb, Centella asiatica (L.) Urban. *Molecules* **2009**, *14*, 3922–3941.

[103] Wang, Z.; Yeats, T.; Han, H.; Jetter, R. Cloning and characterization of oxidosqualene cyclases from Kalanchoe daigremontiana: enzymes catalyzing up to 10 rearrangement steps yielding friedelin and other triterpenoids. *J. Biol. Chem.* **2010**, *285*, 29703–12.

[104] Pina, E. S.; Silva, D. B.; Teixeira, S. P.; Coppede, J. S.; Furlan, M.; França, S. C.; Lopes, N. P.; Pereira, A. M. S.; Lopes, A. A. Mevalonate-derived quinonemethide triterpenoid from in vitro roots of Peritassa laevigata and their localization in root tissue by MALDI imaging. *Sci. Rep.* **2016**, *6*, 22627.

[105] Chandler, R. F.; Hooper, S. N. Friedelin and associated triterpenoids. *Phytochemistry* **1979**, *18*, 711–724.

[106] Shan, W. G.; Zhang, L. W.; Xiang, J. G.; Zhan, Z. J. Natural friedelanes. *Chem. Biodivers.* **2013**, *10*, 1392–1434.

[107] Klaić, L.; Morimoto, R. I.; Silverman, R. B. Celastrol analogues as inducers of the heat shock response. Design and synthesis of affinity probes for the identification of protein targets. *ACS Chem. Biol.* **2012**, *7*, 928–37.

[108] Jiang, F.; Wang, H. J.; Bao, Q. C.; Wang, L.; Jin, Y. H.; Zhang, Q.; Jiang, D.; You, Q. D.; Xu, X. L. Optimization and biological evaluation of celastrol derivatives as Hsp90-Cdc37 interaction disruptors with improved druglike properties. *Bioorganic Med. Chem.* **2016**, *24*, 5431–5439.

[109] Setzer, W. N.; Holland, M. T.; Bozeman, C. A.; Rozmus, G. F.; Setzer, M. C.; Moriarity, D. M.; Reeb, S.; Vogler, B.; Bates, R. B.; Haber, W. A. Isolation and frontier molecular orbital investigation of bioactive quinone-methide triterpenoids from the bark of Salacia petenensis. *Planta Med.* **2001**, *67*, 65–69.

[110] Salminen, A.; Lehtonen, M.; Paimela, T.; Kaarniranta, K. Celastrol: molecular targets of Thunder God Vine. *Biochem Biophys. Res. Commun.* **2010**, *394*, 439–42.

[111] Lewis, M. A.; Graff Yoerg, D.; Bolton, J. L.; Thompson, J. A. Alkylation of 2‘-Deoxynucleosides and DNA by Quinone Methides Derived from 2,6-Di- *tert* -butyl-4-methylphenol. *Chem. Res. Toxicol.* **1996**, *9*, 1368–1374.

[112] Kannaiyan, R.; Shanmugam, M. K.; Sethi, G. Molecular targets of celastrol derived from Thunder of God Vine: potential role in the treatment of inflammatory disorders and cancer. *Cancer Lett.* **2011**, *303*, 9–20.

[113] Salvador, J. A. R.; Santos, R. C.; Figueiredo, S. A. C.; Jing, Y. Antitumor effects of celastrol and semi-synthetic derivatives. *Mini. Rev. Org. Chem.*

2014, *11*, 400–407.

[114] Figueiredo, J. N.; Räz, B.; Séquin, U. Novel quinone methides from Salacia kraussii with in vitro antimalarial activity. *J. Nat. Prod.* **1998**, *61*, 718–23.

[115] Fan, D.; Parhira, S.; Zhu, G. Y.; Jiang, Z. H.; Bai, L. P. Triterpenoids from the stems of Tripterygium regelii. *Fitoterapia* **2016**, *113*, 69–73.

[116] Gomes, J. P. M.; Molina, J.-M.; Carlos, I. Z.; Cardoso, C. R. P.; Vilegas, W. Antitumoral, mutagenic and (anti)estrogenic activities of tingenone and pristimerin. *Braz. J. Phamacogn.* **2011**, *21*, 963–971.

[117] Alvarenga, N.; Ferro, E. A. Bioactive triterpenes and related compounds from celastraceae. In *Studies in Natural Products Chemistry*; **2006**; Vol. 33, pp. 239–307.

[118] Grant, P. K.; Johnson, A. W. Pristimerin. Part I. The nature of the chromophore. *J. Chem. Soc.* **1957**, 4079–4089.

[119] Klaić, L.; Trippier, P. C.; Mishra, R. K.; Morimoto, R. I.; Silverman, R. B. Remarkable stereospecific conjugate additions to the Hsp90 inhibitor celastrol. *J. Am. Chem. Soc.* **2011**, *133*, 19634–19637.

[120] Rodrigues, V. G.; Duarte, L. P.; Silva, R. R.; Silva, G. D. F.; Mercadante-Simões, M. O.; Takahashi, J. A.; Matildes, B. L. G.; Fonseca, T. H. S.; Gomes, M. A.; Filho, S. A. V. Salacia crassifolia (celastraceae): Chemical constituents and antimicrobial activity. *Quim. Nova* **2015**, *38*, 237–242.

[121] Sneden, A. T. Isoiguesterin, a new antileukemic bisnortriterpene from Salacia madagascariensis. *J. Nat. Prod.* **1981**, *44*, 503–7.

[122] Huang, W.; Yang, Y.-J.; Hu, H.; Zhang, S.-B. Seasonal variations in photosystem I compared with photosystem II of three alpine evergreen broad-leaf tree species. *J. Photochem. Photobiol. B.* **2016**, *165*, 71–79.

[123] Sotanaphun, U.; Svttisri, R.; Lippun, V.; Bavovada, R. Quinone-methide triterpenoids from Gliptopetalum Sclerocarpum. *Phytochem.* **1998**, *49*, 1749–1755.

[124] Oramas-Royo, S. M.; Chávez, H.; Martín-Rodríguez, P.; Fernández-Pérez, L.; Ravelo, Á. G.; Estévez-Braun, A. Cytotoxic triterpenoids from Maytenus retusa. *J. Nat. Prod.* **2010**, *73*, 2029–2034.

[125] Chávez, H.; Estévez-Braun, A.; Ravelo, a G.; González, A. G. New phenolic and quinone-methide triterpenes from Maytenus amazonica. *J. Nat. Prod.* **1999**, *62*, 434–6.

[126] Murphy, B. T.; Narender, T.; Kauffman, C. A.; Woolery, M.; Jensen, P. R.; Fenical, W. Saliniquinones A-F, New Members of the Highly Cytotoxic Anthraquinone-γ-Pyrones from the Marine Actinomycete Salinispora arenicola. *Aust. J. Chem.* **2010**, *63*, 929.

[127] Martin, J. D. The structure of dispermoquinone : A triterpenoid quinone methide from Maytenus dispermus. *Tetrahedron* **1973**, *29*, 2997–3000.

[128] Chávez, H.; Rodríguez, G.; Estévez-Braun, A.; Ravelo, A.; Estévez-Reyes, R.; González, A.; Fdez-Puente, J.; García-Grávalos, D. Macrocarpins A-D, new cytotoxic nor-triterpenes from Maytenus macrocarpa. *Bioorg. Med. Chem. Lett.* **2000**, *10*, 759–762.

[129] Rodríguez, F. M.; López, M. R.; Jiménez, I. a.; Moujir, L.; Ravelo, A. G.; Bazzocchi, I. L. New phenolic triterpenes from Maytenus blepharodes. Semisynthesis of 6-deoxoblepharodol from pristimerin. *Tetrahedron* **2005**, *61*, 2513–2519.

[130] T. Morota, C.-X. Yang, T. Ogino, W.-Z. Qin, T. Katsuhara, L.-H. Xu, Y. Komatsu, K.-L. Miao, M. Maruno, B.-H. Y. D:A-friedo-24-noroleanane triterpenoids from Tripterigium Wilford II. *Pergamon* **1995**, *39*, 1159–1163.

[131] Takaishi, Y.; Wariishi, N.; Tateishi, H.; Kawazoe, K.; Nakano, K.; Ono, Y.; Tokuda, H.; Nishino, H.; Iwashima, A. Triterpenoid inhibitors of interleukin-1 secretion and tumour-promotion from Tripterygium wilfordii var. regelii. *Phytochemistry* **1997**, *45*, 969–974.

[132] Morikawa, T.; Kishi, A.; Pongpiriyadacha, Y.; Matsuda, H.; Yoshikawa, M. Structures of new friedelane-type triterpenes and eudesmane-type sesquiterpene and aldose reductase inhibitors from Salacia chinensis. *J. Nat. Prod.* **2003**, *66*, 1191–1196.

[133] Bishayee, A.; Ahmed, S.; Brankov, N.; Perloff, M. Triterpenoids as potential agents for the chemoprevention and therapy of breast cancer. *Front. Biosci.* **2011**, *16*, 980–96.

[134] Setzer, W. N.; Setzer, M. C. Plant-Derived Triterpenoids as Potential Antineoplastic Agents. *Mini Rev. Med. Chem.* **2003**, *3*, 540–556.

[135] Petronelli, A.; Pannitteri, G.; Testa, U. Triterpenoids as new promising anticancer drugs. *Anticancer Drugs* **2009**, *20*, 880–92.

[136] Sogno, I.; Vannini, N.; Lorusso, G.; Cammarota, R.; Noonan, D. M.; Generoso, L.; Sporn, M. B.; Albini, A. Anti-angiogenic activity of a novel class of chemopreventive compounds: oleanic acid terpenoids. *Recent Results Cancer Res.* **2009**, *181*, 209–12.

[137] Tren, Z. K.; Dub, A. Pentacyclic triterpenoic acids: New chemoprotective compounds. *Neoplasma* **2004**, *51*, 327–333.

[138] Shanmugam, M. K.; Nguyen, A. H.; Kumar, A. P.; Tan, B. K. H.; Sethi, G. Targeted inhibition of tumor proliferation, survival, and metastasis by pentacyclic triterpenoids: Potential role in prevention and therapy of cancer. *Cancer Lett.* **2012**, *320*, 158–170.

[139] Eiznhamer, D. A.; Xu, Z.-Q. Betulinic acid: a promising anticancer candidate.

IDrugs **2004**, *7*, 359–73.

[140] Büchele, B.; Zugmaier, W.; Estrada, A.; Genze, F.; Syrovets, T.; Paetz, C.; Schneider, B.; Simmet, T. Characterization of 3alpha-acetyl-11-keto-alpha-boswellic acid, a pentacyclic triterpenoid inducing apoptosis in vitro and in vivo. *Planta Med.* **2006**, *72*, 1285–9.

[141] Frank, M. B.; Yang, Q.; Osban, J.; Azzarello, J. T.; Saban, M. R.; Saban, R.; Ashley, R. A.; Welter, J. C.; Fung, K.-M.; Lin, H.-K. Frankincense oil derived from Boswellia carteri induces tumor cell specific cytotoxicity. *BMC Complement Altern. Med.* **2009**, *9*, 6.

[142] Yu, L.; Yu, T.; Ma, R. Inhibition of the tumor promoting action of 12-O-tetradecanoylphorbol-13-acetate by tubeimoside III isolated from Bolbostemma paniculatum. *Carcinogenesis* **1995**, *16*, 3045–8.

[143] Dzubak, P.; Hajduch, M.; Vydra, D.; Hustova, A.; Kvasnica, M.; Biedermann, D.; Markova, L.; Urban, M.; Sarek, J. Pharmacological activities of natural triterpenoids and their therapeutic implications. *Nat. Prod. Rep.* **2006**, *23*, 394–411.

[144] Foo, J. B.; Saiful Yazan, L.; Tor, Y. S.; Wibowo, A.; Ismail, N.; How, C. W.; Armania, N.; Loh, S. P.; Ismail, I. S.; Cheah, Y. K.; Abdullah, R. Induction of cell cycle arrest and apoptosis by betulinic acid-rich fraction from Dillenia suffruticosa root in MCF-7 cells involved p53/p21 and mitochondrial signalling pathway. *J. Ethnopharmacol.* **2015**, *166*, 270–278.

[145] Zhao, X.; Liu, M.; Li, D. Oleanolic acid suppresses the proliferation of lung carcinoma cells by miR-122/Cyclin G1/MEF2D axis. *Mol. Cell. Biochem.* **2015**, *400*, 1–7.

[146] Sha, M.; Ye, J.; Luan, Z.; Guo, T.; Wang, B.; Huang, J. Celastrol induces cell cycle arrest by MicroRNA-21-mTOR-mediated inhibition p27 protein degradation in gastric cancer. *Cancer Cell Int.* **2015**, *15*, 101.

[147] Lewinska, A.; Adamczyk-Grochala, J.; Kwasniewicz, E.; Deregowska, A.; Wnuk, M. Ursolic acid-mediated changes in glycolytic pathway promote cytotoxic autophagy and apoptosis in phenotypically different breast cancer cells. *Apoptosis* **2017**, *22*, 800–815.

[148] Zhang, H.; Li, J.; Li, G.; Wang, S. Effects of celastrol on enhancing apoptosis of ovarian cancer cells via the downregulation of microRNA‑21 and the suppression of the PI3K/Akt‑NF‑κB signaling pathway in an in vitro model of ovarian carcinoma. *Mol. Med. Rep.* **2016**, *14*, 5363–5368.

[149] Saraswati, S.; Agrawal, S. S.; Alhaider, A. A. Ursolic acid inhibits tumor angiogenesis and induces apoptosis through mitochondrial-dependent pathway in Ehrlich ascites carcinoma tumor. *Chem. Biol. Interact.* **2013**, *206*, 153–165.

[150] Li, L.; Lin, J.; Sun, G.; Wei, L.; Shen, A.; Zhang, M.; Peng, J. Oleanolic acid

inhibits colorectal cancer angiogenesis in vivo and in vitro via suppression of STAT3 and Hedgehog pathways. *Mol. Med. Rep.* **2016**, *13*, 5276–82.

[151] Ni, H.; Zhao, W.; Kong, X.; Li, H.; Ouyang, J. Celastrol inhibits lipopolysaccharide-induced angiogenesis by suppressing TLR4-triggered Nuclear factor-kappa B activation. *Acta Haematol.* **2014**, *131*, 102–111.

[152] Guo, G.; Yao, W.; Zhang, Q.; Bo, Y. Oleanolic acid suppresses migration and invasion of malignant glioma cells by inactivating MAPK/ERK signaling pathway. *PLoS One* **2013**, *8*, e72079.

[153] Yu, X.; Wang, Q.; Zhou, X.; Fu, C.; Cheng, M.; Guo, R.; Liu, H.; Zhang, B.; Dai, M. Celastrol negatively regulates cell invasion and migration ability of human osteosarcoma via downregulation of the PI3K/Akt/NF-κB signaling pathway in vitro. *Oncol. Lett.* **2016**, *12*, 3423–3428.

[154] Lee, B. W.; Seo, W. D.; Gal, S. W.; Yang, M. S.; Park, K. H. Quinone methide triterpenes from Tripterygium regelii. *Agric. Chem. Biotechnol.* **2004**, *47*, 77–80.

[155] Length, W.; Length, W. Celastrol, spectrographic characterization and color tests. *J. Pharm. Sci.* **1942**, *31*, 315–317.

[156] Cascão, R.; Vidal, B.; Lopes, I. P.; Paisana, E.; Rino, J.; Moita, L. F.; Fonseca, J. E. Decrease of CD68 synovial macrophages in celastrol treated arthritic rats. *PLoS One* **2015**, *10*, e0142448.

[157] Venkatesha, S. H.; Dudics, S.; Astry, B.; Moudgil, K. D. Control of autoimmune inflammation by celastrol, a natural triterpenoid. *Pathog. Dis.* **2016**, *74*.

[158] Kim, D. Y.; Park, J. W.; Jeoung, D.; Ro, J. Y. Celastrol suppresses allergen-induced airway inflammation in a mouse allergic asthma model. *Eur J Pharmacol* **2009**, *612*, 98–105.

[159] Peng, X.; Wang, J.; Li, X.; Lin, L.; Xie, G.; Cui, Z.; Li, J.; Wang, Y.; Li, L. Targeting mast cells and basophils with anti-FcεRIα fab-conjugated celastrol-loaded micelles suppresses allergic inflammation. *J. Biomed. Nanotechnol.* **2015**, *11*, 2286–99.

[160] Yu, Y.; Koehn, C. D.; Yue, Y.; Li, S.; Thiele, G. M.; Hearth-Holmes, M. P.; Mikuls, T. R.; O'Dell, J. R.; Klassen, L. W.; Zhang, Z.; Su, K. Celastrol inhibits inflammatory stimuli-induced neutrophil extracellular trap formation. *Curr. Mol. Med.* **2015**, *15*, 401–10.

[161] Jia, Z.; Xu, C.; Shen, J.; Xia, T.; Yang, J.; He, Y. The natural compound celastrol inhibits necroptosis and alleviates ulcerative colitis in mice. *Int. Immunopharmacol.* **2015**, *29*, 552–559.

[162] Yang, H.; Liu, C.; Jiang, J.; Wang, Y.; Zhang, X. Celastrol attenuates multiple sclerosis and optic neuritis in an experimental autoimmune

encephalomyelitis model. *Front. Pharmacol.* **2017**, *8*.

[163] Zhou, L.-L.; Lin, Z.-X.; Fung, K.-P.; Cheng, C. H. K. K.; Che, C.-T.; Zhao, M.; Wu, S.-H.; Zuo, Z. Celastrol-induced apoptosis in human HaCaT keratinocytes involves the inhibition of NF-κB activity. *Eur J Pharmacol* **2011**, *670*, 399–408.

[164] Ding, Q.; Cheng, Y.; Chen, W.; Zhong, H.; Wang, X. Celastrol, an inhibitor of heat shock protein 90β potently suppresses the expression of matrix metalloproteinases, inducible nitric oxide synthase and cyclooxygenase-2 in primary human osteoarthritic chondrocytes. *Eur. J. Pharmacol.* **2013**, *708*, 1–7.

[165] Yu, X.; Tao, W.; Jiang, F.; Li, C.; Lin, J.; Liu, C. Celastrol attenuates hypertension-induced inflammation and oxidative stress in vascular smooth muscle cells via induction of heme oxygenase-1. *Am. J. Hypertens.* **2010**, *23*, 895–903.

[166] Veerappan, K.; Natarajan, S.; Ethiraj, P.; Vetrivel, U.; Samuel, S. Inhibition of IKKB by celastrol and its analogues - an in silico and in vitro approach. *Pharm. Biol.* **2017**, *55*, 368–373.

[167] Zhao, Y.; Zhao, H.; Lobo, N.; Guo, X.; Gentleman, S. M.; Ma, D. Celastrol enhances cell viability and inhibits amyloid-β production induced by lipopolysaccharide in vitro. *J. Alzheimers. Dis.* **2014**, *41*, 835–44.

[168] Zhang, Y.-Q.; Sarge, K. D. Celastrol inhibits polyglutamine aggregation and toxicity though induction of the heat shock response. *J. Mol. Med.* **2007**, *85*, 1421–1428.

[169] Wang, J.; Gines, S.; MacDonald, M. E.; Gusella, J. F. Reversal of a full-length mutant huntingtin neuronal cell phenotype by chemical inhibitors of polyglutamine-mediated aggregation. *BMC Neurosci.* **2005**, *6*, 1.

[170] Cleren, C.; Calingasan, N. Y.; Chen, J.; Beal, M. F. Celastrol protects against MPTP- and 3-nitropropionic acid-induced neurotoxicity. *J. Neurochem.* **2005**, *94*, 995–1004.

[171] Cascão, R.; Fonseca, J. E.; Moita, L. F. Celastrol: A spectrum of treatment opportunities in chronic diseases. *Front. Med.* **2017**, *4*.

[172] Han, L.; Li, C.; Sun, B.; Xie, Y.; Guan, Y.; Ma, Z.; Chen, L. Protective effects of celastrol on diabetic liver injury via TLR4/MYD88/NF-kB signaling pathway in type 2 diabetic rats. *J. Diabetes Res.* **2016**, *2016*, 1–10.

[173] Ma, X.; Xu, L.; Alberobello, A.; Gavrilova, O.; Bagattin, A.; Skarulis, M.; Liu, J.; Finkel, T.; Mueller, E. Celastrol protects against obesity and metabolic dysfunction through activation of a HSF1-PGC1a transcriptional axis. *Cell Metab.* **2015**, *22*, 695–708.

[174] Greenhill, C. Obesity: Celastrol identified as a leptin sensitizer and potential

novel treatment for obesity. *Nat. Rev. Endocrinol.* **2015**, *11*, 444.

[175] Li, M.; Liu, X.; He, Y.; Zheng, Q.; Wang, M.; Wu, Y.; Zhang, Y.; Wang, C. Celastrol attenuates angiotensin II mediated human umbilical vein endothelial cells damage through activation of Nrf2/ERK1/2/Nox2 signal pathway. *Eur. J. Pharmacol.* **2017**, *797*, 124–133.

[176] Tallorin, L.; Durrant, J. D.; Nguyen, Q. G.; McCammon, J. A.; Burkart, M. D. Celastrol inhibits Plasmodium falciparum enoyl-acyl carrier protein reductase. *Bioorg. Med. Chem.* **2014**, *22*, 6053–6061.

[177] Yu, J. S.; Tseng, C. K.; Lin, C. K.; Hsu, Y. C.; Wu, Y. H.; Hsieh, C. L.; Lee, J. C. Celastrol inhibits dengue virus replication via up-regulating type I interferon and downstream interferon-stimulated responses. *Antiviral Res.* **2017**, *137*, 49–57.

[178] Xiao, S.; Zhang, M.; Liang, Y.; Wang, D. Celastrol synergizes with oral nifedipine to attenuate hypertension in preeclampsia: a randomized, placebo-controlled, and double blinded trial. *J. Am. Soc. Hypertens.* **2017**.

[179] Xu, L.; Zhang, D.; Liu, X.; Yang, C.; Wang, Y.; Cao, F. Inhibitory effect of celastrol on cell viability of urinary bladder cancer cell line 5637 cells through JAK2 / STAT3 signaling pathway. **2017**, *10*, 6845–6852.

[180] Shrivastava, S.; Jeengar, M. K.; Reddy, V. S.; Reddy, G. B.; Naidu, V. G. M. G. M. Anticancer effect of celastrol on human triple negative breast cancer: Possible involvement of oxidative stress, mitochondrial dysfunction, apoptosis and PI3K/Akt pathways. *Exp. Mol. Pathol.* **2015**, *98*, 313–327.

[181] Bai, K.-K.; Chen, F.-L.; Yu, Z.; Zheng, Y.-Q.; Li, Y.-N.; Guo, Y.-H. Synthesis of [3β-acetoxy-urs-12-en-28-oyl]-1-monoglyceride and investigation on its anti tumor effects against BGC-823. *Bioorg. Med. Chem.* **2011**, *19*, 4043–50.

[182] Kim, J. H.; Lee, J. O.; Lee, S. K.; Kim, N.; You, G. Y.; Moon, J. W.; Sha, J.; Kim, S. J.; Park, S. H.; Kim, H. S. Celastrol suppresses breast cancer MCF-7 cell viability via the AMP-activated Protein Kinase (AMPK)-induced p53-Polo like Kinase 2 (PLK-2) pathway. *Cell Signal* **2012**, *80*, 1–9.

[183] Raja, S. M.; Clubb, R. J.; Ortega-Cava, C.; Williams, S. H.; Bailey, T. a.; Duan, L.; Zhao, X.; Reddi, A. L.; Nyong, A. M.; Natarajan, A.; Band, V.; Band, H. Anticancer activity of Celastrol in combination with ErbB2-targeted therapeutics for treatment of ErbB2-overexpressing breast cancers. *Cancer Biol. Ther.* **2011**, *11*, 263–276.

[184] Kim, Y.; Kang, H.; Jang, S.; Ko, J. Celastrol inhibits breast cancer cell invasion via suppression of NF-kB -mediated matrix metalloproteinase-9 expression. *Cell Physiol. Biochem.* **2011**, *701*, 175–184.

[185] Jang, S. Y.; Jang, S.-W.; Ko, J. Celastrol inhibits the growth of estrogen positive human breast cancer cells through modulation of estrogen receptor

alfa. *Cancer Lett.* **2011**, *300*, 57–65.

[186] Kannaiyan, R.; Manu, K. A.; Chen, L.; Li, F.; Rajendran, P.; Subramaniam, A.; Lam, P.; Kumar, A. P.; Sethi, G. Celastrol inhibits tumor cell proliferation and promotes apoptosis through the activation of c-Jun N-terminal kinase and suppression of PI3K/Akt signaling pathways. *Apoptosis* **2011**, *16*, 1028–1041.

[187] Meng, Y.; Li, Y.; Li, F.; Song, Y.; Wang, H.; Chen, H.; Cao, B. Synthesis and antitumor activity evaluation of new asiatic acid derivatives. *J. Asian Nat. Prod. Res.* **2012**, *14*, 844–855.

[188] Yadav, V. R.; Sung, B.; Prasad, S.; Kannappan, R.; Cho, S.-G.; Liu, M.; Chaturvedi, M. M.; Aggarwal, B. B. Celastrol suppresses invasion of colon and pancreatic cancer cells through the downregulation of expression of CXCR4 chemokine receptor. *J. Mol. Med.* **2010**, *88*, 1243–1253.

[189] Zhu, H.; Liu, X.-W.; Ding, W.-J.; Xu, D.-Q.; Zhao, Y.-C.; Lu, W.; He, Q.-J.; Yang, B. Up-regulation of death receptor 4 and 5 by celastrol enhances the anti-cancer activity of TRAIL/Apo-2L. *Cancer Lett.* **2010**, *297*, 155–164.

[190] Lu, W.; Jia, G.; Meng, X.; Zhao, C.; Zhang, L.; Ren, Y.; Pan, H.; Ni, Y. Beta-catenin mediates the apoptosis induction effect of celastrol in HT29 cells. *Life Sci.* **2012**, *91*, 279–283.

[191] Sha, M.; Ye, J.; Zhang, L.; Luan, Z.; Chen, Y.; Huang, J. Celastrol induces apoptosis of gastric cancer cells by miR-21 Inhibiting PI3K/Akt-NF-κB signaling pathway. *Pharmacology* **2014**, *93*, 39–46.

[192] Li, P.-P.; He, W.; Yuan, P.-F.; Song, S.-S.; Lu, J.-T.; Wei, W. Celastrol induces mitochondria-mediated apoptosis in hepatocellular carcinoma Bel-7402 cells. *Am. J. Chin. Med.* **2015**, *43*, 137–148.

[193] Zhijuan Cao, Jianying Liang, Caiyun Liu, Jianzhong Lu, Yanhua Sun, K. Z. Polyethylene glycol celastrol and its preparation method and application., Patent CN 102796254 A, **2012**.

[194] Chen, G.; Zhang, X.; Zhao, M.; Wang, Y.; Cheng, X.; Wang, D.; Xu, Y.; Du, Z.; Yu, X. Celastrol targets mitochondrial respiratory chain complex I to induce reactive oxygen species-dependent cytotoxicity in tumor cells. *BMC Cancer* **2011**, *11*, 1–13.

[195] Huang, L.; Zhang, Z.; Zhang, S.; Ren, J.; Zhang, R.; Zeng, H.; Li, Q.; Wu, G.; Wu Inhibitory action of celastrol on hypoxia-mediated angiogenesis and metastasis via the HIF-1α pathway. *Int. J. Mol. Med.* **2011**, *27*, 407–415.

[196] Fan, X.-X.; Li, N.; Wu, J.-L.; Zhou, Y.-L.; He, J.-X.; Liu, L.; Leung, E. Celastrol induces apoptosis in gefitinib-resistant non-small cell lung cancer cells via caspases-dependent pathways and Hsp90 client protein degradation. *Molecules* **2014**, *19*, 3508–3522.

[197] Wang, W.-B. B.; Feng, L.-X. X.; Yue, Q.-X. X.; Wu, W.-Y. Y.; Guan, S.-H. H.; Jiang, B.-H. H.; Yang, M.; Liu, X.; Guo, D.-A. Paraptosis accompanied by autophagy and apoptosis was induced by celastrol, a natural compound with influence on proteasome, ER stress and Hsp90. *J. Cell Physiol.* **2012**, *227*, 2196–206.

[198] Seo, H. R.; Seo, W. D.; Pyun, B.-J.; Lee, B. W.; Jin, Y. B.; Park, K. H.; Seo, E.-K.; Lee, Y.-J.; Lee, Y.-S. Radiosensitization by celastrol is mediated by modification of antioxidant thiol molecules. *Chem. Biol. Interact.* **2011**, *193*, 34–42.

[199] Lee, J. H.; Choi, K. J.; Seo, W. D.; Jang, S. Y.; Kim, M.; Lee, B. W.; Kim, J. Y.; Kang, S.; Park, K. H.; Lee, Y.-S.; Bae, S. Enhancement of radiation sensitivity in lung cancer cells by celastrol is mediated by inhibition of Hsp90. *Int. J. Mol. Med.* **2011**, *27*, 441–446.

[200] Zhang, T.; Hamza, A.; Cao, X.; Wang, B.; Yu, S.; Zhan, C.-G.; Sun, D. A novel Hsp90 inhibitor to disrupt Hsp90/Cdc37 complex against pancreatic cancer cells. *Mol. Cancer Ther.* **2008**, *7*, 162–170.

[201] Ji, N.; Li, J.; Wei, Z.; Kong, F.; Jin, H.; Chen, X.; Li, Y.; Deng, Y. Effect of celastrol on growth inhibition of prostate cancer cells through the regulation of hERG channel in vitro. *Biomed. Res. Int.* **2015**, *2015*, 1–7.

[202] Cao, L.; Zhang, X.; Cao, F.; Wang, Y.; Shen, Y.; Yang, C.; Uzan, G.; Peng, B.; Zhang, D. Inhibiting inducible miR-223 further reduces viable cells in human cancer cell lines MCF-7 and PC3 treated by celastrol. *BMC Cancer* **2015**.

[203] Jo, H.; Loison, F.; Hattori, H.; Silberstein, L. E.; Yu, H.; Luo, H. R. Natural product celastrol destabilizes tubulin heterodimer and facilitates mitotic cell death triggered by microtubule-targeting anti-cancer drugs. *PLoS One* **2010**, *5*, e10318.

[204] Kim, S. H.; Kang, J. G.; Kim, C. S.; Ihm, S.-H.; Choi, M. G.; Yoo, H. J.; Lee, S. J. Cytotoxic effect of celastrol alone or in combination with paclitaxel on anaplastic thyroid carcinoma cells. *Tumor Biol.* **2017**, *39*.

[205] Zhang, X.; Yang, J.; Chen, M.; Li, L.; Huan, F.; Li, A.; Liu, Y.; Xia, Y.; Duan, J.; Ma, S. Metabolomics profiles delineate uridine deficiency contributes to mitochondria-mediated apoptosis induced by celastrol in human acute promyelocytic leukemia cells. *Oncotarget* **2014**, *7*, 46557–46572.

[206] Lu, Z.; Jin, Y.; Qiu, L.; Lai, Y.; Pan, J. Celastrol, a novel HSP90 inhibitor, depletes Bcr-Abl and induces apoptosis in imatinib-resistant chronic myelogenous leukemia cells harboring T315I mutation. *Cancer Lett.* **2010**, *290*, 182–191.

[207] Azmi, A. S.; Wang, Z.; Philip, P. A. Proof of concept : network and systems biology approaches aid in the discovery of potent anticancer drug combinations. *Mol. Cancer Ther.* **2010**, 3137–3144.

[208] Zhu, H.; Liu, X.-W.; Cai, T.-Y.; Cao, J.; Tu, C.; Lu, W.; He, Q.; Yang, B. Celastrol acts as a potent antimetastatic agent targeting beta 1 integrin and inhibiting cell-extracellular matrix adhesion, in part via the p38 mitogen-activated protein kinase pathway. *J. Pharmacol. Exp. Ther.* **2010**, *334*, 489–499.

[209] Ni, H.; Zhao, W.; Kong, X.; Li, H.; Ouyang, J. NF-kappa B modulation is involved in celastrol induced human multiple myeloma cell apoptosis. *PLoS One* **2014**, *9*, e95846.

[210] Tozawa, K.; Sagawa, M.; Kizaki, M. Quinone methide tripterine, celastrol, induces apoptosis in human myeloma cells via NF-κB pathway. *Int. J. Oncol.* **2011**, *39*, 1117–1122.

[211] Morita, H.; Hirasawa, Y.; Muto, A.; Yoshida, T.; Sekita, S.; Shirota, O. Antimitotic quinoid triterpenes from Maytenus chuchuhuasca. *Bioorg. Med. Chem. Lett.* **2008**, *18*, 1050–1052.

[212] Idris, A. I.; Libouban, H.; Nyangoga, H.; Landao-Bassonga, E.; Chappard, D.; Ralston, S. H. Pharmacologic inhibitors of IκB kinase suppress growth and migration of mammary carcinosarcoma cells in vitro and prevent osteolytic bone metastasis in vivo. *Mol. Cancer Ther.* **2009**, *8*.

[213] Li, H.-Y. Y.; Zhang, J.; Sun, L.-L. L.; Li, B.-H. H.; Gao, H.-L. L.; Xie, T.; Zhang, N.; Ye, Z.-M. M. Celastrol induces apoptosis and autophagy via the ROS/JNK signaling pathway in human osteosarcoma cells: an in vitro and in vivo study. *Cell Death Dis.* **2015**, *6*, e1604.

[214] Zheng, L.; Fu, Y.; Zhuang, L.; Gai, R.; Ma, J.; Lou, J.; Zhu, H.; He, Q.; Yang, B. Simultaneous NF-κB inhibition and E-cadherin upregulation mediate mutually synergistic anticancer activity of celastrol and SAHA *in vitro* and *in vivo*. *Int. J. Cancer* **2014**, *135*, 1721–1732.

[215] Jiang, Q.-W.; Cheng, K.-J.; Mei, X.-L.; Qiu, J.-G.; Zhang, W.-J.; Xue, Y.-Q.; Qin, W.-M.; Yang, Y.; Zheng, D.-W.; Chen, Y.; Wei, M.-N.; Zhang, X.; Lv, M.; Chen, M.-W.; Wei, X.; Shi, Z. Synergistic anticancer effects of triptolide and celastrol, two main compounds from Thunder God Vine. *Oncotarget* **2015**, *6*, 32790–804.

[216] Yang, H.; Chen, D.; Cui, Q. C.; Yuan, X.; Dou, Q. P. Celastrol, a triterpene extracted from the Chinese “Thunder of God Vine” is a potent proteasome inhibitor and suppresses human prostate cancer growth in nude mice. *Cancer Res.* **2006**, *66*, 4758–4765.

[217] Pang, X.; Yi, Z.; Zhang, J.; Lu, B.; Sung, B.; Qu, W. Celastrol suppresses angiogenesis-mediated tumor growth through inhibition of AKT/ mammalian target of rapamycin pathway celastrol suppresses angiogenesis-mediated tumor growth through inhibition of AKT/ mammalian target of rapamycin pathway. *Cancer Res.* **2010**, *70*, 1951–1959.

[218] Lin, L.; Sun, Y.; Wang, D.; Zheng, S.; Zhang, J.; Zheng, C. Celastrol

ameliorates ulcerative colitis-related colorectal cancer in mice via suppressing inflammatory responses and epithelial-mesenchymal transition. *Front. Pharmacol.* **2016**, *6*, 1–14.

[219] Ma, J.; Han, L.; Liang, H.; Mi, C.; Shi, H.; Lee, J.; Jin, X. Celastrol inhibits the HIF-1α pathway by inhibition of mTOR/p70S6K/eIF4E and ERK1/2 phosphorylation in human hepatoma cells. *Oncol. Rep.* **2014**, *32*, 235–42.

[220] Gupta, S. C.; Prasad, S.; Aggarwal, B. B. *Anti-inflammatory nutraceuticals and chronic diseases*; Springer International Publishing Switzerland 2016; ISBN:978-3-319-41332-7; **2016**; Vol. 928.

[221] Lin, H.; Hsieh, M.; Hsi, Y.; Lo, Y.; Chuang, Y.; Chen, M.; Chien, S. Celastrol-induced apoptosis in human nasopharyngeal carcinoma is associated with the activation of the death receptor and the mitochondrial pathway. *Oncol. Lett.* **2017**, 1–8.

[222] Lu, L.; Shi, W.; Deshmukh, R. R.; Long, J.; Cheng, X.; Ji, W.; Zeng, G.; Chen, X.; Zhang, Y.; Dou, Q. P. Tumor Necrosis Factor-α sensitizes breast cancer cells to natural products with proteasome-inhibitory activity leading to apoptosis. *PLoS One* **2014**, *9*.

[223] Mi, C.; Shi, H.; Ma, J.; Han, L.; Lee, J.; Jin, X. Celastrol induces the apoptosis of breast cancer cells and inhibits their invasion via downregulation of MMP-9. *Oncol. Rep.* **2014**.

[224] Yang, H.-S.; Kim, J.-Y.; Lee, J.-H.; Lee, B.-W.; Park, K.-H.; Shim, K.-H.; Lee, M.-K.; Seo, K.-I. Celastrol isolated from Tripterygium regelii induces apoptosis through both caspase-dependent and -independent pathways in human breast cancer cells. *Food Chem. Toxicol.* **2011**, *49*, 527–532.

[225] Peng, B.; Xu, L.; Cao, F.; Wei, T.; Yang, C.; Uzan, G.; Zhang, D. HSP90 inhibitor, celastrol, arrests human monocytic leukemia cell U937 at G0/G1 in thiol-containing agents reversible way. *Mol. Cancer* **2010**, *9*, 1–13.

[226] Wu, J.; Ding, M.; Mao, N.; Wu, Y.; Wang, C.; Yuan, J.; Miao, X.; Li, J.; Shi, Z. Celastrol inhibits chondrosarcoma proliferation, migration and invasion through suppression CIP2A/c-MYC signaling pathway. *J. Pharmacol. Sci.* **2017**, *134*, 22–28.

[227] Yu, X.; Zhou, X.; Fu, C.; Wang, Q.; Nie, T.; Zou, F.; Guo, R.; Liu, H.; Zhang, B.; Dai, M. Celastrol induces apoptosis of human osteosarcoma cells via the mitochondrial apoptotic pathway. *Oncol. Rep.* **2015**, *34*, 1129–36.

[228] Liu, X.; Gao, R.; Li, M.; Si, C.; He, Y.; Wang, M.; Yang, Y.; Zheng, Q.; Wang, C. The ROS derived mitochondrial respirstion not from NADPH oxidase plays key role in Celastrol against angiotensin II-mediated HepG2 cell proliferation. *Apoptosis* **2016**, *21*, 1315–1326.

[229] Sung, B.; Park, B.; Yadav, V. R.; Aggarwal, B. B. Celastrol, a triterpene, enhances TRAIL-induced apoptosis through the down-regulation of cell

survival proteins and up-regulation of Death Receptors. *J. Biol. Chem.* **2016**, *291*, 16920–16920.

[230] Mou, H.; Zheng, Y.; Zhao, P.; Bao, H.; Fang, W.; Xu, N. Celastrol induces apoptosis in non-small-cell lung cancer A549 cells through activation of mitochondria- and Fas/FasL-mediated pathways. *Toxicol. Vitr.* **2011**, *25*, 1027–1032.

[231] Nagase, M.; Oto, J.; Sugiyama, S.; Yube, K.; Takaishi, Y.; Sakato, N. Apoptosis induction in HL-60 cells and inhibition of topoisomerase II by triterpene celastrol. *Biosci. Biotechnol. Biochem.* **2003**, *67*, 1883–7.

[232] Yu, X.; Ruan, X.; Zhang, J.; Zhao, Q. Celastrol induces cell apoptosis and inhibits the expression of the AML1-ETO/C-KIT oncoprotein in t(8;21) leukemia. *Molecules* **2016**, *21*, 574.

[233] Rajendran, P.; Li, F.; Shanmugam, M. K.; Kannaiyan, R.; Goh, J. N.; Wong, K. F.; Wang, W.; Khin, E.; Tergaonkar, V.; Kumar, A. P.; Luk, J. M.; Sethi, G. Celastrol suppresses growth and induces apoptosis of human hepatocellular carcinoma through the modulation of STAT3/JAK2 signaling cascade in vitro and in vivo. *Cancer Prev. Res.* **2012**, *5*.

[234] Uttarkar, S.; Dass, E.; Coulibaly, A.; Steinmann, S.; Jakobs, A.; Schomburg, C.; Trentmann, A.; Jose, J.; Schlenke, P.; Berdel, W. E.; Schmidt, T. J.; Carsten, M. Targeting acute myeloid leukemia with a small molecule inhibitor of the Myb/p300 interaction. **2016**, *127*, 1173–1183.

[235] Fribley, A. M.; Miller, J. R.; Brownell, A. L.; Garshott, D. M.; Zeng, Q.; Reist, T. E.; Narula, N.; Cai, P.; Xi, Y.; Callaghan, M. U.; Kodali, V.; Kaufman, R. J. Celastrol induces unfolded protein response-dependent cell death in head and neck cancer. *Exp. Cell Res.* **2015**, *330*, 412–422.

[236] Shao, L.; Zhou, Z.; Cai, Y.; Castro, P.; Dakhov, O.; Shi, P.; Bai, Y.; Ji, H.; Shen, W.; Wang, J. Celastrol suppresses tumor cell growth through targeting an AR-ERG-NF-κB pathway in TMPRSS2/ERG fusion gene expressing prostate cancer. *PLoS One* **2013**, *8*, e58391.

[237] Lee, H.-W.; Jang, K. S. Bin; Choi, H. J.; Jo, A.; Cheong, J.-H.; Chun, K.-H. Celastrol inhibits gastric cancer growth by induction of apoptosis and autophagy. *BMB Rep.* **2014**, *47*, 697–702.

[238] Xu, S.-W. W.; Law, B. Y. K.; Mok, S. W. F.; Leung, E. L. H.; Fan, X. X.; Coghi, P. S.; Zeng, W.; Leung, C.-H. H.; Ma, D.-L. L.; Liu, L.; Wong, V. K. W. Autophagic degradation of epidermal growth factor receptor in gefitinib-resistant lung cancer by celastrol. *Int. J. Oncol.* **2016**, *49*, 1576–1588.

[239] Guo, J.; Mei, Y.; Li, K.; Huang, X.; Yang, H. Downregulation of miR-17-92a cluster promotes autophagy induction in response to celastrol treatment in prostate cancer cells. *Biochem. Biophys. Res. Commun.* **2016**, *478*, 804–810.

[240] Westerheide, S. D.; Bosman, J. D.; Mbadugha, B. N. a; Kawahara, T. L. a; Matsumoto, G.; Kim, S.; Gu, W.; Devlin, J. P.; Silverman, R. B.; Morimoto, R. I. Celastrols as inducers of the heat shock response and cytoprotection. *J. Biol. Chem.* **2004**, *279*, 56053–60.

[241] Hieronymus, H.; Lamb, J.; Ross, K. N.; Peng, X. P.; Clement, C.; Rodina, A.; Nieto, M.; Du, J.; Stegmaier, K.; Raj, S. M.; Maloney, K. N.; Clardy, J.; Hahn, W. C.; Chiosis, G.; Golub, T. R. Gene expression signature-based chemical genomic prediction identifies a novel class of HSP90 pathway modulators. *Cancer Cell* **2006**, *10*, 321–330.

[242] Sreeramulu, S.; Gande, S. L.; Göbel, M.; Schwalbe, H. Molecular mechanism of inhibition of the human protein complex Hsp90-Cdc37, a kinome chaperone-cochaperone, by triterpene celastrol. *Angew. Chem. Int. Ed.* **2009**, *48*, 5853–5.

[243] Zhang, D.; Xu, L.; Cao, F.; Wei, T.; Yang, C.; Uzan, G.; Peng, B. Celastrol regulates multiple nuclear transcription factors belonging to HSP90's clients in a dose- and cell type-dependent way. *Cell Stress Chaperones* **2010**, *15*, 939–946.

[244] Peng, B.; Gu, Y.-J. J.; Wang, Y.; Cao, F.-F. F.; Zhang, X.; Zhang, D.-H. H.; Hou, J. Mutations Y493G and K546D in human HSP90 disrupt binding of celastrol and reduce interaction with Cdc37. *FEBS Open Bio.* **2016**, *6*, 729–734.

[245] Zhang, T.; Li, Y.; Yu, Y.; Zou, P.; Jiang, Y.; Sun, D. Characterization of celastrol to inhibit Hsp90 and Cdc37 interaction. *J. Biol. Chem.* **2009**, *284*, 35381–35389.

[246] Bekki, H.; Kohashi, K.; Maekawa, A.; Yamada, Y.; Yamamoto, H.; Harimaya, K.; Hakozaki, M.; Nabeshima, K.; Iwamoto, Y.; Oda, Y. Elevated expression of HSP90 and the antitumor effect of an HSP90 inhibitor via inactivation of the Akt/mTOR pathway in undifferentiated pleomorphic sarcoma. *BMC Cancer* **2015**, *15*, 804.

[247] Pópulo, H.; Lopes, J. M.; Soares, P. The mTOR signalling pathway in human cancer. *Int. J. Mol. Sci.* **2012**, *13*, 1886–918.

[248] Chen, Y.; Shi, S.; Wang, H.; Li, N.; Su, J.; Chou, G.; Wang, S. A homogeneous polysaccharide from fructus Schisandra chinensis (Turz.) baill induces mitochondrial apoptosis through the Hsp90/AKT signalling pathway in HepG2 cells. *Int. J. Mol. Sci.* **2016**, *17*, 1–19.

[249] Lee, H.-W.; Jang, K. S. Bin; Choi, H. J.; Jo, A.; Cheong, J.-H.; Chun, K.-H. Celastrol inhibits gastric cancer growth by induction of apoptosis and autophagy. *BMB Rep.* **2014**, *47*, 697–702.

[250] Lee, J.-H.; Won, Y.-S.; Park, K.-H.; Lee, M.-K.; Tachibana, H.; Yamada, K.; Seo, K.-I. Celastrol inhibits growth and induces apoptotic cell death in melanoma cells via the activation ROS-dependent mitochondrial pathway

and the suppression of PI3K/AKT signaling. *Apoptosis* **2012**, *17*, 1275–86.

[251] Kuchta, K.; Xiang, Y.; Huang, S.; Tang, Y.; Peng, X.; Wang, X.; Zhu, Y.; Li, J.; Xu, J.; Lin, Z.; Pan, T. Celastrol, an active constituent of the TCM plant Tripterygium wilfordii Hook.f., inhibits prostate cancer bone metastasis. *Prostate Cancer Prostatic. Dis.* **2017**, *20*, 1–9.

[252] Khasigov, P. Z.; Podobed, O. V; Gracheva, T. S.; Salbiev, K. D.; Grachev, S. V; Berezov, T. T. Role of matrix metalloproteinases and their inhibitors in tumor invasion and metastasis. *Biochemistry. (Mosc).* **2003**, *68*, 711–7.

[253] Zhang, X.-X.; Fu, Z.; Zhang, Z.; Miao, C.; Xu, P.; Wang, T.; Yang, L.; Cheng, S. Microcystin-LR promotes melanoma cell invasion and enhances Matrix Metalloproteinase-2/-9 expression mediated by NF-kB activation. *Environ. Sci. Technol.* **2012**, *46*, 11319–11326.

[254] Sethi, G.; Ahn, K. S.; Pandey, M. K.; Aggarwal, B. B. Celastrol, a novel triterpene, potentiates TNF-induced apoptosis and suppresses invasion of tumor cells by inhibiting NF-kB–regulated gene products and TAK1-mediated NF-kB activation. *Blood* **2007**, *109*, 2727–2735.

[255] Li, H.; Li, Y.; Liu, D.; Sun, H.; Liu, J. miR-224 is critical for celastrol-induced inhibition of migration and invasion of hepatocellular carcinoma cells. *Cell. Physiol. Biochem.* **2013**, *32*, 448–58.

[256] Wang, Z.; Zhai, Z.; Du, X. Celastrol inhibits migration and invasion through blocking the NF‑κB pathway in ovarian cancer cells. *Exp. Ther. Med.* **2017**, *14*, 819–824.

[257] Ahmad, A.; Biersack, B.; Li, Y.; Kong, D.; Bao, B.; Schobert, R.; Padhye, S. B.; Sarkar, F. H. Targeted regulation of PI3K/Akt/mTOR/NF-κB signaling by indole compounds and their derivatives: mechanistic details and biological implications for cancer therapy. *Anticancer. Agents Med. Chem.* **2013**, *13*, 1002–13.

[258] Huang, Y.; Zhou, Y.; Fan, Y.; Zhou, D. Celastrol inhibits the growth of human glioma xenografts in nude mice through suppressing VEGFR expression. *Cancer Lett.* **2008**, *264*, 101–106.

[259] Zhou, Y.; Huang, Y. Antiangiogenic effect of celastrol on the growth of human glioma: an in vitro and in vivo study. *Chin. Med. J. (Engl).* **2009**, *122*, 1666–73.

[260] Huang, S.; Tang, Y.; Cai, X.; Peng, X.; Liu, X.; Zhang, L.; Xiang, Y.; Wang, D.; Wang, X.; Pan, T. Celastrol inhibits vasculogenesis by suppressing the VEGF-induced functional activity of bone marrow-derived endothelial progenitor cells. *Biochem Biophys. Res. Commun.* **2012**, *423*, 467–472.

[261] Chou, T.-C. Theoretical basis, experimental design, and computerized simulation of synergism and antagonism in drug combination studies. *Pharmacol. Rev.* **2006**, *58*, 621–681.

[262] Yan, Y.; Guo, Y.; Zhang, W.; Ma, C.; Zhang, Y.; Wang, C.; Wang, H. Celastrol enhanced the anticancer effect of lapatinib in human hepatocellular carcinoma cells in vitro. *J. BUON.* **2014**, *19*, 412–8.

[263] Chen, M.; Rose, A. E.; Doudican, N.; Osman, I.; Orlow, S. J. Celastrol synergistically enhances temozolomide cytotoxicity in melanoma cells. *Mol. Cancer Res.* **2009**, *7*, 1946–1953.

[264] Boridy, S.; Le, P. U.; Petrecca, K.; Maysinger, D. Celastrol targets proteostasis and acts synergistically with a heat-shock protein 90 inhibitor to kill human glioblastoma cells. *Cell Death Dis.* **2014**, *5*, e1216.

[265] Pazhang, Y.; Jaliani, H.; Imani, M.; Dariushnejad, H. Synergism between NF-kappa B inhibitor, celastrol, and XIAP inhibitor, embelin, in an acute myeloid leukemia cell line, HL-60. *J. Cancer Res. Ther.* **2016**, *12*, 155.

[266] Zhu, H.; Yang, W.; He, L.; Ding, W.-J.; Zheng, L.; Liao, S.; Huang, P.; Lu, W.; He, Q.; Yang, B. Upregulating Noxa by ER stress, celastrol exerts synergistic anti-cancer activity in combination with ABT-737 in human hepatocellular carcinoma cells. *PLoS One* **2012**, *7*, 1–12.

[267] Lo Iacono, M.; Monica, V.; Vavalà, T.; Gisabella, M.; Saviozzi, S.; Bracco, E.; Novello, S.; Papotti, M.; Scagliotti, G. V. ATF2 contributes to cisplatin resistance in non-small cell lung cancer and celastrol induces cisplatin resensitization through inhibition of JNK/ATF2 pathway. *Int. J. Cancer* **2015**, *136*, 2598–2609.

[268] Li, Z.; Zhang, J.; Tang, J.; Wang, R. Celastrol increases osteosarcoma cell lysis by γδ T cells through up-regulation of death receptors. *Oncotarget* **2016**, 1–10.

[269] Zhang, J.; Li, C.-Y.; Xu, M.-J.; Wu, T.; Chu, J.-H.; Liu, S.-J.; Ju, W.-Z. Oral bioavailability and gender-related pharmacokinetics of celastrol following administration of pure celastrol and its related tablets in rats. *J. Ethnopharmacol.* **2012**, *144*, 195–200.

[270] Li, Z.; Yao, L.; Li, J.; Zhang, W.; Wu, X.; Liu, Y.; Lin, M.; Su, W.; Li, Y.; Liang, D. Celastrol nanoparticles inhibit corneal neovascularization induced by suturing in rats. *Int. J. Nanomedicine* **2012**, *7*, 1163–73.

[271] Wang, S.; Liu, K.; Wang, X.; He, Q.; Chen, X. Toxic effects of celastrol on embryonic development of zebrafish (Danio rerio). *Drug Chem. Toxicol.* **2011**, *34*, 61–65.

[272] Kusy, S.; Ghosn, E. E. B.; Herzenberg, L. a; Contag, C. H. Development of B cells and erythrocytes is specifically impaired by the drug celastrol in mice. *PLoS One* **2012**, *7*, e35733.

[273] Bai, J.-P.; Shi, Y.-L.; Fang, X.; Shi, Q.-X. Effects of demethylzeylasteral and celastrol on spermatogenic cell Ca2+ channels and progesterone-induced sperm acrosome reaction. *Eur. J. Pharmacol.* **2003**, *464*, 9–15.

[274] Wolfram, J.; Suri, K.; Huang, Y.; Molinaro, R.; Borsoi, C.; Scott, B.; Boom, K.; Paolino, D.; Fresta, M.; Wang, J.; Ferrari, M.; Celia, C.; Shen, H. Evaluation of anticancer activity of celastrol liposomes in prostate cancer cells. *J. Microencapsul.* **2014**, *31*, 501–507.

[275] Song, J.; Shi, F.; Zhang, Z.; Zhu, F.; Xue, J.; Tan, X.; Zhang, L.; Jia, X. Formulation and evaluation of celastrol-loaded liposomes. *Molecules* **2011**, *16*, 7880–92.

[276] Yang, L.; Guo, G.; Sun, L.; Li, C.; Zhang, H. Efficacy and safety of traditional chemotherapies for patients with ovarian neoplasm: a network meta-analysis. *Oncotarget* **2015**, 1–11.

[277] Aqil, F.; Kausar, H.; Agrawal, A. K.; Jeyabalan, J.; Kyakulaga, A. H.; Munagala, R.; Gupta, R. Exosomal formulation enhances therapeutic response of celastrol against lung cancer. *Exp. Mol. Pathol.* **2016**, *101*, 12–21.

[278] Sanna, V.; Chamcheu, J. C.; Pala, N.; Mukhtar, H.; Sechi, M.; Siddiqui, I. A. Nanoencapsulation of natural triterpenoid celastrol for prostate cancer treatment. *Int. J. Nanomedicine* **2015**, *10*, 6835–6846.

[279] Li, Z.; Li, J.; Zhu, L.; Zhang, Y.; Zhang, J.; Yao, L.; Liang, D.; Wang, L. Celastrol nanomicelles attenuate cytokine secretion in macrophages and inhibit macrophage- induced corneal neovascularization in rats. *Int. J. Nanomedicine* **2016**, *11*, 6135–6148.

[280] Chen, Y.; Yuan, L.; Zhou, L.; Zhang, Z.; Cao, W.; Wu, Q. Effect of cell-penetrating peptide-coated nanostructured lipid carriers on the oral absorption of tripterine. *Int. J. Nanomedicine* **2012**, *7*, 4581–91.

[281] Qi, X.; Qin, J.; Ma, N.; Chou, X.; Wu, Z. Solid self-microemulsifying dispersible tablets of celastrol: formulation development, charaterization and bioavailability evaluation. *Int. J. Pharm.* **2014**, *472*, 40–7.

[282] Abbas, S.; Bhoumik, A.; Dahl, R.; Vasile, S.; Krajewski, S.; Cosford, N. D. P.; Ronai, Z. Preclinical studies of celastrol and acetyl isogambogic acid in melanoma. *Clin. Cancer Res.* **2007**, *13*, 6769–6778.

[283] Zhou, Y. Tripterine and tripterine derivatives for treating cancer, inflammation and central nervous system diseases, Patent CN101624415, **2008**.

[284] Liu K., Guan Y., Zhao F., Shao M., Xu H., Z. D. New celastrol-containing alcohol ester for preparing anti-tumor medicine for treating malignant tumors e.g. gastric tumor and for preparing antiinflammation medicine e.g. for treating rheumatoid arthritis, Behcet's syndrome and hepatitis, Patent CN101311187-A, **2009**.

[285] Luchen Shan, Jie Jiang, Hongli Sun, Yuqiang Wang, Lipeng Xu, Pei Yu, G. Z. Tripterine derivate and use thereof, Patent CN 101805390 B, **2012**.

[286] Wei, W.; Wu, S.; Wang, X.; Sun, C. K.-W.; Yang, X.; Yan, X.; Chua, M.-S.; So, S. Novel celastrol derivatives inhibit the growth of hepatocellular carcinoma patient-derived xenografts. *Oncotarget* **2014**, *5*, 5819–5831.

[287] Tang, W. J.; Wang, J.; Tong, X.; Shi, J. B.; Liu, X. H.; Li, J. Design and synthesis of celastrol derivatives as anticancer agents. *Eur. J. Med. Chem.* **2015**, *95*, 166–173.

[288] Shan, W.-G.; Wang, H.-G.; Chen, Y.; Wu, R.; Wen, Y.-T.; Zhang, L.-W.; Ying, Y.-M.; Wang, J.-W.; Zhan, Z.-J. Synthesis of 3- and 29-substituted celastrol derivatives and structure-activity relationship studies of their cytotoxic activities. *Bioorg. Med. Chem. Lett.* **2017**, *27*, 3450–3453.

[289] Hu, L.; Wu, H.; Li, B.; Song, D.; Yang, G.; Chen, G.; Xie, B.; Xu, Z.; Zhang, Y.; Yu, D.; Hou, J.; Xiao, W.; Sun, X.; Chang, G.; Zhang, Y.; Gao, L.; Dai, B.; Tao, Y.; Shi, J.; Zhu, W. Dihydrocelastrol inhibits multiple myeloma cell proliferation and promotes apoptosis through ERK1/2 and IL-6/STAT3 pathways in vitro and in vivo. *Acta Biochim. Biophys. Sin. (Shanghai).* **2017**, *49*, 420–427.

[290] Chadli, A.; Felts, S. J.; Wang, Q.; Sullivan, W. P.; Botuyan, M. V.; Fauq, A.; Ramirez-Alvarado, M.; Mer, G. Celastrol inhibits Hsp90 chaperoning of steroid receptors by inducing fibrillization of the co-chaperone p23. *J. Biol. Chem.* **2010**, *285*, 4224–4231.

[291] Zeng, J.F.; Pan, J.F.; Li, B.Y.; Zhu, Q.; Fang, T.; Ni, H. . Water-soluble triterpene phenol compound having antitumor activities and the preparation method thereof, WIPO Patent Application, Patent WO/2009/067891, **2009**.

[292] Tang, K.; Huang, Q.; Zeng, J.; Wu, G.; Huang, J.; Pan, J.; Lu, W. Design, synthesis and biological evaluation of C(6)-modified celastrol derivatives as potential antitumor agents, molecules. *Molecules* **2014**, *19*, 10177–10188.

[293] Tang, K.; Huang, J.; Pan, J.; Zhang, X.; Lu, W. Design, synthesis and biological evaluation of C(6)-indole celastrol derivatives as potential antitumor agents. *RSC Adv.* **2015**, *5*, 19629–19623.

[294] Zhu, Y.; Chen, Z.; Huang, Z.; Yan, S.; Li, Z.; Zhou, H.; Zhang, X.; Su, Y.; Zeng, Z. AlCl3·6H2O-Catalyzed Friedel-Crafts alkylation of indoles by the para-quinone methide moiety of celastrol. *Molecules* **2017**, *22*, 742.

[295] Li, F.; Zhao, C.; Wang, L. Molecular targeted agents (MTA) combination therapy for cancer: Developments and potentials. *Int. J. Cancer* **2014**, *134*, 1257–69.

[296] Mishra, B. B.; Tiwari, V. K. Natural products: An evolving role in future drug discovery. *Eur. J. Med. Chem.* **2011**, *46*, 4769–4807.

[297] Gonçalves, B. M. F.; Salvador, J. A. R.; Marín, S.; Cascante, M. Synthesis and anticancer activity of novel fluorinated asiatic acid derivatives. *Eur. J. Med. Chem.* **2016**, *114*, 101–117.

[298] Mendes, V. I. S.; Bartholomeusz, G. A.; Ayres, M.; Gandhi, V.; Salvador, J. A. R. Synthesis and cytotoxic activity of novel A-ring cleaved ursolic acid derivatives in human non-small cell lung cancer cells. *Eur. J. Med. Chem.* **2016**, *123*, 317–331.

[299] Rodríguez-Hernández, D.; Demuner, A. J.; Barbosa, L. C. A.; Heller, L.; Csuk, R.; Rodríguez-Hernándeza, D.; Demunera, A. J.; Barbosaa, L. C. A.; Hellerc, L.; Csuk, R. Novel hederagenin–triazolyl derivatives as potential anti-cancer agents. *Eur. J. Med. Chem.* **2016**, *115*, 257–267.

[300] Zhou, Q. Natural diterpene and triterpene quinone methides: structures, synthesis, and biological potentials. In *Quinone Methides*; Richmond, USA, **2009**; Vol. 1, pp. 269–295.

[301] Wu, J.; Zhou, Y.; Wang, L.; Zuo, J.; Zhao, W. Terpenoids from root bark of Celastrus orbiculatus. *Phytochem.* **2012**, *75*, 159–168.

[302] Zhou, Y.; Li, W.; Wang, M.; Zhang, X.; Zhang, H.; Tong, X.; Xiao, Y. Competitive profiling of celastrol targets in human cervical cancer HeLa cells via quantitative chemical proteomics. *Mol. BioSyst.* **2017**.

[303] Lokwani, D.; Bhandari, S.; Pujari, R.; Shastri, P.; Shelke, G.; Pawar, V. Use of Quantitative Structure–Activity Relationship (QSAR) and ADMET prediction studies as screening methods for design of benzyl urea derivatives for anti-cancer activity. *J. Enzyme Inhib. Med. Chem.* **2010**, *26*, 319–331.

[304] Gaware, R.; Khunt, R.; Czollner, L.; Stanetty, C.; Cunha, T. Da; Kratschmar, D. V.; Odermatt, A.; Kosma, P.; Jordis, U.; Claben-Houben, D. Synthesis of new glycyrrhetinic acid derived ring A azepanone, 29-urea and 29-hydroxamic acid derivatives as selective 11b-hydroxysteroid dehydrogenase 2 inhibitors. *Bioorganic Med. Chem.* **2011**, *19*, 1866–1880.

[305] Sommerwerk, S.; Heller, L.; Kuhfs, J.; Csuk, R. Urea derivates of ursolic, oleanolic and maslinic acid induce apoptosis and are selective cytotoxic for several human tumor cell lines. *Eur. J. Med. Chem.* **2016**, *119*, 1–16.

[306] Devlin, J. P. Derivatives of pentacyclic nortriterpene quinone methides as compounds useful in the treatment of inflammatory, neurodegenerative, and neoplastic diseases, Unitated States, Patent US 2004/0220267 A1, **2004**.

[307] Nakanishi, K.; Takahashi, Y.; Budzikiewicz, H. Pristimerin. Spectroscopic properties of the dienone-phenol-type rearrangement products and other derivatives. *J. Org. Chem.* **1965**, *30*, 1729–1734.

[308] Leathen, M. L.; Peterson, E. A. Facile preparation of protected benzylic and heteroarylmethyl amines via room temperature Curtius rearrangement. *Tetrahedron Lett.* **2010**, *51*, 2888–2891.

[309] Salvador, J. A. R.; Silvestre, S. M. Bismuth-catalyzed allylic oxidation using t-butyl hydroperoxide. *Tetrahedron Lett.* **2005**, *46*, 2581–2584.

[310] Ramesh, C.; Mahender, G.; Ravindranath, N.; Das, B. A mild, highly selective and remarkably easy procedure for deprotection of aromatic acetates using ammonium acetate as a neutral catalyst in aqueous medium. *Tetrahedron* **2003**, *59*, 1049–1054.

[311] Trott, A.; West, J. D.; Klaic, L.; Westerheide, S. D.; Silverman, R. B.; Morimoto, R. I.; Morano, K. A. Activation of heat shock and antioxidant responses by the natural product celastrol: transcriptional signatures of a thiol-targeted molecule. *Mol. Biol. Cell* **2008**, *19*, 1104–1112.

[312] Shapiro, G. I.; Harper, J. W. Anticancer drug targets : cell cycle and checkpoint control. *J. Clin. Invest.* **1999**, *104*, 1645–1653.

[313] Stacey Ricci, M.; Zong, W. Chemotherapeutic approaches for targeting cell death pathways. *Oncologist* **2006**, *11*, 342–357.

[314] Vermes, I.; Haanen, C.; Steffens-Nakken, H.; Reutelingsperger, C. A novel assay for apoptosis. Flow cytometric detection of phosphatidylserine expression on early apoptotic cells using fluorescein labelled Annexin V. *J. Immunol. Methods* **1995**, *184*, 39–51.

[315] Taatjes, D. J.; Sobel, B. E.; Budd, R. C. Morphological and cytochemical determination of cell death by apoptosis. *Histochem. Cell Biol.* **2008**, *129*, 33–43.

[316] Fulda, S.; Debatin, K.-M. Extrinsic versus intrinsic apoptosis pathways in anticancer chemotherapy. *Oncogene* **2006**, *25*, 4798–4811.

[317] Vousden, K. H.; Lu, X. Live or let die: the cell's response to p53. *Nat. Rev. Cancer* **2002**, *2*, 594–604.

[318] Mullany, L. K.; Wong, K. K.; Marciano, D. C.; Katsonis, P.; King-Crane, E. R.; Ren, Y. A.; Lichtarge, O.; Richards, J. A. S. Specific TP53 mutants overrepresented in ovarian cancer impact CNV, TP53 activity, responses to Nutlin-3a, and cell survival. *Neoplasia* **2015**, *17*, 789–803.

[319] Bressac, B.; Galvin, K.; Liang, T.; Isselbacher, K.; Wands, J.; Ozturk, M. Abnormal structure and expression of p53 gene in human hepatocellular carcinoma. *Pnas* **1990**, *87*, 1973–1977.

[320] Breen, L.; Heenan, M.; Amberger-Murphy, V.; Clynes, M. Investigation of the role of p53 in chemotherapy resistance of lung cancer cell lines. *Anticancer Res.* **2007**, *27*, 1361–1364.

[321] Whitesell, L.; Lindquist, S. L. HSP90 and the chaperoning of cancer. *Nat. Rev. Cancer* **2005**, *5*, 761–72.

[322] Taldone, T.; Gozman, A.; Maharaj, R.; Chiosis, G. Targeting Hsp90: small-molecule inhibitors and their clinical development. *Curr. Opin. Pharmacol.* **2008**, *8*, 370–374.

[323] Duan, Y.; Jin, H.; Yu, H.; Wang, Z.; Zhang, L.; Huo, J. Computational

investigation of interactions between Cdc37 and celastrol. *Mol. Simul.* **2013**, *39*, 270–278.

[324] Holmes, D. Ovarian cancer: beyond resistance. *Nat. Outl.* **2015**, *527*, S217–S219.

[325] Yu, H.; Gou, S.; Wang, Z.; Chen, F.; Fang, L. Toward overcoming cisplatin resistance via sterically hindered platinum(II) complexes. *Eur. J. Med. Chem.* **2016**, *114*, 141–152.

[326] Raja, F. A.; Chopra, N.; Ledermann, J. A. Optimal first-line treatment in ovarian cancer. *Ann. Oncol.* **2012**, *23*.

[327] Shaloam, D.; Tchounwou, P. B. Cisplatin in cancer therapy: Molecular mechanisms of action. *Eur. J. Pharmacol.* **2014**, *740*, 364–378.

[328] Florea, A.; Büsselberg, D. Cisplatin as an anti-tumor drug: cellular mechanisms of activity, drug resistance and induced side effects. *Cancers* **2011**, 2315–2325.

[329] Chou, T. C.; Talalay, P. Quantitative analysis of dose-effect relationships: the combined effects of multiple drugs or enzyme inhibitors. *Adv. Enzyme Regul.* **1984**, *22*, 27–55.

[330] Jeong, B.; Kim, Y. C.; Lee, E.-S.; Zhao, L.; Park, H.; Jew, S.; Lee, M. K.; Kim, Y. C.; Thapa, P.; Karki, R.; Jahng, Y.; Jeong, B.; Lee, E.-S. Modification of C2, 3, 23, 28 functional groups on asiatic acid and evaluation of hepatoprotective effects. *Bull. Korean Chem. Soc.* **2007**, *28*, 977–982.

[331] Salvador, J. A. R.; Leal, A. S.; Alho, D. P. S.; Gonçalves, B. M. F.; Valdeira, A. S.; Mendes, V. I. S.; Jing, Y. Highlights of pentacyclic triterpenoids in the cancer settings. In *Studies in Natural Products Chemistry*; Elsevier; ISBN: 15725995, **2014**; Vol. 41, pp. 33–73.

[332] Salvador, J. A. R.; Leal, A. S.; Valdeira, A. S.; Alho, D. P. S.; Figueiredo, S. A. C.; Silvestre, S. M.; Mendes, V. I. S. Oleanane-, ursane-, and quinone methide friedelane-type triterpenoid derivatives: recent advances in cancer treatment. *Eur. J. Med. Chem.* **2017**.

[333] Chang, Y.; Zhou, S.; Li, E.; Zhao, W.; Ji, Y.; Wen, X.; Sun, H.; Yuan, H. Fragment-based discovery of novel pentacyclic triterpenoid derivatives as cholesteryl ester transfer protein inhibitors. *Eur. J. Med. Chem.* **2017**, *126*, 143–153.

[334] He, Z.; Liang, F.; Lu, J.; Pan, Y. Cytotoxic triterpenoids from Lysimachia parvifolia. *Eur. J. Med. Chem.* **2013**, *67*, 390–397.

[335] Sommerwerk, S.; Heller, L.; Kuhfs, J.; Csuk, R. Selective killing of cancer cells with triterpenoic acid amides - The substantial role of an aromatic moiety alignment. *Eur. J. Med. Chem.* **2016**, *122*, 452–464.

[336] Moreira, V. M.; Salvador, J. A. R.; Simões, S.; Destro, F.; Gavioli, R. Novel

oleanolic vinyl boronates: Synthesis and antitumor activity. *Eur. J. Med. Chem.* **2013**, *63*, 46–56.

[337] Sommerwerk, S.; Heller, L.; Kerzig, C.; Kramell, A. E.; Csuk, R. Rhodamine B conjugates of triterpenoic acids are cytotoxic mitocans even at nanomolar concentrations. *Eur. J. Med. Chem.* **2017**, *127*, 1–9.

[338] Heller, L.; Kahnt, M.; Loesche, A.; Grabandt, P.; Schwarz, S.; Brandt, W.; Csuk, R. Amino derivatives of platanic acid act as selective and potent inhibitors of butyrylcholinesterase. *Eur. J. Med. Chem.* **2017**, *126*, 652–668.

[339] Liu, Z.; Ma, L.; Zhou, G.-B. The main anticancer bullets of the Chinese medicinal herb, Thunder God Vine. *Molecules* **2011**, *16*, 5283–5297.

[340] Ma, J.; Dey, M.; Yang, H.; Poulev, A.; Pouleva, R.; Dorn, R.; Lipsky, P. E.; Kennelly, E. J.; Raskin, I. Anti-inflammatory and immunosuppressive compounds from Tripterygium wilfordii. *Phytochemistry* **2007**, *68*, 1172–1178.

[341] Wong, K.-F.; Yuan, Y.; Luk, J. M. Tripterygium wilfordii bioactive compounds as anticancer and anti-inflammatory agents. *Clin. Exp. Pharmacol. Physiol.* **2012**, *39*, 311–320.

[342] Hu, Y.; Qi, Y.; Liu, H.; Fan, G.; Chai, Y. Effects of celastrol on human cervical cancer cells as revealed by ion-trap gas chromatography-mass spectrometry based metabolic profiling. *Biochim. Biophys. Acta* **2013**, *1830*, 2779–2789.

[343] Figueiredo, S. A. C.; Salvador, J. A. R.; Cortés, R.; Cascante, M. Novel celastrol derivatives with improved selectivity and enhanced antitumour activity: Design, synthesis and biological evaluation. *Eur. J. Med. Chem.* **2017**, *138*, 422–437.

[344] Ghosh, A. K.; Brindisi, M. Organic carbamates in drug design and medicinal chemistry. *J. Med. Chem.* **2015**, *58*, 2895–2940.

[345] Saito, A.; Yamashita, T.; Mariko, Y.; Nosaka, Y.; Tsuchiya, K.; Ando, T.; Suzuki, T.; Tsuruo, T.; Nakanishi, O. A synthetic inhibitor of histone deacetylase, MS-27-275, with marked in vivo antitumor activity against human tumors. *Proc. Natl. Acad. Sci.* **1999**, *96*, 4592–7.

[346] Snodgrass, R. G.; Collier, A. C.; Coon, A. E.; Pritsos, C. A. Mitomycin C inhibits ribosomal RNA: a novel cytotoxic mechanism for bioreductive drugs. *J. Biol. Chem.* **2010**, *285*, 19068–19075.

[347] Bencharit, S.; Morton, C. L.; Howard-Williams, E. L.; Danks, M. K.; Potter, P. M.; Redinbo, M. R. Structural insights into CPT-11 activation by mammalian carboxylesterases. *Nat. Struct. Biol.* **2002**, *9*, 337–342.

[348] Quinney, S. K.; Sanghani, S. P.; Davis, W. I.; Hurley, T. D.; Sun, Z.; Murry, D. J.; Bosron, W. F. Hydrolysis of capecitabine to 5'-deoxy-5-fluorocytidine

by human carboxylesterases and inhibition by loperamide. *J. Pharmacol. Exp. Ther.* **2005**, *313*, 1011–1016.

[349] Morgan, D. M. L. Tetrazolium (MTT) assay for cellular viability and activity. In *Polyamine Protocols. Methods in Molecular Biology, vol 79*; Humana Press; ISBN: 978-1-59259-565-5: New Jersey, **1998**; pp. 179–184.

[350] Thornberry, N. A.; Laebnik, Y. Caspases: enemies within. *Science* **1998**, *281*, 1312–1316.

[351] Chaitanya, G. V.; Steven, A. J.; Babu, P. P. PARP-1 cleavage fragments: signatures of cell-death proteases in neurodegeneration. *Cell Commun. Signal.* **2010**, *8*.

[352] Westphal, D.; Dewson, G.; Czabotar, P. E.; Kluck, R. M. Molecular biology of Bax and Bak activation and action. *Biochim. Biophys. Acta - Mol. Cell Res.* **2011**, *1813*, 521–531.

[353] Jemal, A.; Murray, T.; Ward, E.; Samuels, A.; Tiwari, R. C.; Ghafoor, A.; Feuer, E. J.; Thun, M. J.; Manager, M. Cancer Statistics, 2005. *CA. Cancer J. Clin.* **2005**, *55*, 10–30.

[354] Ferlay, J.; Soerjomataram, I.; Dikshit, R.; Eser, S.; Mathers, C.; Rebelo, M.; Parkin, D. M.; Forman, D.; Bray, F. Cancer incidence and mortality worldwide: Sources, methods and major patterns in GLOBOCAN 2012. *Int. J. Cancer* **2015**, *136*, E359–E386.

[355] Neijt, J. P.; Engelholm, S. A.; Tuxen, M. K.; Sorensen, P. G.; Hansen, M.; Sessa, C.; de Swart, C. A.; Hirsch, F. R.; Lund, B.; van Houwelingen, H. C. Exploratory phase III study of paclitaxel and cisplatin versus paclitaxel and carboplatin in advanced ovarian cancer. *J. Clin. Oncol.* **2000**, *18*, 3084–92.

[356] Markman, M.; Kennedy, A.; Webster, K.; Peterson, G.; Kulp, B.; Belinson, J. Combination chemotherapy with carboplatin and docetaxel in the treatment of cancers of the ovary and fallopian tube and primary carcinoma of the peritoneum. *J. Clin. Oncol.* **2001**, *19*, 1901–5.

[357] Ferrero, J.-M.; Weber, B.; Geay, J.-F.; Lepille, D.; Orfeuvre, H.; Combe, M.; Mayer, F.; Leduc, B.; Bourgeois, H.; Paraiso, D.; Pujade-Lauraine, E. Second-line chemotherapy with pegylated liposomal doxorubicin and carboplatin is highly effective in patients with advanced ovarian cancer in late relapse: a GINECO phase II trial. *Ann. Oncol.* **2006**, *18*, 263–268.

[358] Zhang, X.; Liu, Y.; Kim, Y. J.; Mac, J.; Zhuang, R.; Wang, P. Co-delivery of carboplatin and paclitaxel via cross-linked multilamellar liposomes for ovarian cancer treatment. *RSC Adv.* **2017**, *7*, 19685–19693.

[359] Toteva, M. M.; Richard, J. P. The generation and reactions of quinone methides. *Adv. Phys. Org. Chem.* **2011**, *45*, 39–91.

[360] Parra, A.; Tortosa, M. Para-quinone methide: A new player in asymmetric

catalysis. *ChemCatChem* **2015**, *7*, 1524–1526.

[361] Wuts, P. G. M. *Greene's protective groups in organic synthesis*; 5th; **2014**.

[362] Torii, S.; Tanaka, H.; Inokuchi, T.; Tomozane, K. Electrolytic decarboxylation. A convenient synthesis of 3-(cis-3-hexenyl)-2-cyclopentenone, a precursor of cis-Jasmone synthesis. *Bull. Chem. Soc. Jpn.* **1982**, *55*, 3947–3948.

[363] Chaikin, S. W.; Brown, W. G. Reduction of aldehydes, ketones and acid chlorides by sodium borohydride. *J. Am. Chem. Soc.* **1949**, *71*, 122–125.

[364] Patrick, G. L. *An Introduction to Medicinal Chemistry*; Oxford University Press; ISBN: 9780199234479: Oxford; **2009**; Vol. 40.

[365] Ouyang, A.; Skibo, E. B. Iminium ion chemistry of mitosene DNA alkylating agents. Enriched 13C NMR and isolation studies. *Biochemistry* **2000**, *39*, 5817–5830.

[366] Hassani, M.; Cai, W.; Holley, D. C.; Lineswala, J. P.; Maharjan, B. R.; Ebrahimian, G. R.; Seradj, H.; Stocksdale, M. G.; Mohammadi, F.; Marvin, C. C.; Gerdes, J. M.; Beall, H. D.; Behforouz, M. Novel lavendamycin analogues as antitumor agents: synthesis, in vitro cytotoxicity, structure−metabolism, and computational molecular modeling studies with NAD(P)H:quinone oxidoreductase-1. *J. Med. Chem.* **2005**, *48*, 7733–7749.

[367] Fryatt, T.; Pettersson, H. I.; Gardipee, W. T.; Bray, K. C.; Green, S. J.; Slawin, A. M.; Beall, H. D.; Moody, C. J. Novel quinolinequinone antitumor agents: structure-metabolism studies with NAD(P)H:quinone oxidoreductase (NQO1). *Bioorg. Med. Chem.* **2004**, *12*, 1667–1687.

[368] Kretzschmar, M.; Hodík, T.; Schneider, C. Brønsted acid catalyzed addition of enamides to ortho-quinone methide imines-an efficient and highly enantioselective synthesis of chiral tetrahydroacridines. *Angew. Chemie Int. Ed.* **2016**, *55*, 9788–9792.

[369] Frasinyuk, M. S.; Mrug, G. P.; Bondarenko, S. P.; Khilya, V. P.; Sviripa, V. M.; Syrotchuk, O. A.; Zhang, W.; Cai, X.; Fiandalo, M. V; Mohler, J. L.; Liu, C.; Watt, D. S. Antineoplastic isoflavonoids derived from intermediate ortho-quinone methides generated from mannich bases. *ChemMedChem* **2016**, *11*, 600–11.

[370] Garuti, L.; Roberti, M.; Pizzirani, D. Nitrogen-containing heterocyclic quinones: a class of potential selective antitumor agents. *Mini Rev. Med. Chem.* **2007**, *7*, 481–9.

[371] Scriven, E. F. V.; Turnbull, K. Azides: their preparation and synthetic uses. *Chem. Rev.* **1988**, *88*, 297–368.

[372] Leogane, O.; Lebel, H. One-pot Curtius rearrangement processes from carboxylic acids. *Synthesis* **2009**, 1935–1940.

[373] Fleming, F. F.; Yao, L.; Ravikumar, P. C.; Funk, L.; Shook, B. C. Nitrile-containing pharmaceuticals: Efficacious roles of the nitrile pharmacophore. *J. Med. Chem.* **2010**, *53*, 7902–7917.

[374] Rokita, S. E. *Quinone methides*; John Wiley & Sons, Inc., Publication; ISBN: 0470452870; **2009**; Vol. 1.

[375] Weinert, E. E.; Ruggero Dondi; Colloredo-Melz, S.; Frankenfield, K. N.; Mitchell, C. H.; Freccero, M.; Rokita, S. E. Substituents on quinone methides strongly modulate formation and stability of their nucleophilic adducts. *J. Am. Chem. Soc.* **2006**, *128*, 11940–11947.

[376] Silvestre, S. M.; Salvador, J. A. R. Allylic and benzylic oxidation reactions with sodium chlorite. *Tetrahedron* **2007**, *63*, 2439–2445.